PHYSICAL CONTROLS ON THE DISTRIBUTION OF CONTAMINANTS ON STURGEON BANK, FRASER RIVER DELTA, BRITISH COLUMBIA

by

Tracey Dawn Feeney

B.Sc. University of British Columbia, 1989

A THESIS SUBMITTED IN PARTIAL FULFILMENT OF

THE REQUIREMENTS FOR THE DEGREE OF

MASTER OF SCIENCE

in

THE FACULTY OF GRADUATE STUDIES

Oceanography

We accept this thesis as conforming

to the required standard

THE UNIVERSITY OF BRITISH COLUMBIA

December, 1995

In presenting this thesis in partial fulfilment of the requirements for an advanced degree at the University of British Columbia, I agree that the Library shall make it freely available for reference and study. I further agree that permission for extensive copying of this thesis for scholarly purposes may be granted by the head of my department or by his or her representatives. It is understood that copying or publication of this thesis for financial gain shall not be allowed without my written permission.

Department of Oceanography

The University of British Columbia
Vancouver, Canada

Date Dec. 19/95

ABSTRACT

The physical controls on the distribution of contaminants on the environmentally sensitive Sturgeon Bank tidal flat of the Fraser River delta is being studied to define the locations of erosion and deposition, and migration pathways of sediment and associated contaminants. Sediment erodibility was measured at 10 sites using an *in-situ* benthic annular flume called the Sea Carousel. At each site, InterOcean S4 current meters were also deployed for one month to determine current speed and direction, and suspended sediment concentrations were measured twice weekly for 2 months. Grain size analysis was performed on sediments collected from these 10 sites and an additional 56 sites. The 56 sites were also analyzed for major and minor element composition. Sea Carousel data reveal that sediments on the inner bank are not suspended by the current velocities measured at these stations due to surface cohesion in fine-grained material. Unlike the inner bank, sediments on the outer bank are suspended by wave-induced currents and in some cases tidal currents, especially in the fine sand-dominated sediments on the outer southern area of the bank. Eroded sediments from this area appear to be transported shoreward. Current meter data reveal that currents are variable both spatially and temporally on the bank. In general, flow is bidirectional with flooding currents on the outer bank (seaward) having higher average velocities. Currents on the inner bank (shoreward) show no consistent orientation of peak velocities. Suspended sediment data show an increase in concentration shoreward and a marked increase as wave height increases. Geochemical results reveal that surface sediments on Sturgeon Bank show very little contamination in Pb, Cu, Zn, Ni, Cr and V. The distribution of these elements on Sturgeon Bank is controlled primarily by sediment texture and physical controls on sediment transport. The coarse-grained nature and

relatively low clay content of sediments on the bank result in a decreased accumulation of minor elements. Cobalt concentrations are unusually high in some surface sediments, a result not explainable in the scope of this study. Results indicate that contaminated sediments known to have been deposited in the past on Sturgeon Bank due to sewage discharge are not present at the surface. This probably reflects more recent deposition of less contaminated sediments transported from the Fraser River distributaries and/or deposition of sediments resuspended from the outer bank which have been transported shoreward.

TABLE OF CONTENTS

LIST OF FIGURES

Page No.

ACKNOWLEDGEMENTS

I would like to express my sincere thanks to my supervisor, Dr. Paul LeBlond for never putting any pressure on me in one of the most difficult years of my life. Your words of wisdom and positive outlook were always appreciated. Dr. John Luternauer and the entire staff of the Cordilleran Division of the Geological Survey of Canada provided funding and many hours of discussion. Dr. Luternauer was a master of finding more things for me to think about. Dr. Carl Amos, from the Atlantic Geoscience Centre, provided the impetus for this study and was patient in all of the hundreds of phone conversation we had while I learned about sediment transport. Dr. Tom Pedersen and Dr. Steve Calvert taught me a great deal about a subject I was relatively unfamiliar with - geochemistry. Dr. Steve Pond graciously loaned me five S4 current metres and allowed me to deploy them in an area of high risk. If not for his rigorous testing, the data may never have been collected in such a difficult environment. A special thanks goes to the members of the Canadian Coast Guard hovercraft search and rescue unit who made sampling on the delta much more enjoyable; they were always cheerful, patient and their skill was greatly appreciated. Dr. Peter Mustard was always supportive, helpful and spent many hours with me reducing data and writing programs. I would like to thank the many people who volunteered to collect mud and water samples over the years of this study; despite the ride in the hovercraft, it was long and tedious work at times. Finally I would like to thank my friends and family, especially my sister, Heather, who put up with sections of my thesis strewn all over the apartment and my untidiness in those last few weeks, and Paul who always made me feel that I could do it.

Chapter 1. INTRODUCTION

1.1. THE PROBLEM WITH THE INTERTIDAL

The study of sediment dynamics in the marine environment locates areas of erosion, deposition, and pathways of sediment migration. This allows determination of the stability of the environment and the pathways of contaminants associated with these sediments. Intertidal zones are dynamic systems with physical processes such as waves, tides and river runoff contributing to their ever-changing morphology. To understand the sediment dynamics associated with the intertidal environment, a knowledge of the physical parameters and processes at work is required. Conventional field programs conducted on land or at sea must be redesigned for intertidal studies to maximize the quality of information. Data collection is difficult because access by boat is limited by shallow water and access by foot is limited by harsh environments. Instruments commonly used at sea are not designed for sampling while exposed to air, and instruments commonly used on land are not designed for sampling while inundated for several hours. Other unusual considerations include boundary conditions such as the shore and manmade structures, shifting tidal channels, tides, seasonal river discharge variations and many others. The presence of contaminants from natural and anthropogenic sources complicates the problem even more. The fate of these contaminants is further complicated by the influence from the mineralogy, grain size and organic content of the sediments and the physical processes which control their deposition. It is for these reasons that the grey area between the land and the sea known as the "intertidal" has often been avoided when research is undertaken.

The Fraser River in southwestern British Columbia, has historically been an important

transport route and fishery. The port city of Vancouver and the Lower Mainland, built both on and adjacent to the Fraser River delta, is the second largest city in Canada. The rapid expansion of Vancouver increases the impact from industry, agriculture, sewage, and channel confinement on the Fraser River. The importance of intertidal areas to fish and wildlife have only recently been recognized and, although not yet completely understood, studies are being actively pursued to determine the extent of human influence and the impacts which we have had on the organisms that use both the river and the intertidal as required habitats.

1.2. REGIONAL SETTING

The Fraser River is more than 1400 km in length, drains an area of approximately 230,000 km^2 and enters the ocean in southern British Columbia adjacent to the city of Vancouver, Canada. In its upper reaches, the Fraser River drops 1 km in elevation in 100 km, but over the next 900 km, to the town of Hope, it levels out to more moderate gradients (Milliman, 1980). Downstream from Hope, the river becomes more mature, passing through alluvial flood plains for 200 km until it reaches its terminus at the Strait of Georgia, forming the Fraser River delta. At New Westminster, approximately 25 km upstream from the mouth, the river bifurcates into the North Arm and the Main Arm (Figure 1). The North Arm, which carries ~16% of the total river discharge, bifurcates again at Richmond where ~30% of the flow (~5% of the total Fraser River flow) exits via the Middle Arm while the remaining 70% (9% of the total Fraser River flow) exits via the North Arm (Luternauer and Murray, 1973). The Fraser River distributary channels flow through an active deltaic system which includes marshes, intertidal sand and mud flats, and foreslope sediments. Two large intertidal flats, Roberts and Sturgeon Bank, lie on the

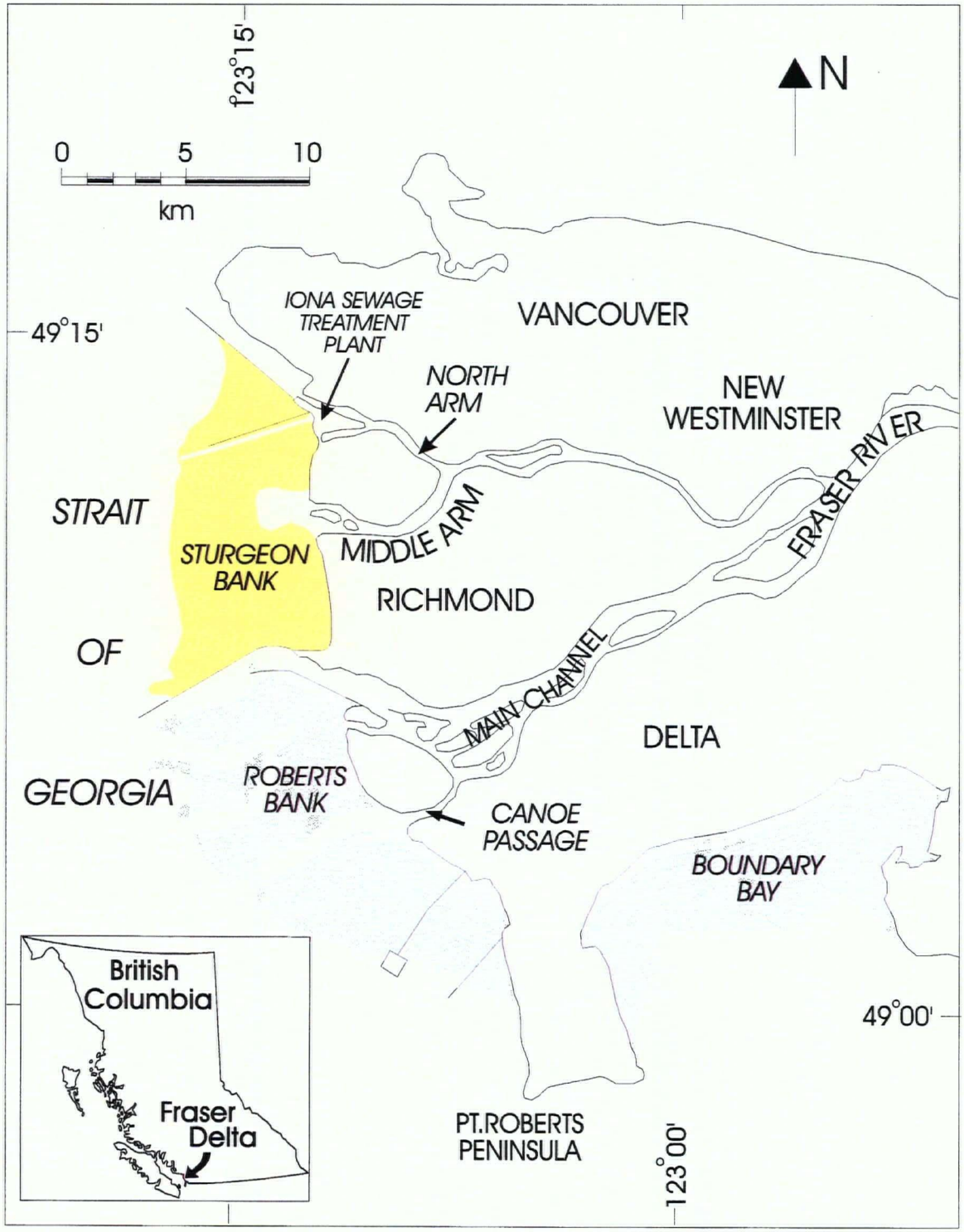

Figure 1: The Fraser River delta, British Columbia.
Colored section outlines Sturgeon Bank study area.

deltas western edge (Figure 1).

The mean discharge of the Fraser River (measured at Hope) is 3,400 m^3/s (McLean and Church, 1986); however flows in the late spring and early summer due to snowmelt average up to 10,000 m^3/s (McLean and Church, 1986; Milliman, 1980), and flows in the late fall to early spring average 1500 m^3/s (Milliman, 1980).

The Fraser transports an average of 20 X 10^6 m^3 of sediment annually with 80% of the sediment load being discharged in the spring freshet. It has been presumed that only 3-9% of the total sediment load in the Fraser River enters the North Arm (Church et al., 1990). The sediment load consists primarily of very coarse silt and sand with an average of 35% of the suspended sediment transported comprising sand (McLean and Tassone, 1991). The high sand content is probably related to the coarse nature of the Pleistocene glacial deposits which form a major Fraser River sediment source (Pharo, 1972; Armstrong, 1956), the seasonality of the river flow and the fact that the river is not dammed at any point. Mathews and Shepard (1962) reported that the delta in the region of the Main Arm advances at a rate of ~2.3 m per year at the low water mark. However, recent bathymetric measurements suggest that the slope off Sturgeon Bank is stable, whereas the southernmost portion of Roberts Bank is retreating (Luternauer and Murray, 1973; Luternauer, 1975).

The Fraser River delta is Holocene in age, formed since the end of the last glaciation 11,000 - 13,000 years BP (Clague et al., 1983) and is 975 km^2 in area (Mathews and Shepard, 1962). The delta deposits, which overlie late Pleistocene till, have an average thickness of 110 m (Johnston, 1921; Mathews and Shepard, 1962).

Tides in the Strait of Georgia are mixed semi-diurnal with mean tidal ranges over the

delta slope of 2.7 m and over the tidal flats 2.6 m (Canadian Hydrographic Service, 1972; Thomson, 1977). The average range for spring tides over the seaward edge of the delta is 4.7 m, however extreme tides can reach 5.4 m (Canadian Hydrographic Service, 1972). Maximum significant wave heights in the Strait of Georgia are approximately 1.5 m and average heights are approximately 0.6 m (Hoos and Packman, 1974). Based on these values, the most probable maximum waves reaching the delta foreshore would be 2.9 m (Thomson, 1977). During periods of low river discharge and spring tides mixing is enhanced and the estuary is classified as moderately stratified (Hodgins et al., 1977). During high river discharges, mixing is restricted and the estuary is classified as a salt-wedge system (Kostaschuk et al., 1989).

Waves generated by wind from the NW have the longest fetch (>100 km) and therefore presumably are the largest; contributing the most to wave-related processes on the delta-front. Wind waves breaking tangentially to the delta slope and breaking internal gravity waves may contribute to longshore drift of sediment and suspended material along the delta-front with flows reaching 50 cm/s (Thomson, 1975). Surface currents over the foreslope flow northward at 0.3-0.5 m/s (Tabata et al., 1971) and a general northward flow of fresh turbid water from the Main Arm across Sturgeon Bank has been observed (Tabata, 1972). Medley (1978) suggests that waves do not break on the flats but dissipate their energy across the bank.

1.3. STURGEON BANK STUDY AREA

Sturgeon Bank is situated on the western edge of the Fraser River delta between the Main Arm and the North Arm of the Fraser River (Figure 1). It is an intertidal sand and mudflat approximately 83 km^2 in area. Sturgeon Bank is 6 km wide on average and slopes gently

westwards towards the Strait of Georgia at an angle of 0.08°. The southern portion of Surgeon Bank is complicated by the presence of active drainage channels draining the adjacent marsh. A detailed bathymetric map of the area was constructed using a Global Positioning System (GPS) survey which employed two geodetic quality GPS receivers. Contours of Sturgeon Bank elevations were developed (Figure 2) using the Geographical Information System (GIS) Arc/Info program and a three-dimensional perspective was created using the contours (Figure 3). Details of the GPS survey can be found in Aitken and Feeney (1994) and Feeney (1994) and a general description of the survey is provided in Appendix I.

The tidal flats are bioturbated and pelletized which is the result of a diverse invertebrate infauna dominated by polychaete worms (Manayunkia aestuaria, Amphicteis sp., Eteone longa, Pygospio elegans, Capitella capitata, hemipodus borealis), bivalves (Macoma balthica, Macoma inconspicua, Mya arenaria, Cryptomya californica), amphipods (Corophium salmonis, Amphithoe humeralis), isopods (Gnorimosphaeroma lutra and Argeia pugettensis) and decapods (Callianassa californiensis), plus oligochaeta, nematode worms and harpacticoid copepods (B.C. Research, 1977; Bawden et al, 1973; Otte and Levings, 1975; Levings et al., 1983; Harrison, 1981). In addition, twenty-seven species of fish, including commercial species such as salmon, have been reported on Sturgeon Bank (Birtwell et al., 1983).

The shoreline of Sturgeon Bank is bordered by a marsh, 3.5 m above chart datum, composed primarily of sedges (Carex sp.) and bulrushes (Scirpus sp.) (B.C. Research, 1975). Benthic macrophytes include Ulva lactuca and Entomoropha sp. and their abundance suggests an increased nutrient concentration (Hoos and Packman, 1974). Benthic microalgae (primarily diatoms) on top of the sediment or within the first centimetre suggests that benthic primary

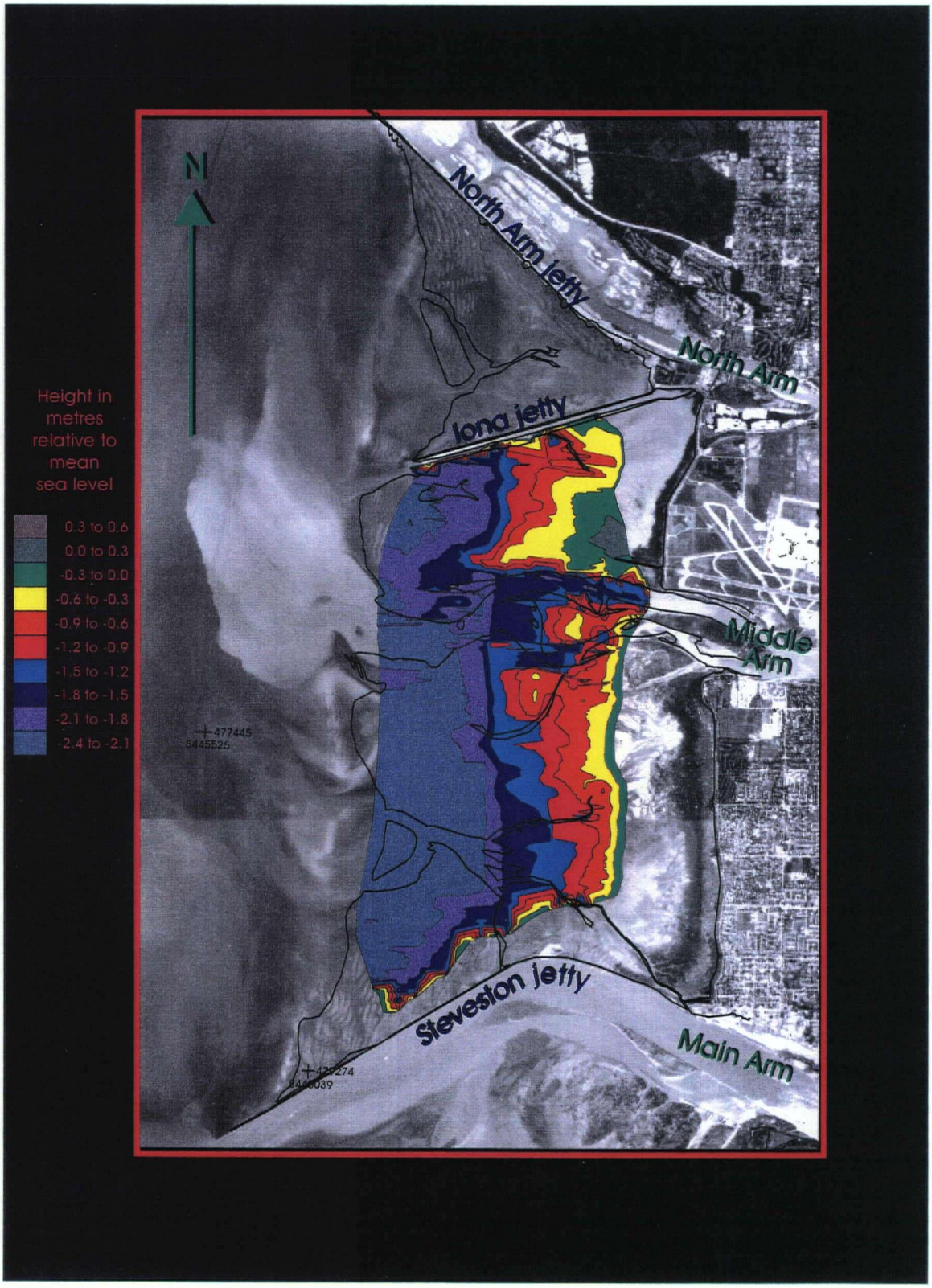

Figure 2: Elevation map of Sturgeon Bank generated from GPS kinematic survey

Figure 3: Three-dimensional perspective of Sturgeon Bank generated from GPS survey

productivity is considerable based on estimates of chlorophyll a concentrations (Harrison, 1981).

The Sturgeon Bank region has been severely altered by the construction of jetties, the disposal of dredge spoil on the inner flats and the disposal of primary treated sewage effluent from the Iona sewage treatment plant (Figure 4). Jetty construction included the Steveston jetty, North Arm jetty, Iona jetty, and the airport jetty. Prior to 1959, the McDonald Arm of the Fraser River was permitted to discharge onto Sturgeon Bank (similar to the Middle Arm); however at that time, a causeway which blocked this confluence was built to allow access to Iona Island. In addition, the bank has been altered by high metal values which have been observed in both sediments (Benedict et al., 1973; Hall and Fletcher, 1974; Hall et al., 1974) and benthic organisms (Parsons et al., 1973; Bawden et al., 1973) due to the discharge of metal-rich sewage on Sturgeon Bank (Hall et al., 1975).

1.4. SEWAGE EFFLUENT DISCHARGE HISTORY

The Iona sewage treatment plant, began operation in 1962 and underwent three expansions prior to 1985. Prior to its opening, a jetty 4.5 km in length was constructed on Sturgeon Bank, spanning almost the entire width of the intertidal area. The jetty was built to control the flow of effluent discharged from the plant to ensure that it did not end up on populated beach areas nearby. From 1962 until 1988 storm and sanitary sewage effluent from the Iona Sewage Treatment Plant was discharged into a shallow dredged channel which ran parallel to the Iona jetty on its south side (Coastline Environmental Services Ltd., 1985). The effluent discharged at this time varied from 376.4 x 10^3 m^3/day for average flows between May and October, and 581.4 x 10^3 m^3/day for winter months (Coastline Environmental Services Ltd.,

1985). Effluent flow rates of less than 942 x 10^3 m^3/day were given primary treatment (i.e. screening, grit, scum and grease removal, sedimentation, and chlorination from May 1 to September 30 to reduce bacterial coliform counts during the summer) (Rawn et al., 1953; S&S Consultants, 1983) but flows exceeding this level received little or no treatment (Birtwell et al., 1983).

During low tide, the effluent flowed seaward in the channel for almost 7 km. However, during high tide, the channel was essentially ineffective at moving the effluent off the bank and it was dispersed over inner Sturgeon Bank resulting in rapid environmental degradation of the area. The effects of deposition of this sewage-laden particulate matter onto Sturgeon Bank included elevated levels of heavy metals, total organic carbon (TOC), coliform bacteria, and sediment oxygen demand which resulted in numerous fish kills in the area (Birtwell et al., 1983) and impacts on the benthic communities adjacent to the outfall (B.C. Research, 1973, 1975, 1977; McGreer, 1982). In response to this problem a deep-water outfall extension was constructed in 1987 which extended from the end of the existing jetty into the Strait of Georgia, where effluent is now discharged through a diffuser at 107 metres depth on the delta slope. During severe rainstorms overflow effluent is still discharged through the original pipe onto Sturgeon Bank, but this rarely occurs more than once or twice per year (Iona Sewage Treatment Plant operator, pers. comm., 1993).

Sewage releases heavy metals such as mercury, cadmium and vanadium (Hall et al., 1974) which can be adsorbed onto sediments and may accumulate in organisms (Parsons et al., 1973). Additional potential pollutants are those discharged from the Fraser River system that may be transported to the tidal flats, including industrial, agricultural and urban runoff.

Upon installation of the deep outfall pipe, the Department of Fisheries and Oceans began monitoring the recovery of the area, but had many concerns about the final deposition sites of the contaminated sediments. It was believed that burial of the sediments by recent sedimentation would eventually lead to their withdrawal from the environment. Erosion of these sediments could mean their complete removal, but also could result in resuspension increasing the risk of entrance into the biological food chain, or transport of the contaminated sediments to other important habitats. The need to address these issues provided the impetus for this study.

1.5. PROJECT OVERVIEW

Sediments form important habitats for organisms. They are also often either a temporary or permanent sink for metals. Both natural and anthropogenic controls allow metals to accumulate to high levels in some sediments, thus increasing the possibility that they may become incorporated into the biota. Although aquatic organisms require certain trace metals to metabolize, when these metals, and others not used in the metabolic process, are available in excess they may exert toxic effects.

Although determining the fate of contaminated sediments on Sturgeon Bank is critical, the processes which control sediment transport are practically unstudied. The main objective of this study was to determine the major processes controlling sediment transport on Sturgeon Bank and relate these processes to the fate of contaminants deposited within them. These objectives were carried out by conducting several analyses: 1) In order to determine the erosional processes sediment erodibility was determined *in situ* using a benthic field flume; 2) the physical oceanographic processes were determined using *in situ* measurements of currents; 3) the

suspended sediment processes were determined using *in situ* measurements of suspended sediment concentration; 4) the sediment textural properties were determined by measuring grain size and sorting; 5) the sediment geochemical properties were determined by measuring the major/minor element concentration and organic content permitting the examination of the areal extent of contaminant dispersal on Sturgeon Bank.

This study employed innovative data collection techniques in non-traditional sampling environments. Although work on *in situ* sediment erodibility measurements have been done, these studies are not common and, until now have never been attempted on the Fraser delta. *In situ* current velocity and directional information and suspended sediment concentration measurements have never been collected on Sturgeon Bank and GPS kinematic surveys to determine intertidal bathymetry have only recently been attempted and never on the Fraser delta. These studies constitute important baseline information that may now be used in future studies.

Sample sites were chosen using the air-photo based sediment classification of Medley and Luternauer (1976) (Figure 4). Ten primary stations were used in this study, occupying 3 transects. The density of stations was highest adjacent to the Iona jetty where 6 stations were selected (S1, S2, S3, S4, S5, and S6). Three stations running parallel to the Steveston jetty were chosen (S11, S12, and S13) and one station adjacent to the Middle Arm was selected (S14). An additional 56 stations on Sturgeon Bank were chosen, including stations north of the Iona jetty, for grain size/sorting measurements and major/minor element analyses. These sites were sampled to provide an areal distribution of grain size, sorting, and contaminant concentrations over the entire area of Sturgeon Bank. The grain size and erodibility results measured at the 10 primary sites were believed to be representative of the results at sites elsewhere on the bank with

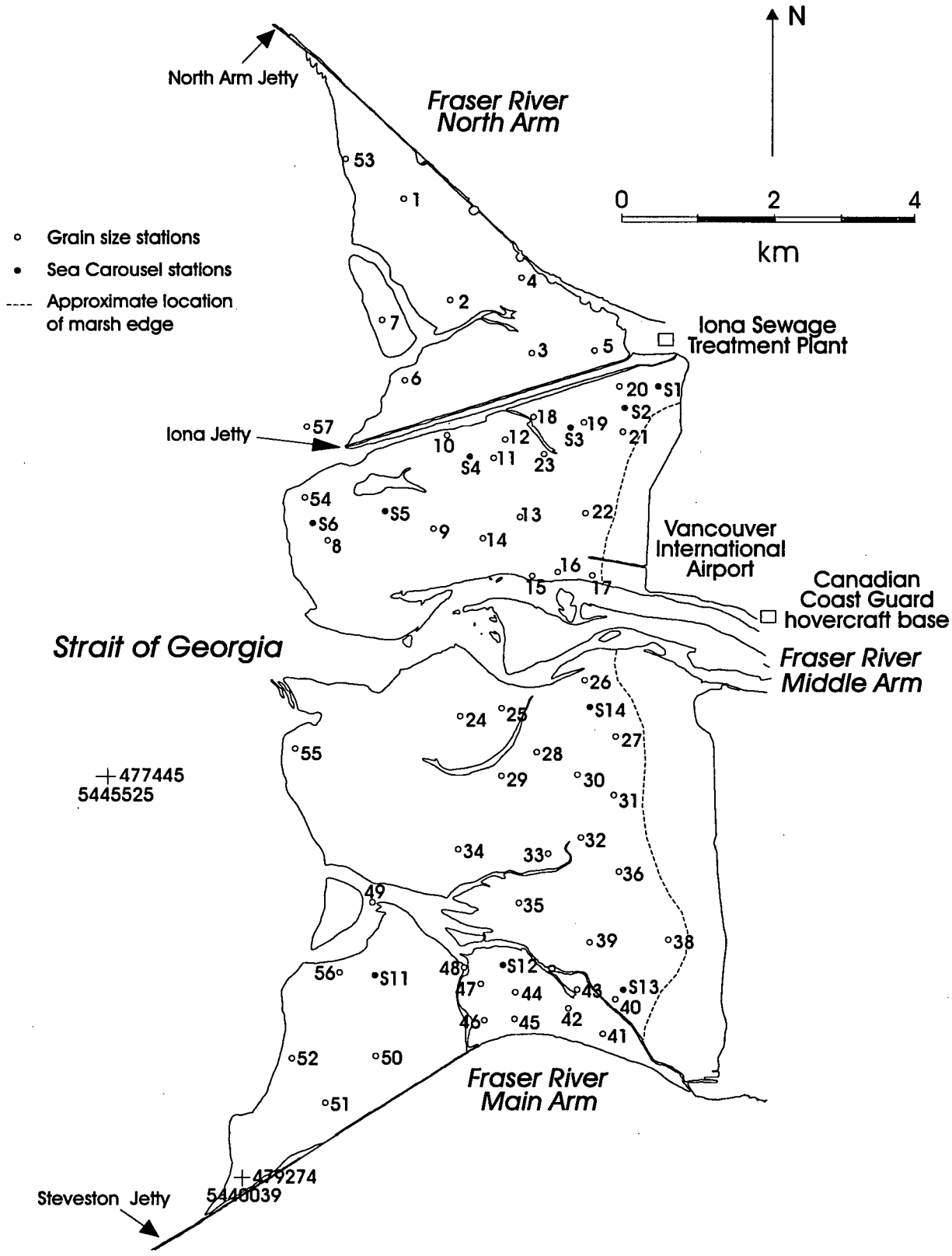

Figure 4: Sturgeon Bank study area and station locations

similar sediment characteristics. However, this was not the case as the variability in measured parameters between stations was large and therefore extrapolation was not realistic, thus not attempted. Results of data collected from the area north of the Iona jetty have been included for reference purposes, however, the focus of this study is centred around the area of Sturgeon Bank between the Iona and Steveston jetties and more specifically the 10 primary stations. Major and minor element concentrations were not determined on sediments collected from the Sea Carousel stations due to an inadequate supply of sediment sampled. Due to the vast amount of data collection required to understand the physical processes and sediment properties of the marsh area on Sturgeon Bank, an independent study would be needed. Therefore the marsh area was not sampled in this study. It is important to note, however, that the marsh may play a significant role in the accumulation of contaminants on Sturgeon Bank.

For ease in interpretation, the bank has been divided into three zones in this study, namely northern Sturgeon Bank between the North Arm and Iona jetties, central Sturgeon Bank between Iona jetty and the Middle Arm of the Fraser River, and southern Sturgeon Bank between the Middle Arm and the Steveston jetty. Geographical station locations are listed in Appendix II. Conditions at stations varied from rippled sand to thick mud, the latter making the occupation of some sites impossible by traditional methods. Because of the difficulty in accessing such a large area during successive high tides or low tides and unstable sediment conditions at some stations, a Canadian Coast Guard hovercraft was employed as a sampling vehicle. The hovercraft's manoeuvrability on both land and water allowed access to sampling stations at any time during the tidal cycle quickly and easily. Data collection began in July, 1992 with the majority of sampling occurring in May and June, 1993.

Chapter 2. SEDIMENT ERODIBILITY

2.1. THE SEA CAROUSEL AND FIELD SAMPLING

An instrument known as the Sea Carousel was deployed at 10 stations on Sturgeon Bank to determine sediment response to currents. The instrument is an annular benthic field flume designed for use in intertidal and sub-tidal settings. The Sea Carousel comprises an annulus, 2 metres in diameter, 0.3 metres high, and 0.15 metres wide, within which flow is induced; an underwater pod containing controllers and battery power for electronic sensors; and a ship-board monitor, computer and power supply. The output voltages from all sensors were digitized and transformed to scientific units on a Campbell Scientific CR10 data logger and stored on a Campbell Scientific SM 192 storage module. The data logger is programmed from the surface using the computer through an RS232 interface. A more detailed description of the Sea Carousel is given in Amos et al. (1992a).

A flow is set up via the computer by rotating a mobile lid equipped with 8 paddles within the annulus. The flow is increased at 10 minute intervals up to an azimuthal velocity of 1.0 m/s (Amos et al., 1992b). Vertical and azimuthal current speed is recorded by a Marsh McBirney current meter located in the annulus at a height of 0.25 metres above the bed. Three Optical Backscatter Sensors (OBS) located in the annulus measure the amount of sediment in suspension at each induced current velocity. Two of the sensors are located on the inner wall of the annulus at heights of 0.07 and 0.22 m above the base of the annulus (the seabed), hereby referred to as the lower and upper OBS. The third OBS is located outside the annulus to detect ambient particle concentration. A video camera monitors the seabed through a window in the flume wall.

A horizontal skirt situated 0.04 metres above the base of the annulus ensures a standardized penetration of the flume into the seabed. The OBS's give a linear response to particle concentration for mud and sand over a range in concentrations of 0.1 to 50 g/l (Downing and Beach, 1989). The OBS's are calibrated by analyzing water samples pumped from the annulus through a sampling port 0.2 metres above the skirt for suspended sediment concentration (SSC).

The physical properties of the sediment are expected to vary across the tidal flats due to differences in grain size, relative exposure (Anderson and Howell, 1984), and biological influences (Amos et al., 1988; Underwood and Paterson, 1993). The biological influences include benthic diatoms (Grant et al., 1986; Paterson, 1989; Paterson et al., 1990), vegetation, animal tracking, pelletization and bioturbation (Nowell et al., 1981; Jumars et al., 1981).

The Sea Carousel was towed to stations S1 through S14 (See Figure 4) at high tide on a floating pontoon and the instrument lowered to the seafloor slowly to ensure minimal water and seabed disturbance. This allowed the measurements of the natural, saturated substrate erosional properties *in situ*. Each station was occupied between July 18 and July 28, 1992. For a detailed description of the study and its results refer to Amos et al. (in prep).

2.2. DATA REDUCTION

A time series plot of the vertical and azimuthal current velocities, the three measures of suspended sediment concentration and the erosion rate were generated after time-averaging (20 second) and despiking the data between 2 standard deviations of the 20 second mean values (Amos et al., in prep.). Erodibility was interpreted from the rate of change in SSC detected in the annulus with time throughout each deployment (Amos et al., 1992b) The total suspended

mass was determined as the product of mass concentration per unit volume of the annulus (0.216 m^3). The eroded depth (mm) was determined by dividing the total suspended mass times the annulus volume by the sediment bulk density dry weight (determined from samples collected when the bank was exposed) times the annulus area. It was assumed that the depth of erosion was equal over the area of the flume. Erosion rates ($kg/m^2/s$) were determined from the change in suspended mass per unit time divided by the area of the annulus ($0.873m^2$). The bed shear stress was determined from a transform of the azimuthal flow using the following equation $\tau_0 = \tau_{C0}(10^{-0.000176(SSC)})^2$ (Amos et al., in prep) which takes into account the bed shear stress reduction due to suspended sediment concentration (Amos et al., 1992a) where τ_{C0} = the clear water bed shear stress = ρu^{*2}, ρ is the density of the overlying water (~1015 kg/m^3), SSC is the suspended sediment concentrations, and u^* is the induced friction velocity.

The cohesive strengths of the sediments at stations 1, 2, 3, 13, and 14 were determined through examination of bivariate plots of effective stress (transform from eroded depth explained below) and applied bed shear stress. The surface intercepts of these plots yield the surface cohesion or the surface critical shear stress for erosion (τ_c). This is defined as the maximum shear stress that a sediment can withstand before failure occurs (Brown et al., 1989). The linear failure envelope of the sediment profile is proportional to the internal friction angle (ϕ) of the sediment, calculated by transforming depth into effective stress $\sigma' = \gamma z - P = 1.0z$ (where γ is the unit bulk weight of the sediment, z is the depth in mm and P is the excess pore pressure, assumed to be zero). Then $\phi = \tan\text{-}1(\Delta\tau/\Delta\sigma')$, where the higher the value of ϕ, the more resistant the bed is to erosion. The type of erosion (Type I or Type II) was determined from the trends in erosion rate through each 10 minute velocity increment. Type I shows an asymptotic

decrease in erosion rate while Type II erosion shows continuous erosion rate through time.

The surface critical shear stress for erosion for stations 4, 5, 6, 11, and 12 could not be determined using this method because grain size composition at these stations consisted of fine to medium sands. Sandy sediments do not possess cohesive strength and therefore behave differently than cohesive sediments under applied stress. Cohesive sediments are lifted as clumps or flocs and non-cohesive sediments are lifted as individual grains. For this reason the bivariate scatter plot of applied bed stress to SSC was examined to determine the shear stress at which sediments were suspended for the sandy sediments. The migration of sand through ripples resulted in scattered sediment concentrations recorded from the lower OBS. The upper OBS results were used to determine the onset of sediment erosion because results were significantly less variable as only the suspended sediment load and not the bed load was measured. Because sands move through traction, saltation and suspension, the time series of erosion rates and the bivariate scatter plot of eroded depth versus applied shear stress were not plotted. The reason for this is that no mean sediment depth could be determined because of the movement of sand as ripples rather than bed erosion and transport. Determining the rate of bedload transport is a difficult task and has not been undertaken in this study. For the fine sands on Sturgeon Bank we will assume that bed load transport is minor relative to suspended load transport; however, for medium sands this assumption cannot be made so easily. This is because fine sands behave somewhat like silts in that they do not go through a bedload stage (Brown et al., 1989).

Velocity measurements at the seabed are extremely difficult to obtain because instruments deployed close to the bed become obstacles and consequently interfere with the flow and sediment dynamics. Therefore instruments are deployed at some measured distance above the

seabed. The critical shear stress at the bed can be converted to a critical shear velocity at the bed and subsequently converted into an equivalent velocity at any height above the bed. This is true because the velocity profile in the turbulent layer decreases logarithmically towards the bed due to friction (Brown et al., 1989). The conversion of the surface critical bed shear stress for erosion to current velocities at a height of 50 cm above the bed was determined using the equation for the Law of the Wall or von Karman-Prandtl equation: $u_y=(u^*/\kappa)\ln(y/y_0)$, where u_y is the current velocity at a height y above the bed, κ is the von Karman constant with a value of 0.4, y is the height above the bed in metres, y_0 is Nikuradse's roughness length which for transitional and rough turbulent flow conditions is equal to d/30 where d is the diameter of the flocs or height of the bed ripples, and u^* is the friction velocity which, at the bed, is equal to $(\tau_c/\rho)^{0.5}$ (Dyer, 1986) where τ_c is the critical shear stress for erosion and ρ is the density of the overlying water column. The flow roughness is determined through the flow Reynolds number and in all cases on the bank the erosion process began under turbulent transitional flows.

Suspended sediment transport rates ($kg/m^2/s$) were determined by multiplying the current velocity and the suspended sediment concentration. The transport rate was then plotted against applied shear stress and an equation relating the transport rate to both the applied shear stress and the equivalent current velocity at 50 cm from the bed were determined.

2.3. RESULTS AND DISCUSSION

The calibration of the two internal OBS sensors yielded linear and consistent results between stations following the functions: SSC(upper) = 4.11(OBS-upper) - 115 (r^2=0.89) and SSC(lower) = 3.18(OBS-lower) - 32 (r^2=0.88) (Amos et al., in prep).

2.3.1. COHESIVE SEDIMENTS

2.3.1.1. *Erosion rates*

A time series plot of the vertical and azimuthal current velocities, the three measures of suspended sediment concentration and the erosion rate for stations S1, S2, S3, S13, and S14 are plotted in Appendix III. It is evident that Type I erosion dominates the initial stages of bed erosion with erosion rates peaking sharply within 30 seconds of flow increase and then decreasing exponentially to zero within 5 minutes (Amos et al., in prep). Two erosion types are evident when referring to Type I erosion behavior. Type IA erosion is observed on the video camera and described as the removal of loose floccules, pellets and organic aggregates found on the sediment surface, probably ephemeral deposits from slack water tidal deposition. Erosion of Type IA was observed only at stations S2, S3 and S14 (Appendix III) with values of 0.0003, 0.0011and 0.0026 $kg/m^2/s$, respectively. Type IB erosion is described as the erosion of a consolidated seabed possessing a yield strength so the critical shear stress for erosion is measurable. Type IB erosion dominated the non-cohesive sediments on Sturgeon Bank (Appendix III). Erosion rates for Type IB erosion at stations S1, S2, and S14 are similar with values of 0.0018, 0.00125 and 0.00133 ($\pm$ 0.0005) $kg/m^2/s$, respectively. Stations S3 and S13 show Type IB erosion rates significantly lower with values of 0.00032 and 0.00024 ($\pm$0.00005) $kg/m^2/s$, respectively. Type II erosion dominates the latter stages of bed erosion with no significant peak in erosion rate being detected but a continuous erosion rate through time. Type II erosion was only observed at stations S1, S2, and S3 (Appendix III) with peak erosion rates of 0.00067, 0.000155 and 0.0004 ($\pm$0.00005) $kg/m^2/s$, respectively. The transition from Type IB to Type II erosion occurred in all cases at current speeds of 0.7 - 0.9 m/s.

2.3.1.2. *Erosion thresholds*

The surface critical shear stresses for erosion at stations S1, S2, S3, S13, and S14 are 1.6, 2.2, 2.0, 1.0, and 1.5 Pa, respectively. These values correspond to friction velocities at the bed of 4.0 4.7, 4.4, 3.1, and 3.8 cm/s. In order to obtain these critical shear velocities at the bed and initiate bed erosion, velocities at a height 50 cm above the bed would need to be 73, 86, 80, 57, and 69 cm/s, for stations S1, S2, S3, S13, and S14, respectively. That is, currents of this speed are required at a height of 50 cm from the seabed before erosion at the bed may occur.

Erosion thresholds measured at depth in the sediments vary considerably but generally follow an increase in sediment strength with depth. Station S1 has a weak layer at depth between 0.3 and 0.5 mm in the sediments which is evident by the negative friction angle indicating a decrease in bed strength with depth (Figure 5). At depths greater than 0.5 mm the sediment strength increases twice with corresponding positive friction angles of 73° and 85°. Station S2 behaves similarly to station S1 with a weak sediment layer between 0.05 and 0.25 mm in the sediments as shown by the negative friction angle (Figure 6). At depths below this the sediment strength increases with depth with a friction angle of 65°. Despite the high surface cohesion values at stations S1 and S2, the concentration of sediment suspended during the experiment is significantly higher than all of the other stations. This may, in large part, be due to the weak sediment layer present with depth at both stations.

Station S3 has a surface critical shear stress for erosion similar to station S2, however, no weak layer is observed in the sediments at this station. The increase in sediment strength with depth following a high friction angle of 87° results in a depth of erosion of 0.3mm over the entire sampling time (Figure 7), significantly lower than the depth of 1.2 mm recorded at stations S1

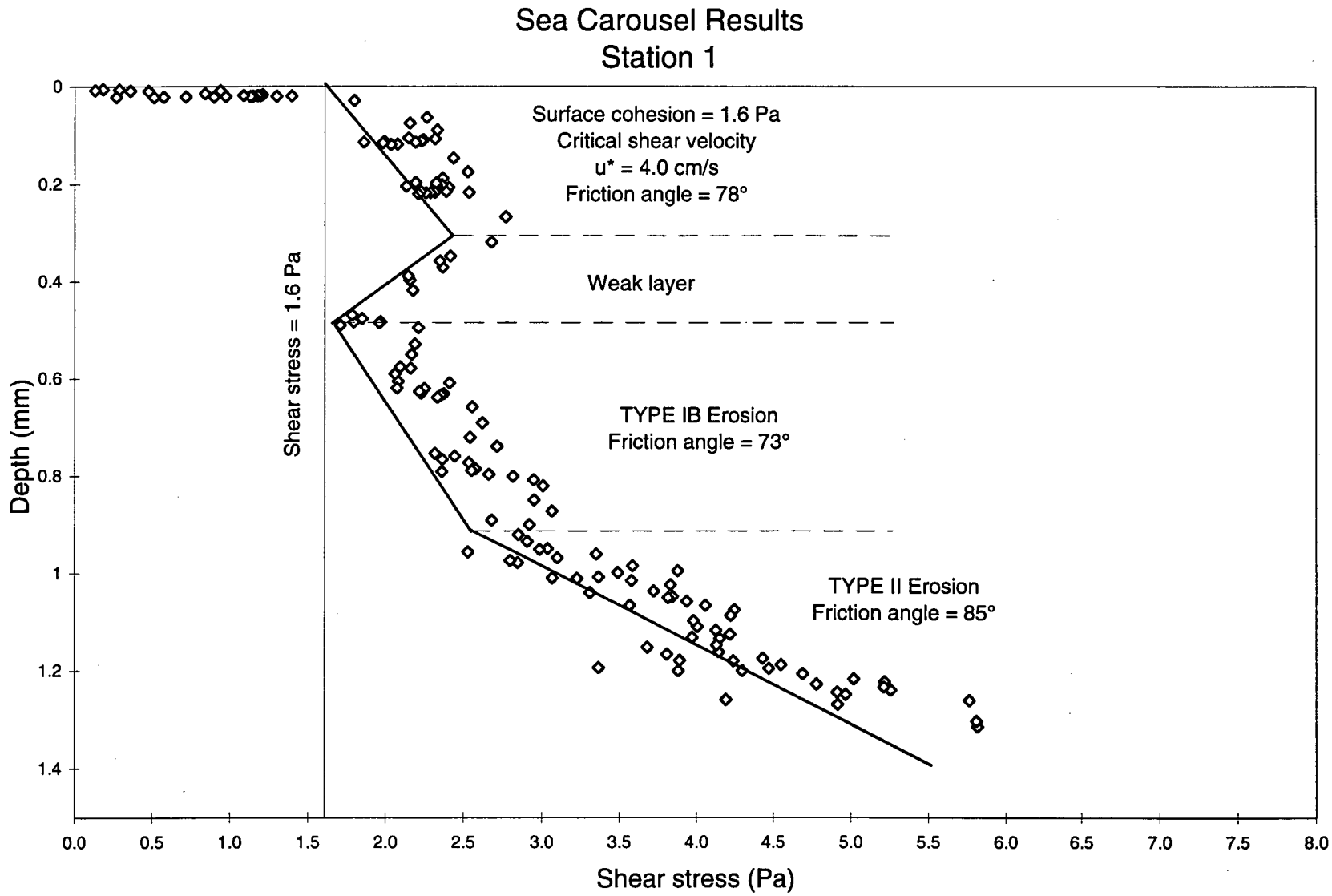

Figure 5: Sediment strength with depth at station 1

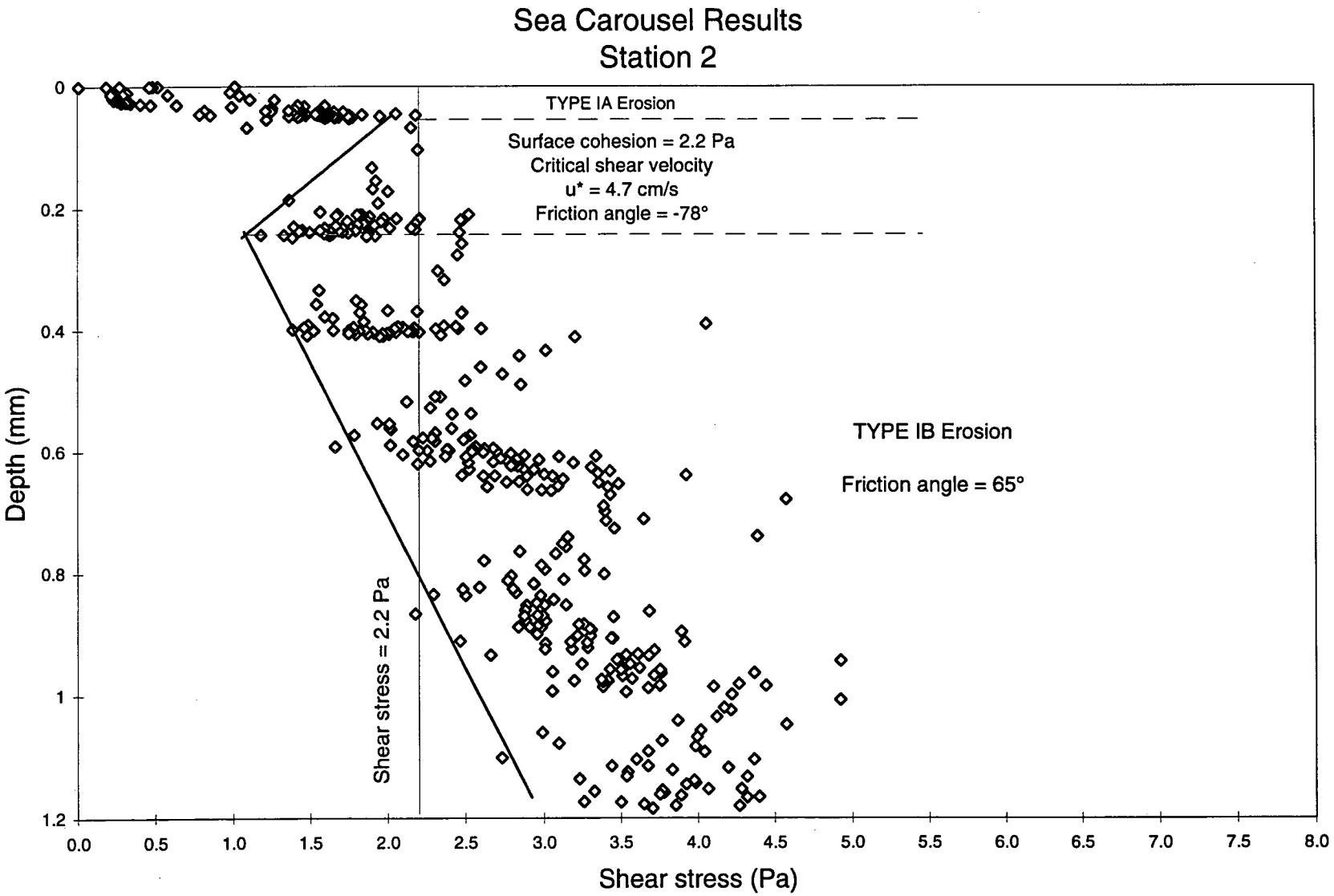

Figure 6: Sediment strength with depth at station 2

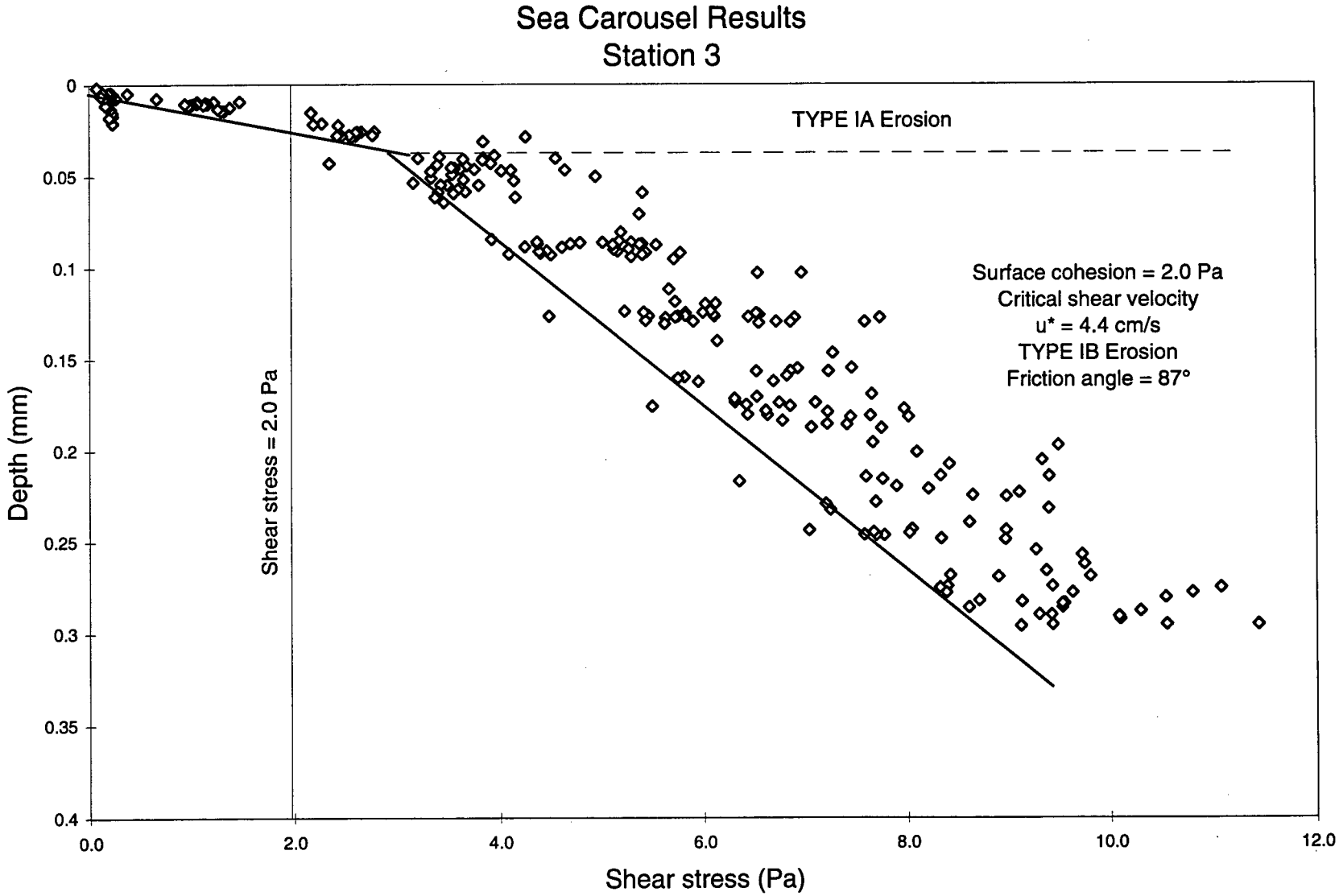

Figure 7: Sediment strength with depth at station 3

and S2 over the same time interval.

Station S13 behaves similarly to station S3 with an eroded depth of only 0.11 mm over the sampling time interval. The sediment strength increases with depth twice with corresponding friction angles of 89° and 87° with no reversals indicative of weak layers (Figure 8). The sediment behavior with depth at station S14 is unlike any other station in that the eroded depth seems to decrease with increasing applied shear stress. This behaviour can not be explained, however the increase in sediment strength with depth follows an approximate friction angle of 69° (Figure 9).

2.3.2. NON-COHESIVE SEDIMENTS

A time series plot of the vertical and azimuthal current velocities and the three measures of suspended sediment concentration for stations S4, S5, S6, S11, and S12 are plotted in Appendix III. Sandy sediments do not exhibit Type I and Type II erosion as bed failure in non-cohesive sediments is not the same as cohesive sediments. Non-cohesive sediments lack the physio-chemical interactions that exist between clay particles and therefore are free to move independently.

The surface critical shear stress for erosion at stations S4, S5, S6, S11, and S12 were determined using the suspended sediment concentration versus the applied bed shear stress plot and are ~0.9, 1.25 1.2, 0.0?, and 0.4 Pa, respectively (Figures 10, 11, 12, 13, and 14). These values correspond to friction velocities at the bed of ~3.0, 3.5, 3.4, 0.0, and 2.0 cm/s for stations S4, S5, S6, S11, and S12, respectively and current velocities at 50 cm above the bed of ~49, 58, 56, 0, and 33 cm/s, respectively in order to initiate sediment suspension.

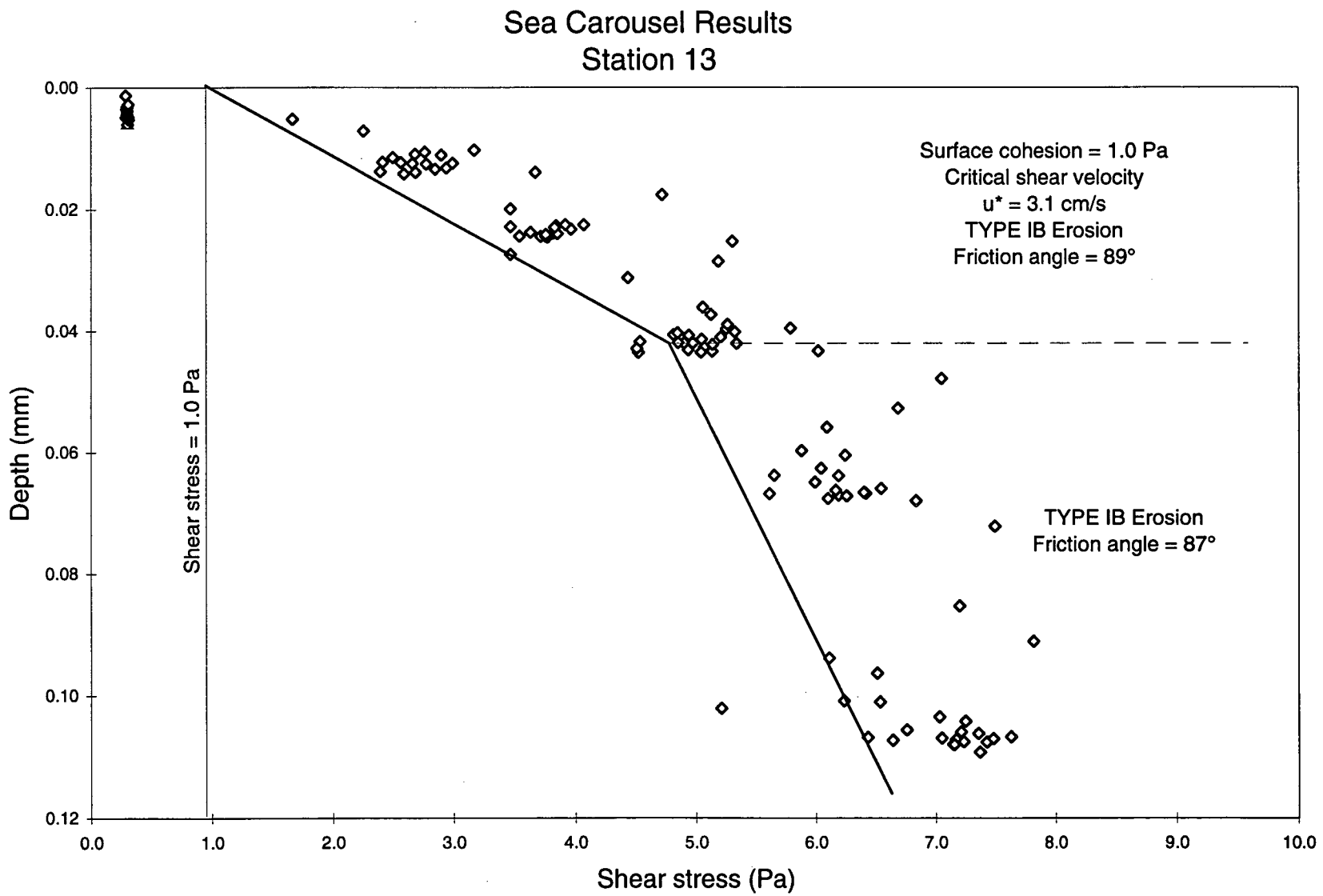

Figure 8: Sediment strength with depth at station 13

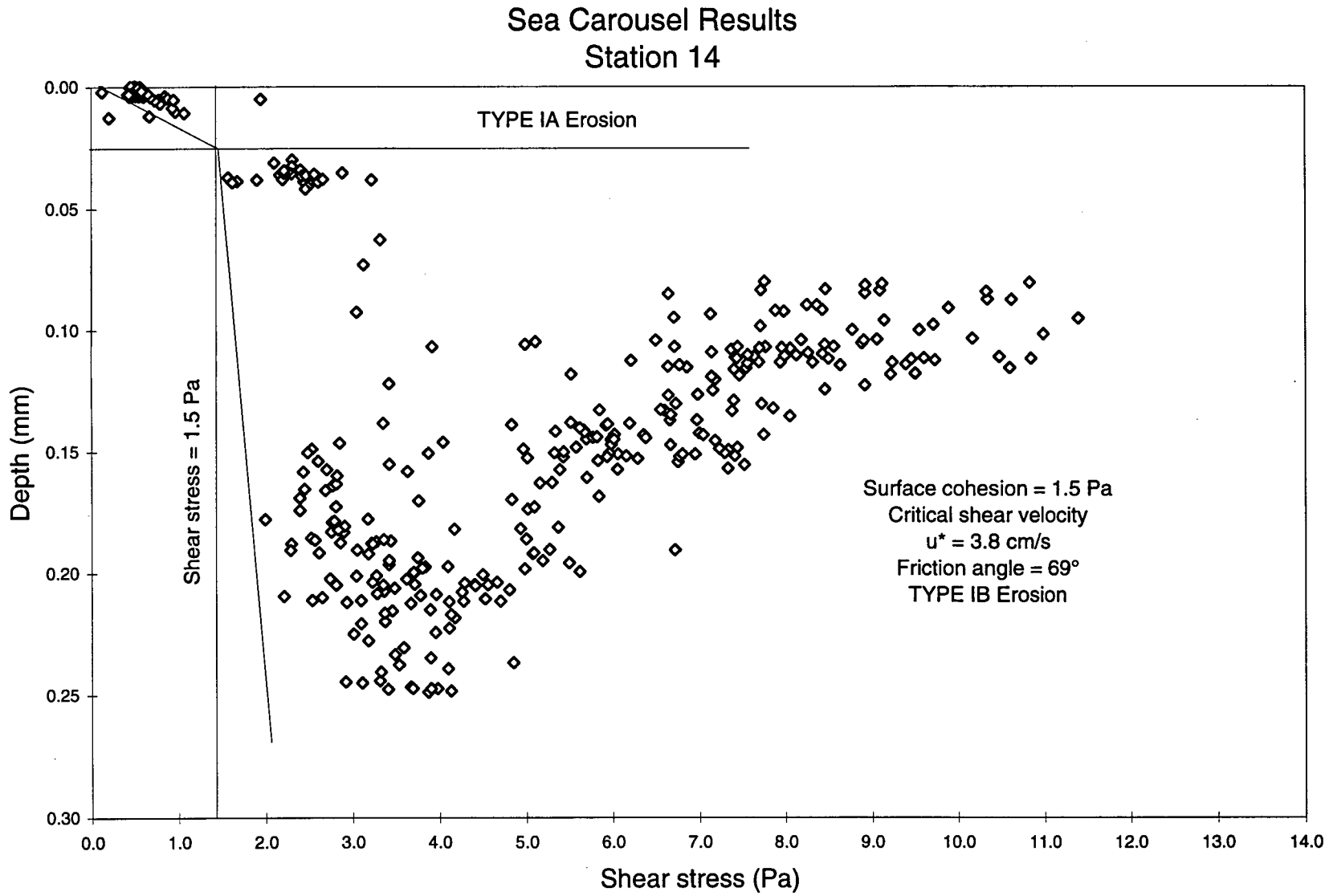

Figure 9: Sediment strength with depth at station 14

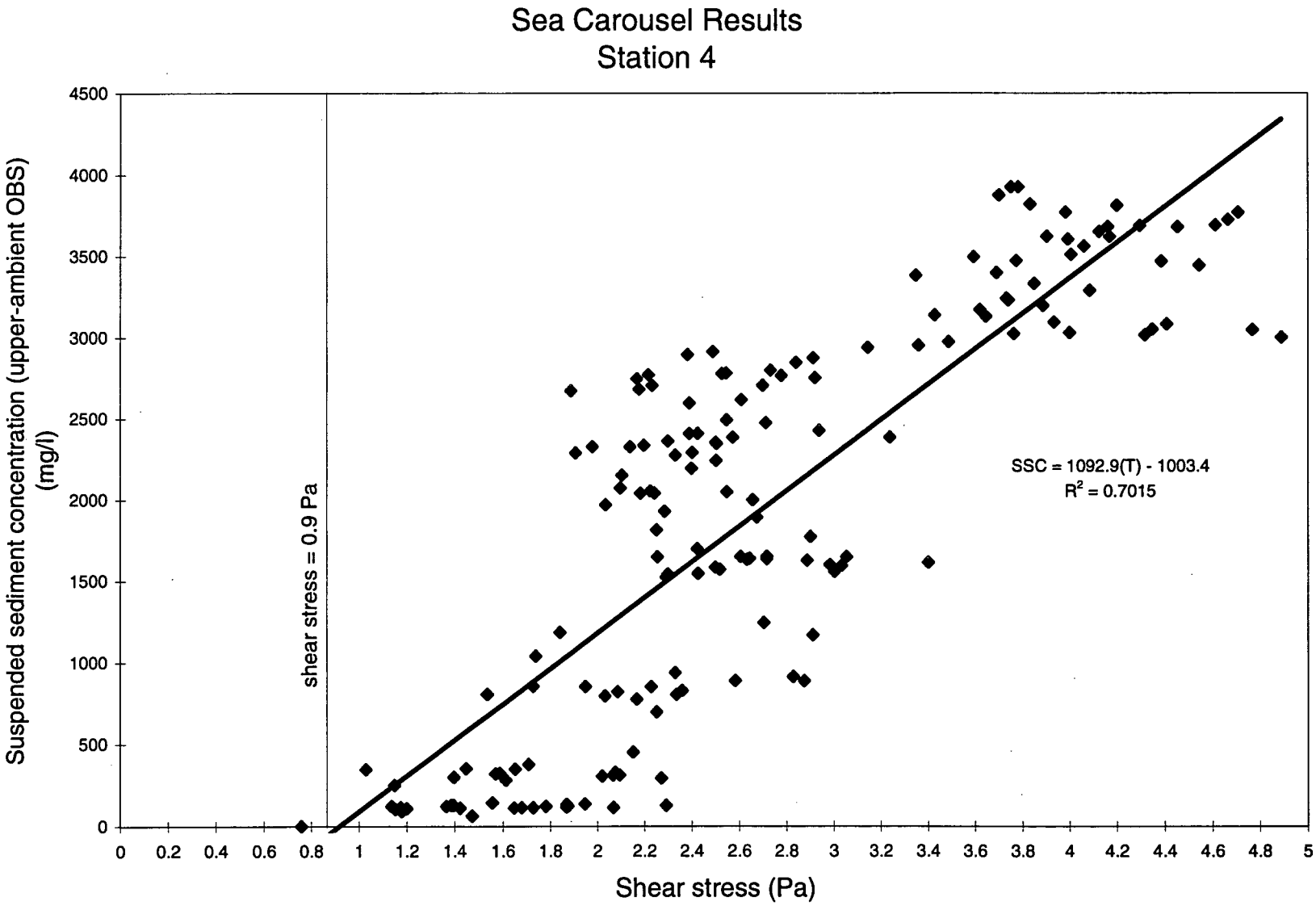

Figure 10: Suspended sediment concentration (upper OBS - ambient OBS) versus applied bed shear stress at station 4

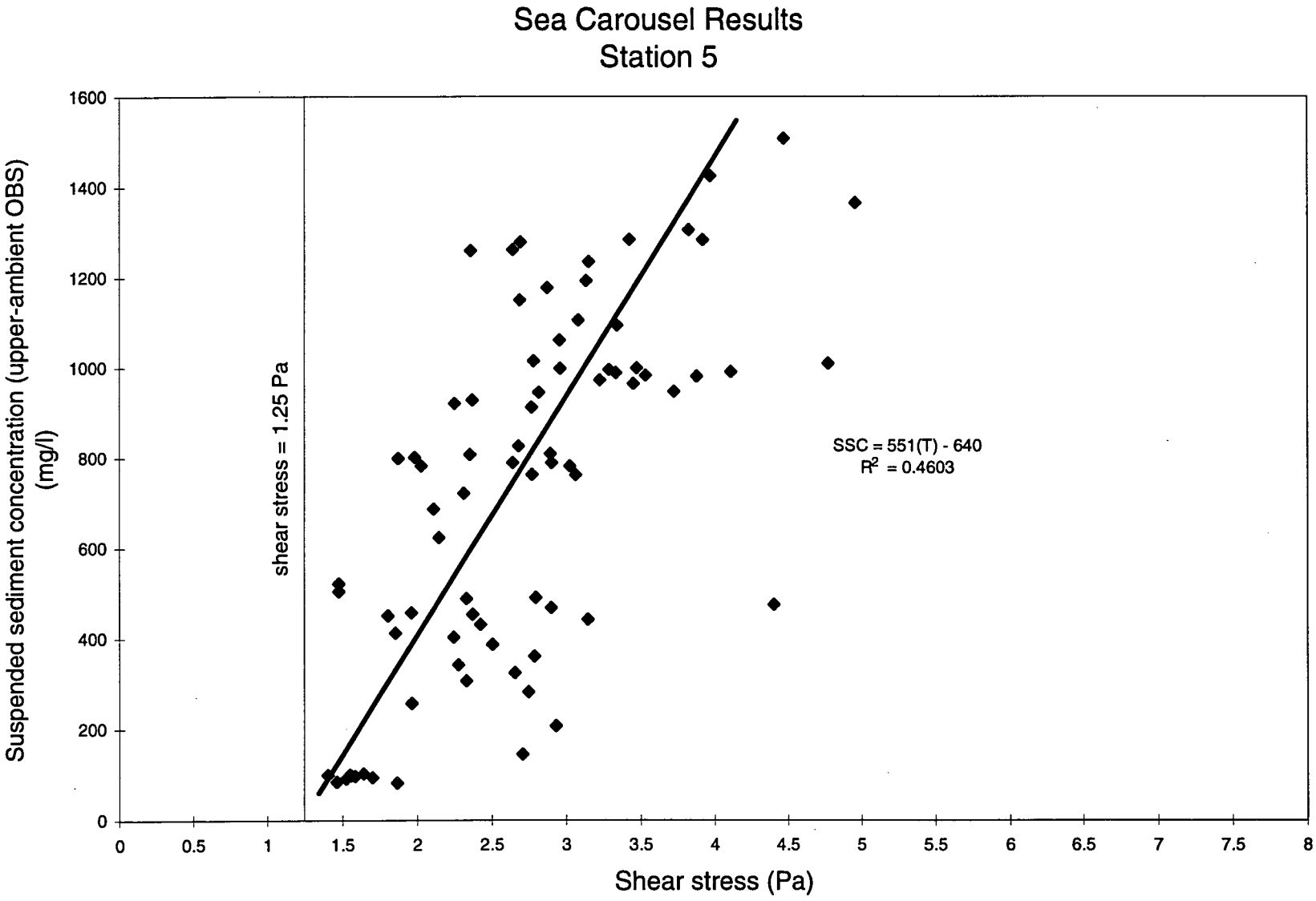

Figure 11: Suspended sediment concentration (upper OBS - ambient OBS) versus applied bed shear stress at station 5

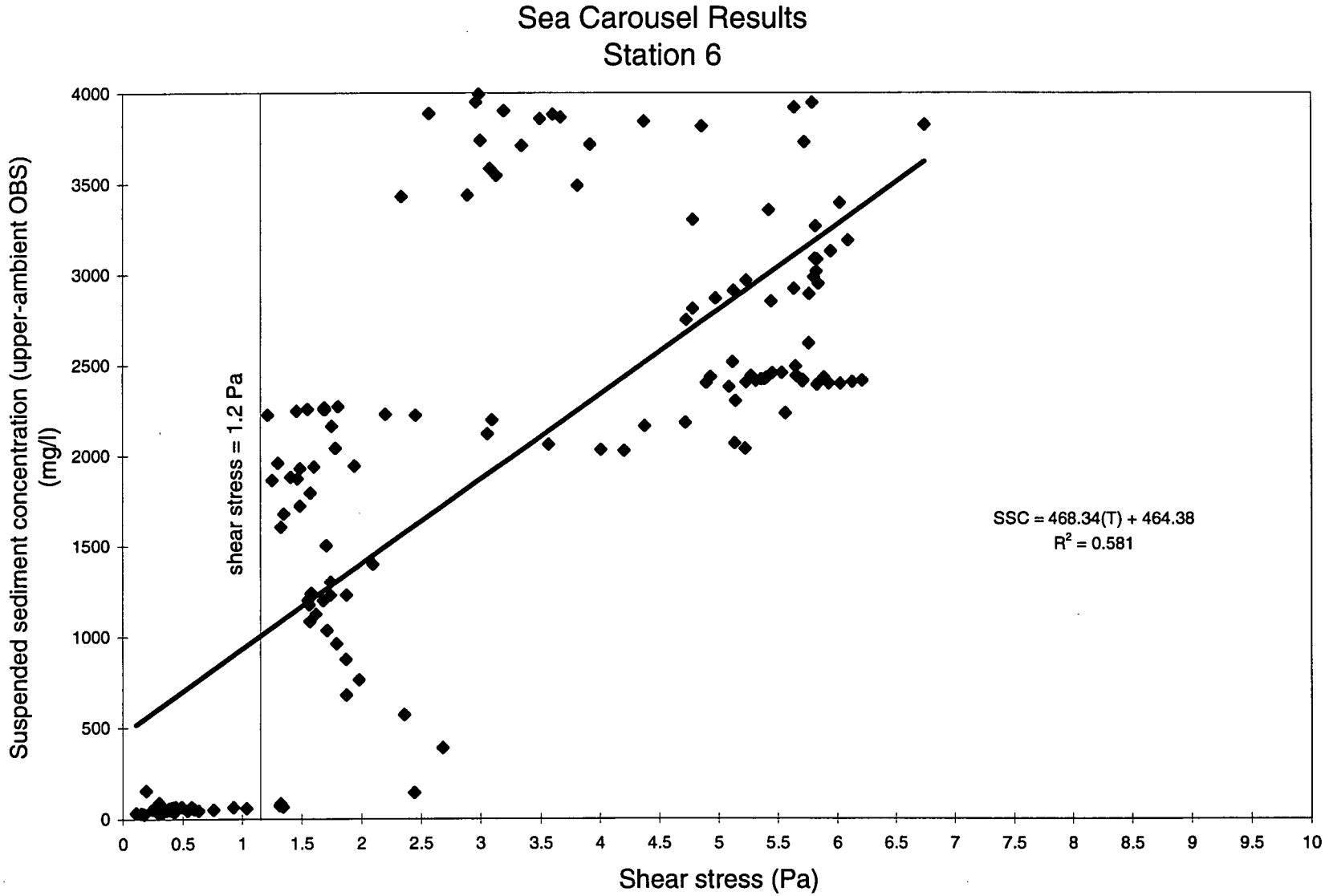

Figure 12: Suspended sediment concentration (upper OBS - ambient OBS) versus applied bed shear stress at station 6

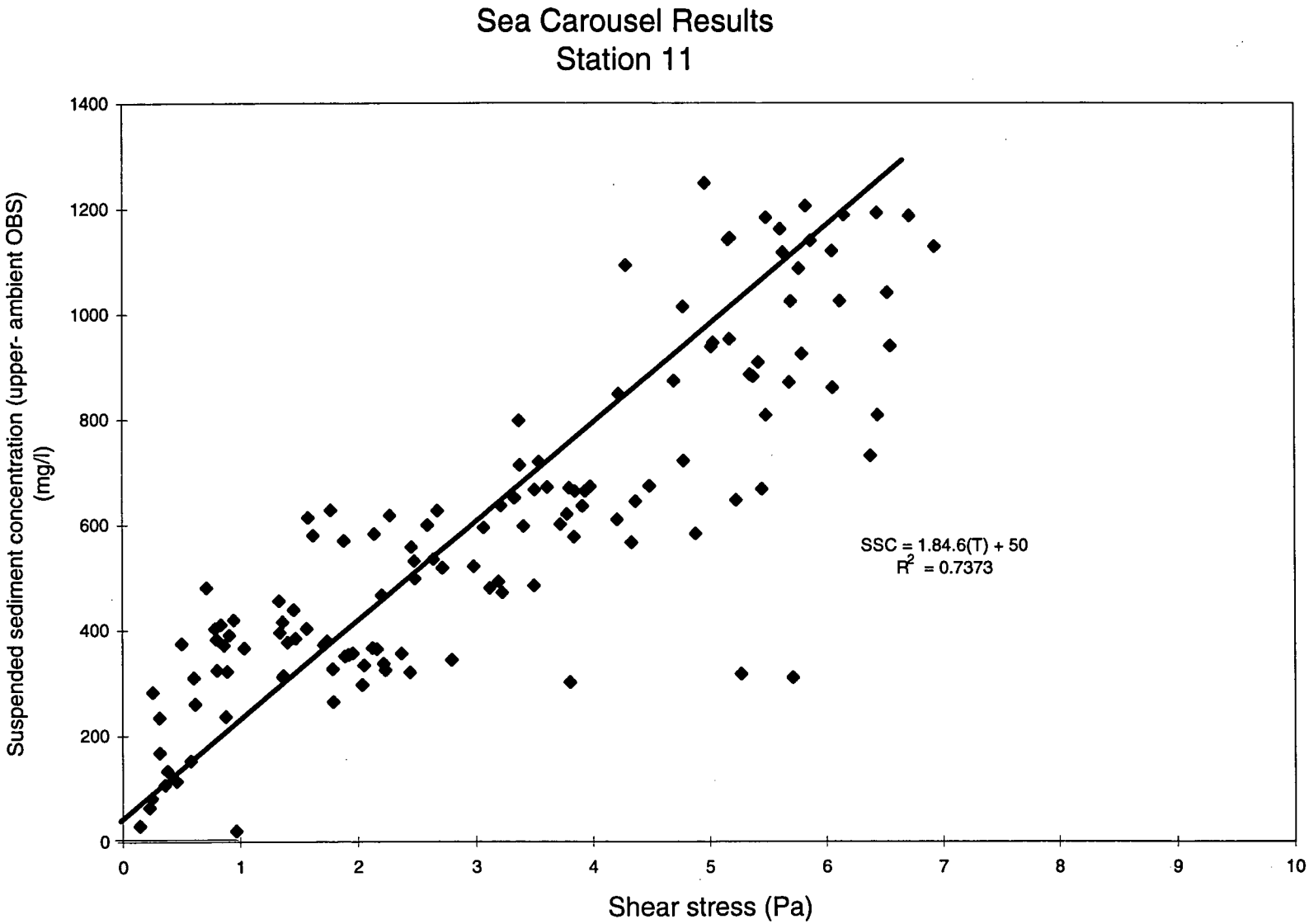

Figure 13: Suspended sediment concentration (upper OBS - ambient OBS) versus applied bed shear stress at station 11

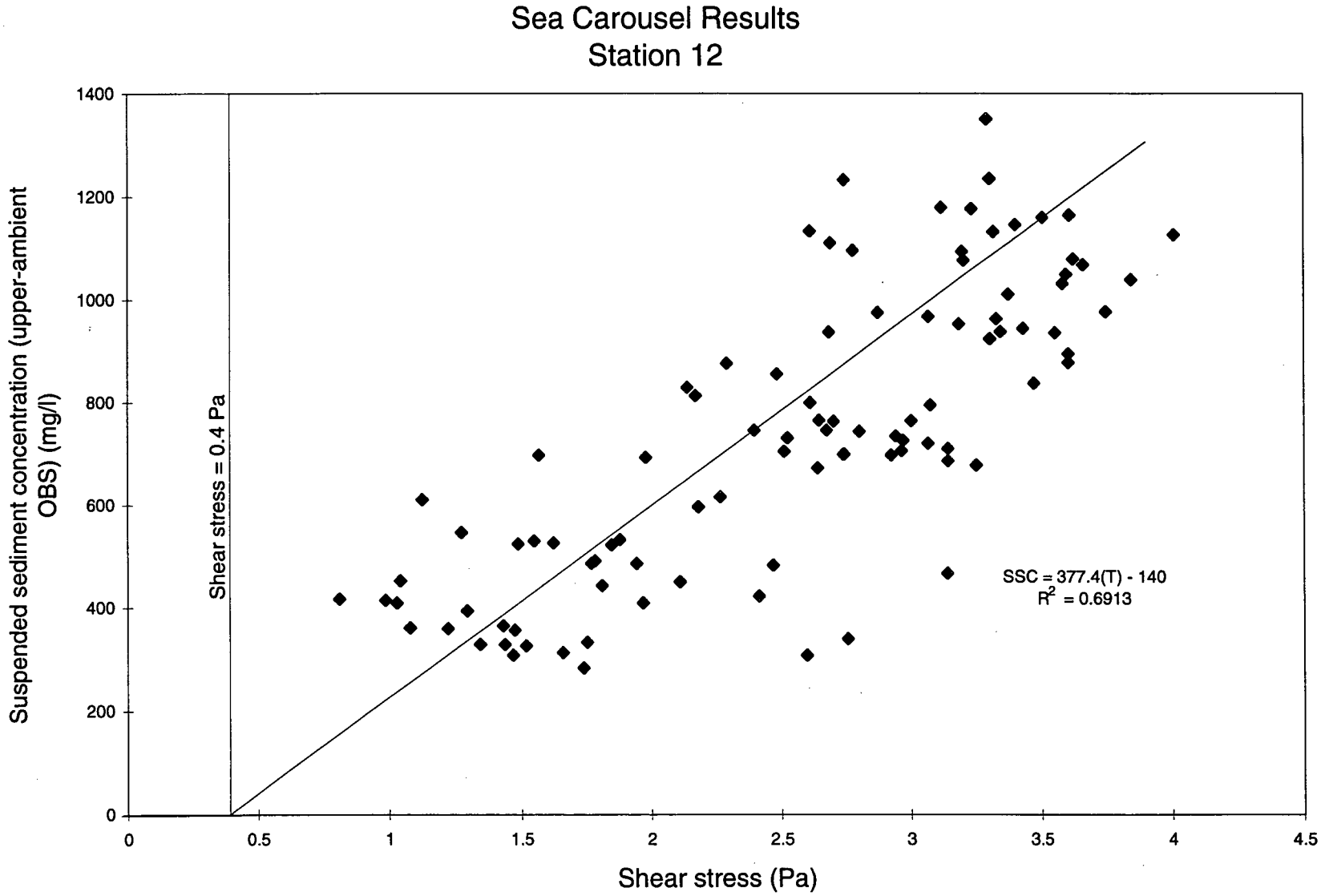

Figure 14: Suspended sediment concentration (upper OBS - ambient OBS) versus applied bed shear stress at station 12

2.3.3. SEDIMENT TRANSPORT RATES

Only the suspended sediment transport rates (SSTR in $kg/m^2/s$) have been examined in this thesis as bedload transport rates are difficult to obtain and assumed to be minor compared to the suspended load. The best fit regression line was used to describe the sediment transport rate versus applied shear stress and applied current velocity 50 cm from the bed. In many cases the equation followed the power law while in other cases a linear regression best described the data. The slope of the corresponding sediment transport equation gives an indication of the quantity of sediment transported.

Station S1 transport rates follow the equation $SSTR = 1.70(\tau) - 1.95$ where τ is the applied bed shear stress (Figure 15a). Converting this equation to represent a function of the SSTR using the velocity at 50 cm from the bed results in the following relationship $SSTR = 8.99(u_{50}) - 5.84$ (Figure 15b). This equation is valid for bed shear stresses with values up to 2.9 Pa ($u_{50} = 98$ cm/s) and then the following relationship describes transport behavior more closely $SSTR = 0.74(\tau) + 1.04$ and $SSTR = 5.15(u_{50}) + 1.83$ using the velocity 50 cm from the bed. The equation showing the relationship of applied current velocity at 50 cm from the bed will hereby be given in square brackets preceding the applied shear stress relationship. Station S2 shows a constant increase in SSTR with increasing applied shear stress following the equation $SSTR = 1.26(\tau) - 1.73$ (Figure 16a) [$SSTR = 7.02(u_{50}) - 4.85$ (Figure 16b)]. The suspended sediment transport equation for station S3 is a power function following the equation $SSTR = 0.008(\tau)^{2.02}$ (Figure 17a) [$SSTR = 0.078(u_{50})^{4.03}$ (Figure 17b)]. Station S13 behaves similar to station S3 in that it follows it follows the power law with an increase in SSTR with increasing applied shear stresses following the relationship $SSTR = 0.002(\tau)^{2.33}$ (Figure 18a) [$SSTR = 0.027(u_{50})^{4.67}$

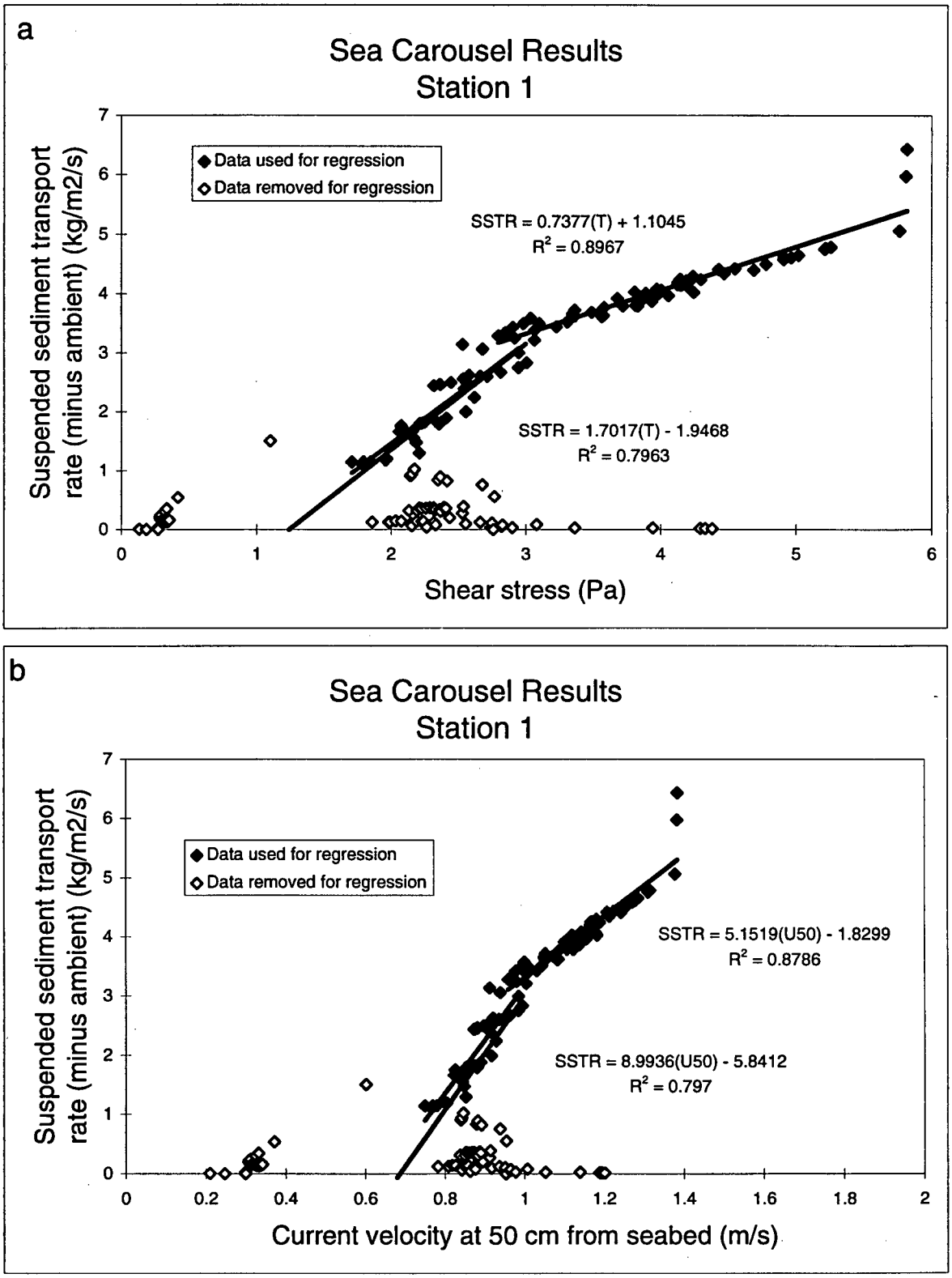

Figure 15: Suspended sediment transport rate for sediments at station 1.

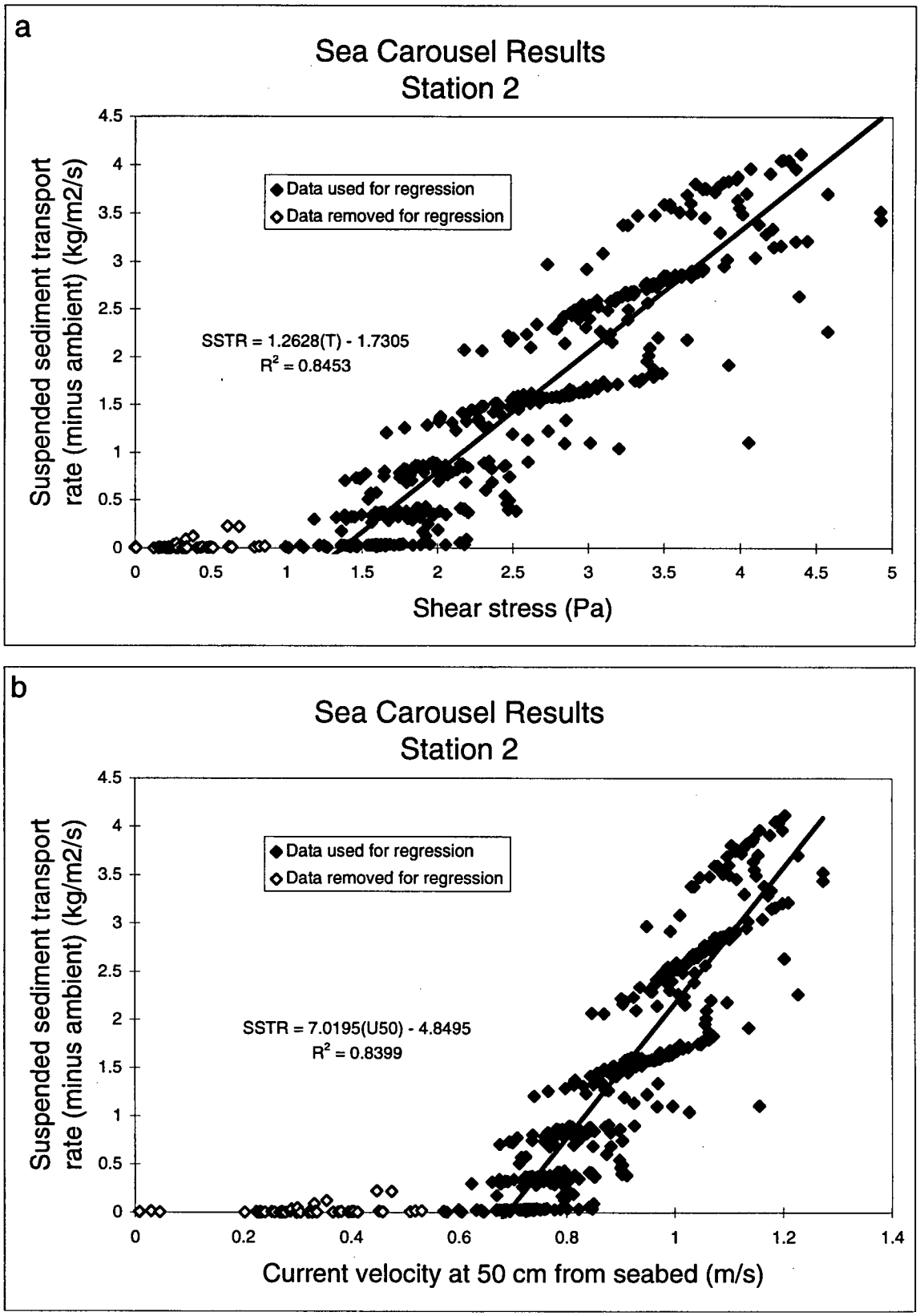

Figure 16: Suspended sediment transport rates for sediments at station 2.

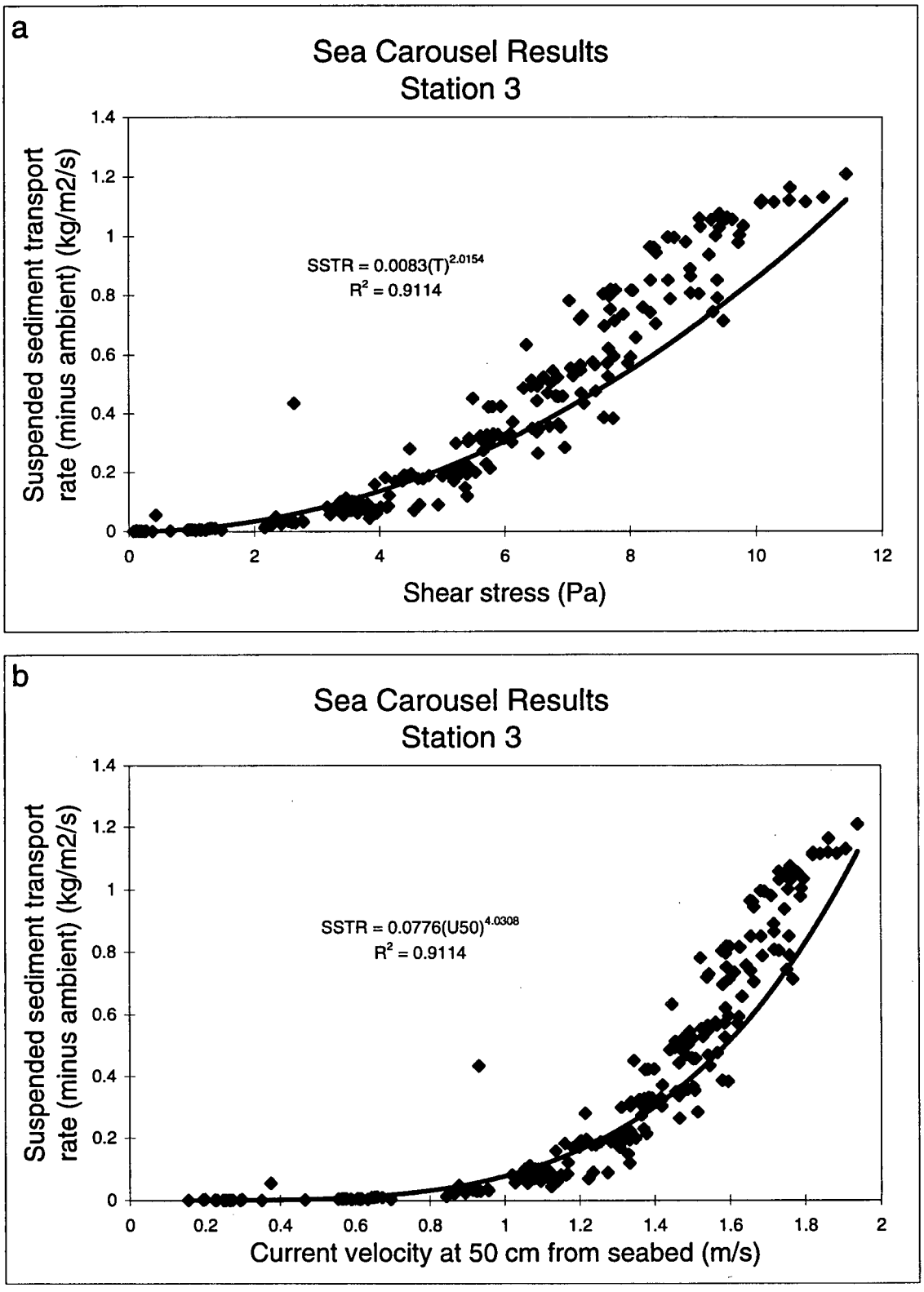

Figure 17: Suspended sediment transport rate for sediments at station 3.

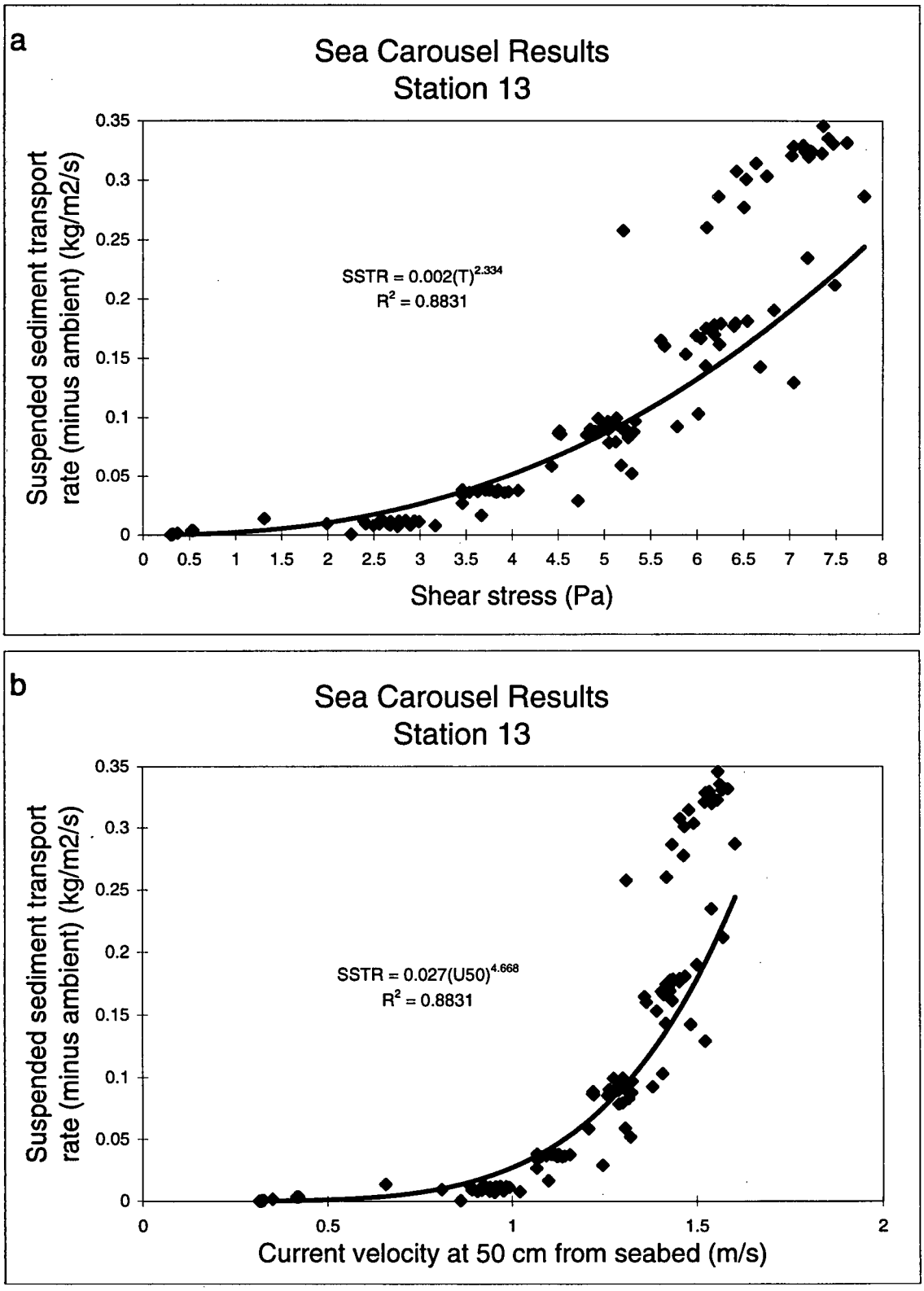

Figure 18: Suspended sediment transport rate for sediments at station 13.

(Figure 18b)]. Station S14 shows two distinct trends in sediment transport behavior and, like station S1, transport rates increase faster at lower applied shear stresses following the relationship SSTR = 0.55(τ) - 1.01 (Figure 19a) [SSTR = 3.47(u_{50}) - 2.79 (Figure 19b)] up to an applied shear stress of 4.3 Pa (u_{50} = 120 cm/s) and then follow the relationship SSTR = 0.25(τ) + 0.37 [SSTR = 2.32(u_{50}) + 1.38] for applied stress greater than 4.3 Pa.

The data for suspended sediment transport rates for sandy sediments are somewhat more scattered than for the cohesive sediments probably because of the influence from saltating particles. Suspended sediment transport at station S4 is best described by the following power law equation SSTR = 0.044(τ)$^{2.88}$ (Figure 20a) [SSTR = 1.98(u_{50})$^{5.76}$ (Figure 20b)], while suspended sediment transport at station S5 follows the power law equation SSTR = 0.025(τ)$^{2.46}$ (Figure 21a) [SSTR = 0.66(u_{50})$^{4.91}$ (Figure 21b)]. Suspended sediment transport rates are difficult to decipher at station S6 because of the large scatter in the data, however the approximate power function SSTR = 0.062(τ)$^{2.16}$ (Figure 22a) [SSTR = 1.08(u_{50})$^{4.31}$ (Figure 22b)] best describes the transport behavior here. The suspended sediment transport behavior at station S11 follows the power law relationship SSTR = 0.66(τ)$^{1.28}$ (Figure 23a) [SSTR = 0.36(u_{50})$^{2.55}$ (Figure 23b)]. The almost zero intercept for the SSTR equation implies that sediments start eroding almost at the onset of any applied stress. Although this is not likely, it is obvious that the sediments at station S11 are being suspended at very low applied shear stresses, probably less than 0.25 Pa (u_{50} = 26 cm/s). Station S12 shows a power function increase in SSTR with increasing applied shear stress following the relationship SSTR = 0.074(τ)$^{1.54}$ (Figure 24a) [SSTR = 0.57(u_{50})$^{3.08}$ (Figure 24b)].

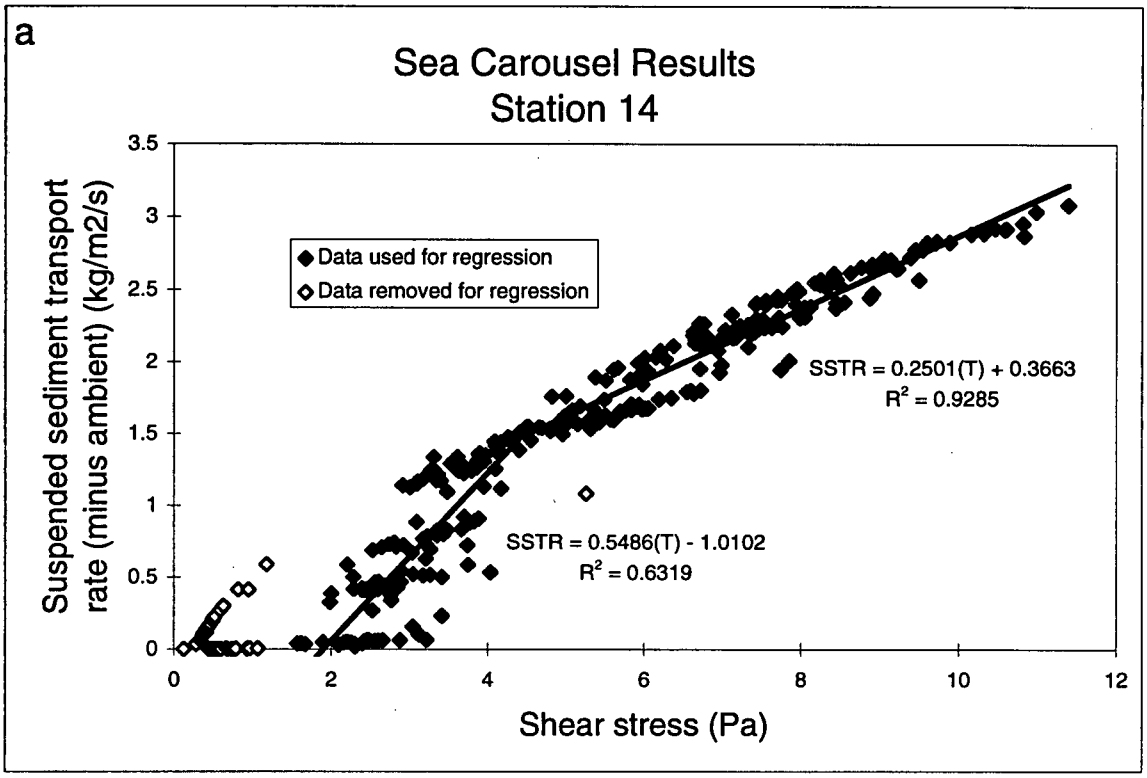

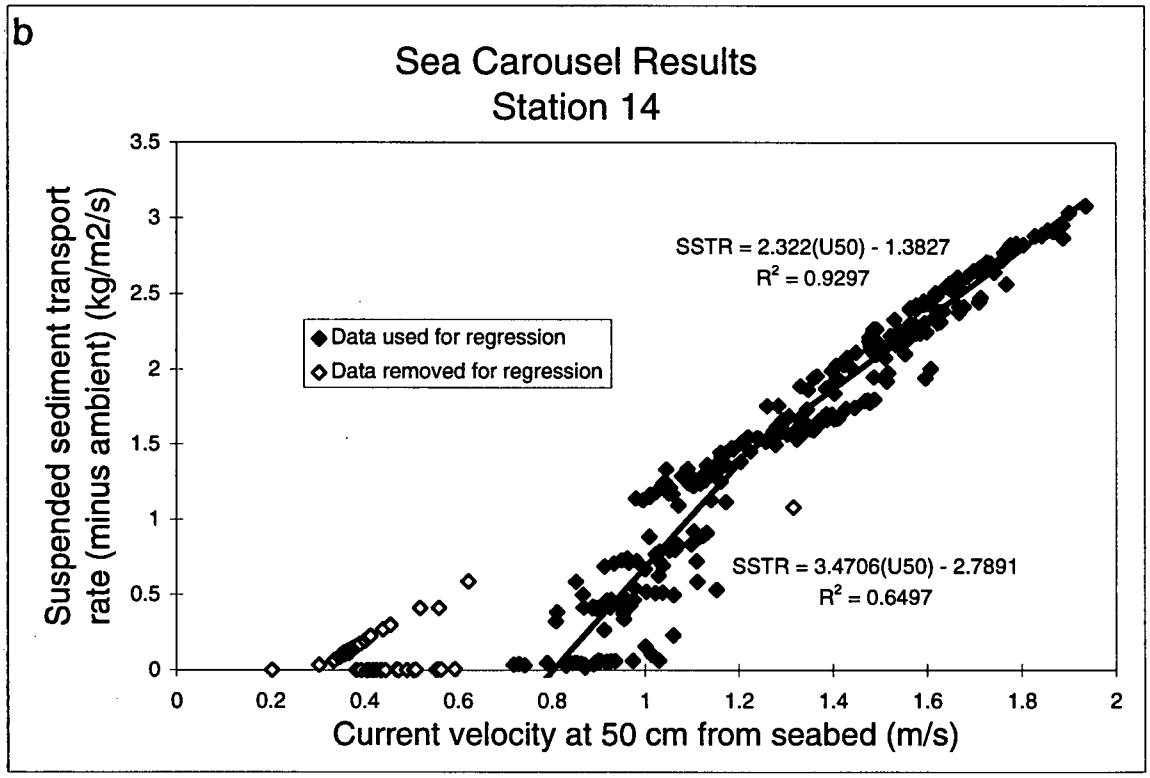

Figure 19: Suspended sediment transport rate for sediments at station 14.

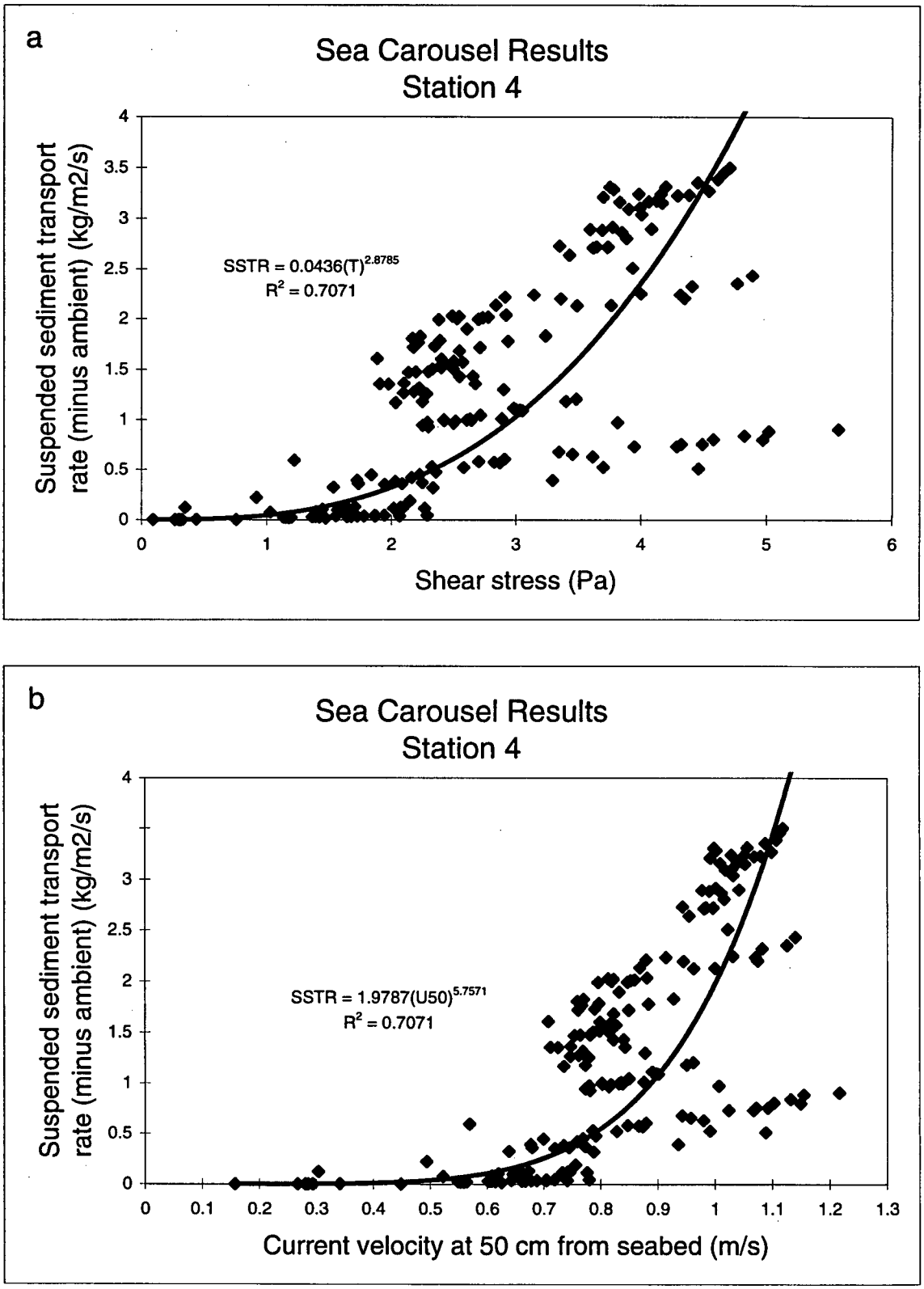

Figure 20: Suspended sediment transport rate for sediments at station 4.

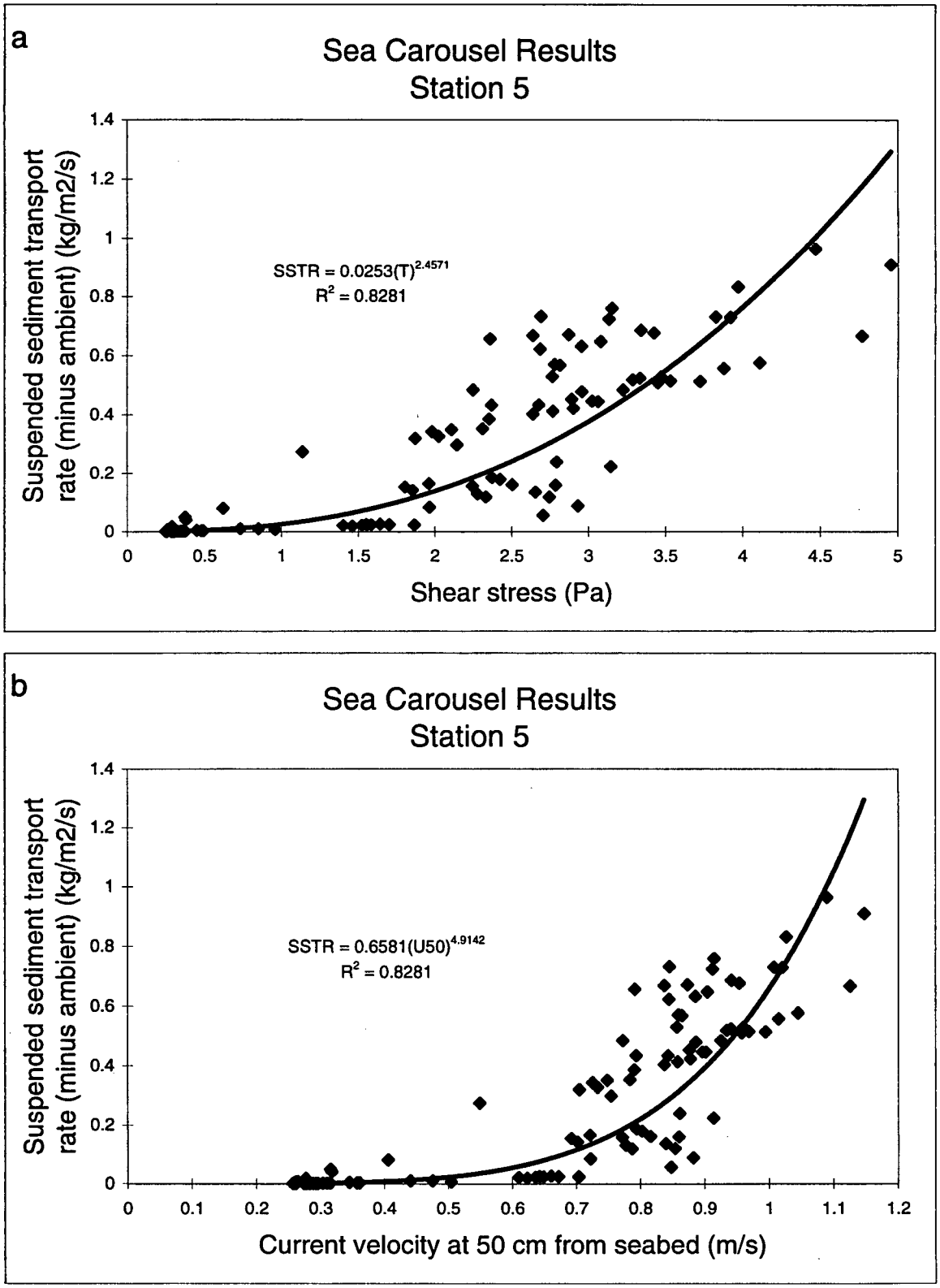

Figure 21: Suspended sediment transport rate for sediments at station 5.

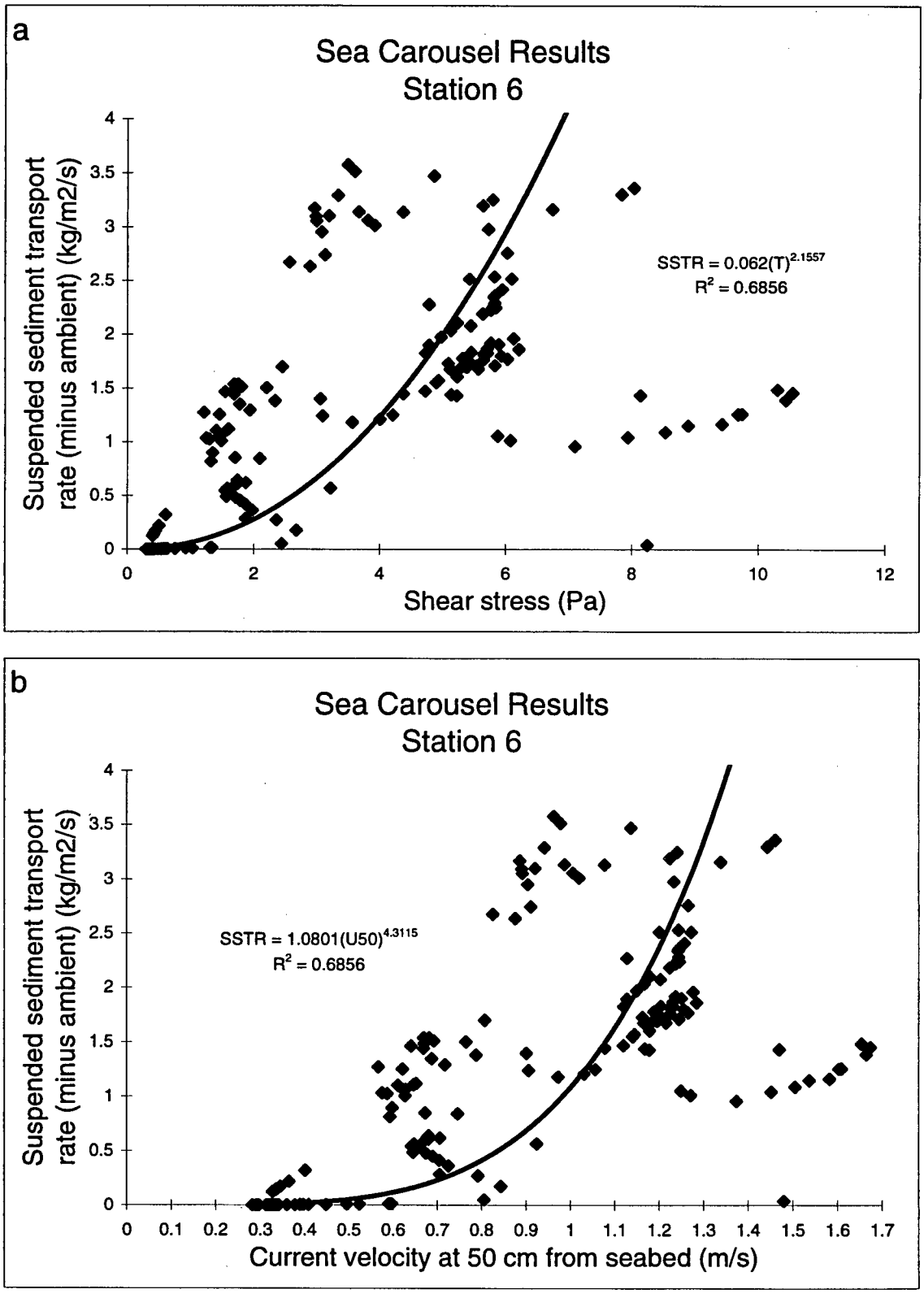

Figure 22: Suspended sediment transport rate for sediments at station 6.

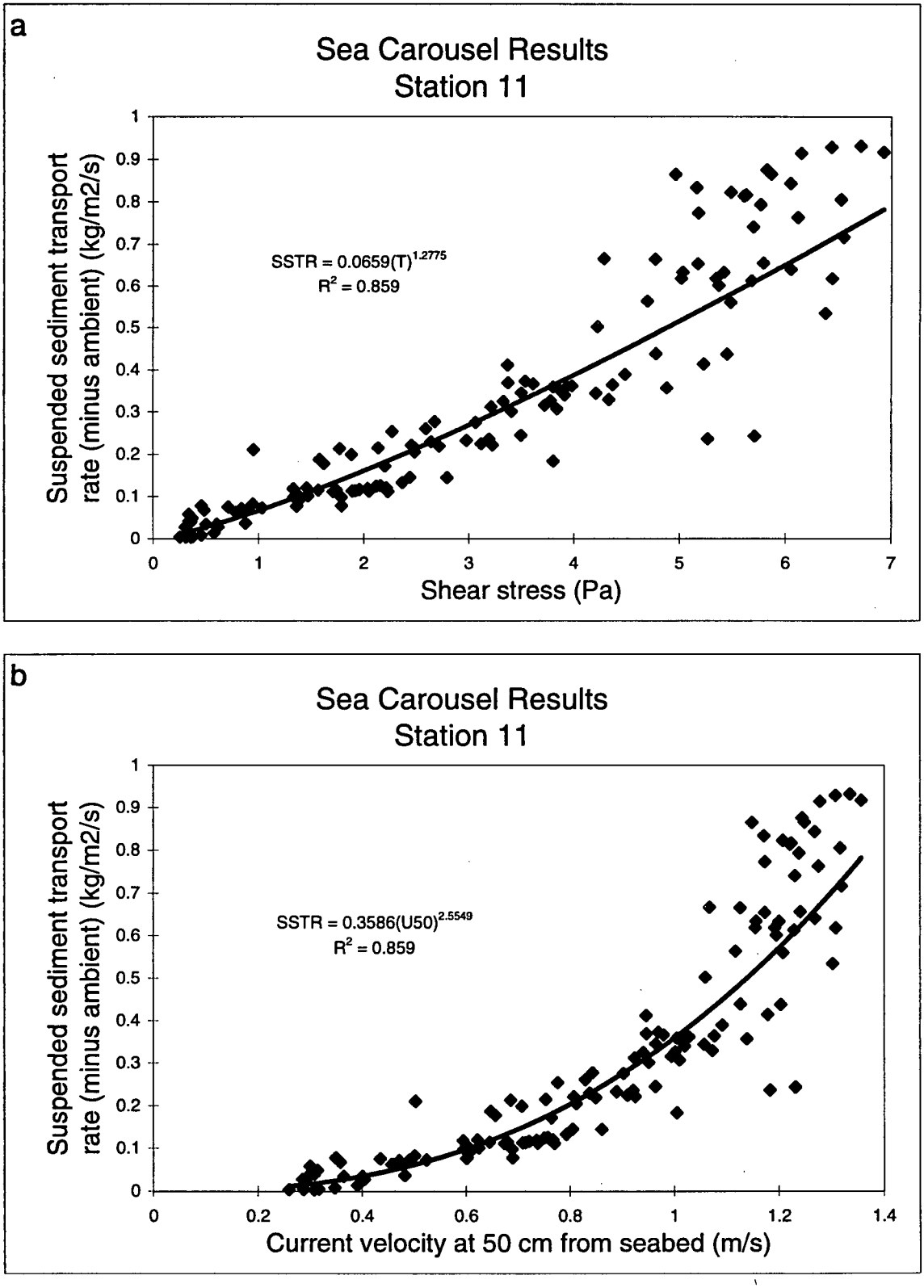

Figure 23: Suspended sediment transport rate for sediments at station 11.

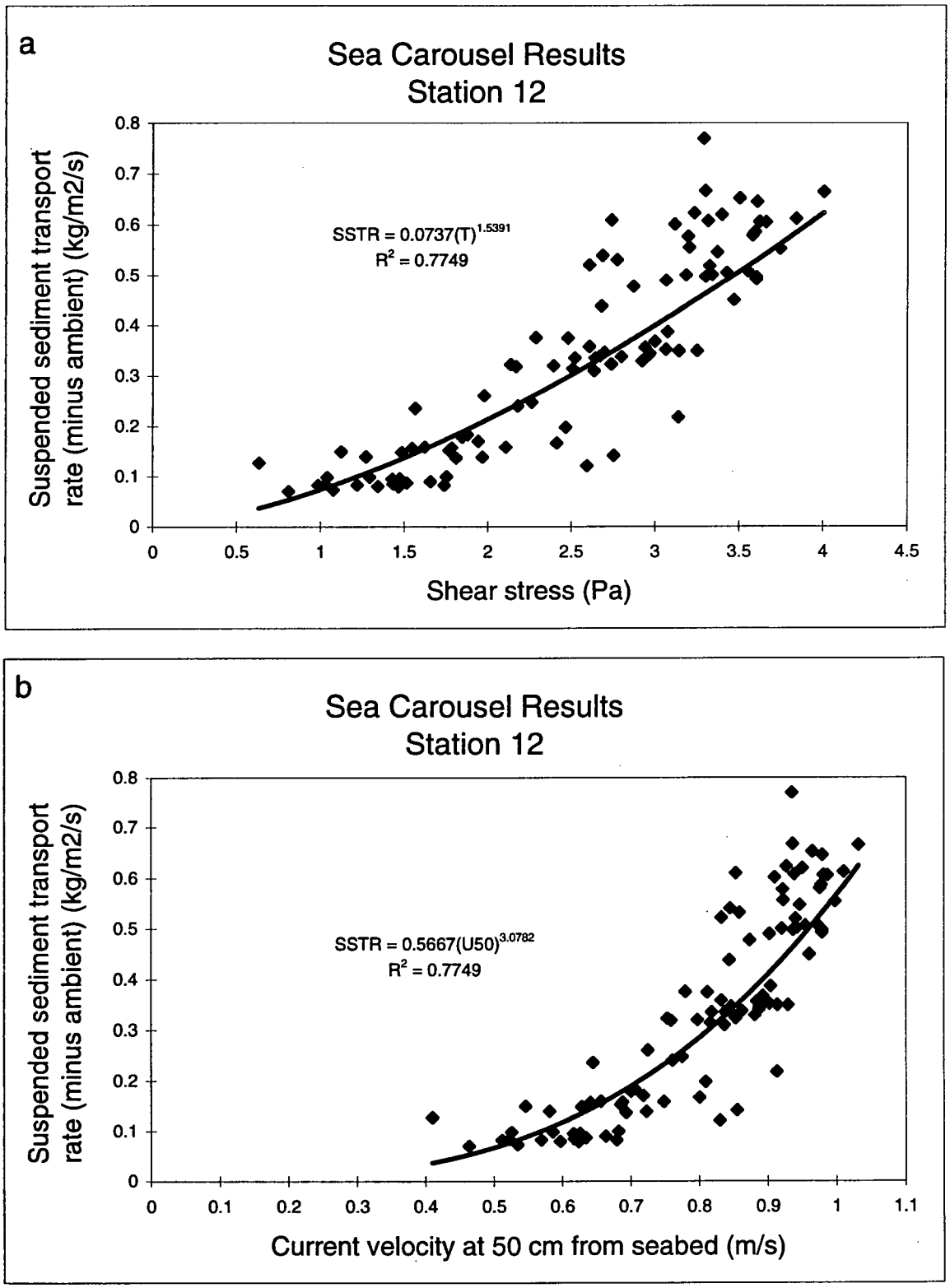

Figure 24: Suspended sediment transport rate for sediments at station 12.

Chapter 3. PHYSICAL OCEANOGRAPHY

3.1. THE S4 CURRENT METERS AND FIELD SAMPLING

Physical oceanographic data were collected from 10 sites on Sturgeon Bank during May and June, 1993. The sampling stations corresponded with the Sea Carousel sites and the sampling time overlapped with both the Fraser River freshet which peaked on May 20 at 8890 m^3/s and suspended sediment sampling. An InterOcean S4 current meter was deployed at stations S2, S4, S6, S12, and S14 from May 7 to June 3 and a current meter was deployed at stations S1, S3, S4, S5, S11, and S13 from June 3 to June 30 (See Figure 4). A description of the study is also found in Feeney (1994).

The current meters were calibrated in the laboratory for salinity, temperature, direction, and velocity. They were also cold-temperature-tested to insure they would continue data collection if temperatures on the bank decreased drastically. Aluminum poles, 1-1.5 m in length, were screwed into the base of the current meter and then shoved, by hand, into the sediments. A plexiglass plate was placed on the rod 30 cm below the base of the current meter to ensure that it did not sink further into the sediments over the month of deployment. The electrodes which measured current velocity and direction were situated 50 cm from the seabed, while the instruments collecting temperature, salinity and depth measurements were situated on the top of the current meter approximately 75 cm from the seabed.

Each current meter was programmed to sample every 1.5 seconds for speed and direction of currents. After 10 data entries (15 seconds) an additional line of information which included conductivity, temperature, density and salinity were recorded. This procedure was repeated 3

times (a total of 1 minute) after which the instrument shut itself off for the following 59 minutes. On the next hour, the S4 would "wake up" and begin sampling again every 1.5 seconds for one more minute, recording additional data at the end of every 15 seconds.

3.2. DATA REDUCTION

See Appendix IV for a detailed description of the physical oceanographic data. The data were carefully analyzed to determine when the tide was at a sufficient height to cover the electrodes on the current meter. This was possible because the current meter deployed at station S4 was equipped with a pressure sensor to measure depth of inundation. The depths at station S4 acted as a guide to determine the times when current meters at the other stations were inundated. Data from station S4 were not used unless a depth of 0.5 m was recorded which ensured that the electrodes collecting the measurements were sufficiently submersed. Data collected at station S5 were not used unless a depth of 0.5 m was being recorded at station S4, while data collected at stations S6, S11and S12, were not used unless a depth of 0.1 m was being recorded at station 4. For stations S2, S3, S13 and S14, data were not used unless a depth of 1 m was being recorded at station S4 and station S1 data were not used unless a depth of 1.5 m was being recorded at station S4. Conductivity measurements assisted in the determination of current meter exposure or inundation. Ignoring the first and last hour of data collected with good conductivity measurements ensured that no questionable data were included.

Current directional data for each station were divided into 10° increments and plotted as frequency of occurrence. Both a rose diagram and frequency histogram were produced for ease in data visualization. The velocities associated with each 10° class interval were averaged and

plotted on frequency diagram to show the current velocities associated with their directions (See Appendix IV - Figures 91, 96, 101, 108, 109, 119, 124, 129, 136, 141, 146).

Velocities were also determined by averaging all the data points produced in one minute (See Appendix IV - Figures 89, 84, 99, 104, 105, 116, 122, 127, 132, 139, 144). It was assumed that wave periods did not exceed a few seconds in duration and therefore averaging the data over one minute effectively filtered out the effects of waves. High-frequency velocity fluctuations which are assumed to result from waves were determined directly from the S4 data by considering each individual data point in each one minute sampling interval (See Appendix IV - Figures 90, 95, 100, 106, 107, 117, 118, 123, 128, 133, 134, 135, 140, 145). Sampling periods were selected randomly, choosing intervals where wave current velocities were higher than average, then these values were plotted against direction. This allowed visualization of the dominant current directions and their associated velocities in a way similar to the method described for the 10° increment data.

Temperature and salinity measurements were plotted for the entire sampling period for each station (See Appendix IV - Figures 92, 93, 97, 98, 102, 103, 110, 111, 112, 113, 120, 121, 125, 126, 130, 131, 137, 138, 142, 143, 147, 148). The current meter at station 4 was equipped with a pressure sensor which measured depth and therefore depth was plotted for the sampling period (See Appendix IV - Figures 114, 115).

3.3. RESULTS AND DISCUSSION

3.3.1. 10° INCREMENT-AVERAGED VELOCITY AND DIRECTIONAL DATA

Current directional data on Sturgeon Bank are variable (Figure 25). Stations S3, S4, S5,

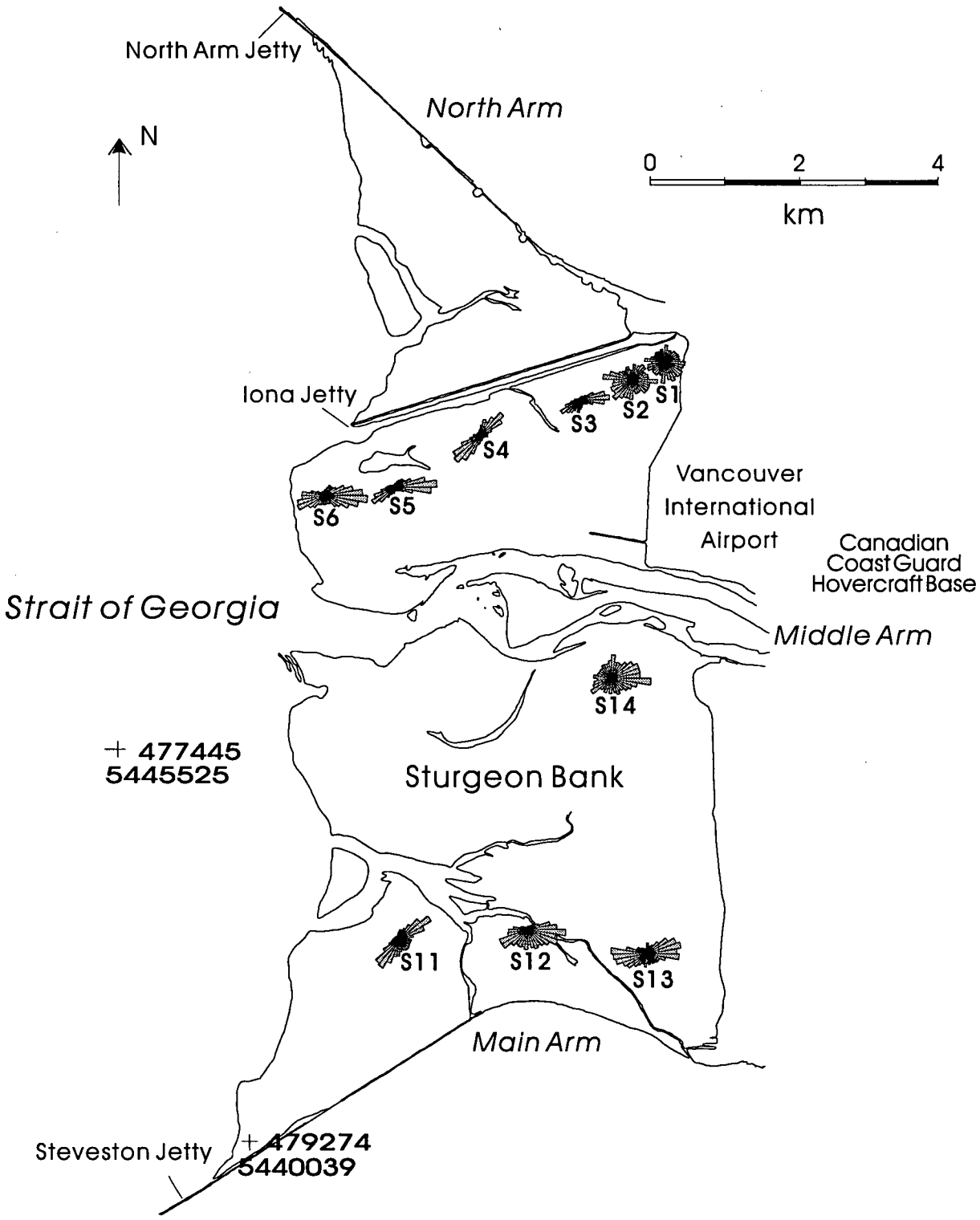

Figure 25: Current direction plots for 10° averaged increments

S6, S11, S12, and S13 show strong bidirectional flows due to flooding and ebbing tides, while stations S1, S2, and S14 show a more random distribution of flow frequencies in all directions. Flows at stations S4 and S11 are dominantly toward 50° in a flooding direction and 225° in an ebbing direction, while flows at stations S3 and S5 are dominantly toward 85° and 235°. Flooding and ebbing flow directions at station S6 are dominantly toward 95° and 250°, respectively, with flooding and ebbing flow directions at station S13 being less focussed and dominantly toward 80° and 270°, respectively. Although station S12 has a strong bidirectional flow toward 95° and 240° for flooding and ebbing tides respectively, an additional component of flow southwards toward the Steveston jetty may be indicative of flow towards an opening in the Steveston jetty on a flooding tide.

Particular stations on Sturgeon Bank seem to be more affected by currents in a flooding direction while others are more affected by currents in an ebbing direction. This is likely the result of the seabed morphology which focusses tidal flows to certain areas of the bank. Flooding directions, averaged over 10° increments, occur more often at stations S3, S5, S6, S12, and S14 (Appendix IV - Figures 101, 119, 124, 136, 146). Ebbing directions, averaged over 10° increments, occur more often at station S4 in May and station S13, while ebbing and flooding directions occur equally at station S4 in June and station S11 (Appendix IV - Figures 108, 141, 109, 129). Average velocities associated with each 10° increment are higher in the flood direction at stations S1, S2, S3, S4, S5, S11, and S12, with values of 7.8, 8.3, 17.5, 23.0, 23.0, 21.0, and 18.0 cm/s, respectively, while velocities in the ebb direction are higher at stations S6, S13 and S14 with values of 24.0, 11.0, and 15.0 cm/s, respectively (Figure 26a-k). Direct station comparisons must be made cautiously because in some cases the data has been collected in

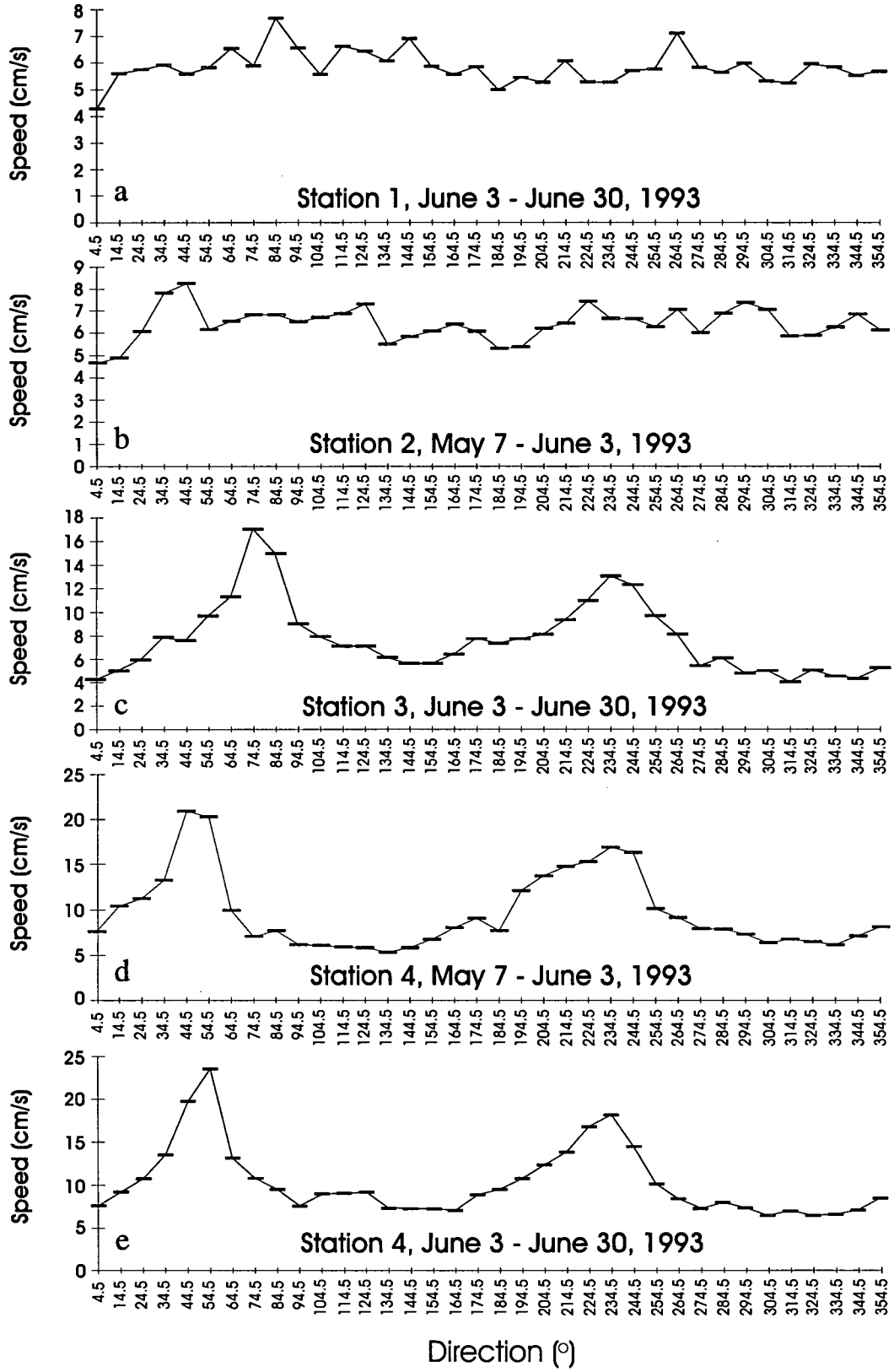

Figure 26 a-e: Current speed plots for 10° averaged increments for stations 1, 2, 3, 4 (May), and 4 (June), respectively

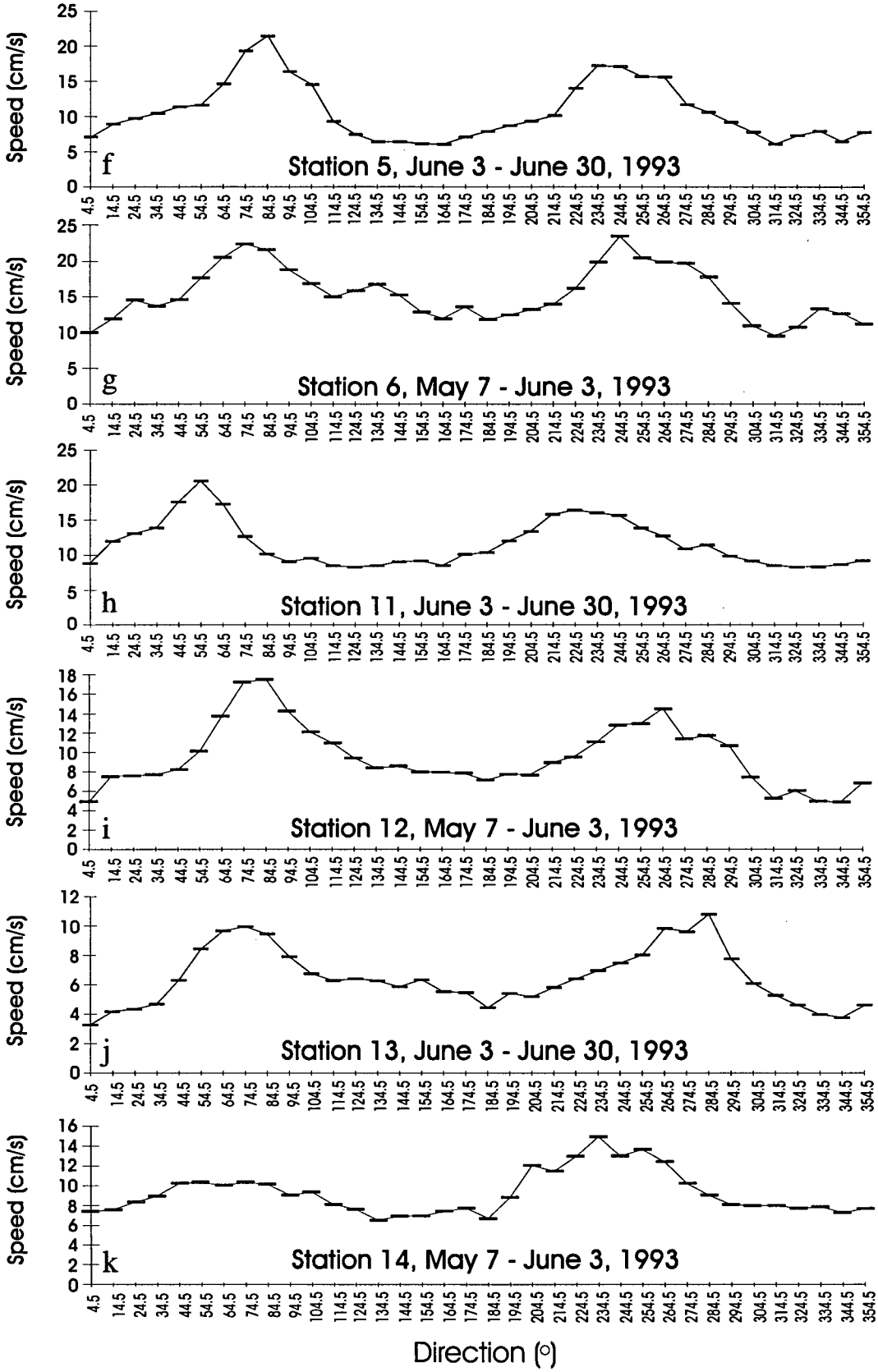

Figure 26 f-k: Current speed plots for 10° averaged increments for stations 5, 6, 11, 12, 13, and 14, respectively

different months.

Higher ebbing velocities at lower frequencies at stations S6 and S14 may be the result of a strong influence from the Middle Arm of the Fraser River on ebbing tides. Because the frequency of flow in the ebbing direction is low, these speeds must only be reached for short times during the tidal cycle. Station S14 is situated adjacent to the south side of the mouth of the Middle Arm and station S6 is on the outer bank where flow from the Middle Arm (or a channel from the Middle Arm) reaches the edge of the bank. The influence of the Middle Arm flow at these two stations would be supported by strong variations in salinity and temperature within sampling intervals as the salt water from the Strait of Georgia is replaced by fresh water from the river on an ebbing tide. This pattern is observed at both stations S6 and S14, where observed variations in salinity and temperature are higher relative to all the other stations on the bank (Appendix IV - Figures 125, 126, 147, 148). Salinity at station S14 remains lower compared to station S6 because of its proximity to the shore, which results in tidal inundation for shorter periods of time. Lower salinities occur at all of the inner bank stations for the same reason.

Based on the results from station S4, ebbing tidal directions occur more frequently in May than in June (Appendix IV - Figures 108, 109), likely due to the effect of a larger source of water from offshore because of the increasing Fraser River flow and the slight increase in spring tidal height in June. The higher frequency of occurrence of ebbing tidal directions in June at station S13 is therefore likely preceded by an even higher frequency in May. Station S13 is the only station where the ebbing velocities are both higher than flooding velocities and occur more often (Appendix IV - Figure 141). Station S13 is situated close to a channel connected to the Main Arm of the Fraser River through an opening in the Steveston jetty and therefore probably

maintains a large degree of flow seaward even at higher tides.

3.3.2. ONE-MINUTE-AVERAGED VELOCITY DATA

The highest velocities averaged over 1 minute recorded in May occurred primarily in the sampling interval May 11 (1900 h) to May 12 (0100 h) with the May 12 (0600-1300 h) and the May 28 (1800 h) to May 29 (0600 h) intervals also recording high velocities at stations S12 and S4, respectively (See Appendix IV - Figures 94, 104, 122, 132, 144). The highest tidal velocities recorded in June occurred in several sampling intervals including June 3 (1400 h) to June 4 (0900 h), June 4 (1400 h) to June 5 (0900 h), June 6 (1500 h) to June 7 (1100 h), June 9 (2100 -2400 h), June 21 (1900-2200), June 23 (1800 h) to June 24 (0100 h), June 24 (1600 h) to June 25 (0400 h), June 25 (1700 h) to June 26 (0300 h), and June 26 (1900 h) to June 27 (0300 h) (See Appendix IV - Figures 89, 99, 105, 116, 127, 139).

The highest velocities averaged over one minute were recorded at stations S6, S12 and S14 in the May 11-12 sampling interval with values of 27.8, 24.92, and 20.4 cm/s, respectively (Appendix IV - Figures 122, 132, 144). It must be observed that these values represent the average velocities over a one minute sampling period and therefore incorporate currents due to waves if they are high in that minute of sampling. Averaging these one minute intervals over the whole inundation period tends to filter out some of these high hourly fluctuations. However, if waves remain high throughout the entire sampling inundation, the higher average velocity recorded in that interval may be largely the result of persistent waves rather than tides. Examination of the high-frequency velocity fluctuations revealed that high averaged velocities recorded on May 11 and 12 and June 4, 6, and June 21 were likely due to the waves which

persisted throughout each of these sampling intervals and not due solely to tidal currents. The high one minute averaged velocities recorded in the other intervals mentioned above also show some degree of influence from the wave climate that existed on the bank at the time of sampling.

The one minute averaged velocity values obtained from stations S12 are considerably higher than the values obtained from more seaward station S11 (Appendix IV - Figures 132, 127), perhaps because of its proximity to a tidal channel (See Figure 4). The values obtained from station S14 are considerably higher than stations S1, S2, S3, and S13, also adjacent to the shore, and stations S4 and S5 in the middle bank area probably due to the influence of the Middle Arm flow (Appendix IV - Figures 148, 89, 94, 99, 139, 104, 105, 116). At station S4, where data was collected in both May and June, the average velocity over each month was the same, however, the highest one-minute-averaged velocities recorded within a sampling interval at station S4 occurred in June (Appendix IV - Figures 104, 105). Average velocities, in general, are higher at the stations sampled in June. The analysis of surface currents at the seaward edge of Sturgeon Bank conclude that currents flow north at 26 to 51cm/s (Giovando and Tabata, 1970; Tabata et al., 1971). These results are not consistent with the results obtained from this survey where average velocities at the edge of the bank are commonly twice as high as those observed in the previous study. Current meters used in this study measured currents 50 cm from the seabed rather than the sea surface, so the results of the studies cannot be directly compared.

3.3.3. HIGH-FREQUENCY VELOCITY FLUCTUATIONS (WAVES)

High frequency sampling results (waves) are similar to low frequency (averages) patterns on Sturgeon Bank in that they vary widely. Maximum wave velocities reach 90 cm/s at station

S11, 90 cm/s at station S6 and 83 cm/s at station S12 (Figure 27i, j, k) . Stations S1, S2 and S13 show the lowest with maximum values of 38, 43, and 42 cm/s, respectively (Figure 27a, b, d), and stations S3, S4, S5, and S14 show maximum velocities of 47, 53, 62, and 60 cm/s, respectively (Figure 27c, f, g, h, e). Maximum wave velocities at station S4 are slightly higher in June than in May and high velocities are reached almost 3 times more often in June (Appendix IV - Figures 106, 107). Wave velocities in a flooding direction generally exceed those in an ebbing direction except station S14. Ebbing velocities also have a large influence at stations S6, S11, S12 and S13 and the maximum wave velocities at all stations often occur in ebbing directions (Appendix IV - Figures 145, 123, 128, 133, 134, 135, 140).

3.3.3.1. *Erosional capabilities of currents on Sturgeon Bank*

Velocities capable of eroding sediments on Sturgeon Bank are never reached on the inner bank at stations S1, S2, S3, S13 and S14 (Figure 27 a-e) and are only reached at stations S4, S5, S6, S11, and S12 (Figures 27 f-k) if high-frequency fluctuations are considered. Wave energy dissipates as it moves shoreward across the bank in a method consistent with that described by Medley (1978). The critical shear velocity for erosion of sediments at station S4 (i.e. 49 cm/s at a height of 50 cm from the seabed) is reached only once in May (Figure 27f) and 12 times in June (Figure 27g). Using the sediment transport equation determined in chapter 2, 0.04 $kg/m^2/s$ of sediment is transported in an ebbing direction in May and 0.56 $kg/m^2/s$ of sediment is transported in a flooding direction in June at station S4. Currents at station S5 reach the critical shear velocity for erosion (i.e. 58 cm/s at a height of 50 cm from the seabed) only 6 times in one month of data collection (Figure 27h) and resulting sediment transport values are 0.17 $kg/m^2/s$ in an

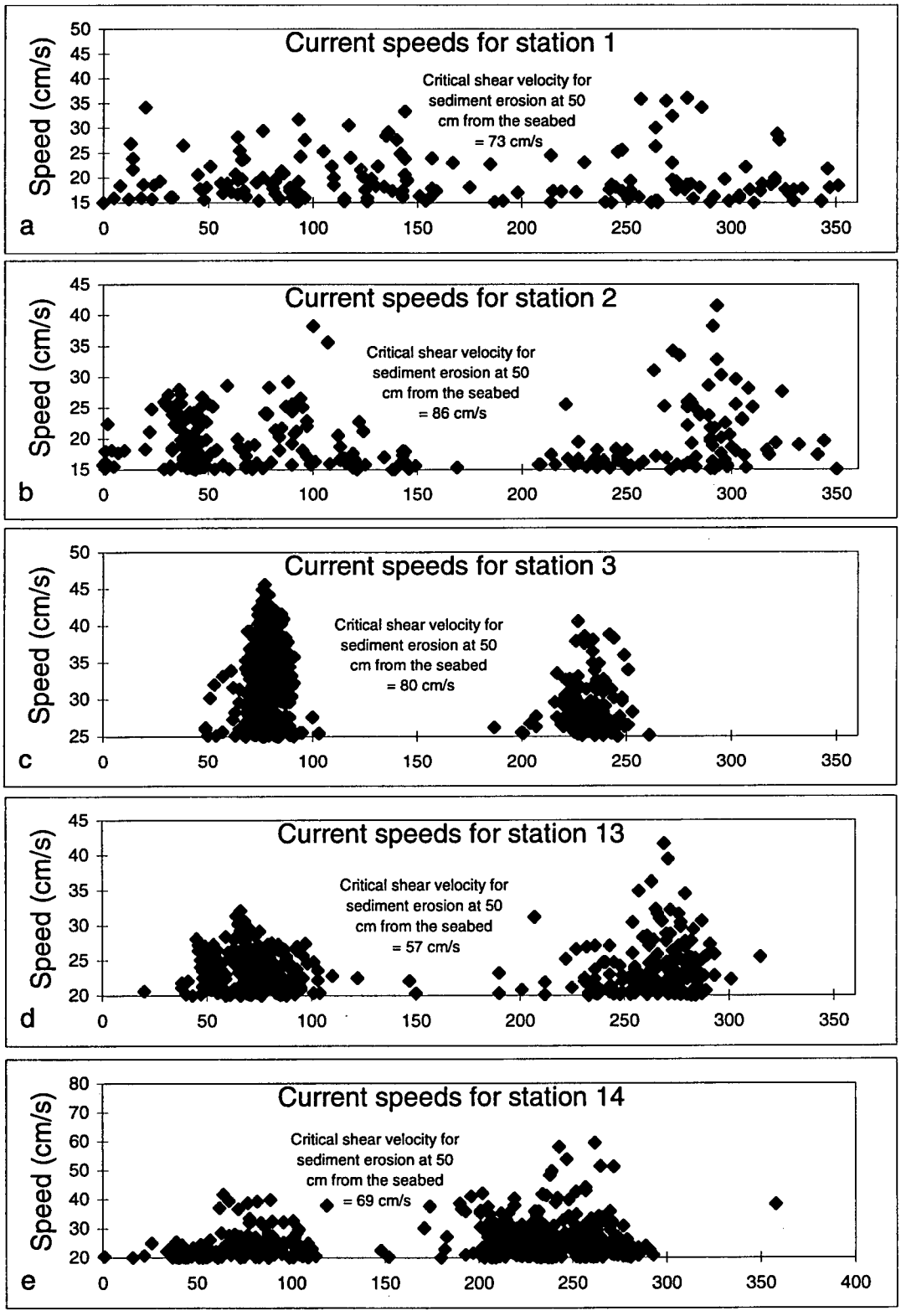

Figure 27: Highest current velocities recorded at each station through one month S4 deployments

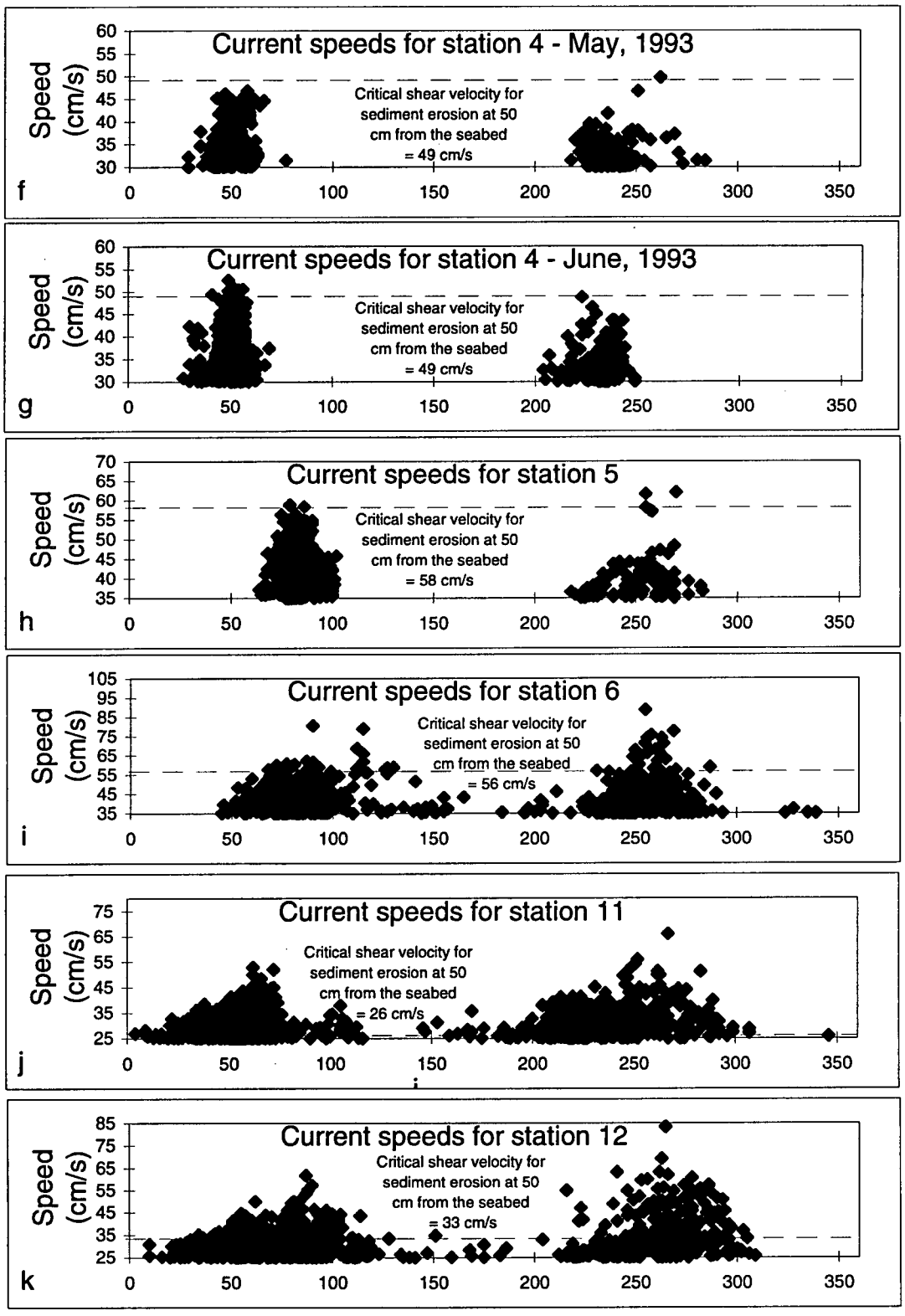

Figure 27 cont'd: Highest current velocities recorded at each station through one month S4 deployments

ebbing direction and 0.14 kg/m^2/s in a flooding direction. The critical shear velocity for erosion of sediments at station S6 (i.e. 56 cm/s at a height of 50 cm from the seabed) is reached 56 times in the month of current meter deployment (Figure 27i). Despite the higher frequency of occurrence of velocities over 56 cm/s in the flooding direction, the higher overall velocities in the ebbing direction result in a higher sediment transport rate. Sediment transport in the flooding direction at station S6 over the month of May was 4.24 kg/m^2/s, while sediment transport in the ebbing direction was 4.88 kg/m^2/s. Station S11 shows sediment transport rates significantly higher than other stations on Sturgeon Bank because of the low critical shear velocity for erosion (i.e. ~26 cm/s at a height of 50 cm from the seabed). The critical shear velocity for erosion is reached 1771 times with the highest frequency of occurrence in the flooding direction (Figure 27j). This high-frequency results in a sediment transport rate in the month of June at station S11 of 21.87 kg/m^2/s in the flooding direction and 11.69 kg/m^2/s in the ebbing direction. Station S12 current velocity data is similar to station S6 in that the critical shear velocity for erosion is reached more often in a flooding direction but is exceeded by a much greater amount in the ebbing direction (Figure 27k). However, unlike station S6, the sediment transport rate in the flooding direction 9.11 kg/m^2/s is greater than the sediment transport rate in the ebbing direction 7.14 kg/m^2/s.

Critical shear velocities for sediment erosion are reached less than 0.3% of the total inundated sampling time at stations S4, S5 and S6 and therefore sediment transport at these stations is very low. Critical shear velocities for sediment erosion at station S11 and S12 are reached 8.4% and 2.5% of the total inundated sampling time, respectively, significantly more often than the other stations and therefore sediment transport rates are considerably higher.

Unfortunately, some of the data may not be included in these sediment transport calculations. Currents which act on the seabed as the tide (and waves if they exist) approaches and departs from the station may have a significant effect on the sediment transport, including at stations on the inner bank. However, these current data have not been collected because the electrodes on the current meter are at a height of 50 cm from the seabed requiring at least this water depth before reasonable data is recorded. Data collection, therefore, is missed on the initial incoming tide and on the final outgoing tide. It is very difficult to collect current velocity and directional information at or near the surface of the bed because of instrument interference on current dynamics. It is therefore likely that all sediment transport rates on Sturgeon Bank are higher than what has been calculated here.

Current meters deployed in the month of May recorded the highest wave velocities in the interval May 11 (1900 h) to May 12 (0100 h) with station S12 also showing high values in the intervals May 12 (0600-1300 h) and May 23 (0500-0900 h) (Appendix IV- Figures 95, 106, 123, 133, 134, 135). Wind speeds on May 11, 12 and 23 were the maximum recorded for the month of May (Environment Canada-Monthly meteorological summary, May/June, 1993) with average speeds during each interval of 26.6 (WNW), 29.1 (WNW), and 26.6 (WNW) km/hr, respectively and maximum daily gusts occurring during the May 11 and May 12 intervals with values of 46 and 48 km/hr. Critical shear velocities capable of eroding sediments at stations sampled in May (i.e. S4, S6 and S12) are all reached in the May 11 interval. Wind-induced waves are likely responsible for a majority of the sediment erosion and transport on the bank as eroding velocities are rarely reached unless storm conditions persist.

The highest wave velocities were recorded in several intervals in June, including June 4

(1400 h) to June 5 (1900 h), June 6 (2300 h) to June 7 (1000 h), June 19 (0400-0800 h), June 20 (1600-1700), and June 21 (1900-2200 h) with only stations S4 and S11 and stations S5 and S12 showing highest values in the same interval (Appendix VI - Figures 90, 100, 107, 117, 118, 128, 140). Wind speeds on June 4, 6, 19, 20 and 21 are variable with average speeds during each interval of 13.7 (WNW), 23.8 (WNW), 8.83 (E), 19.0 (WNW) and 17.75 (NW) km/hr, respectively and maximum daily gusts occurring during only the June 21 interval with a value of 35 km/hr. Critical shear velocities capable of eroding sediments at stations sampled in June (i.e. S4, S5 and S11) are reached in a number of sampling intervals, especially at station 11, however a majority of these high velocities are reached in the June 4 - June 5 interval. Since the wind speeds in the June 4 June 5 interval are low, and the interval corresponds to the maximum spring tidal cycle, it is possible that currents associated with this large tide as well as wind generated currents are capable of eroding sediments at these stations in June. The maximum wave velocities in the month of June do not correspond to average daily wind speed measurements, however they do show a much greater association with the spring/neap tidal cycle than the values recorded in May. It is clear that the presence of waves affects the current velocities everywhere on the bank, however, current velocities are also influenced by tidal effects. The tidal influence on current velocities on Sturgeon Bank is more apparent in June.

3.3.4. TEMPERATURE AND SALINITY VARIATIONS

Temperature measurements throughout the sampling period show the influence of the spring/neap tidal cycle with warmer water occurring during neap times due to lower tidal heights. High winds have a tendency to bring colder deep Strait of Georgia water to the surface and

consequently to Sturgeon Bank which may explain the large temperature drop on June 21 at the stations sampled during this month (Appendix IV - 92, 111, 120, 130, 142). Temperature ranges throughout the sampling period are highest in May with temperatures dropping to lower values during this month (Appendix IV - Figures 97, 110, 125, 137, 147). Typical temperatures ranged from 9 to 26°C with the highest temperatures recorded on the inner bank. The largest temperature ranges throughout the survey occur at stations S1 and S2 with maximum ranges of 11 and 14°C, respectively (Appendix IV - Figures 92, 97). This is likely the result of the predominantly shallow water at these stations which tends to be heated more quickly than the deeper water at other stations. Each station varied in temperature over both the sampling period and each sampling interval. Temperature variations within single sampling intervals are highest at stations S2, S5, and S14, reaching 7° C, and lowest at stations S1 and S3 (Appendix IV - Figures 97, 120, 147, 92, 102).

Salinity measurements throughout the sampling period show only slight influence from spring/neap tidal effects. This is due to the large within-interval salinity variations which effectively mask the trace of monthly tidal influences. Salinity varies widely at each station with variation throughout the sampling period showing a range from 0‰ to 30‰ and the variation within a single sampling interval reaching 21‰ (Appendix IV - Figures 93, 98, 103, 112, 113, 121, 126, 131, 138, 143, 148). The highest degree of variation occurs at station 6 with the outer bank stations generally showing the largest variations. The range in salinity values recorded at the stations is higher in May than in June likely because of the larger influence from the more saline Strait of Georgia water which is able to reach the bank more easily in May than in June when the less saline Fraser River water dominates flow on the bank.

Chapter 4. SUSPENDED SEDIMENT

4.1. FIELD SAMPLING

Suspended sediment samples were collected from stations S1, S2, S3, S4, S5, S6, S11, S12, S13, and S14 on Sturgeon Bank (See Figure 4) every third or fourth day from May 14 to June 28, 1993. The sampling stations corresponded with the Sea Carousel and current meter sampling sites and overlapped with the deployment time of the current meters. Suspended sediment sampling also coincided with the peak in Fraser River discharge on May 20.

Samples were collected using a DH48 bottle sampler at times as close to high-water slack-tide as possible to remove the effects of the flooding and ebbing tidal currents. It was not always possible to adhere to these sampling times because of the availability of the hovercraft. The water depth was tested prior to the deployment of the sampler and then the instrument was lowered from the hovercraft slowly and at a constant speed until a depth just above the seafloor was reached. The sampler was then brought to the surface at the same speed as the descent. The DH48 sampler is designed to collect a depth-integrated water sample by controlling the speed at which the water enters the sampling bottle. Unfortunately, the rate at which the sampler was lowered and raised was difficult to maintain because of hovercraft movement in the presence of waves or swells.

Each station was sampled three times. Where the water depth was less than 1 metre, the sampling bottles were dipped by hand into the water to a depth of approximately 0.5 metres to collect the sample. This procedure had to be adopted because the draft of the hovercraft tended to stir up the bottom sediments too quickly to take the samples with the DH48 at water depths

less than 1 metre. Suspended sediment concentrations measured at stations S1 and S2 were most susceptible to this problem and therefore their results should be viewed cautiously.

4.2. ANALYTICAL TECHNIQUES

Water samples were filtered through 0.045 μm Millipore® filters no more than 48 hours after sampling. This pore size corresponds to the defined boundary between dissolved and suspended sediment and the suspended sediment concentration (SSC) is operationally defined as the amount of sediment retained on the type of filter being used (Loring and Rantala, 1992). Millipore filters have well-defined pore sizes that give them a relatively precise cutoff in the size of particles they retain. They are made of a polycarbonate material which is relatively metal-free and hydrophobic, making them easy to tare and reweigh after sample collection. However, since the build up of particles modifies the effective pore size of the filter, the material retained on the filter includes additional particles smaller than the original pore size. The dried filters were weighed both before and after filtering and the weight gain was recorded as suspended sediment mass. The volume of the sample bottles was measured and the suspended sediment concentration was determined by dividing the weight of the sediment retained on the filter by the volume of water in the sampling bottle. The three replicate sample concentrations taken from each station were averaged to remove as much sample error as possible and to test the consistency of results from replicate samples. Results are recorded in mg/l and are shown in Appendix V. Sampling dates have been converted to cumulative days so that the time between sampling days could be more readily visualized.

4.3. RESULTS AND DISCUSSION

4.3.1. SHOREWARD INCREASE IN SSC

Suspended sediment concentrations decrease seaward with stations S1, S2, S3, S4, S5, and S6 showing typical concentrations of 50, 40, 30, 15, 10, and 5 mg/l, respectively and stations S14, S13, S12, and S11 showing typical concentrations of 45, 30, 10 and 5 mg/l, respectively (Figure 28). Upon initial examination of the higher suspended sediment concentrations on the inner bank, one may be tempted to suggest that the inner bank sediments are eroded more easily than sediments on the outer bank and therefore are the source of sediments to the outer bank. The implication of this behavior would be the eventual retreat of the mudflat and adjacent marshes because sediment was being removed and transported seaward. However, the higher SSC on the inner bank can be explained when one understands how sediments supplied from the Fraser River move headwards onto the tidal flats. The mechanics of tidally-driven sediment motion onto and across a tidal flat was postulated by Postma (1961, 1967) and van Straaten and Kuenen (1957) to be the product of "settling and scour lag" due to the change in sediment behavior from high to low tides because of tidal asymmetry. Postma stated:

> "Towards high tide, when the flood current velocity has decreased sufficiently, nearly all material sinks to the bottom. The sediment is not again brought into suspension by the returning ebb current before the latter has reached a velocity considerably higher than that of the flood current at the moment of deposition. In this manner the material is resuspended in a water mass, the relative position of which is farther inward than that of the water mass which carried the material during the flood."

As the tide moves across the bank, the heaviest material settles out quickly and the fine-grained material is transported to the inner bank, consequently producing higher concentrations of suspended sediments in shore. This headward flux of suspended sediments due to tidal

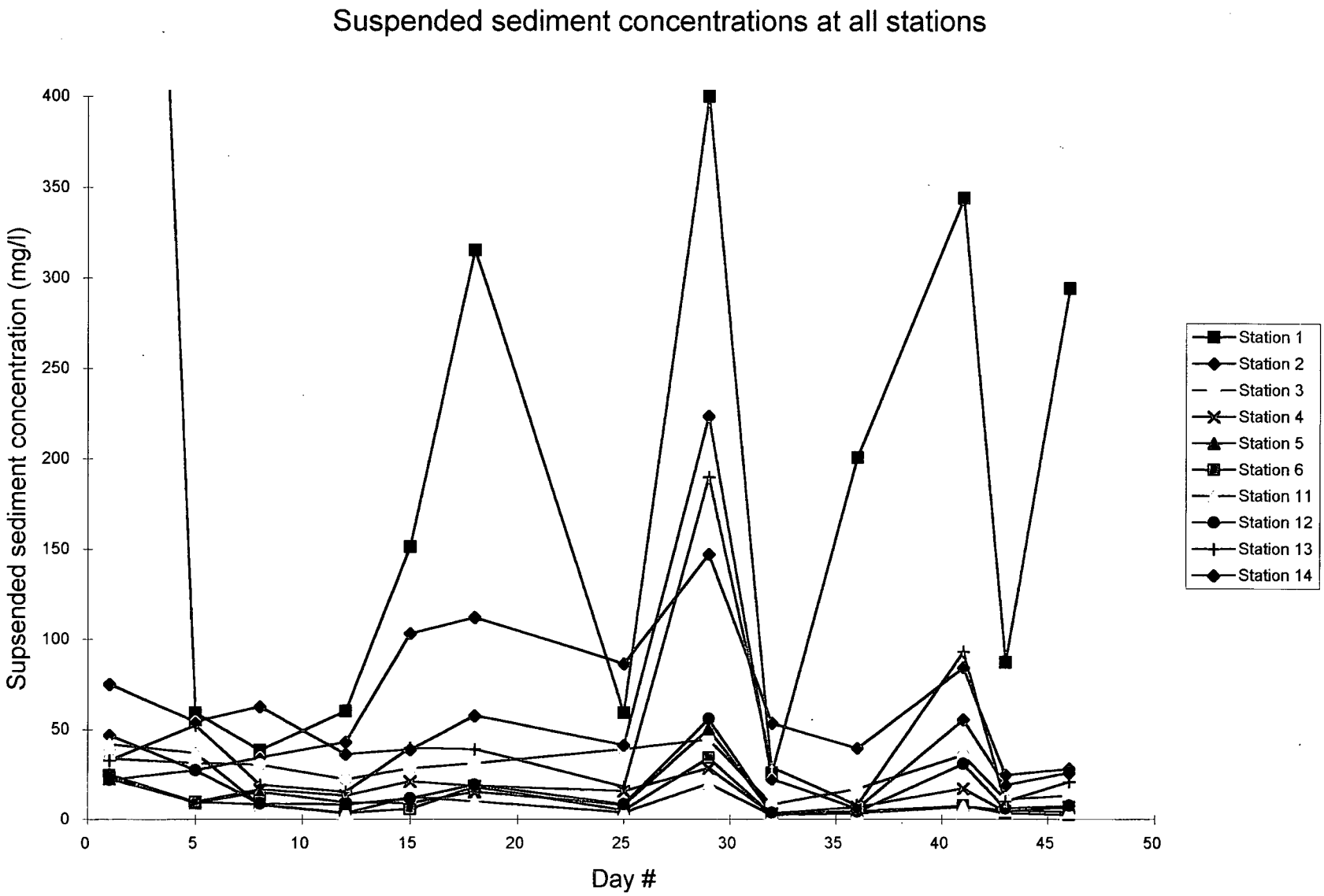

Figure 28: Suspended sediment concentrations on Sturgeon Bank through May and June, 1993

asymmetry should be balanced by a seaward diffusion due to a seaward-decreasing SSC-gradient creating a dynamic equilibrium through diffusive rather than advective processes (Amos, 1995).

4.3.2. DECREASING SSC THROUGHOUT SAMPLING PERIOD

In general, stations S3, S4, S5, S6, S11, S12, and S14 show trends to decreasing concentration over the length of the survey implying that one source of sediments being supplied to the bank is diminishing throughout the survey. This suggests an additional source of sediments, other than those resuspended by waves or tidal currents, must be available and is likely the Fraser River. Water discharge in the Fraser River is low in the winter and rises rapidly in the spring in response to snowmelt then gradually declines during the summer to a low flow in the fall. The suspended sediment concentration follows this pattern but peaks slightly earlier than the discharge and drops very rapidly in the early spring as the supply of fine sediment in the Fraser River basin is exhausted (Kostaschuk et al., 1989; Church et al., 1990). This loop-shaped relation between sediment transport and water discharge occurring through a flood event has been observed in many rivers and is known as the hysteresis effect (Bogen, 1980; Church and Gilbert, 1975; Gregory and Walling, 1973; Statham, 1977; and Walling, 1974). Fraser River discharge rates for May and June, 1993 are shown in Figure 29 with peak river flow occurring on May 20, day 6 of the SSC survey. Unfortunately, suspended sediment measurements in the Fraser River at Mission were unavailable for 1993 at this time. Suspended sediment concentrations in the Fraser River should peak slightly before May 20 and should be declining by the start of the suspended sediment survey on May 14 which is the trend observed on the bank at stations S3, S4, S5, S6, S11, S12, and S14.

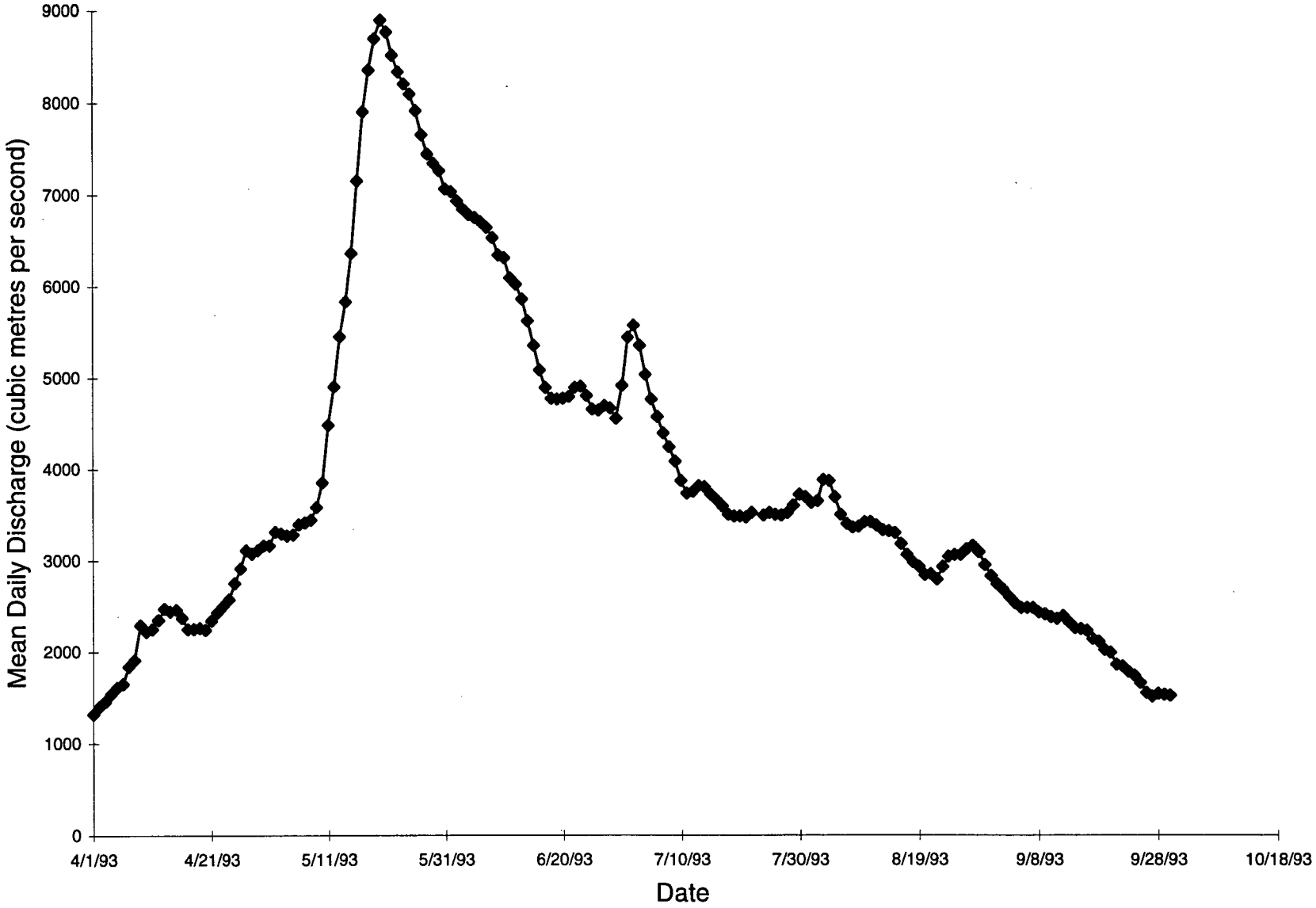

Figure 29: Fraser River mean daily discharge for May to October, 1993

4.3.3. INCREASE IN SSC DUE TO WIND AND WAVES

Suspended sediment does not remain stable at the concentrations described above as large peaks and drops in SSC occur at all stations on the bank frequently. Peaks in SSC throughout the sampling period suggest resuspension by waves may be occurring. Suspended sediment peaks on day 29 (June 11) at all stations on Sturgeon Bank except station S11, with values as high as 400, 150, 45, 50, 35, 56, 190, and 224 mg/l measured at stations S2, S3, S4, S5, S6, S12, S13, and S14, respectively. The most prominent peaks on day 29 occur at stations S12 and S13 and indicate that these stations are more affected by sediment suspension through wave action. Station S12 also demonstrated a strong influence from the Fraser River discharge as described above. Station S1 was not sampled on June 11 because the water depth was not conducive for a representative sample.

Hourly wind speeds on June 11 reached 35 km/hr from the west, the maximum hourly wind speed recorded in the month of June. Peak wind gusts on June 11 during the period of suspended sediment sampling reached 43 km/hr. Current speeds measured at all stations on June 11 are high however station S11 suspended sediment concentration peaked on day 1 (May 14) of the survey reaching 42 mg/l rather than day 29 suggesting that the Fraser River influence is important at this station and that tidal as well as wave particle velocities are responsible for sediment erosion here.

Suspended sediments at other stations also show high concentrations on May 14 despite the relatively low wave particle velocities. Hourly wind speeds on May 14 ranged from 10 to 20 km/hr from the southeast. Suspended sediment concentrations are also noticeably high on days 15 (May 28), 18 (May 31) and 41 (June 23) when wind speeds were 20 to 24 km/hr from the

east/southeast, 6 to 20 km/hr from the west/southwest and 24 to 30 km/hr from the west, respectively. Current velocities on day 15 are similar to day 1 in that they are low at all stations relative to other suspended sediment sampling days implying that the peak in SSC on days 1 and 15 may be the result of Fraser River influence rather than resuspension by waves. These two days are characterized by winds from the east/southeast which seem to have an effect on increasing the concentration of suspended sediment without increasing current velocities over the bank. High suspended sediment concentrations measured on days 18 and 41 can be explained by high current velocities which persisted on these day relative to other SSC sampling days. Unfortunately, suspended sediment concentrations were not measured on May 11 and 12 when high current velocities were persistent.

The majority of sediment in suspension on the bank is likely derived from the Fraser River discharge with a smaller amount being derived from erosion of the bank itself. However waves can strongly influence the concentration of suspended sediment on Sturgeon Bank. Suspended sediment concentrations increase considerably when wind speeds are greater than 25 km/hr. Even lower wind speeds of longer duration do not seem to generate waves large enough to resuspend the amount of sediment that winds of higher speed and shorter duration are capable of. The greatest amount of sediment suspension is measured generally when the winds are blowing from the west where the fetch is the longest; however winds from the southeast are capable of increasing SSC if speeds are high enough.

4.3.4. LIMITATIONS OF SUSPENDED SEDIMENT CONCENTRATION DATA

In order to assess the error associated with suspended sediment sampling at least

6 replicate samples would need to be taken and statistically analyzed. Since this was not done, sample error can only be estimated by the variability in the three replicate samples. Replicate sampling, although not statistically sufficient, indicate that the method of suspended sediment collection should be examined. Sample replicates vary in concentration by as much as 169% from the average, with most varying only 1 to 30% of the average. In many instances one of the three replicate samples accounted for the majority of the variability. When these values were removed from the data set the variability decreased dramatically in most cases. Although one cannot simply remove data, the exercise confirmed that the method of suspended sediment collection may be subject to many errors. Some of the variability in replicate sampling could be due to the variability in the water column. It is more likely, however, that the problems in bottom disturbance by the sampling vehicle, inconsistent rates of ascent and descent with the sampling instrument, seabed contact with the sampling instrument in rough conditions, and collection of particles finer than 0.045 μm on clogged filters are responsible for a large part of the sample inconsistency.

It is difficult to collect suspended sediment rapidly because typical sample collection times ranged from 2 to 3 hours for 10 stations depending on the weather. This meant that sampling could not be carried out everyday because of hovercraft and human time constraints. Thus it is difficult to get a precise picture of the suspended sediment changes on a daily or even hourly time frame which would be necessary to determine the true suspended sediment dynamics on the bank.

Chapter 5. GRAIN SIZE ANALYSIS

5.1. FIELD SAMPLING

Bulk sediment samples were taken from 56 sites on Sturgeon Bank (See Figure 4). Bulk sediment samples were also taken from the 10 Sea Carousel sites. Samples comprise the top two centimetres of sediment at each site and were collected using an 8 cm diameter plexiglass tube pushed into the exposed sediment at low tide on June 30 and July 1, 1992. Samples were collected from the Sea Carousel sites by scooping a thin veneer of sediments from the surface to a depth of approximately 2 cm on July 10, 1991. Five samples were collected at station 19 in a 10 metre east-west transect using 2 metre sample spacing to examine the variability in sediment grain size between adjacent samples.

5.2. ANALYTICAL TECHNIQUES

Sediment samples were dried in an oven at 80°C overnight and disaggregated with a spatula. Dried samples were weighed and then washed through a 230 (63 μm) mesh in a process known as wet sieving to collect the sand fraction. Once washed the sand fraction was transferred to a beaker, dried in an 80°C oven, then reweighed and the weight loss recorded as mud weight. The dried sand fraction was split into 2.0 g sub-samples and then run through a settling tube with and internal diameter of 20 cm and a height of 2 m. The instrument contained a plexiglass plate suspended from a Mettler balance at the bottom of the tube. The deflection of the balance increased with accumulating weight and using Stokes law ($w_s = [(\rho_s-\rho)g/18\mu]d^2$; where w_s is the settling velocity, d the particle diameter, $\rho_s-\rho$ the density difference between the particles and the

fluid, and μ the viscosity of the fluid) a computer calculated the particle size by correlation with time of particle descent. The sampling introduction devices consisted of two discs having a slight convexity onto which the sample was uniformly distributed and wetted with Kodak Photoflo in a method similar to that described by Gibbs (1972). The sample-loaded disc was inverted, then lowered into the top of the tube until, upon touching the water surface, surface tension was broken and the sample was released. This procedure allowed minimum disturbance of the sample upon introduction. Upon contact with the water surface a timer begins recording the time of descent of the particles. The distilled water in the settling tube was allowed to equilibrate with room temperature for several hours prior to use in order that no convection currents would disturb the settling velocities of the spheres. Two samples were run so that an average particle size could be calculated. A description of the statistical analyses and grain size results are given in Appendix VI.

Samples were visually inspected for mud and those which contained more than 5% mud (silt and clay) were washed through the 230 (63 μm) mesh sieve and the wash water collected in a plastic bucket below the sieve. The wash water was transferred to half litre plastic cups and then spun in a centrifuge at 2000 R.P.M. for 90 minutes to separate the mud. The supernatant was poured off and the mud was transferred to plastic bags and freeze-dried for 2 days. Once dried, 2.5 g sub-samples of the mud were transferred into plastic sedigraph cups and the cups filled with approximately 30 ml of 0.05% sodium hexametaphosphate, an anti-coagulant which prevents particle flocculation. The mixture was then stirred, run through a sonic bath and then run through a Sedigraph® 5100 analyzer. The sedigraph determines particle size in the silt and clay range down to 14ϕ by using a finely collimated X-ray beam to measure particle

concentration in terms of transmitted intensity of the X-ray beam through the sample relative to a clear fluid.

5.3. RESULTS AND DISCUSSION

5.3.1. SEDIMENT GRAIN SIZE

Sediments have been classified into appropriate grain size using the Wentworth classification scheme according to their mean grain size in phi units using the first moment statistical method (See Appendix VI-1). A ternary diagram (Figure 30) demonstrates the abundance of sand and silt in the sediments collected on Sturgeon Bank. A majority of the sediments collected on the bank fall into the fine sand category (44% of the samples collected), while only 9% of the samples were fine silt, 7% were medium silt, 13% were coarse silt, 10% were very fine sand, and 17% were medium sand (Figure 31). Grain size contours drawn on Figure 31 have been constructed by hand and represent the Wentworth size classes. The medium sand samples contain 98 to 100 wt. % sand and the fine sand samples contain 93.5 to 99 wt. % sand with the remaining fraction consisting of silt-sized particles.

The proportion of sand to mud reflects the amount of winnowing at the site of deposition. Mud values are defined as the sum of the silt and clay fraction in the sample. The remainder of the sediment sample collected from Sturgeon Bank that was not mud consisted of sand. Sturgeon Bank samples contain a relatively small amount of clay, consequently most of the mud fraction in the sediment is comprised of silt-sized particles. The clay content in sediments from Sturgeon Bank ranges from 0 to 26 wt. % with the highest clay content being found in sediments collected from stations 21, 40, S2, S3, S13 and S14 where clay-sized particles comprise 20 wt. % or more

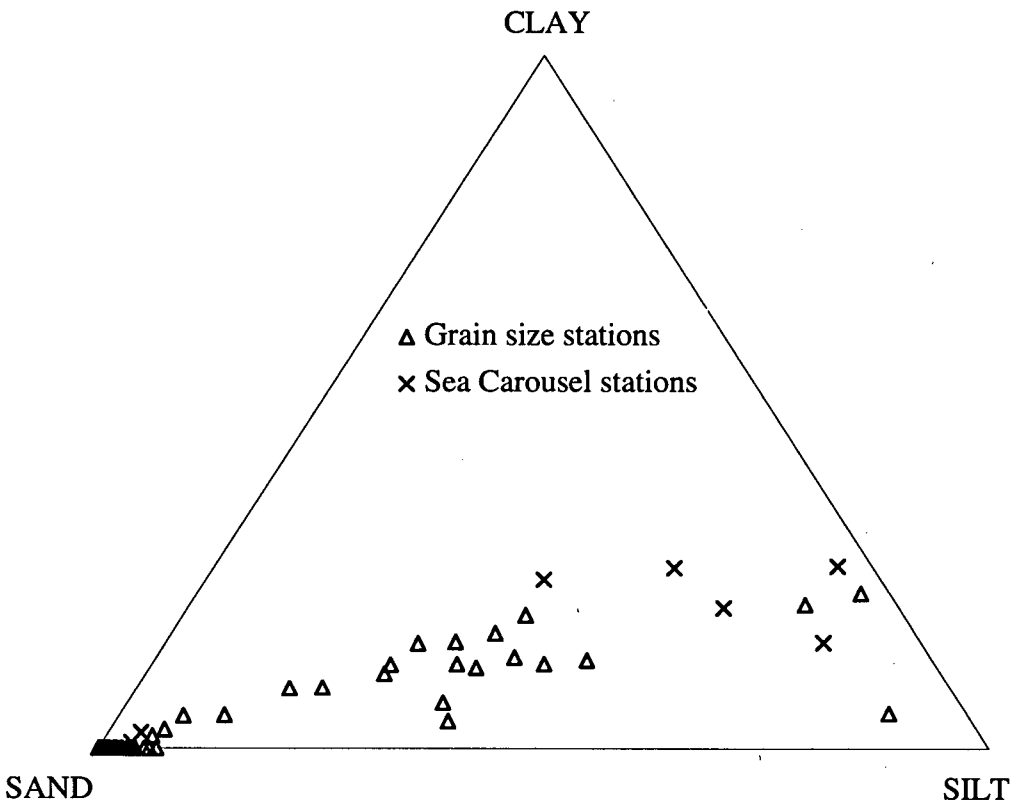

Figure 30: Ternary diagram indicating percent sand/silt/clay for sediments on Sturgeon Bank

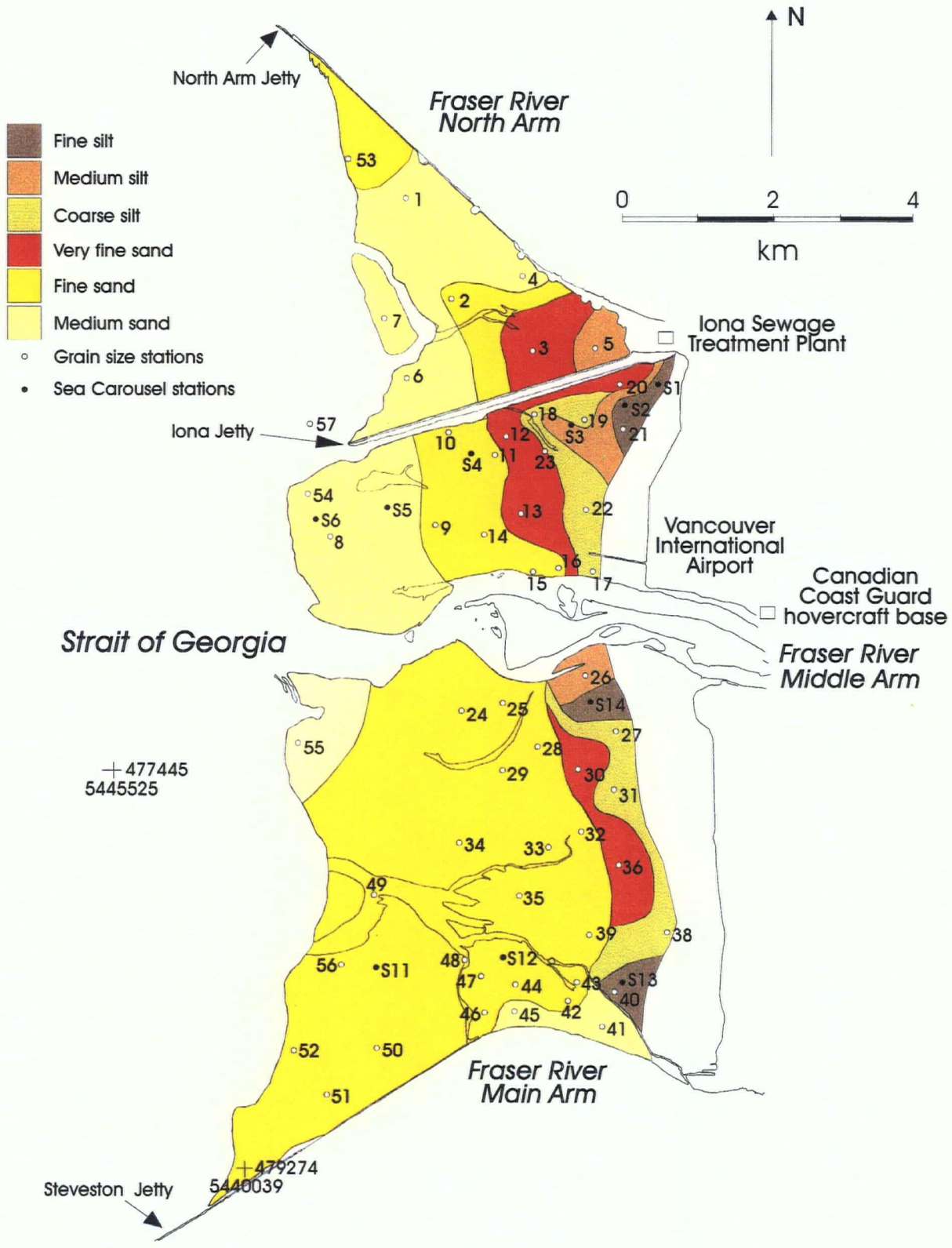

Figure 31: Sediment Grain Size on Sturgeon Bank using Wentworth classification

of the sample. The fine and medium sand samples collected contain no clay while all of the very fine sand samples contain minor amounts of clay. Stations 20 and 23, in particular, contain 9 wt. % clay, higher than their other very fine sand counterparts. The coarse silt sediment class contains between 10 - 15 wt. % clay and 27 to 49 wt. % silt with an anomaly in the coarse silt sediments collected from station 5 which contain 86 wt. % silt, higher than any other sediment sample collected from Sturgeon Bank in this study.

5.3.2. SEDIMENT SORTING

Sediments have been classified into appropriate sorting classes using the Pettijohn et al. (1973) classification scheme modified from Folk (1968) according to their standard deviation in phi units using the second moment statistical method (See Appendix VI-1). Sorting depends on 4 major factors (Folk, 1968), (1) the size range of the material supplied to the environment, (2) the type of deposition (i.e. beach vs. river etc.), (3) the current characteristics, that is, the best sorting is obtained by currents of intermediate and constant strength as opposed to very strong, very weak or currents which fluctuate rapidly which are not efficient sorters, and (4) time, that is, the rate of supply of detritus compared to the efficiency of the sorting agent.

Sorting on Sturgeon Bank varies between 0.31 (very well sorted) to 2.7 (very poorly sorted) (Figure 32). In general sediments become more well sorted in a seaward direction, however, poorly sorted sediments extend to the middle of the central bank at stations 12, 13 and S4. Very poorly sorted sediments dominate the area adjacent to the Iona jetty and the airport on central Sturgeon Bank with slightly better sorting in sediments at stations 21 and S1. On southern Sturgeon Bank, very poorly sorted sediments occupy the inner bank adjacent to the

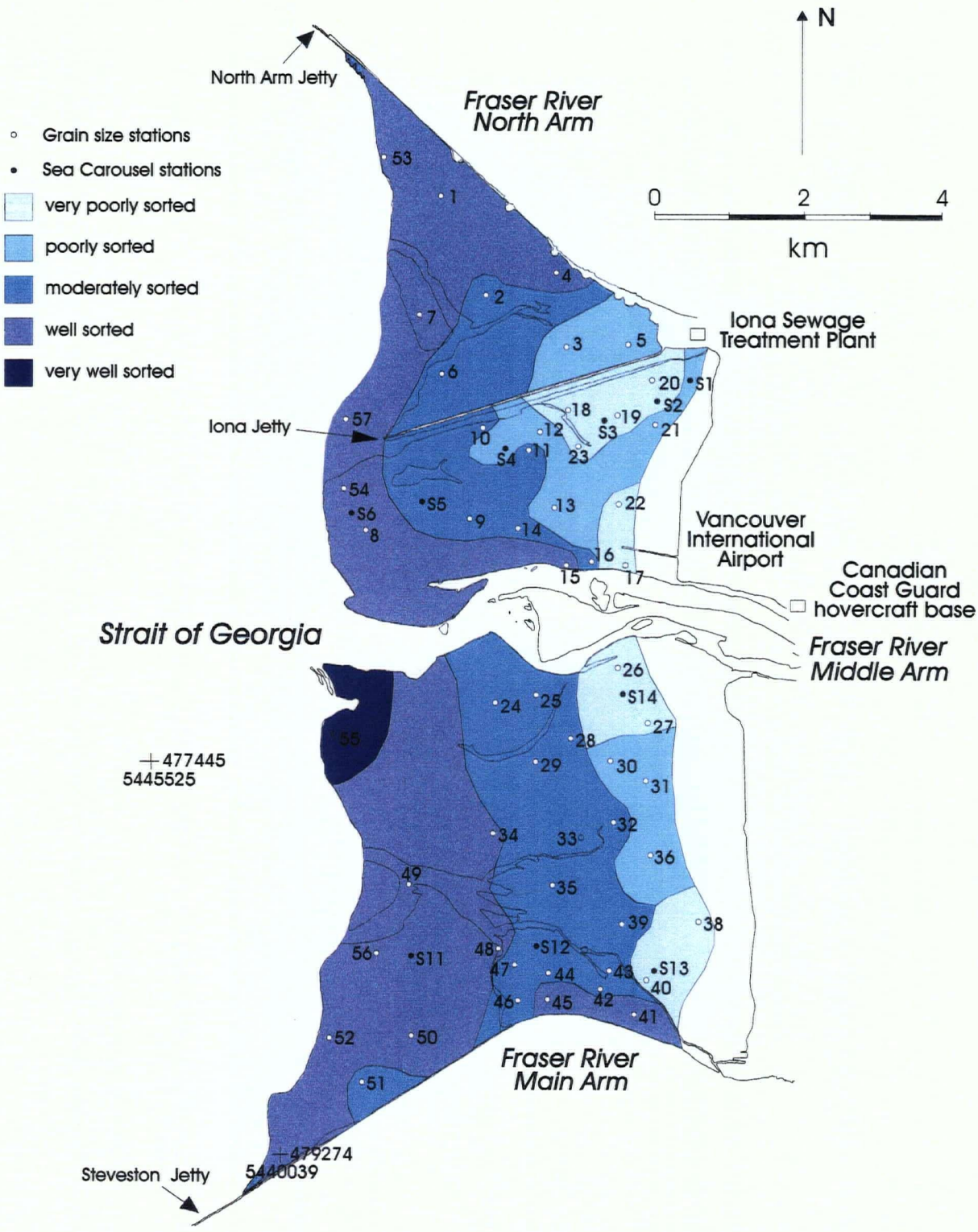

Figure 32: Degree of sorting in sediments on Sturgeon Bank

Middle Arm and the the inner bank at stations 38, 40 and S13. Sediments adjacent to the Steveston jetty on the inner bank are well sorted unlike other sediments collected this far shoreward. Sediments collected from station 51 are only moderately sorted, unlike the well-sorted sediments collected from stations this far seaward. Sediment sorting at stations 30, 31 and 36 is better than other stations on the inner bank similar to the trend seen in sediments found at stations 21 and S1 on central Sturgeon Bank. Sediments collected from station 55, south of the Middle Arm show the highest degree of sorting on the bank.

Sorting is strongly dependent on grain size which can be seen by constructing a scatter plot of mean size versus sorting (Figure 33). The highest degree of sorting is found in the medium sands on Sturgeon Bank and then decreases through the fine and very fine sands with the poorest sorting present in the coarse and medium silts. There is a slight increase in the degree of sorting in the fine silts. This trend in sorting values is consistent with many grain size studies and can be partially explained by nature which produces three basic populations of detrital grains to rivers and beaches (Wentworth, 1922). The first is a pebble population which results from rocks which break along joint or bedding planes. This population is not found in Sturgeon Bank sediments. The second is a sand coarse-silt population which represents the stable residual products from the weathering of granular rocks and the third is a clay population which represents the reaction products of chemical decay of unstable minerals in soil. This sorting by nature results in a scarcity of sediments in the granule to coarse sand (0 to -2ϕ) particles, and fine silts (6 to 8ϕ) particles and suggests that sediments of these sizes must be a mixture of either sand with pebbles or sand or coarse silt with clay and therefore will be more poorly sorted than the pure end members of gravel, sand, or clay.

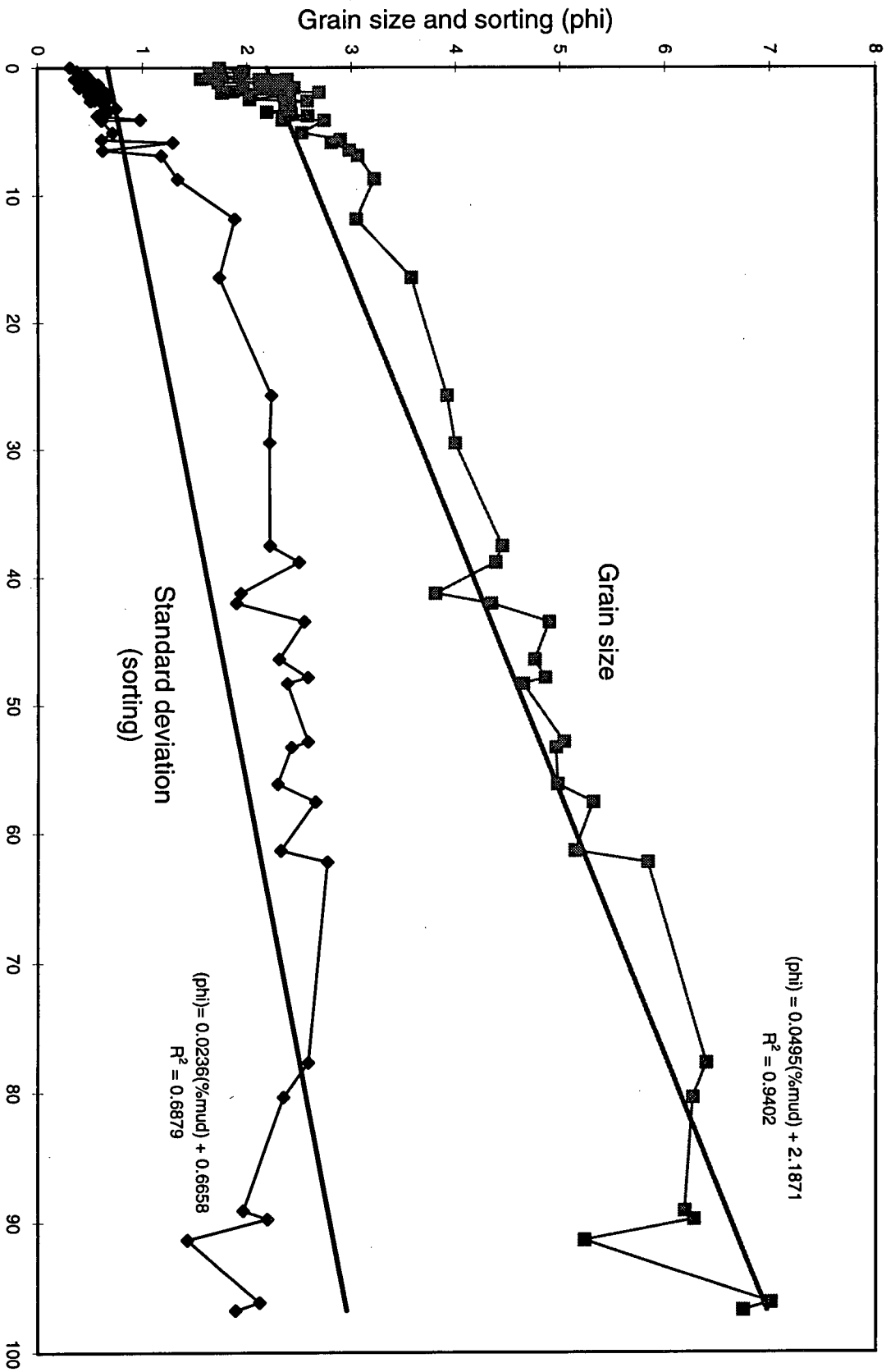

Figure 33: Percent mud versus sorting and grain size (in phi units)

5.3.3. GRAIN SIZE AND SORTING CONTROLS ON ERODIBILITY

The fine-silt sediments collected from station S1 have less clay than the fine-silt sediments from station S2, which is likely the reason for the higher erosion threshold at station S2. Sediments collected from stations S13 and S14, however, both have clay contents over 20% and show much lower erosion thresholds. This may be the result of higher sand contents at these two stations. It seems reasonable to say that sediments with clay contents over ~20% and high silt contents are more difficult to erode than sediments with clay contents over ~20% and high sand contents. Station S3 sediments show a high erosion threshold (relative to stations S13 and S14) despite the low silt and high sand content. The reason for this may be the coarser-grained nature of the sand-sized sediments.

Sediments collected from station S11 contain 99% fine-sand with no clay and consequently erode easily. Fine-sand samples which contain clay require a higher surface shear stress to initiate erosion as stations S4 and S12 demonstrate. The medium-sand samples at stations S5 and S6 show similar erosion thresholds, higher than the fine-sand sediments due likely to the size and weight of the sand grains being eroded.

Sediments which are poorly sorted are more difficult to erode than sediments which are well sorted. This behavior can be seen especially in the fine and medium-sand size fractions. This is not the case in the fine silts where sediments from station S1 are more difficult to erode despite the better sorting than sediments from stations S13 and S14. Station S1 possesses a high surface sediment strength despite its' low clay content, high silt content, and better sorting than the other inner bank stations. It is suggested that some sort of biostabilization on the sediment

surface has taken place at station S1, possibly diatoms.

5.3.4. SEDIMENT GRAIN SIZE VARIABILITY

Station 19 was sampled 5 times in an east-west transect with a sample spacing of 2 metres. Station 19a was the closest to the shoreward edge of the bank while station 19e was the closest to the seaward edge of the bank. All samples were classified as coarse silts with very poor sorting according to the Wentworth and Pettijohn classification schemes. Sand contents varied from 42 to 61 wt. % in the five samples with corresponding silt contents varying from 39 to 27 wt. %. In general there is an increase in sand content (decrease in silt content) in a seaward direction, however sample 19b, closer to the shore contains a higher sand content than its more seaward counterparts, 19c and 19d. Initially the 56 stations sampled for grain size were thought to behave similarly to sediments collected from the 10 Sea Carousel sites. That is, if fine sand sediments were easily eroded at station 11 then fine sand sediments should be easily eroded at other stations on the bank. However, the degree of variability in sediment grain size results within a 10 metre spacing reveals how difficult it is to extrapolate values across the bank. Grain size and their corresponding erodibility results should therefore be assumed to be site specific.

Chapter 6. SEDIMENT GEOCHEMISTRY

6.1. FIELD SAMPLING

Bulk sediment samples were taken from 56 sites on Sturgeon Bank (see Figure 4). The sites corresponded with the grain size sampling stations and geochemical analyses were performed on the same sediment sample as grain size determination. Samples comprise the top two centimetres of sediment at each site and were collected using an 8 cm diameter plexiglass tube pushed into the exposed sediment at low tide on June 30 and July 1, 1992. Five samples were collected at station 19 in a 10 metre east-west transect using 2 metre sample spacing to examine the variability in sediment geochemistry between adjacent samples.

6.2. ANALYTICAL TECHNIQUES

Sediment samples were dried in an oven at 60° overnight and then ground in a tungsten carbide mill for two minutes. Ground samples were analyzed for major and minor element concentration, inorganic and total carbon content, and nitrogen content. Major element compositions were determined on fused glass discs using X-ray fluorescence following Norrish and Hutton (1969) and are reported as wt.% abundance of the element. Minor element compositions were determined on pressed powder pellets using X-ray fluorescence and reported as parts per million (ppm). Total carbon and nitrogen were determined by gas chromatography/thermal conductivity on a Carlo-Erba CNS analyzer (model NA-1500) and carbonate carbon (inorganic carbon) was determined by coulometry. Details of major and minor element analyses, a description of X-ray fluorescence spectrometry, total carbon and nitrogen

analyses, inorganic carbon analyses, major and minor element results, XRF instrument settings, analytical precision and accuracy of all analyses, and carbon/nitrogen analyses are given in Appendix VII - 1, 2, 3, 4, 5, 6, 7, 8, 9, 10, 11, 12, and 13, respectively.

6.3. RESULTS AND DISCUSSION

6.3.1. CONTROLLING FACTORS ON THE COMPOSITION OF SEDIMENTS

Nearshore sediments vary widely in mineralogical composition mainly because they are deposited in environments where physical conditions are continually changing. Sediments are composed of three main components which are detrital, authigenic and biogenous in origin (Calvert, 1976). Detrital components are rocks fragments and minerals derived from the land through geochemical weathering which are subsequently deposited via rivers, ice, or wind. These include insoluble primary minerals and new minerals formed in the weathering environment, principally clays and oxides of iron and aluminum. Authigenic components are those derived from inorganic precipitates which form both in the water and after deposition of the bulk sediment through diagenesis. Biogenous components are those derived from skeletal remains including carbonate, silica and phosphate and the degradation of organic material, including humic materials and other insoluble organics. The elemental composition of a sediment is determined by the influence of each of these components whose proportions can vary widely. On the west coast of Canada the detrital component dominates due to the high precipitation, high relief and (because most of Canada has been glaciated in recent geological history), the large amount of glacial flour produced by the abrasion of bedrock.

Textural control also plays a major role in the elemental makeup of a given sediment and

therefore cannot be overlooked in any geochemical study. Certain elements are enriched in coarser (sand and silt) fractions while others are concentrated in the finer portions (mud and clay) (Calvert, 1976). Therefore, regional comparisons of elemental concentrations can only be made using texturally equivalent sediment size fractions (Loring and Rantala, 1992; Calvert, 1976).

Sediments offer many sites and possibilities for metal associations. Metals may exist as constituent elements present in the insoluble primary minerals produced by physical weathering, also known as the lattice-bound elements. The degree to which minor elements, including trace metals, are incorporated into detrital minerals depends on their ability to substitute for the major ions (i.e. similar ionic radii) in the crystal lattices of the principal rock-forming mineral. Metals may also exist in a variety of secondary forms such as adsorbed on surfaces (coprecipitated with iron and manganese oxides; clays; humic flocs (Francois, 1987)); associated with organic matter (Troup and Bricker, 1975; Carpenter et al., 1975) as a result of either uptake by the living organism or by complexation and chelation; associated with authigenic sulfides in ion-exchange processes during the weathering of clay minerals; in the lattice positions in secondary minerals or in amorphous iron or manganese oxides (Campbell et al., 1988).

Most minor elements show an affinity for fine-grained sediments (Krauskopf, 1979). The surface area of the particles making up the sediments increases with decreasing grain size and therefore, the minor elements being hosted within these minerals will tend to be enriched in the fine-grained material. Organic material and fine-grained sediments tend to be deposited together in low energy environments (Kuenen, 1965; Calvert, 1983). This is because of the adsorptive affinity of fine-grained material for certain organic compounds during deposition (Premuzic, et al., 1982) and the low-density nature of organic debris which allows it to behave hydraulically

equivalent to clay or fine silt sized detritus.

A major source of sediment on the Fraser delta is Pleistocene glacial deposits from the interior of British Columbia (Pharo, 1972). Geochemical analyses in deltaic sediments from Sturgeon Bank have been discussed by Grieve (1977); Grieve and Fletcher (1976); B.C. Research (1973, 1975, 1977); Birtwell et al., (1983) Coastline Environmental Services Ltd. (1985) and provide the most extensive data collected to date. Grieve and Fletcher's (1976) work discovered a close correlation between trace-metal concentrations, sediment texture, and Fe and Mn content. Their studies also indicated that within the sediments, the bulk of the trace metals are present in a non-labile form associated with the detrital silicate minerals and 10-20% are associated with hydrous oxides of Fe (and Mn) which form coatings on detrital grains. The authors concluded that the dominant controls on trace-metal distribution patterns on the delta-front and upper fore-slope were the physical processes influencing sediment transport and size-fractions distributions. All studies on the geochemistry of sediments on Sturgeon Bank found abnormally high concentrations of labile trace metals in sediments adjacent to the Iona sewage treatment plant where discharge of metal rich sewage took place from 1962 until 1988. Unfortunately, results of the sediment geochemical studies to date have been determined using a variety of analytical methods and therefore caution should be exercised when comparing results. Total element analyses are easier to compare than analyses which extract only a certain component of the minor elements (i.e. the labile component) unless the analytical techniques are the same. It is however, more difficult to determine what is biologically available to organisms using the total element analytical method.

6.3.2. MAJOR ELEMENTS

6.3.2.1. *Aluminum*

Feldspars, micas, pyroxenes and amphiboles are important Al-bearing minerals (Rankama and Sahama, 1950). The distribution of Al in sediments likely reflects the distribution of fine-grained material associated with the minerals described above. The Al% content in sediments on Sturgeon Bank ranges from 5.0 to 7.2 ± 1.05% by weight with the highest concentrations in the fine silt-rich sediments at stations 21 and 40 (Figure 34). The lowest concentrations were found on outer southern Sturgeon Bank, stations 33, 44 and on a small area north of the middle Arm at station 16. Aluminum correlates negatively with grain size ($r = -0.77$) (Figure 35) indicating concentration in the finer size fraction; it is therefore a reasonable proxy for grain size.

6.3.2.2. *Silicon*

The distribution of silica in sediments likely reflects the distribution of quartz, a resistant mineral left after weathering that dominates the sand and silt size ranges. It tends to be found in the coarser fractions of sediments and to accumulate in turbulent depositional environments where finer-grained sediment constituents such as clay minerals and organic matter are resuspended (Rankama and Sahama, 1950). The content of silicon in surface sediments from Sturgeon Bank varies from 29.7 to 36.9 wt. % ± 0.85% (Figure 36). These values are up to twice those obtained from sediments in Howe Sound (Drysdale, 1990) and could reflect the differing grain sizes present in these environments. The highest concentrations for this study were found on outer Sturgeon Bank, in particular at station 54 in the medium sand size fraction, and at stations 48 and 35. The lowest concentrations were found at stations 21 and 40. This

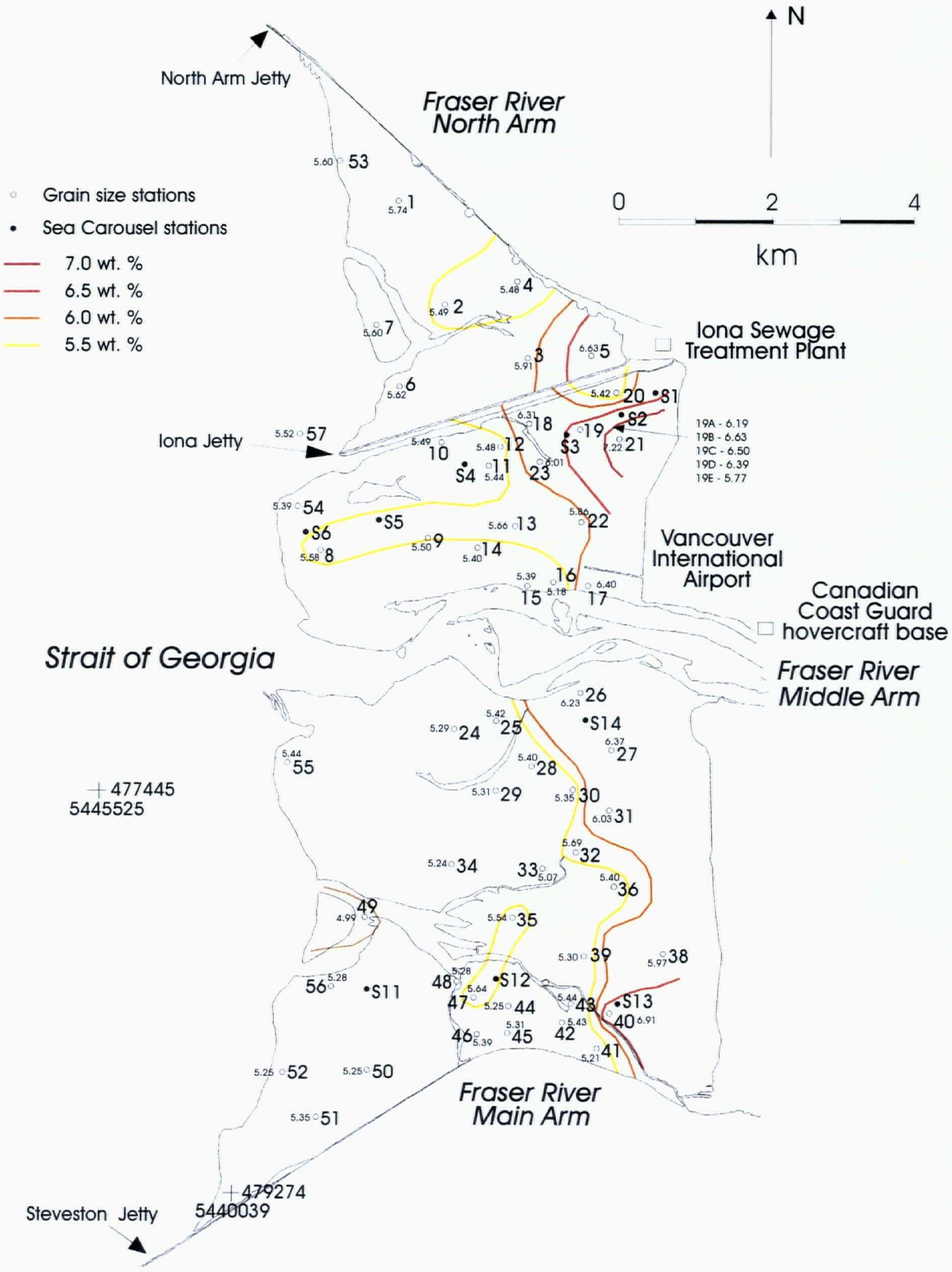

Figure 34. Areal distribution of aluminum content on Sturgeon Bank

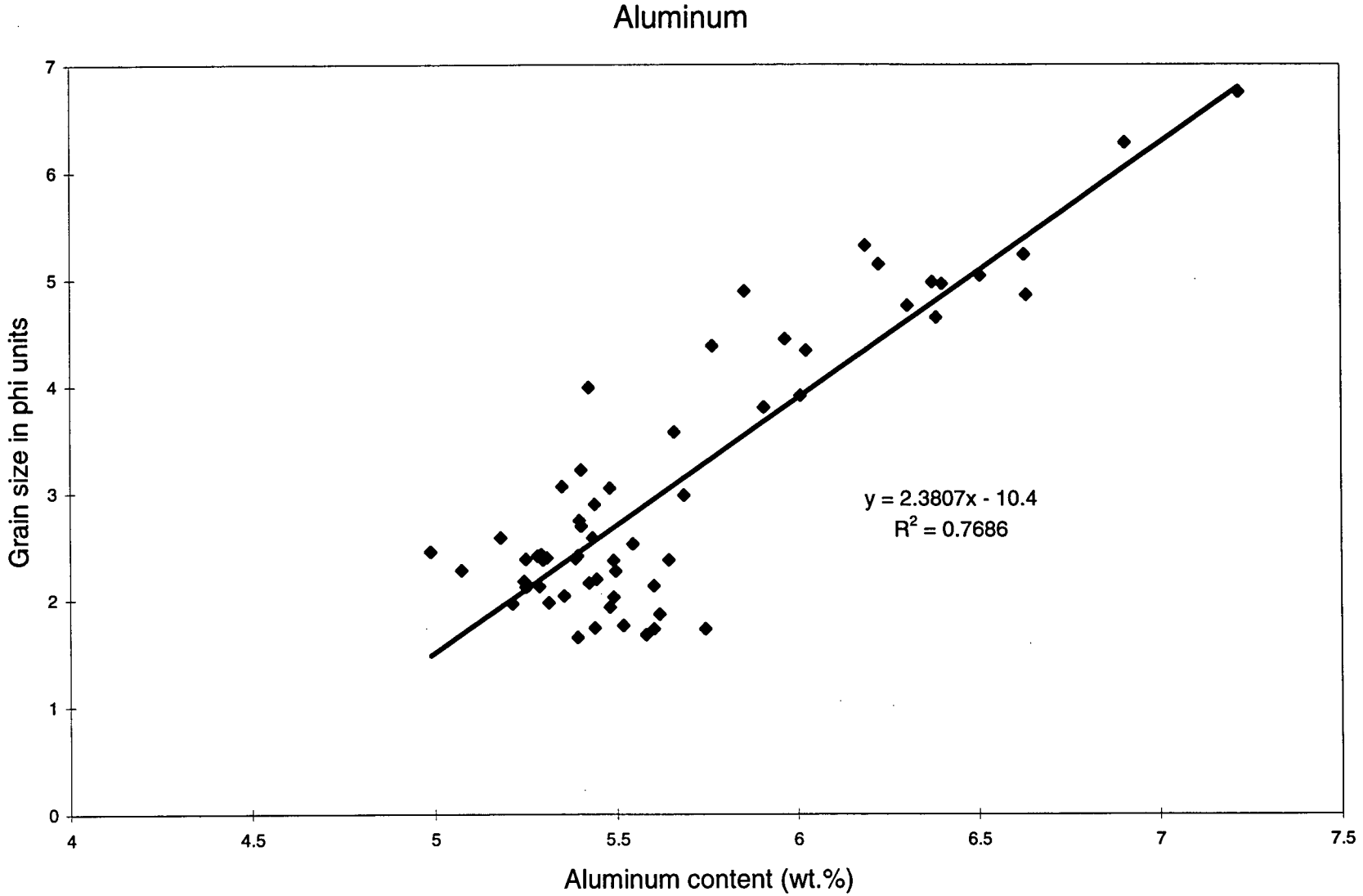

Figure 35: Aluminum content versus grain size

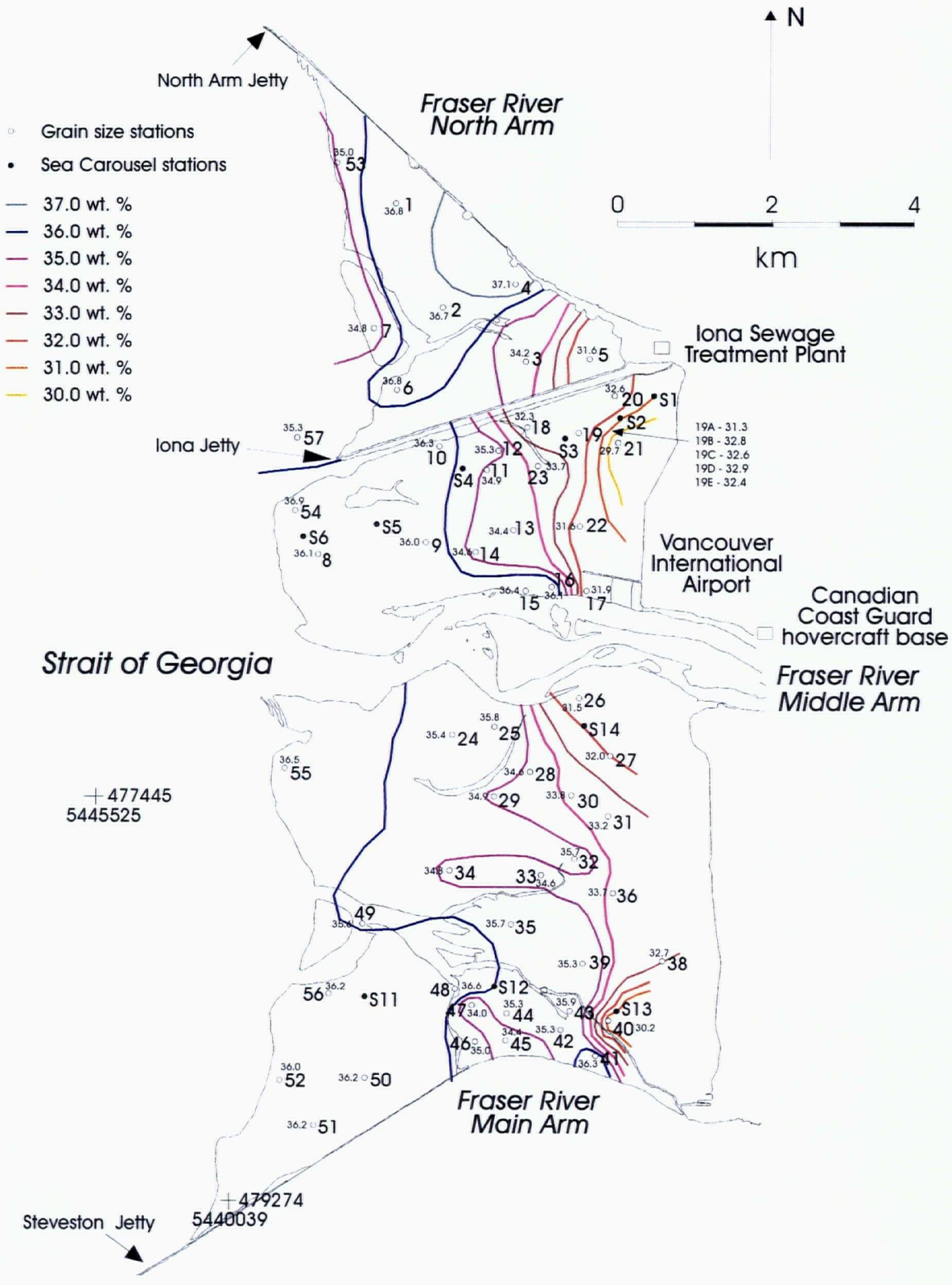

Figure 36: Areal distribution of silicon content on Sturgeon Bank

distribution shows the opposite trend to Al, as expected, because Si is more enriched in the coarser-grained sediments. Silica correlates positively with grain size (r = +0.87) (Figure 37) and is indicative of quartz enrichment in the sand and coarse silt size fractions.

The variation of elemental concentrations in sediments does not necessarily reflect the input of certain minerals, since varying degrees of dilution by other components may be operating (Calvert, 1976). In order to avoid misinterpretation of data caused by these effects, ratios of one element to another are commonly used rather than the absolute abundance of an element. Aluminum is often used to normalize element concentrations because it is an element essentially exclusive to silicate minerals. In this way it can be used to determine whether changes in elemental concentrations represent changes in mineralogy of the source rocks or whether they are due simply to dilution by other materials. The areal distribution of the Si/Al ratio varies from 4.11 to 7.13 with the highest values occurring on the outer bank of central and southern Sturgeon Bank and the lowest values occurring at stations 21 and 40 (Figure 38). These ratios are higher than those obtained by Drysdale (1990) in Howe Sound sediments and Francois (1987) in Saanich Inlet sediments.

6.3.2.3. *Titanium*

The concentration of titanium in sediments on Sturgeon Bank ranges from 0.2 to 0.7 wt.% ± 0.85% (Figure 39). The highest values occur on the inner bank and at station 14. The highest content was found at station 36 with a noticeable difference in Ti content between stations 40 and 41, 510 metres apart. The grain size difference between these two stations is likely the cause of such wide variation as station 40 is composed of fine silt and station 41 is composed of medium

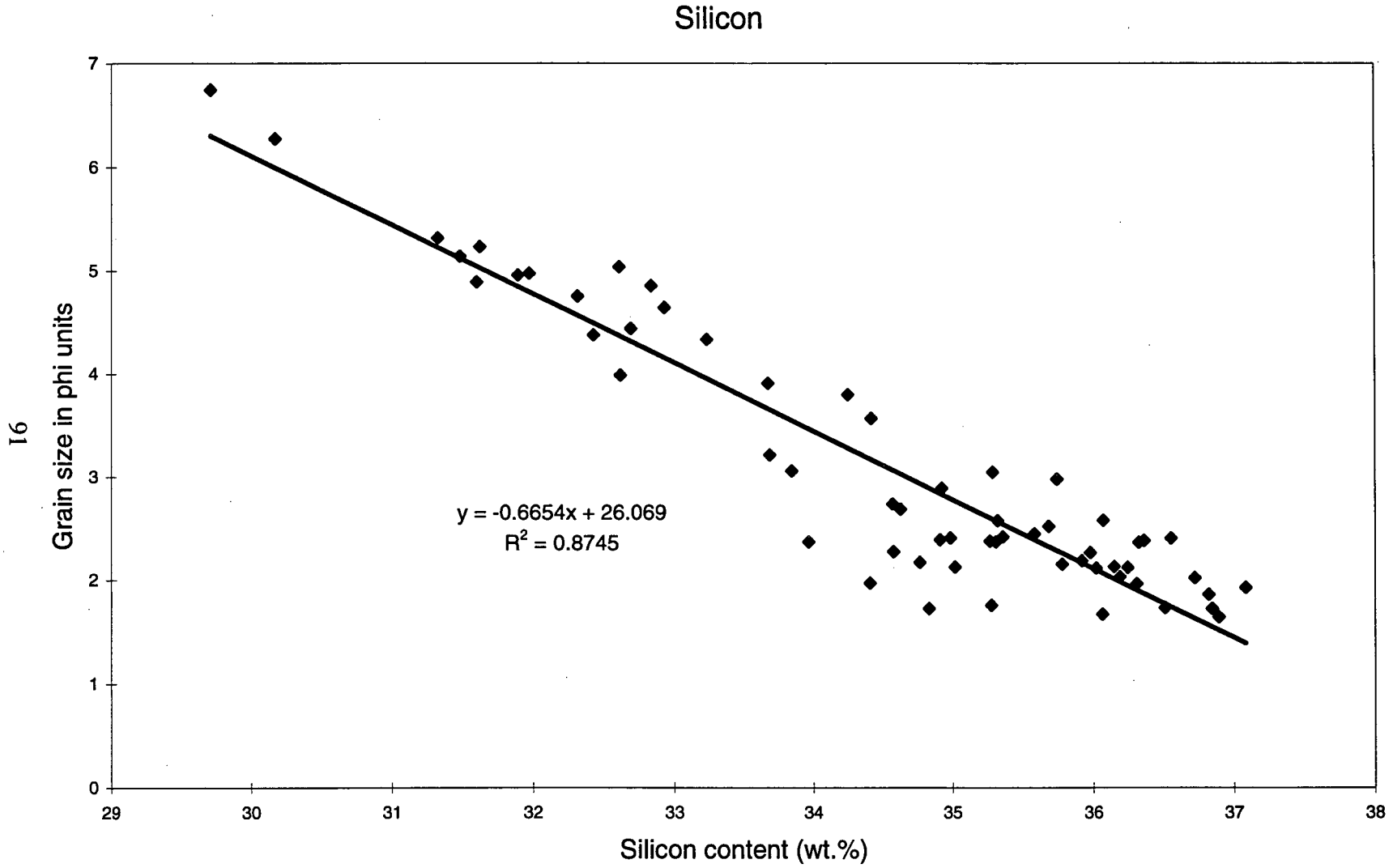

Figure 37: Silicon content versus grain size

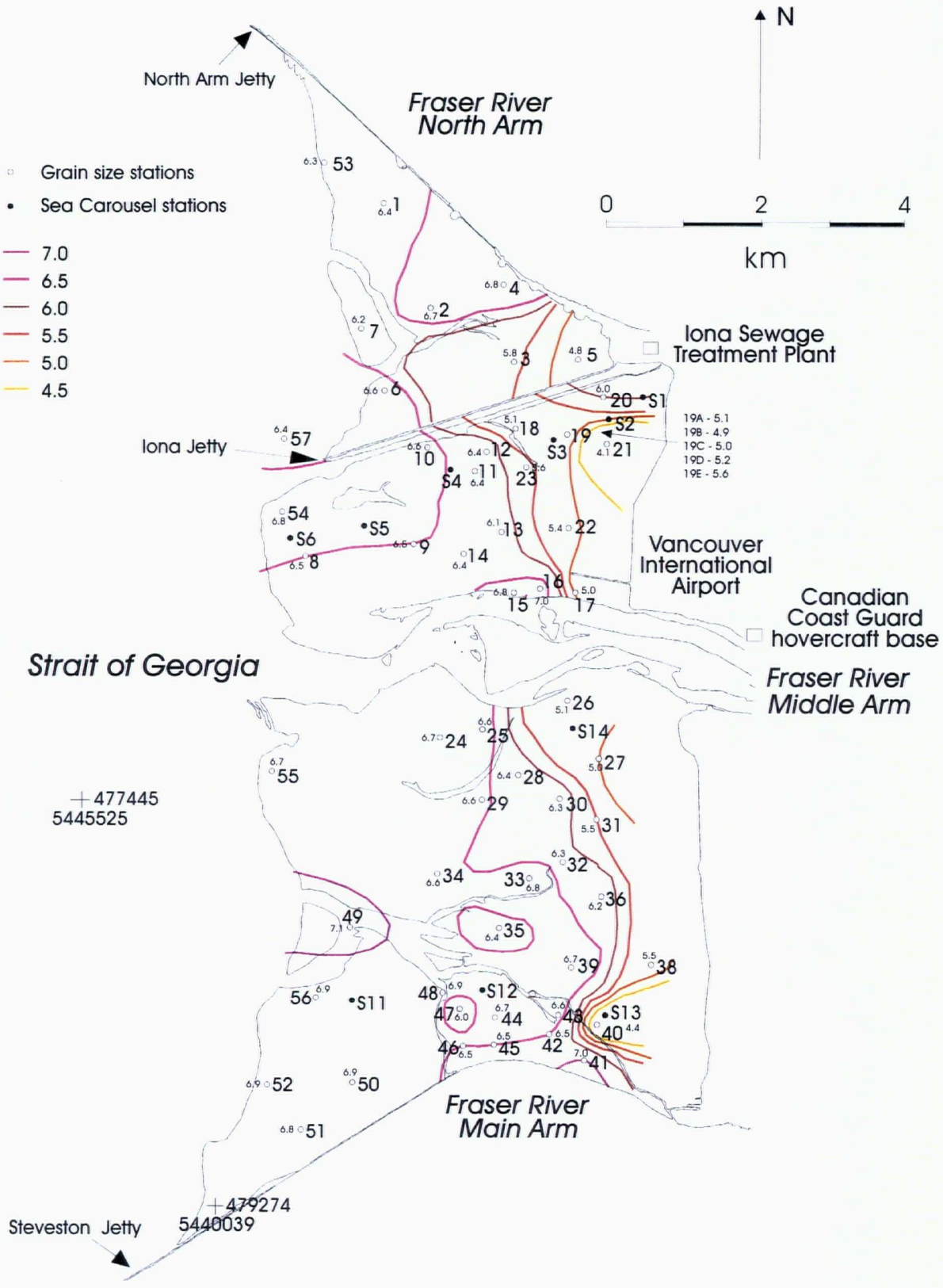

Figure 38: Areal distribution of Si/Al on Sturgeon Bank

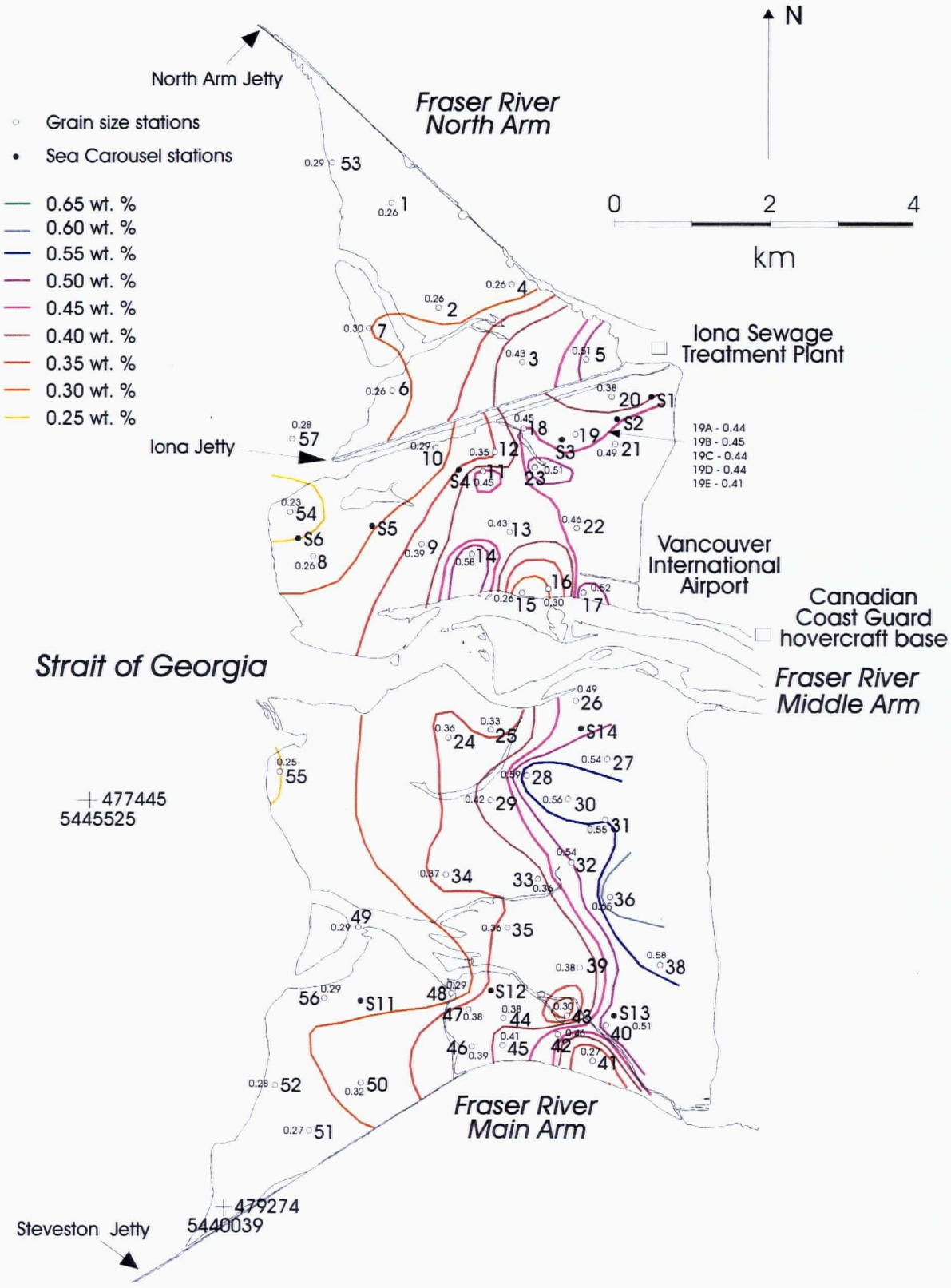

Figure 39: Areal distribution of titanium content on Sturgeon Bank

sand. Titanium may occur in marine sediments as ilmenite ($FeTiO_3$), rutile (TiO_2), anatase (TiO_2) or brookite (TiO_2) which are refractory oxides concentrated in the sand fraction, as finely disseminated cryptocrystalline rutile which adsorbs to clay minerals in the finer fraction, or substituting for Al in clay minerals (Rankama and Sahama, 1950; Degens, 1965). The distribution of Ti/Al reflects the distribution of Ti with the highest ratios present in sediments from stations 14, 28, 30, 36 and 38 (Figure 40).

Titanium correlates only reasonably positively with grain size (r= +0.44) (Figure 41a) suggesting that the element is concentrated in the fine to very fine sand fraction of sediments on the bank. Medium sand-dominated sediments show Ti contents generally less than 0.5 wt. %. In contrast, titanium shows a positive correlation with iron (r = +0.89) (Figure 41b) indicating that Ti-content may be largely due to the iron-bearing clay mineral phase associated with ilmenite. However ilmenite is likely only present as a trace constituent and therefore the host for Ti in Fe-bearing minerals is not known.

6.3.2.4. *Iron*

Iron occurs in detrital sediments in illite, ferro-magnesian micas, amphiboles (general formula: $W_{0-1}X_2Y_5Z_8O_{22}(OH)_2$, pyroxenes (general formula: $XYSi_2O_6$) (where W cations include Na and K, X cations include Ca, Mg, Fe and Y cations include Mg, Fe, Al), some K-feldspars, and in the authigenic mineral glauconite $[(K,Na)(Fe^{3+},Al,Fe^{2+},Mg)_2(Si,Al)_4O_{10}(OH)_2]$ (Rankama and Sahama, 1950). Dissolved Fe usually flocculates as it passes from fresh into saline waters (by ~ 15‰) where it is then incorporated into hydroxide and oxyhydroxide coatings on mineral particles (Burton and Liss, 1970). The most common hydroxide and oxyhydroxide phases in oxic

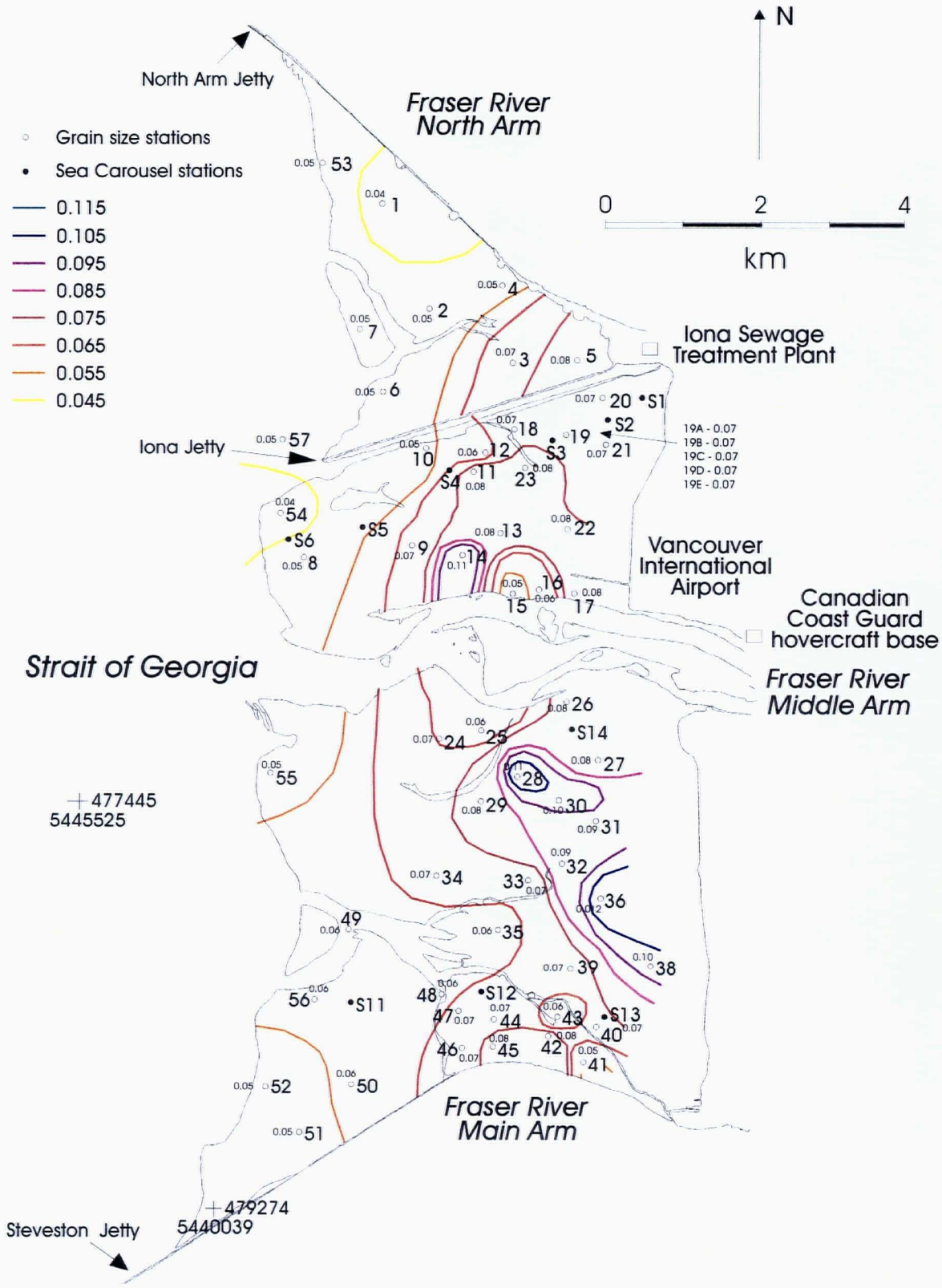

Figure 40: Areal distribution of Ti/Al on Sturgeon Bank

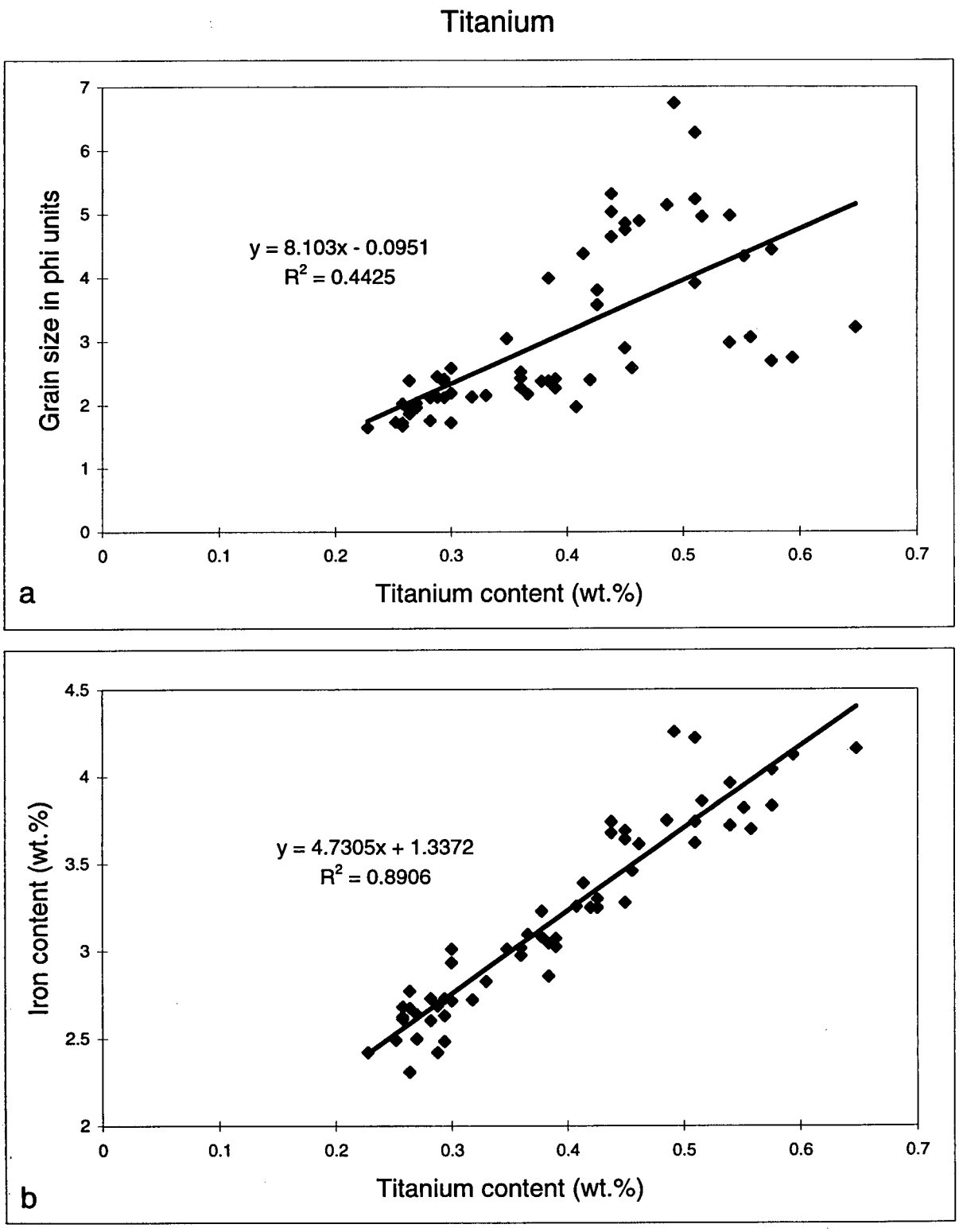

Figure 41: (a) Titanium content versus grain size
(b) Titanium content versus iron content

sediments are hematite (Fe_2O_3), geothite ($\alpha FeO(OH)$) and lepidocrocite ($\gamma FeO(OH)$) (Degens, 1965) while the most common hosts in anoxic sediments are pyrite (FeS_2) and siderite ($FeCO_3$) (Krauskopf, 1979).

Iron concentrations in the sediments on Sturgeon Bank range from 2.3 to 4.3 wt.% ± 3.4%, are highest at stations 21 and 40 and other stations on the inner bank, and decrease in concentration seaward (Figure 42). Sediments collected from stations 15 and 16 contain considerably less Fe than others in the same area. The plot of Fe/Al ratios in surface sediments show values ranging from 0.42 to 0.77 (Figure 43). Ratios on northern Sturgeon Bank are highest on the inner bank but lower concentrations are found adjacent to the north arm jetty but then increase seaward. Sediments on the central bank show Fe/Al ratios which increase seawards with the exception of station 20 where low values were found and station 14 where high values were found. Southern Sturgeon Bank sediments show a similar trend to those on the northern and central banks with the addition of local highs in Fe/Al ratio located at stations 28 and 36.

Iron shows good positive correlation with grain size (r= +0.60) with the highest concentrations generally occurring in the finest grained sediments (Figure 44a). There is, however, a significant addition of coarser grained sediments with high Fe contents such as station 45 (medium sand), stations 14, 28, 32 and 42 (fine sand) and stations 23, 30 and 36 (very fine sand). The high Fe content in some fine sands may be the result of some Fe-bearing sand-sized material such as the mineral pyrite (FeS_2) or more likely the mineral magnetite (Fe_3O_4). Chlorite [$(Mg,Al,Fe)_3(Si,Al)_4O_{10}(OH)_2 \cdot (Mg,Al,Fe)_3(OH)_6$] is likely associated with the coarsest-grained clay-sized sediment and therefore the higher Fe in some coarse silts and very fine sands may be due to the presence of Fe-rich chlorite which is common in the Fraser River sediments (Pharo,

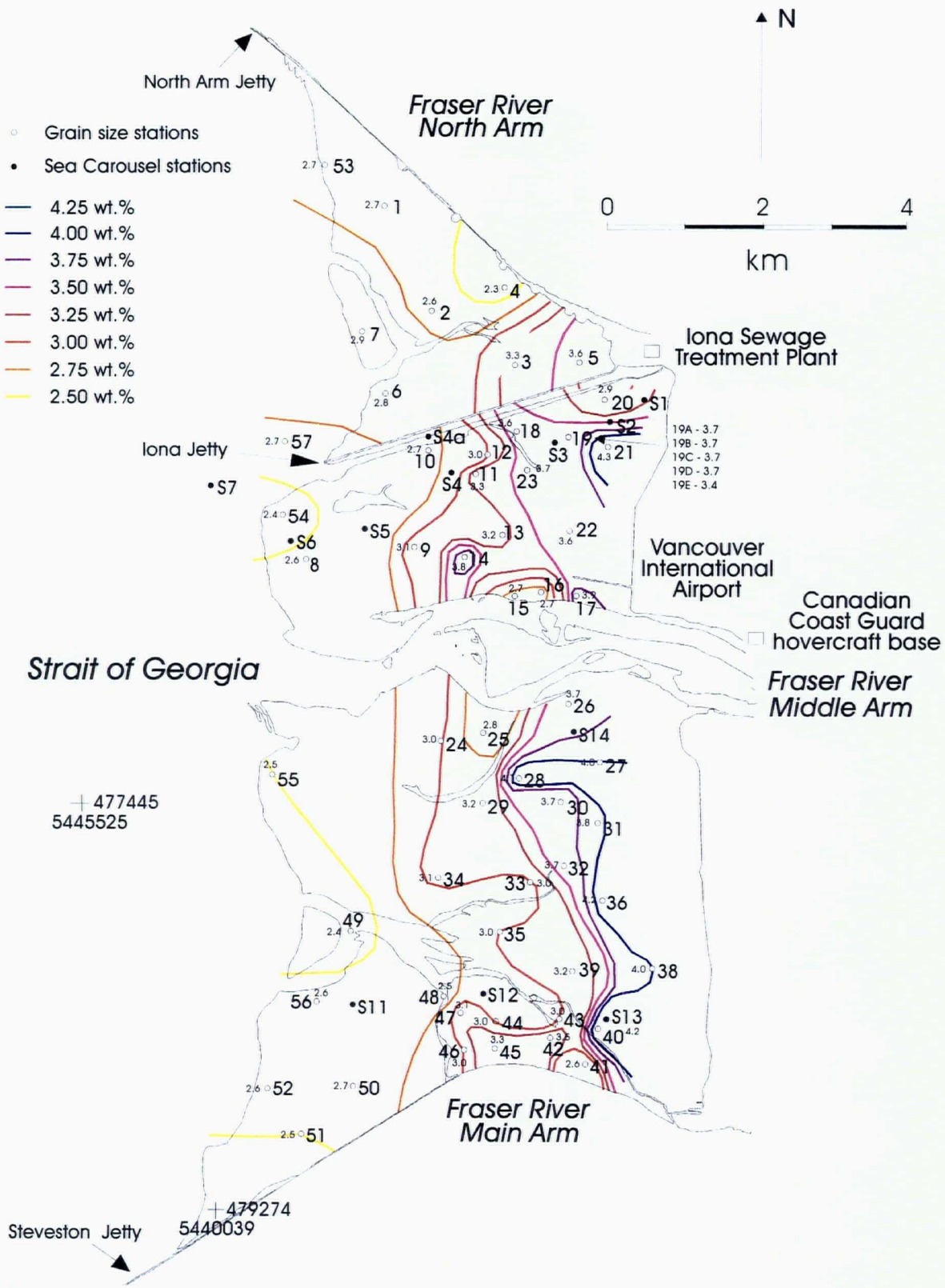

Figure 42: Areal distribution of iron content on Sturgeon Bank

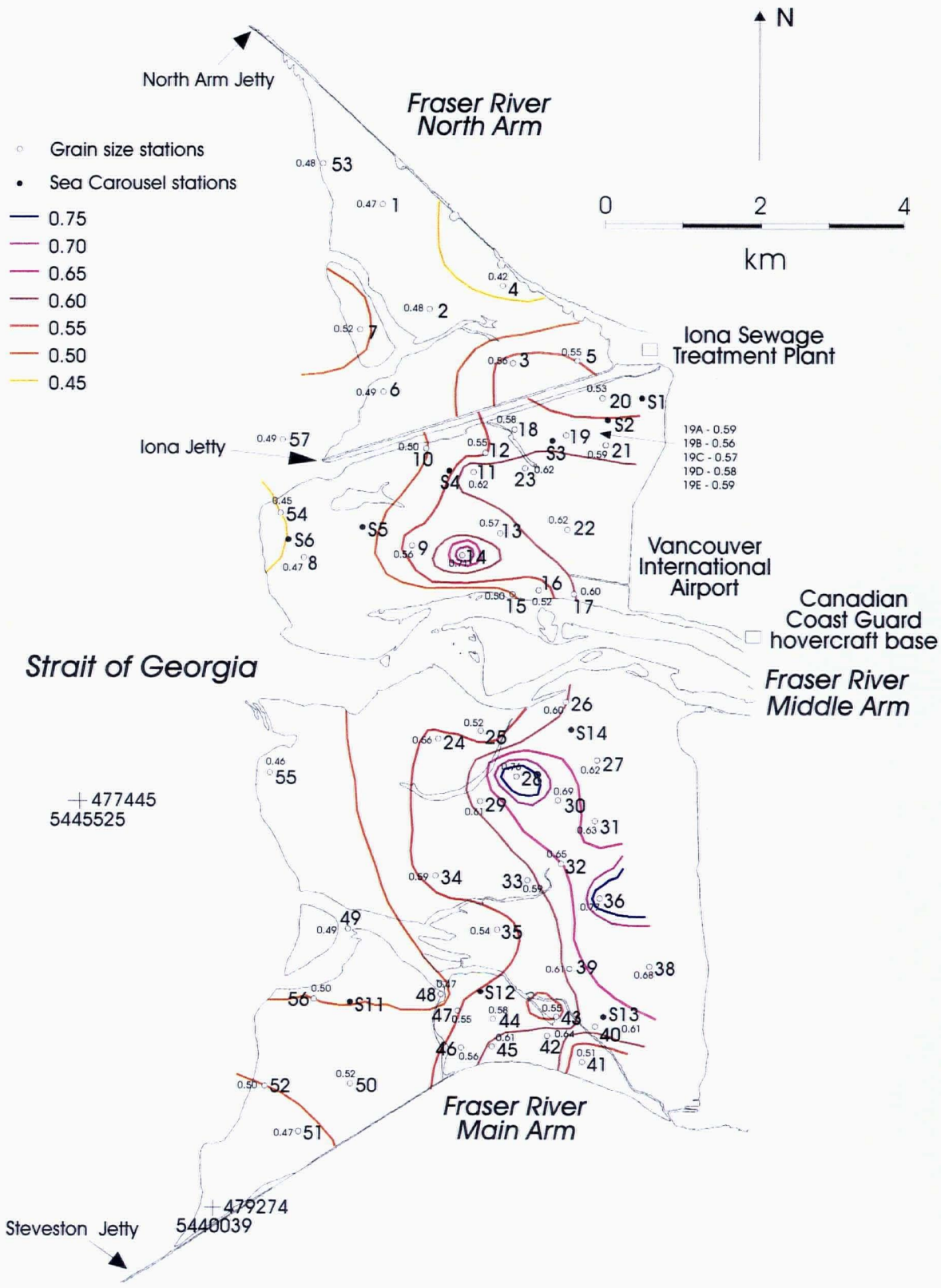

Figure 43: Areal distribution of Fe/Al on Sturgeon Bank

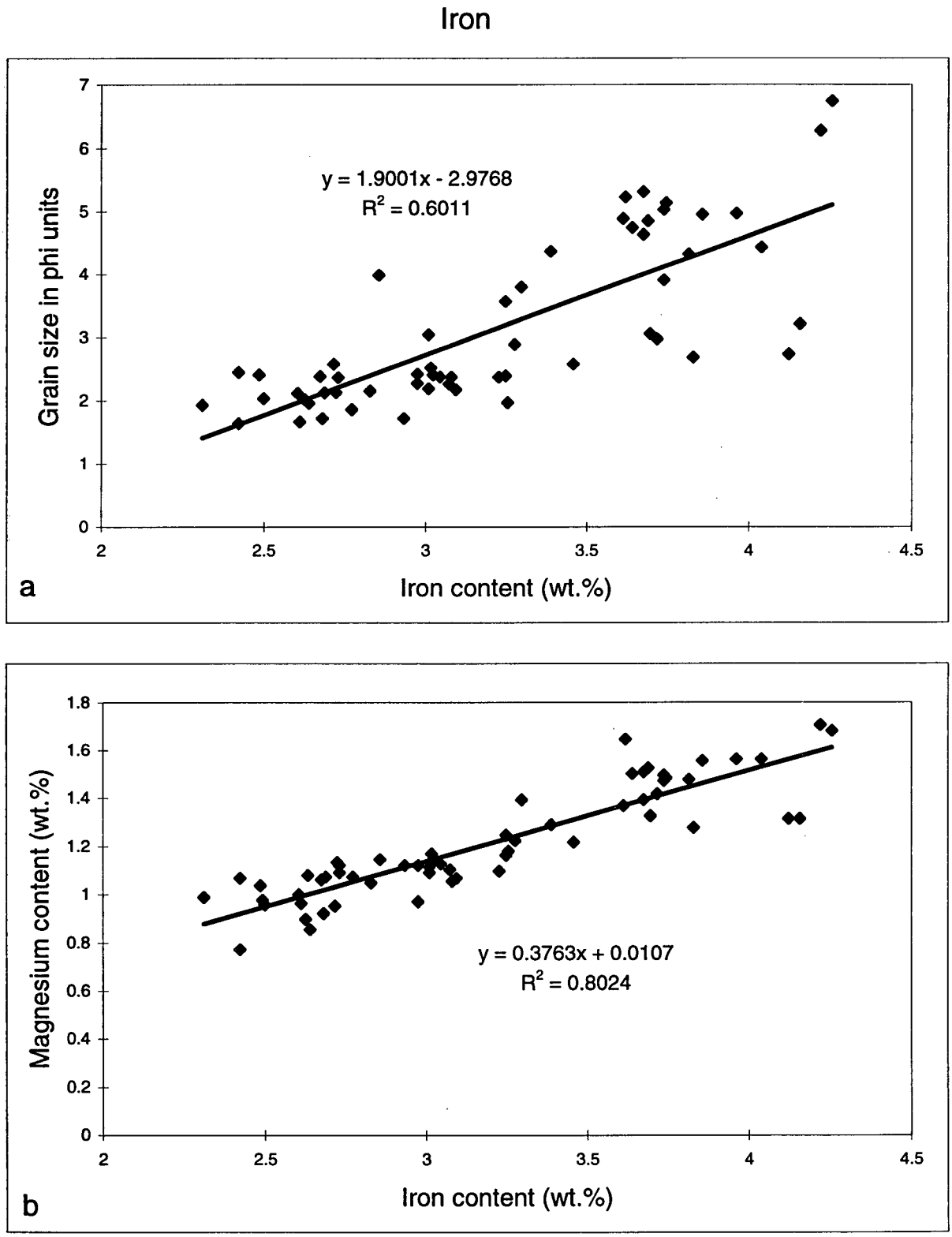

Figure 44: (a) Iron content versus grain size
(b) Iron content versus magnesium content

1972). Iron-rich sediments could therefore be indicative of Fraser River source material. The observation that chlorite may be responsible for a large part of the iron content found on Sturgeon Bank is consistent with the positive correlation between Fe and Mg (r= +0.80) shown in Figure 44b. The Fe and Mg correlation may also be due to biotite-vermiculite $[K_2(Mg,Fe)_3AlSi_3O_{10}(OH,O,F)_2]$-$[(Mg,Ca)(Mg,Fe^{2+})_5(Fe^{3+},Al)(Si_5,Al_3)O_{20}(OH)_4 \cdot 8H_2O]$ or hornblende $[(Na,K)_{0-1}Ca_2(Mg,Fe^{2+},Fe^{3+},Al)_5(Si,Al)_8O_{22}(OH)_2]$; however, iron and potassium correlate poorly (r= +0.38) and indicate that the influence from Fe-K minerals (eg. biotite) is negligible. The strong correlation between Fe and Mg indicates that most of the iron present on Sturgeon Bank is associated in lattice-bound form rather than as oxides and therefore is not likely biologically available to organisms.

6.3.3. CARBON AND NITROGEN

Primary production in estuaries contributes organic carbon to the environment along with contributions from terrestrial drainage and anthropogenic activity in and around the estuary. The distribution of organic carbon in Sturgeon Bank sediments is shown in Figure 45. High values (> 0.5% ± 4.84 % by weight) are found at stations 5, 17, 18, 19, 21 and 40 with stations 3, 12, 13, 16, 20, 23, 45, 26, 27, and 31 also demonstrating C_{org} enrichments. The highest C_{org} value was found at station 21 (1.11%) adjacent to the once active Iona sewage outfall. All other stations on the bank have C_{org} contents of less than 0.2% by weight. These values are fairly typical of many nearshore estuarine environments (for example, Calvert, 1976; Krom and Sholokovitz, 1977; Rosenfeld, 1979; Francois, 1987; McNichol et al., 1988 and Drysdale, 1990) which have high marine productivity and/or high terrigenous inputs.

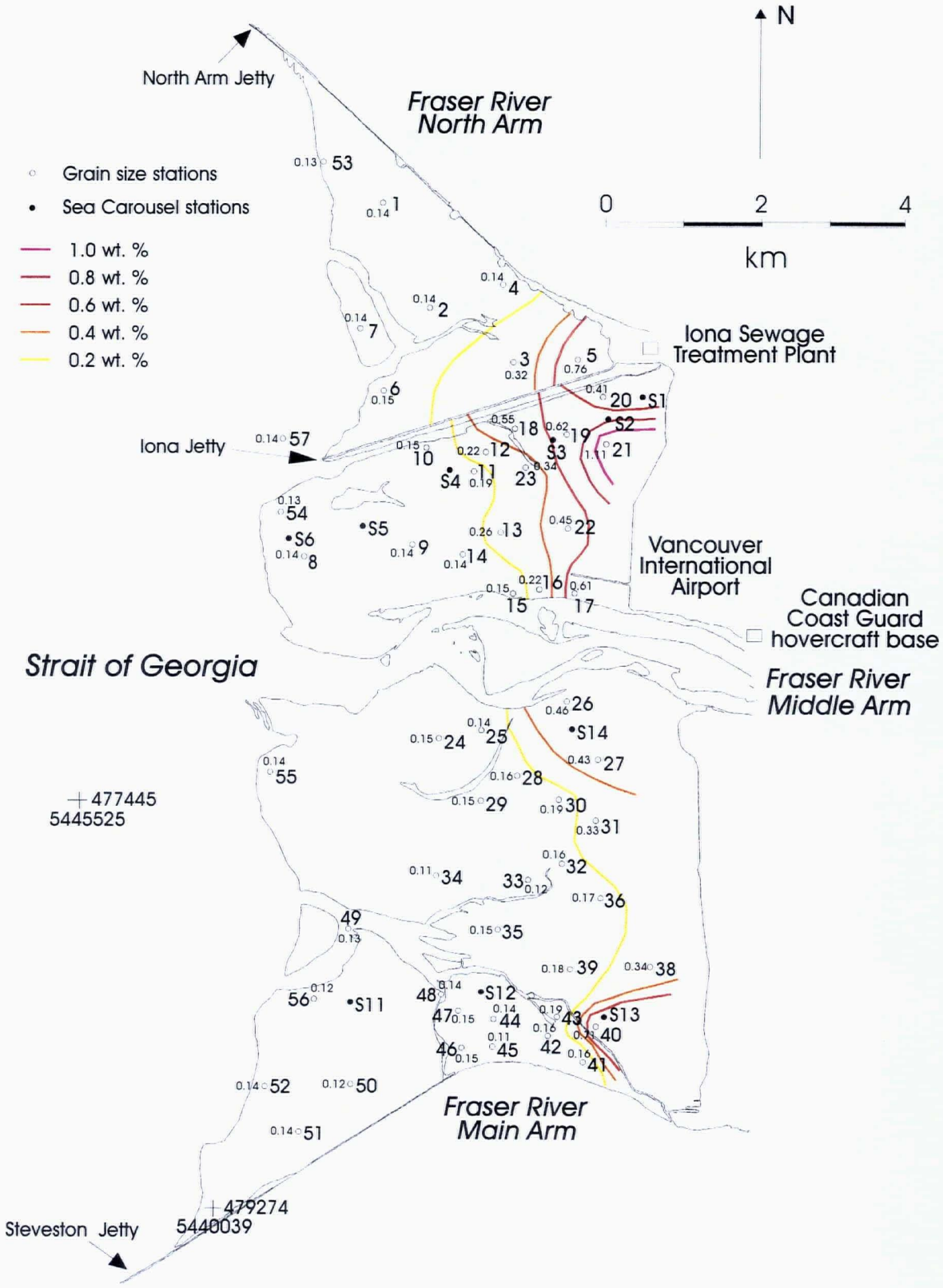

Figure 45: Areal distribution of organic carbon on Sturgeon Bank

The positive correlation between C_{org} and grain size is very good (r = +0.88) showing a decrease in grain size with a corresponding increase in C_{org} (Figure 46) confirming that hydraulic sorting plays a major role in determining the organic carbon content and explaining the preferential accumulation of organic carbon in fine-grained sediments. It is clear then that textural controls dominate the content of organic carbon on the bank but the composition of organic carbon depends on its source.

C_{org}/N ratios for terrestrial material are generally higher (> 15) because terrestrial material (leaves, bark etc.) contain less nitrogen than marine plankton (C_{org}/N ~ 6). C_{org} /N ratios are therefore used as an index of the relative contributions of marine and terrestrial material (Borodowskiy, 1965; Müller, 1977). Organic carbon/nitrogen ratios in Sturgeon Bank sediments range from 4.9 at station 44 to 13.6 at station 5 (Figure 47). The highest C_{org}/N ratios occur in the coarse silt-dominated fraction. The highest C_{org} value was found at station 21 and is accompanied by a C_{org}/N value of 8.71 whereas lower C_{org} contents at stations 5, 17, 26, and 40, have C_{org}/N ratios greater than 11. These results indicate that high C_{org}, low C_{org}/N sediments found at station 21 and stations adjacent to the once active Iona outfall are potentially more reactive than fine-grained sediments elsewhere on the bank.

6.3.4. MINOR ELEMENTS

Minor elements occur in concentrations of a few tenths of a percent or less by weight (Richardson and McSween, 1989) and their geochemistry is affected by changes in temperature, salinity, pH and redox potential of the waters that surround them (Troup and Bricker, 1975). Therefore minor elements participate in a variety of biogeochemical reactions in the water and

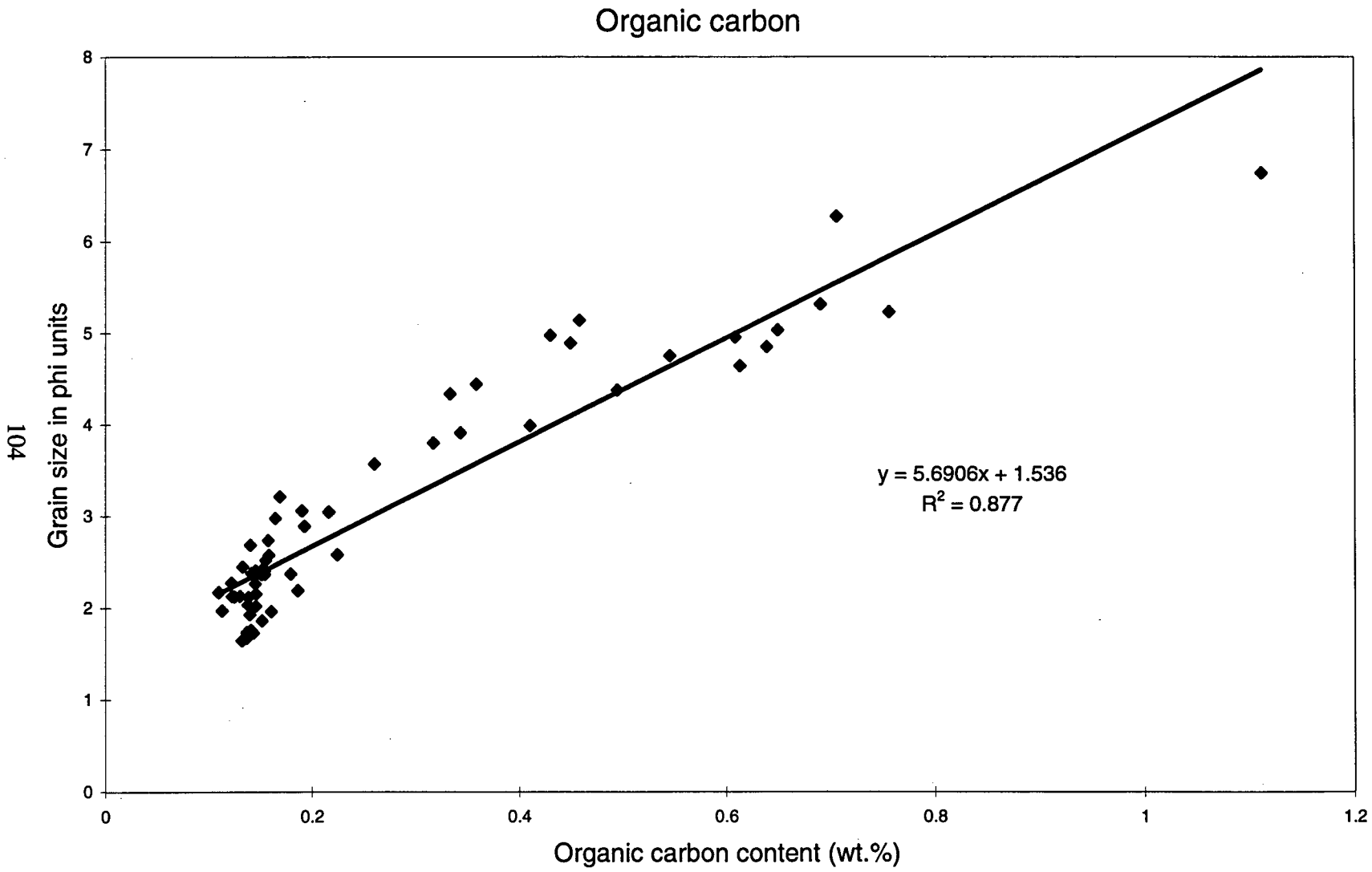

Figure 46: Organic carbon content versus grain size

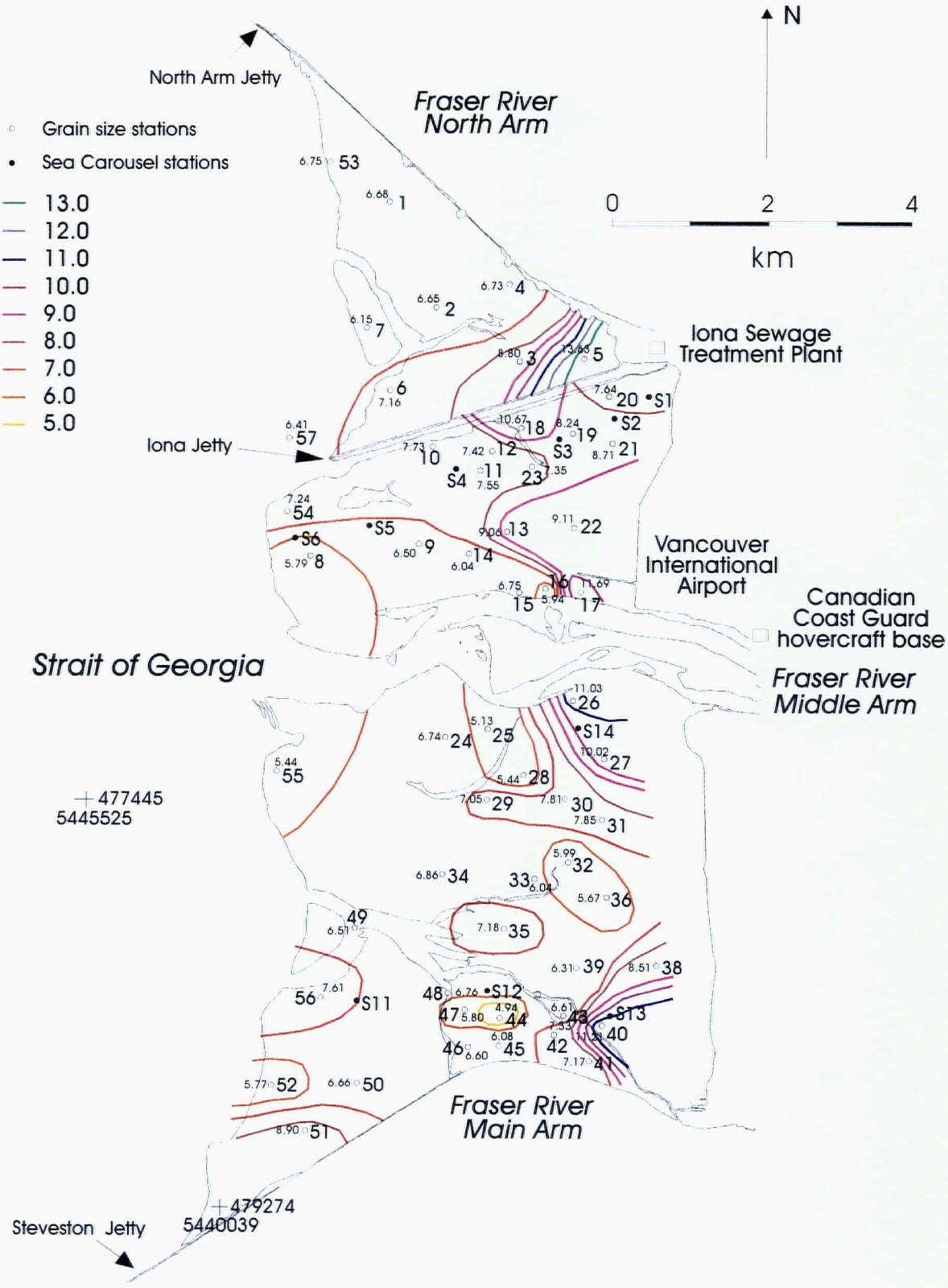

Figure 47: Areal distribution of C(org)/N on Sturgeon Bank

sediments unlike most major elements which behave nearly conservatively (Troup and Bricker, 1975). The concentrations of minor elements in sediments depends in part on their ability to substitute for the major ions in the crystal lattices of principal minerals (Krauskopf, 1979).

6.3.4.1. *Cobalt*

Cobalt is a transition metal with an ionic radius similar to Fe and Mg and therefore it substitutes for these major elements in the crystal lattices of early-forming Fe and Mg minerals of ultramafic rocks (olivine and pyroxene groups) and some basalts (Rankama and Sahama, 1950). Cobalt forms no independent minerals in igneous rocks; however it substitutes for iron in the pyrite and sphalerite structures forming minerals like CoS_2 (cattierite), Co_3S_4 (linnaeite; 51% Co), CoAsS (cobaltite; 35.4%Co) and $CoAs_{3-2}$ (smaltite; ~ 28% Co) (Rankama and Sahama, 1950). The bulk of cobalt found in igneous rocks is incorporated in silicate minerals.

The elemental abundance of Co in sediments on Sturgeon Bank ranges from 40 ppm to 138 ppm ± 28.86% (Figure 48), significantly higher than values found in Howe Sound sediments (Drysdale, 1990) and in reported values for shales, sandstones and sediments (Mason and Moore, 1982). Cobalt is enriched in sediments from stations 5, 12, 20, 25, 29, 30, 48 and 52 with stations 4, 18 and 22 showing the highest concentrations. The plot of Co/Al distribution in surface sediments show high local values at stations 4, 12, 18, 20, 22, 25, 29, 30, 48 and 52 with highest values found at stations 4 and 22 (Figure 49).

The Co vs. grain size plot shows no correlation; however it does illustrate that the fine silt sediments contain the lowest Co contents (Figure 50a). The coarse silt sediments have Co concentrations ranging from 32 to 138 ppm covering almost the entire range of Co content found

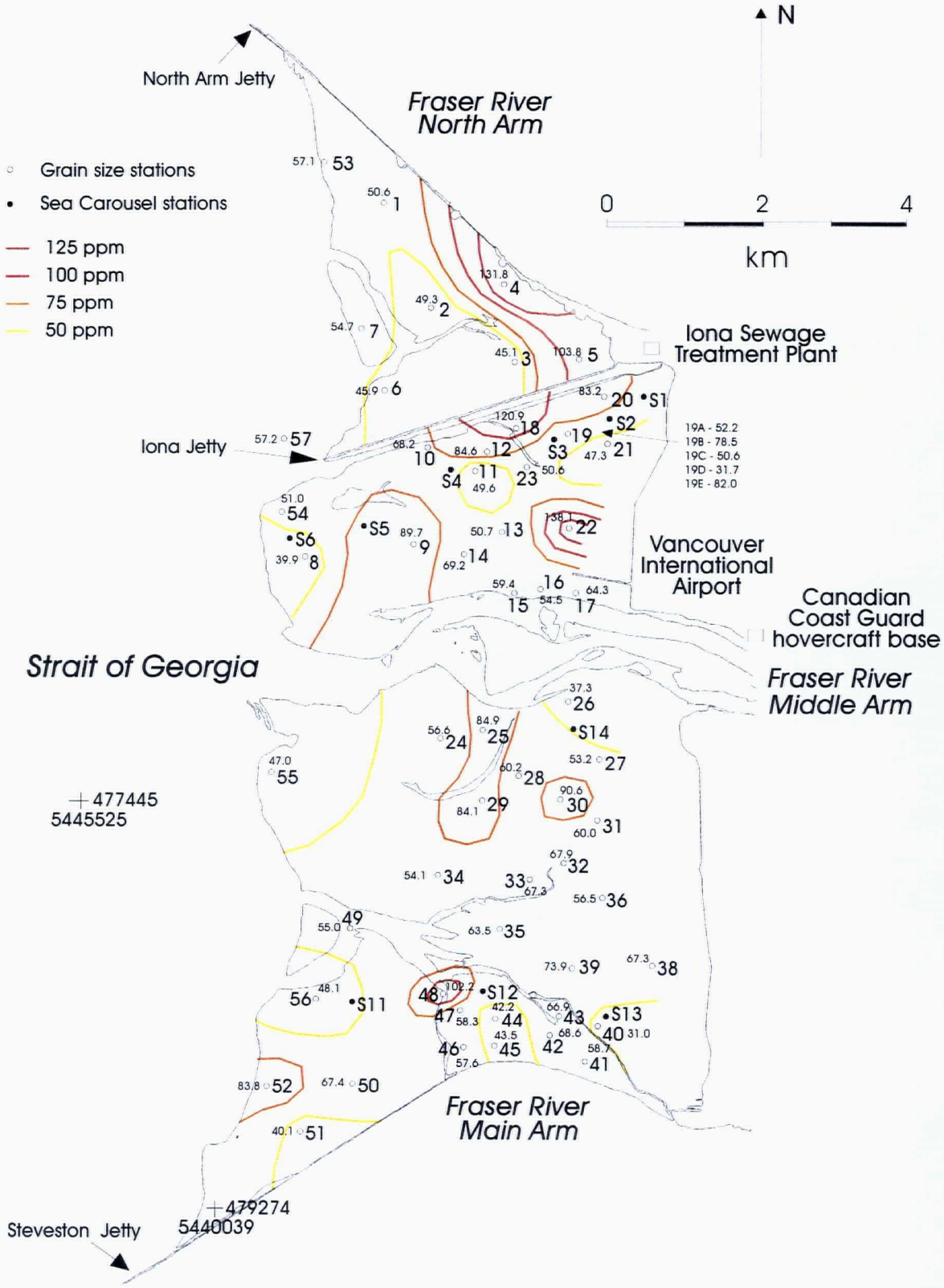

Figure 48: Areal distribution of cobalt content on Sturgeon Bank

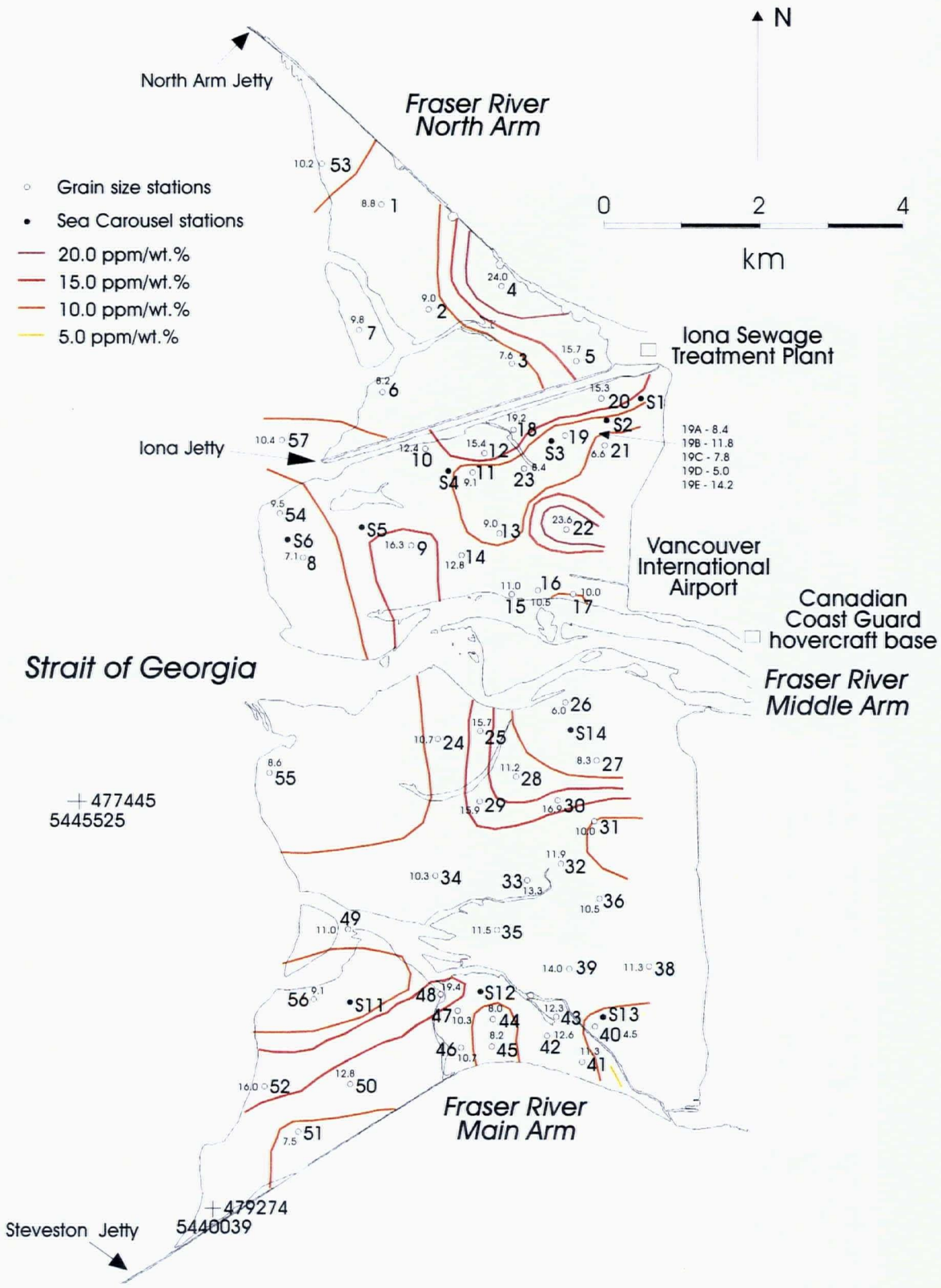

Figure 49: Areal distribution of Co/Al on Sturgeon Bank

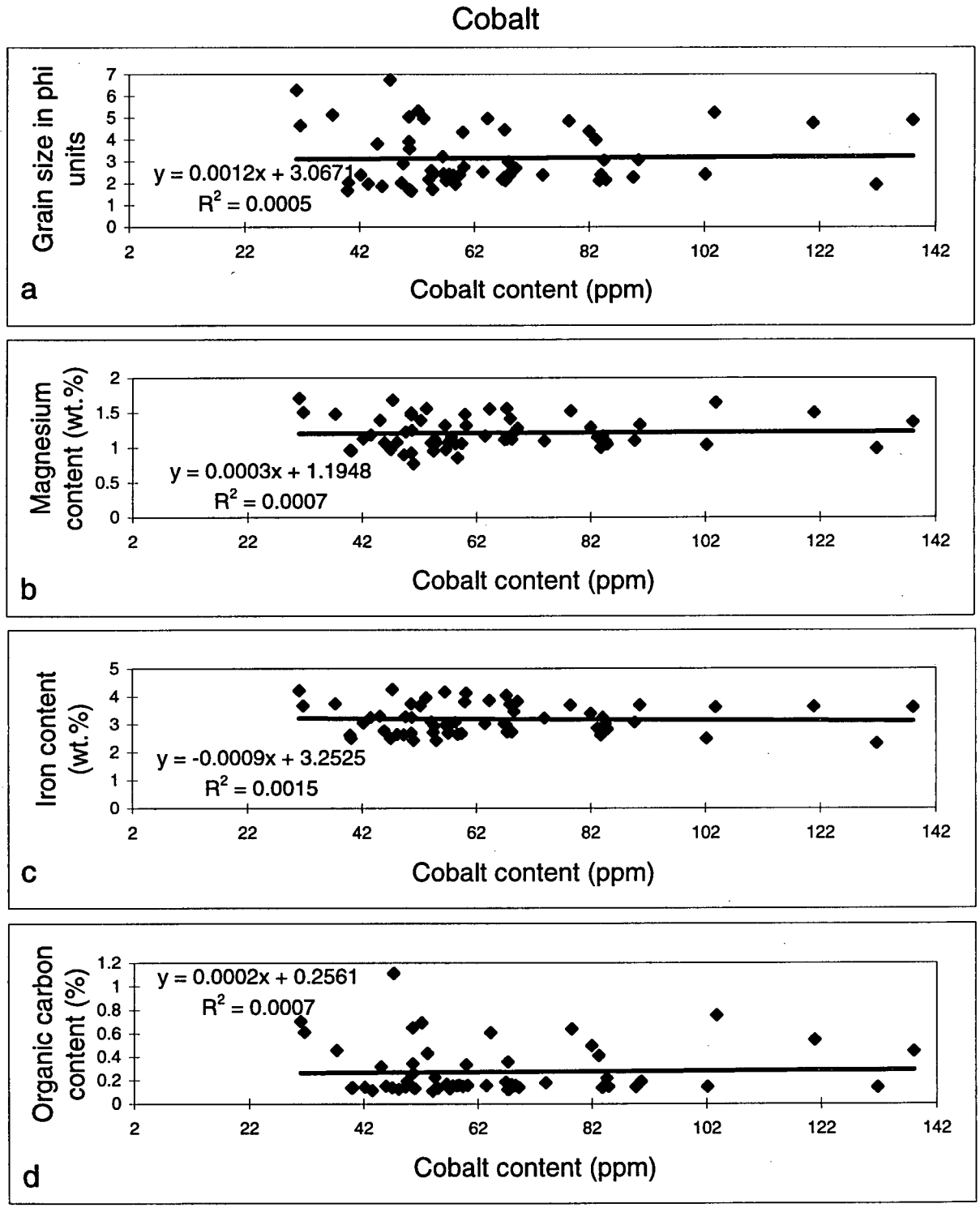

Figure 50: (a) Cobalt content versus grain size
(b) Cobalt content versus magnesium content
(c) Cobalt content versus iron content
(d) Cobalt content versus organic carbon content

in sediments on Sturgeon Bank. Cobalt content in medium sands is generally in the 40 to 60 ppm range with the exception of station 4 where Co content reaches 132 ppm. No correlation between Co vs. Mg (Figure 50b), Co vs. Fe (Figure 50c) or Co vs. C_{org} (Figure 50d) exists indicating that there is no association of Co with specific mafic minerals or organic matter. The absence of cobalt association with major or minor elements, organic carbon or grain size implies that the source of Co on Sturgeon Bank is unknown. The availability of high concentrations of Co to organisms using the bank would require further investigation.

6.3.4.2. *Chromium*

Chromium, like cobalt substitutes for Mg and Fe in early-crystallized olivine rocks or dunites (Rankama and Sahama, 1950). In igneous rocks chromium occurs both in oxide and in silicate minerals. The only independent chromium minerals are the chromian members of the spinel group, magnesiochromite, $MgCr_2O_4$ and chromite, $FeCr_2O_4$ (Rankama and Sahama, 1950).

Chromium abundance in sediments on Sturgeon Bank ranges from 54 to 216 ppm ±7.45% (Figure 51), considerably higher than values found in igneous rocks (Mason and Moore, 1982) and in Howe Sound sediments (Drysdale, 1990). The Cr vs. Al areal distribution plot (Figure 52) shows a similar trend to the Cr-content plot with high Cr/Al ratios found at stations 14, 28 and 36.

High Cr concentrations are not consistent with any particular grain sizes (r = +0.16) (Figure 53a). Like cobalt, chromium is carried in the fine to very fine sand and coarse silts. Chromium correlates reasonably well with Mg (r = +0.41) (Figure 53b) and Fe (r = +0.70) (Figure 53c) implying chromium substitution for Fe and Mg in mafic minerals. Earlier

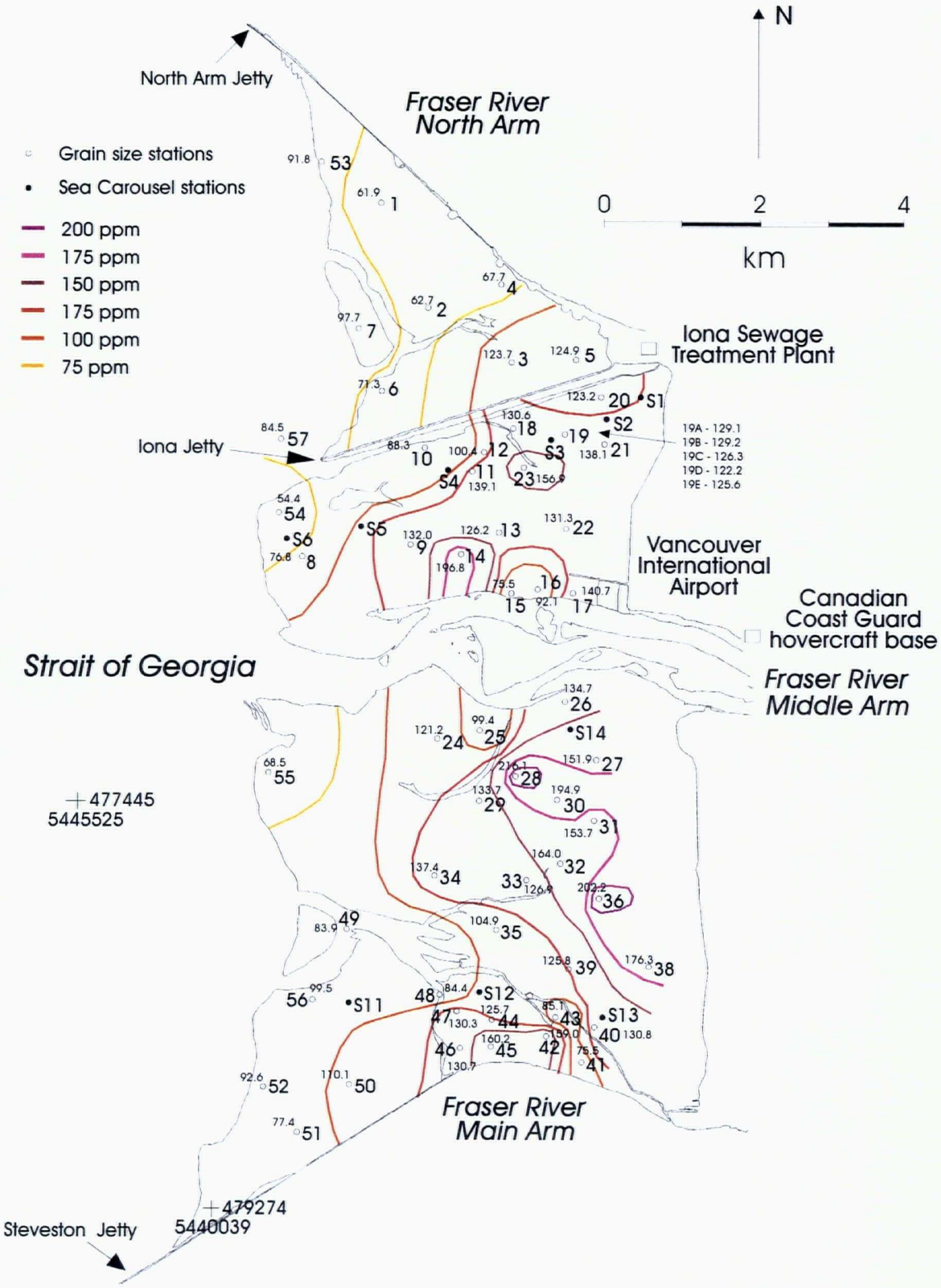

Figure 51: Areal distribution of chromium content on Sturgeon Bank

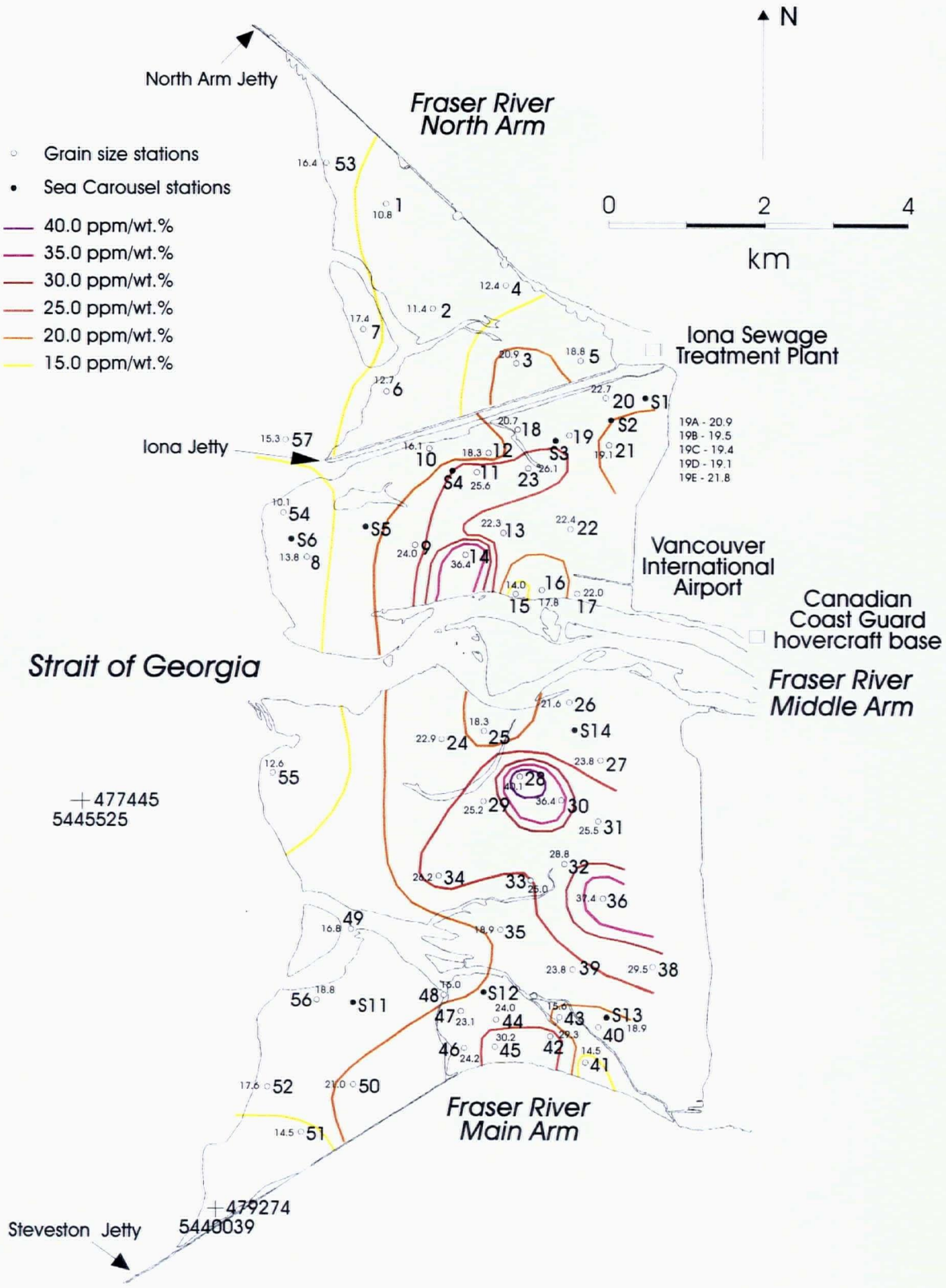

Figure 52: Areal distribution of Cr/Al on Sturgeon Bank

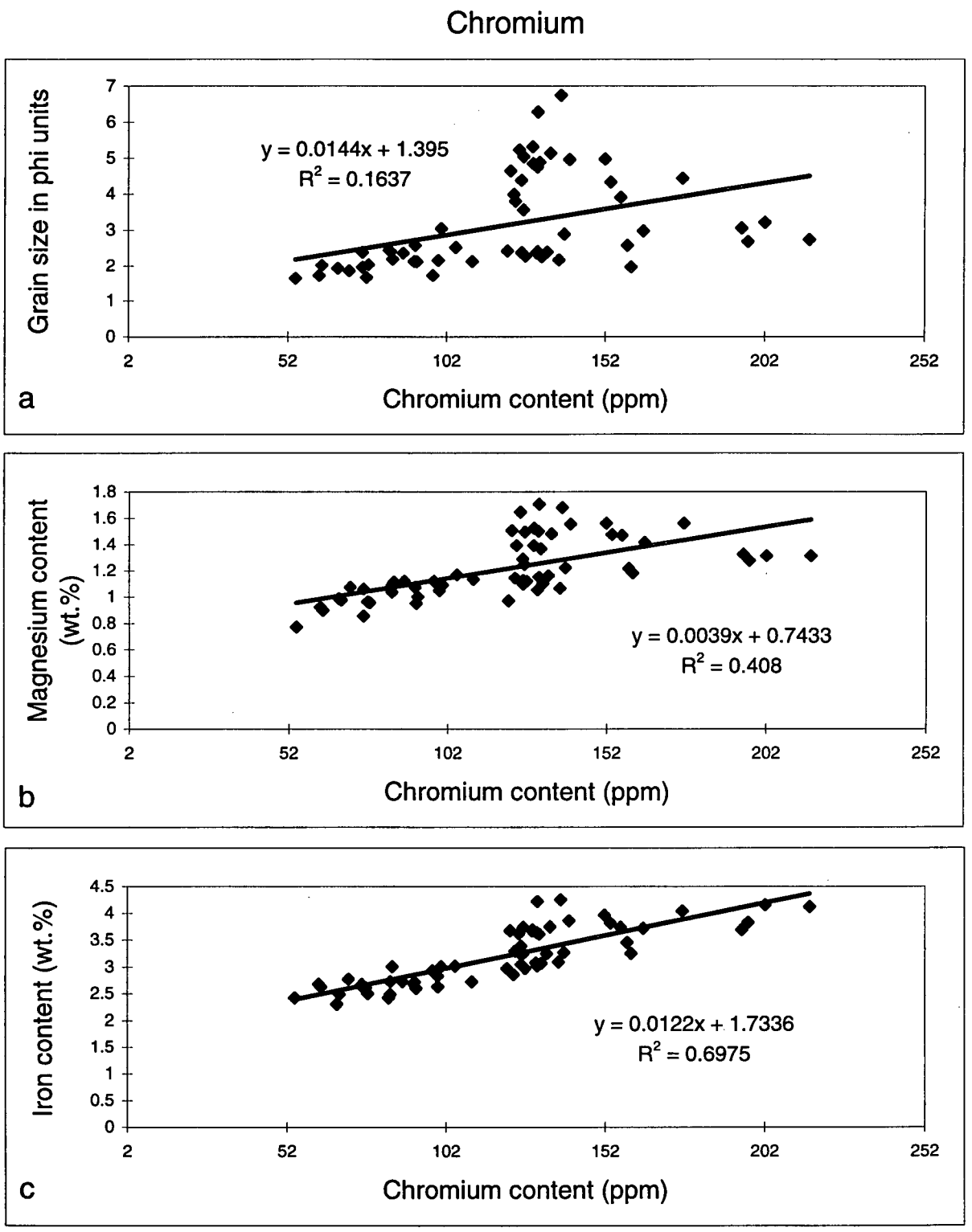

Figure 53: (a) Chromium content versus grain size
(b) Chromium content versus magnesium content
(c) Chromium content versus iron content

suggestions that the Mg-Fe phase in the fine to very fine sand phases may be chlorite supports the substitution of Cr for Fe and Mg in these coarser grained sediments. Chromite may also be the host for Cr in these coarser-grained sediments, however like ilmenite, it is a trace constituent and therefore unlikely to be a significant source of Cr on the bank. Both the chlorite and chromite are probably finer grained than the sand they are travelling with but because of hydraulic equivalence are concentrated in this size fraction at some stations.

6.3.4.3. *Nickel*

Like chromium and cobalt, the distribution of Ni in igneous rocks is closely related to the distribution of Mg and Fe (Krauskopf, 1979). The nickel ion has essentially the same radius and the same charge as magnesium and consequently may be substituting in magnesium minerals. The bulk of Ni found in igneous rocks is incorporated in silicate minerals.

Nickel abundance in Sturgeon Bank sediments is highest on the inner bank, decreases seaward and ranges from 26 to 51 ppm ± 7.2% (Figure 54). Nickel vs. aluminum distribution plots show higher values at stations 14, 23, 28, 36 and 38 (Figure 55), similar to the chromium distribution. The high Ni content in sediments collected from station 40 is not reflected in the Ni/Al value because of the high Al content found at this site.

The Ni vs. grain size plot shows a stronger positive correlation (r=0.58) (Figure 56a) than chromium and shows that the Ni is concentrated in the finer size fraction of sediments rather than the coarser fraction where Cr and Co are found. Nickel and chromium are known to behave similarly (Krauskopf, 1979). Nickel shows positive correlations with Mg (r = +0.75) (Figure 56b) and Fe (r = +0.83) (Figure 56c) and indicates that Mg and Fe minerals are likely hosts for

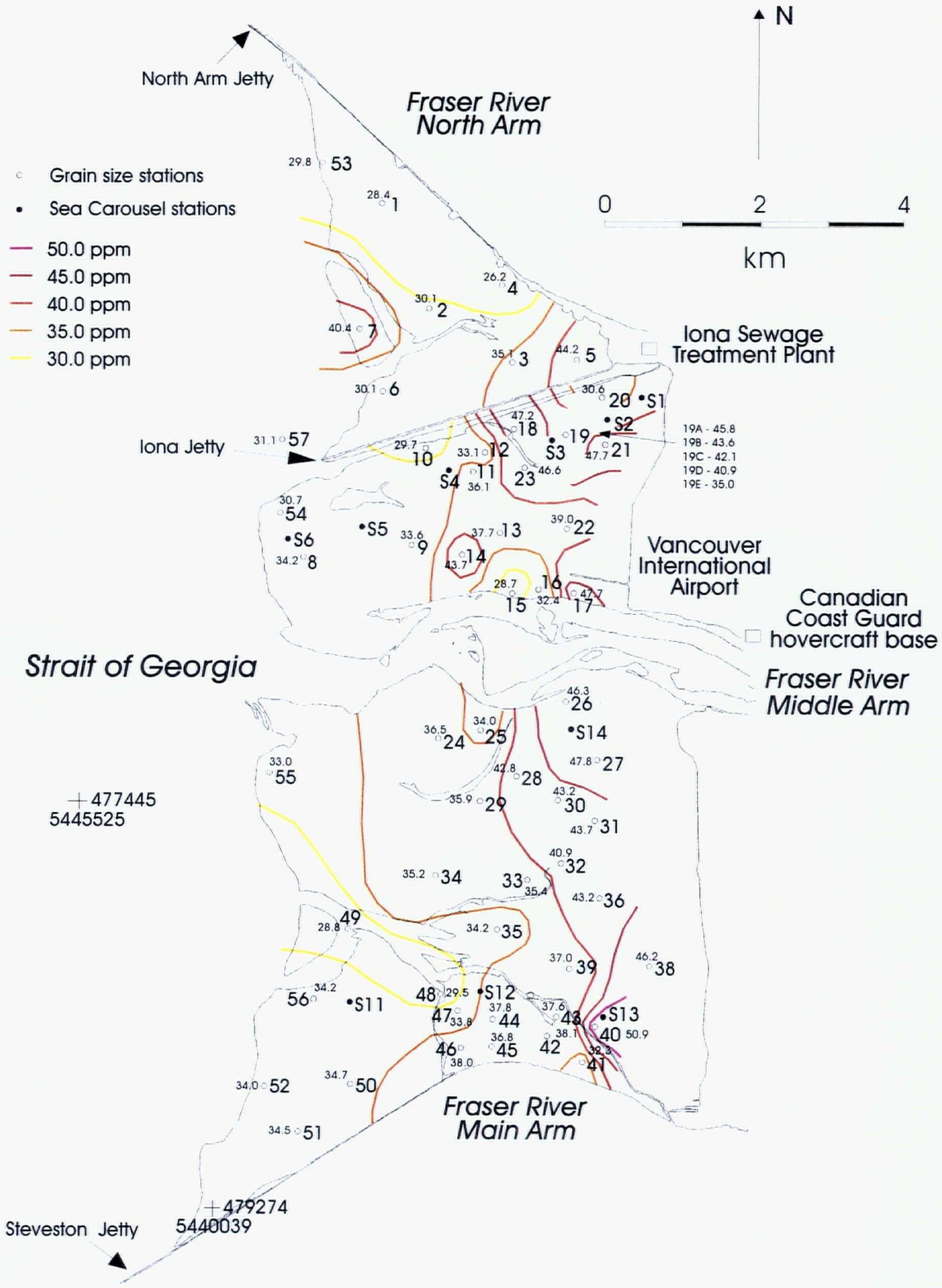

Figure 54: Areal distribution of nickel content on Sturgeon Bank

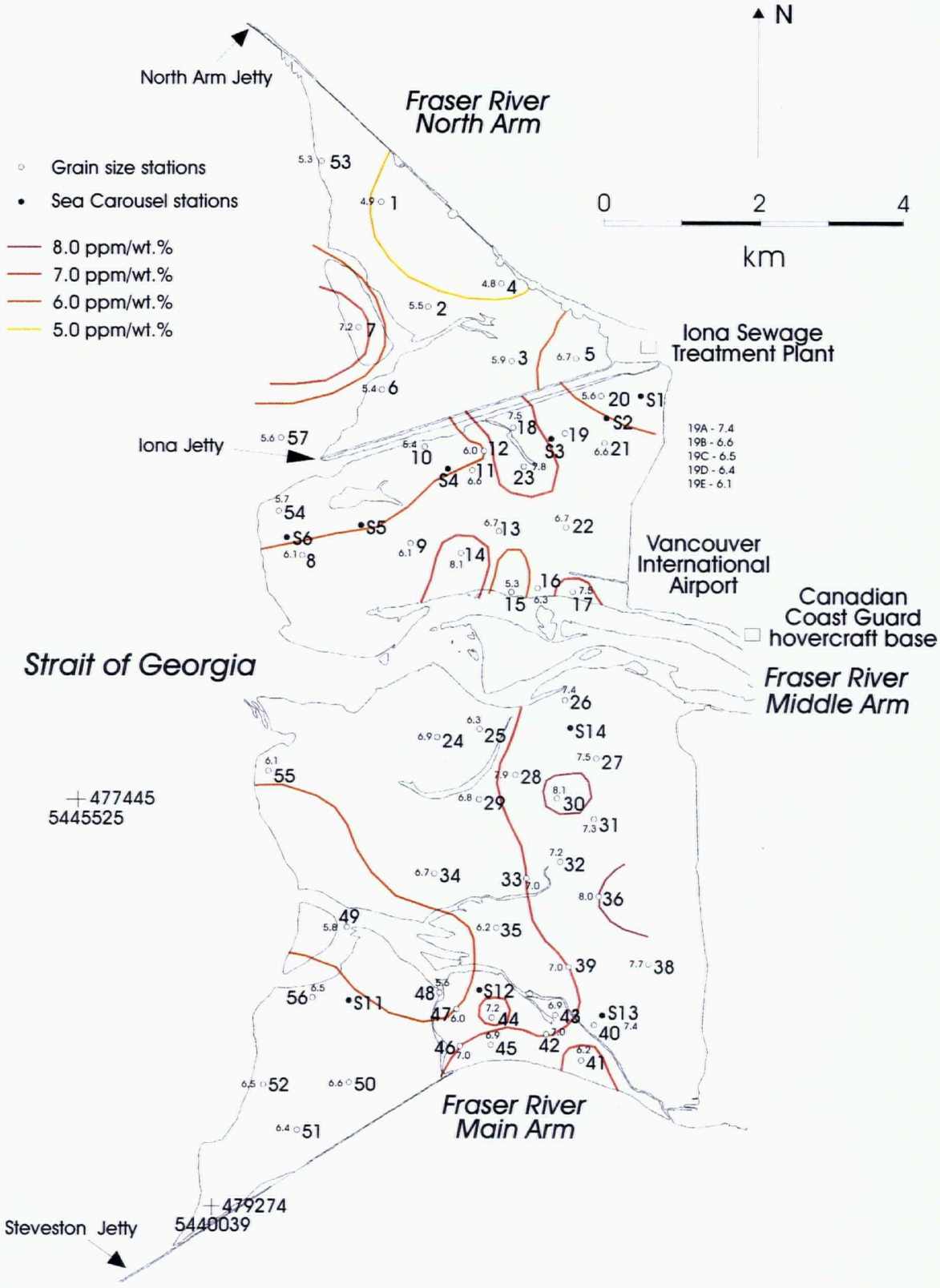

Figure 55: Areal distribution of Ni/Al on Sturgeon Bank

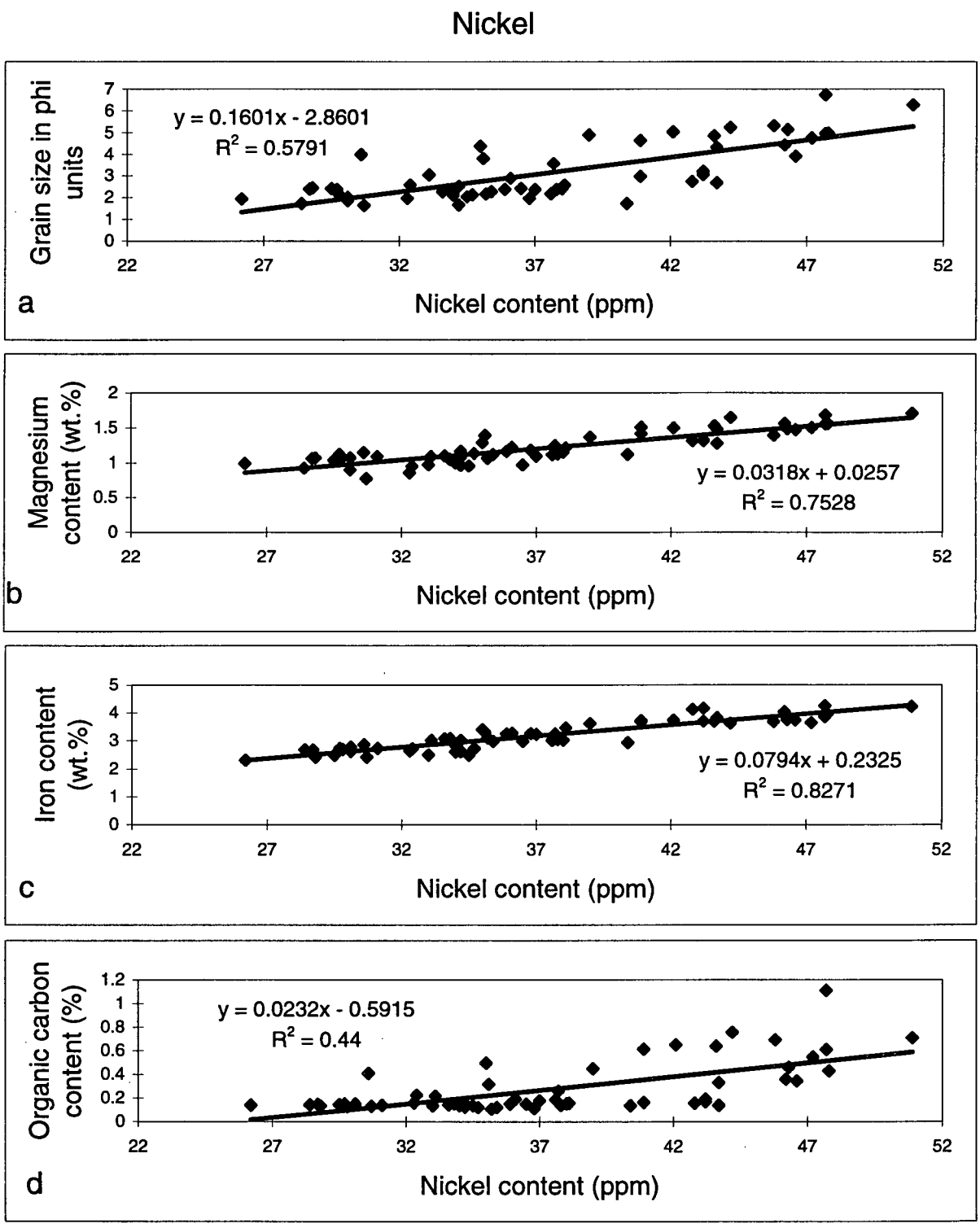

Figure 56:
(a) Nickel content versus grain size
(b) Nickel content versus magnesium content
(c) Nickel content versus iron content
(d) Nickel content versus organic carbon content

Ni where they are concentrated in the finer fraction. Correlation between Ni and C_{org} (r = +0.44) (Figure 56d) indicates that some of the Ni content in the sediments may be hosted by organic material supporting the observation that Ni preferentially accumulates in the finer size fractions.

6.3.4.4. *Vanadium*

Vanadium is strongly enriched in basic rocks and often correlates closely with Fe and Mg (Krauskopf, 1979). Vanadium is enriched in early-formed magnetite (Fe_3O_4) but also occurs in pyroxenes, amphiboles, and biotite (Mason and Moore, 1982).

In general, vanadium concentrations decrease in a seaward direction and range from 83 to 144 ppm ± 9.6% (Figure 57). The V vs. Al distribution shows highest values in sediments from stations 14, 28, 36, 42 and 44 (Figure 58), similar to Cr and Ni distributions. The low V content in sediments from stations 20 and 41 and the high V content in sediments from stations 21 and 23 are not reflected in the V/Al distribution.

The V vs. grain size plot shows positive correlation (r = +0.50) with V being enriched in some very fine, fine and medium sands (Figure 59a). A plot of V vs. Fe shows a very strong positive correlation (r = +0.94) (Figure 59b) and indicates that V is substituting for Fe in Fe-minerals, probably biotite or chlorite in the finer grained material but also magnetite and chlorite in the finer sand material. The relatively low abundance of V and its strong correlation with Fe implies that its presence in Sturgeon Bank surface sediments can be explained by textural effects rather than the result of previous sewage discharge. The low V content adjacent to the Iona sewage treatment plant indicates that surface sediments are relatively uncontaminated with respect to vanadium supporting the observation that V distribution is texturally-controlled.

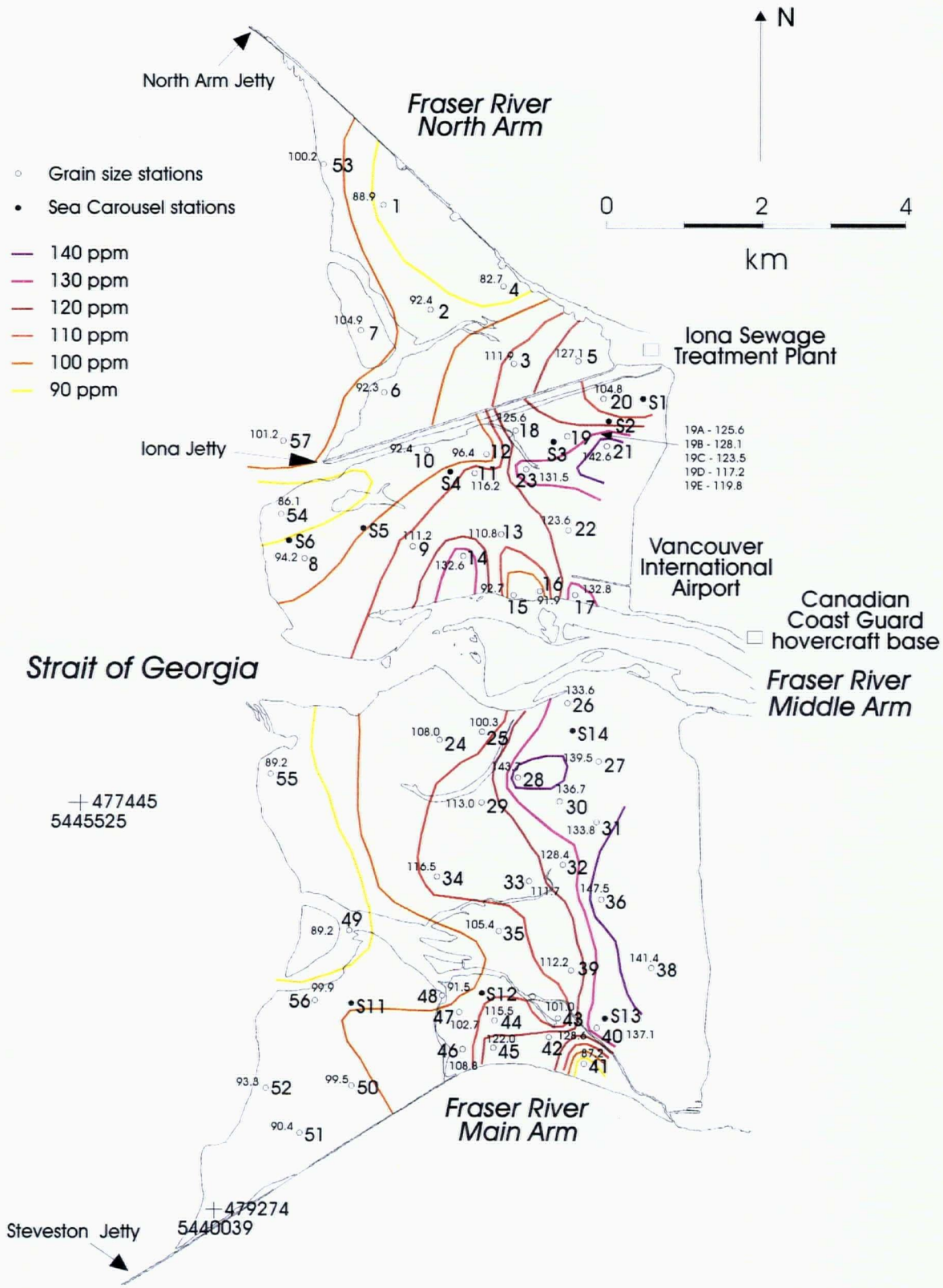

Figure 57: Areal distribution of vanadium content on Sturgeon Bank

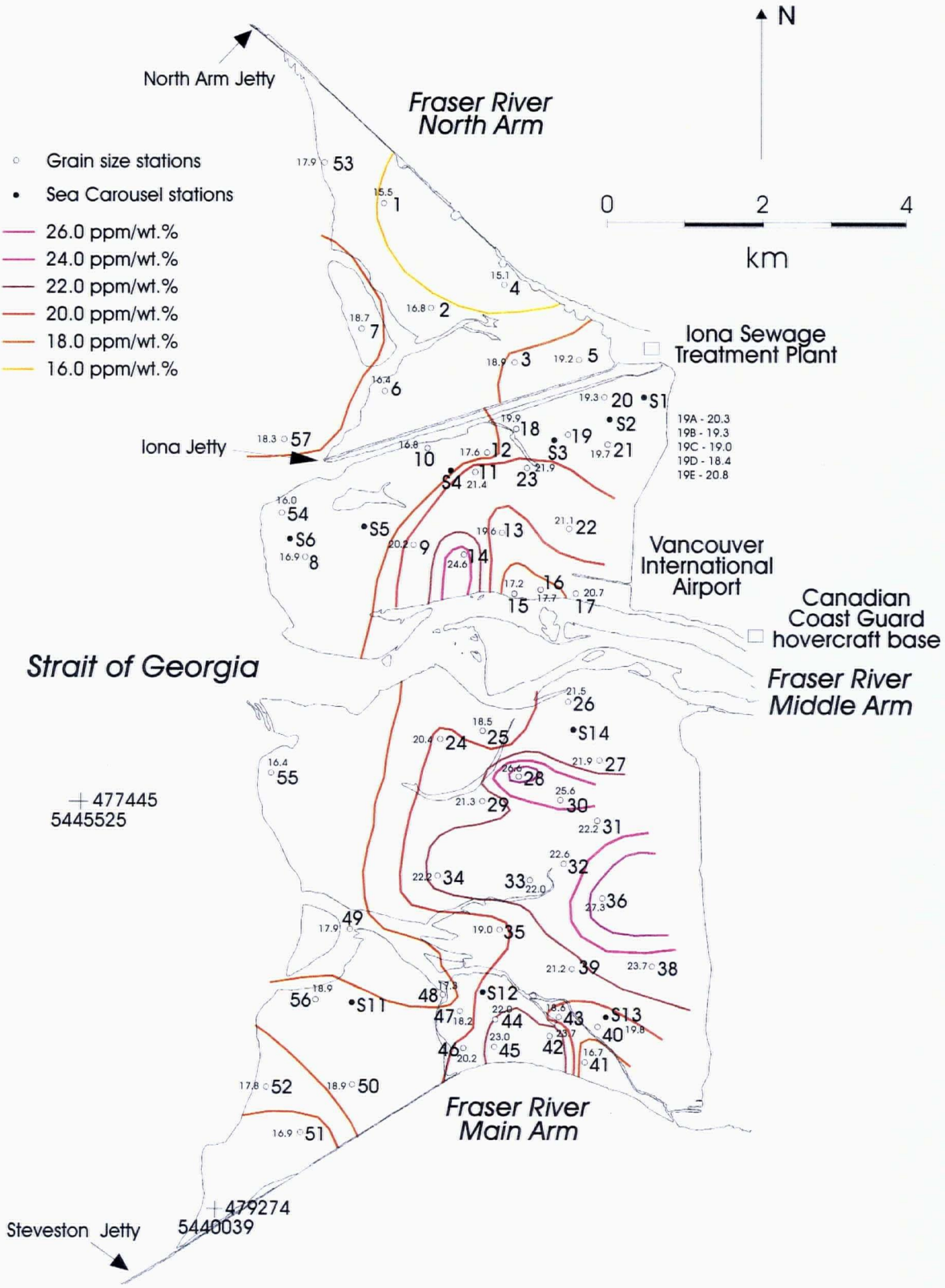

Figure 58: Areal distribution of V/Al on Sturgeon Bank

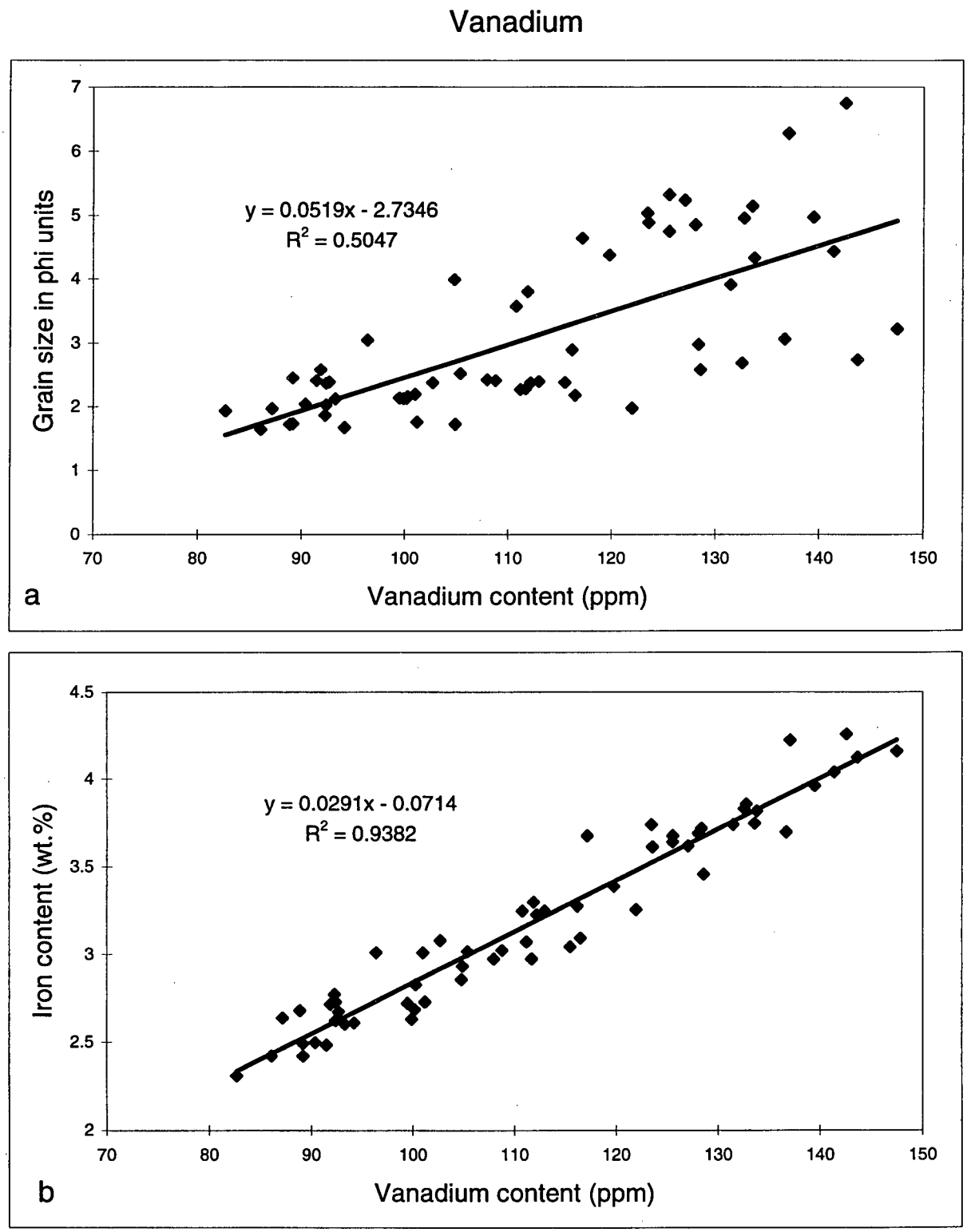

Figure 59: (a) Vanadium content versus grain size
(b) Vanadium content versus iron content

6.3.4.5. *Manganese*

Manganese behaves in a complex manner geochemically and therefore its distribution in sediments is difficult to interpret. Manganese can be partitioned into several terrigenous, biogenous and hydrogenous phases. Mn has a similar ionic radius to Fe and therefore substitutes into early-formed mafic minerals (Krauskopf, 1979) where it is enriched in biotite and hornblende but depleted in feldspars, micas and apatite (Mason and Moore, 1982). Mn is also found to form silicates, sulphides, carbonates and oxides. In addition to the difficulty in deciphering what phase Mn is present in, it also has a complex diagenetic behaviour. Mn-oxides are reduced just below the oxic zone in sediments and the dissolved Mn^{2+} which is formed migrates upwards towards lower concentrations until it comes in contact with oxygen where it repreciptates as amorphous Mn oxides. This typically creates manganese enrichment at the base of the oxic zone in the sediments. Such enrichments can occur within millimetres of the sediment-water interface and therefore this diagenetic behavior must be taken into consideration when interpreting Mn distribution in sediments.

Samples collected from Sturgeon Bank contain the top 2 cm of sediment and do not indicate the presence of any high-Mn layers formed diagenetically. Manganese concentrations range from 472 to 975 ppm ± 6.4% and show a random distribution on the bank (Figure 60). On northern Sturgeon Bank, the concentration is lowest shoreward and increases in a seaward direction toward the highest Mn contents found at stations 1 and 7, while on the central bank Mn concentrations are lowest adjacent to the Iona jetty and increase in a southerly direction. On southern Sturgeon Bank, Mn content is lowest in a strip along the inner bank which extends from Steveston jetty northward and then heads seaward at station 49. Higher Mn contents were found

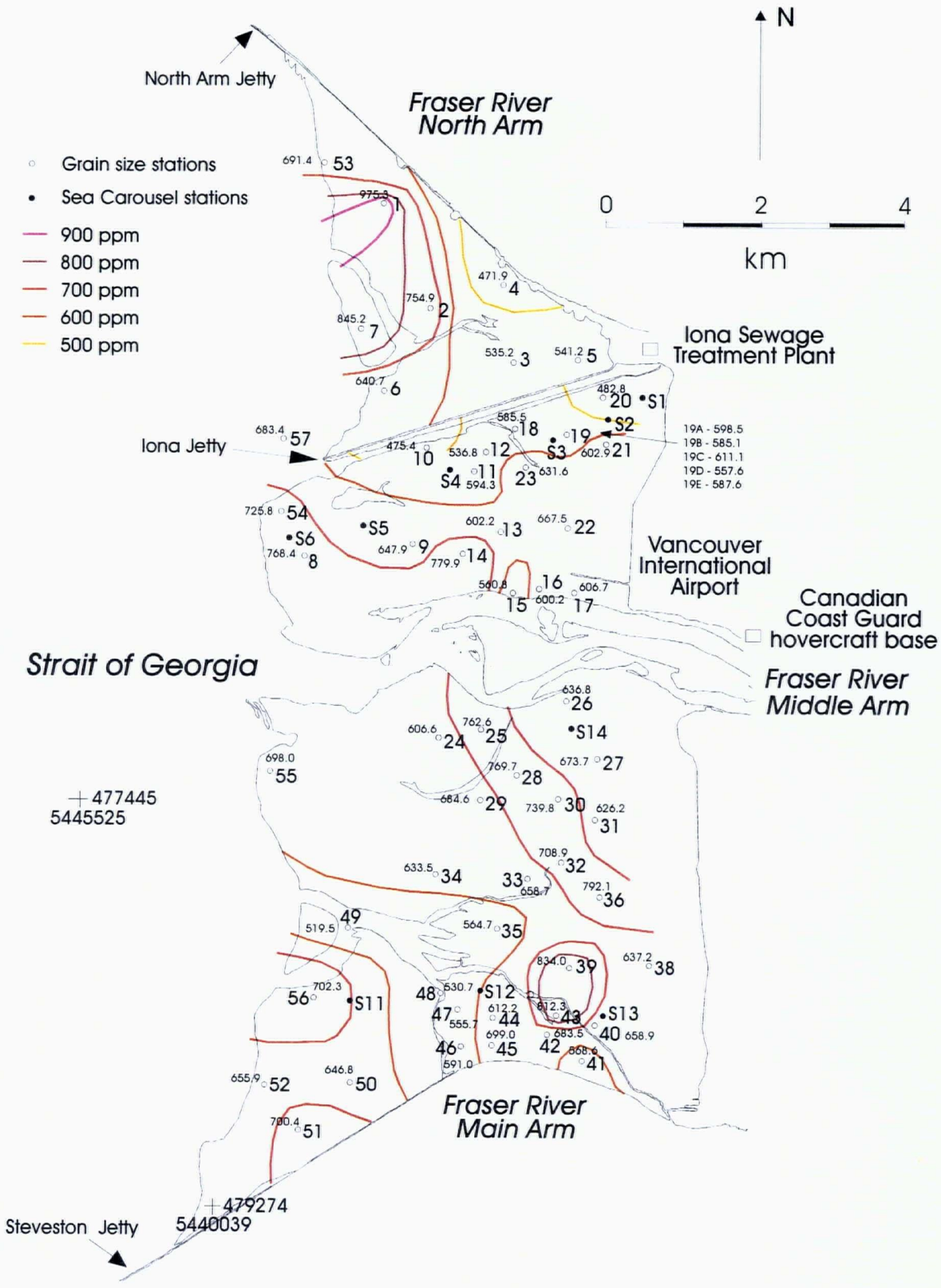

Figure 60: Areal distribution of manganese content on Sturgeon Bank

at stations 39 and 43. The Mn/Al distribution plot (Figure 61) reflects the Mn distribution. The relatively low Mn concentrations on Sturgeon Bank, especially in the area adjacent to the inactive sewage outfall, indicate that Mn-oxides are not abundant and therefore can not be a significant host for trace metals on Sturgeon Bank.

Manganese does not correlate with grain size (r = -0.10) (Figure 62a), Mg (r = -0.03) (Figure 62b), or Fe (r = 0.00) (Figure 62c) further supporting the absence of Mn-oxides in fine-grained sediments on the bank. The high Mn/Al ratios found on the outer northern Sturgeon Bank may represent Mn-oxides, however, these stations are composed of medium sands and therefore this is unlikely.

6.3.4.6. *Copper*

Copper tends to be concentrated in residual minerals because it is not capable of forming its own minerals and does not easily substitute for common ions in silicate rocks (Krauskopf, 1979). Copper is found in Cu sulphides such as CuO (tenorite), $Cu_2CO_3(OH)_2$ (malachite), $Cu_3(CO_3)_2(OH)_2$ (azurite), $CuFeS_2$ (chalcopyrite), Cu_5FeS_4 (bornite), Cu_2S (chalcocite), Cu_2O (cuprite), CuS (covellite) (Klein and Hurlbut, 1977; Nesse, 1986) and other common minerals.

The highest copper content is found at station 21 (49 ppm ± 13.3%) (Figure 63) considerably lower than even the lowest values found in Howe Sound sediments (Drysdale, 1990) and values reported for marine clays, shales and sandstones (Bowen, 1979). Concentrations of Cu elsewhere on the bank are lower than 27 ppm. Sediments from uncontaminated inlets on the west coast of British Columbia range from 4 to 37 ppm (Harding and Goyette, 1989) and are similar to the values found in surface sediments on Sturgeon Bank.

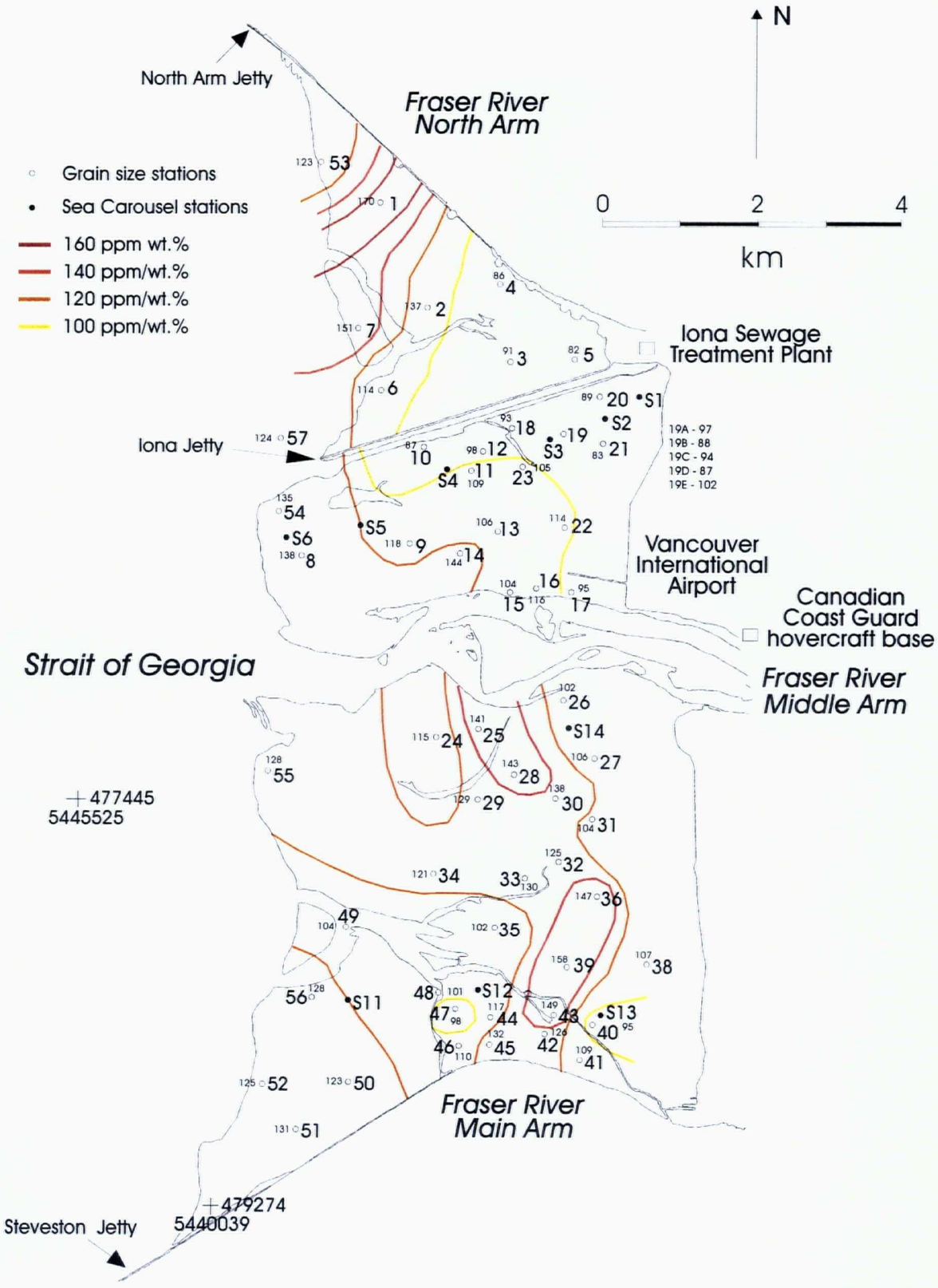

Figure 61: Areal distribution of Mn/Al on Sturgeon Bank

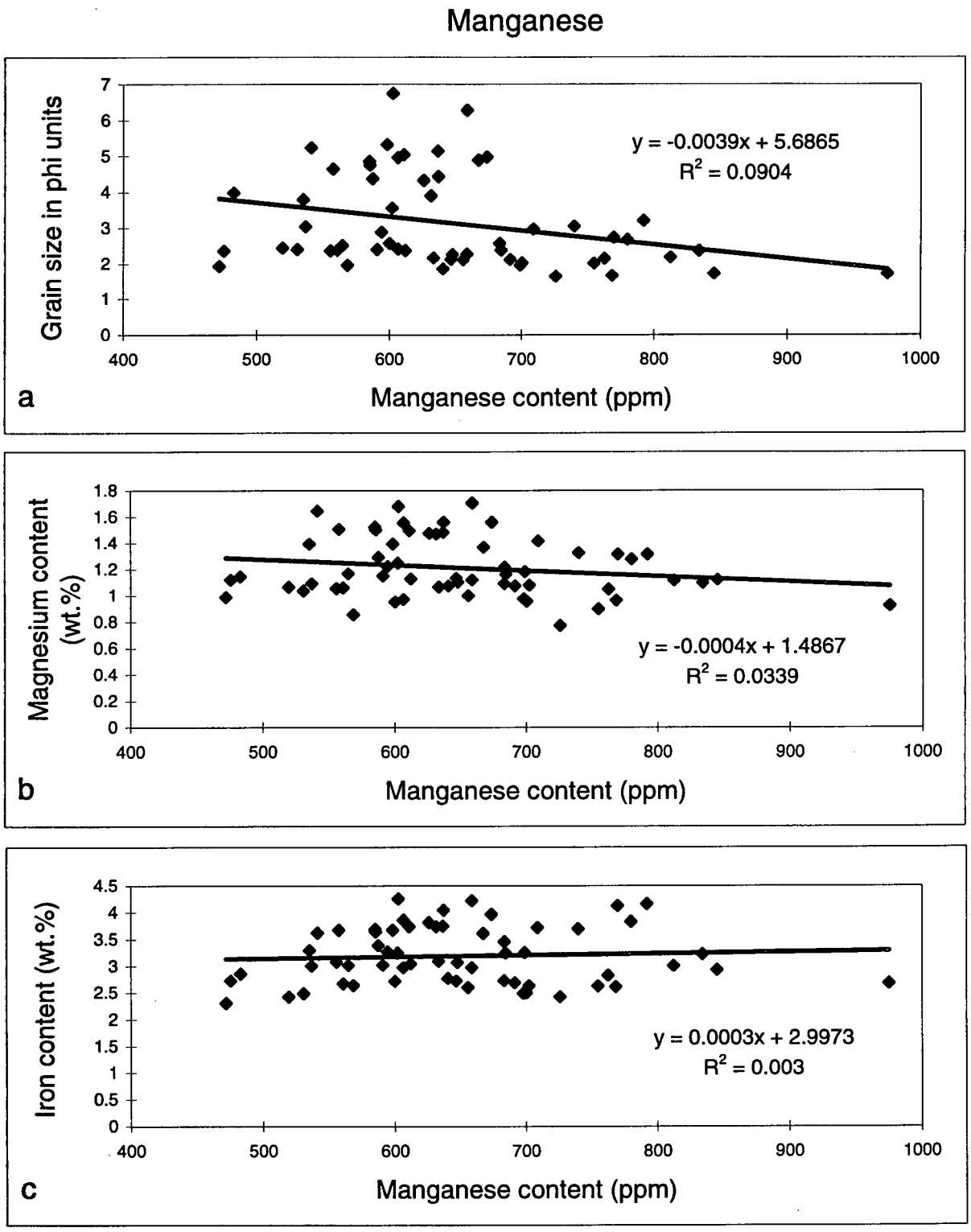

Figure 62: (a) Manganese content versus grain size
(b) Manganese content versus magnesium content
(c) Manganese content versus iron content

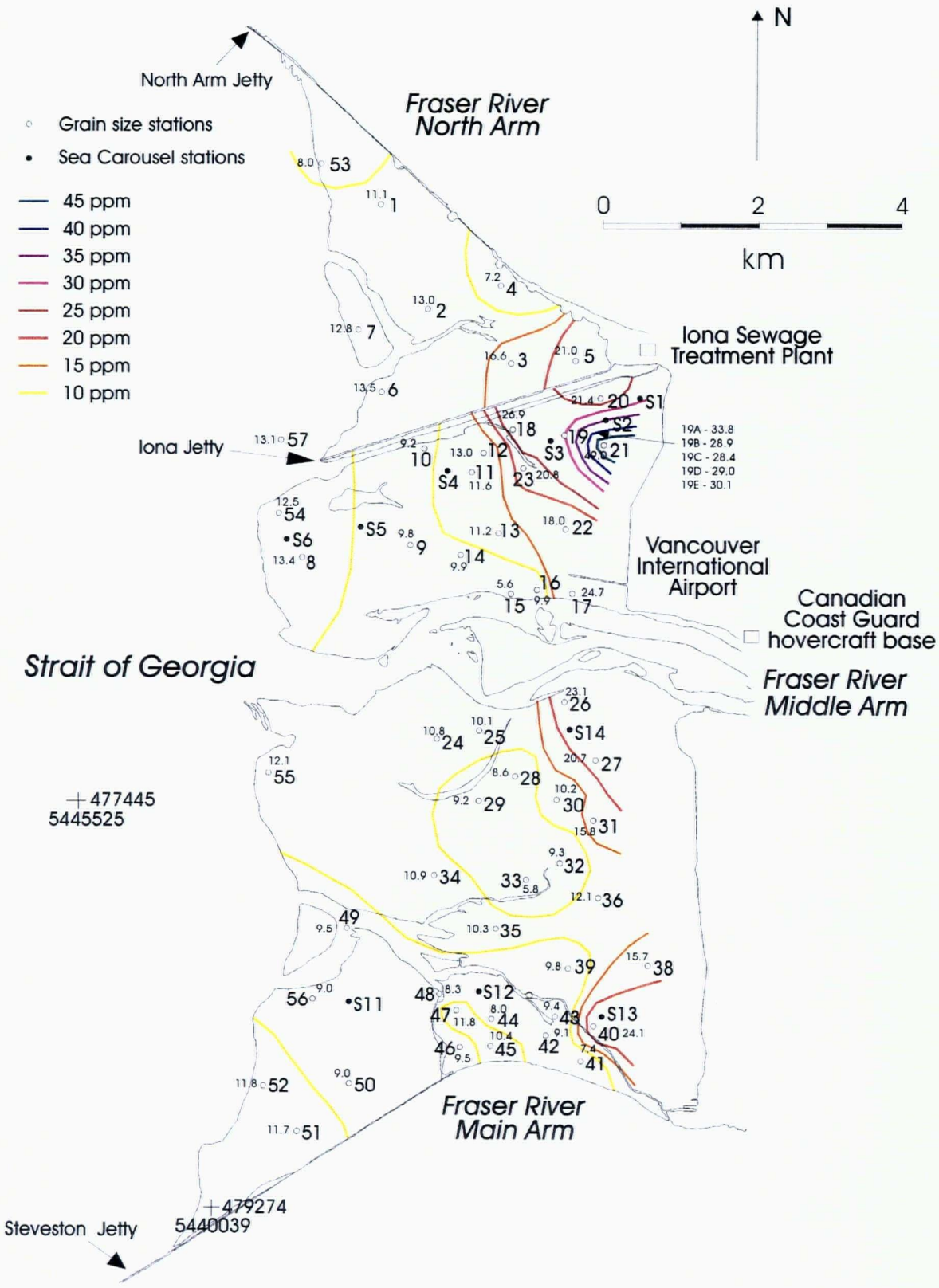

Figure 63: Areal distribution of copper content on Sturgeon Bank

Copper is concentrated in the finer grain sizes with the exception of stations 3, 20 and 23 which are composed of very fine sand and lie adjacent to the once active Iona sewage outfall. The Cu/Al distribution plot reflects the Cu distribution, particularly on the northern and central Sturgeon Bank (Figure 64). The Cu/Al ratio from sediments collected from station 21 adjacent to the now inactive Iona sewage treatment plant outfall is considerably higher than the ratios from sediments of surrounding stations. The fine silt-dominated sediments found at station 40 do not exhibit the same Cu enrichment as those from station 21 which suggests the sediments found at station 21 have been contaminated by an additional source of Cu. This source was likely the Iona sewage effluent whereby Cu still remains enriched in the finer-grained surface sediments of station 21. Higher Cu concentrations at station 21 could also reflect the composition of organic matter here which, as explained previously, may be more reactive than the organic material present at station 40. It is important to note, however, that the concentration of Cu in the sediments from station 21 is low and does not show considerable contamination.

Copper correlates positively with grain size ($r = +0.73$) (Figure 65a) reflecting surface area adsorption. Copper shows weak correlations with Fe (Figure 65b) and Pb (Figure 65c) ($r = +0.33$, $r = +0.33$, respectively) but good correlation with Zn ($r = +0.78$) (Figure 65d), reflecting grain size preference. As observed with vanadium, copper concentrations on Sturgeon Bank indicate that Cu distribution is texturally controlled and surface sediments are relatively uncontaminated with respect to copper.

6.3.4.7. *Zinc*

Zinc, like copper, is enriched in residual solutions and therefore is concentrated in felsic

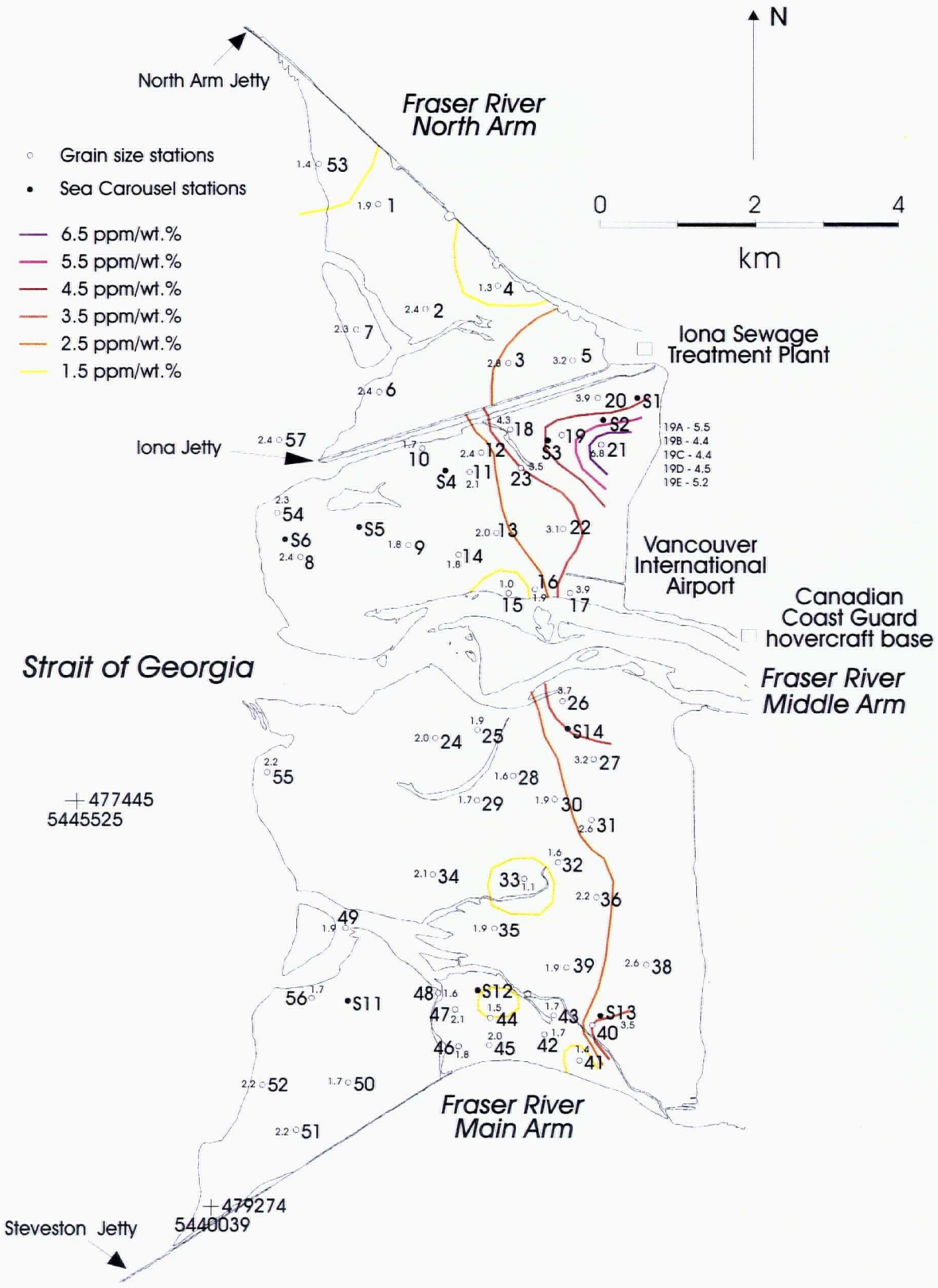

Figure 64: Areal distribution of Cu/Al on Sturgeon Bank

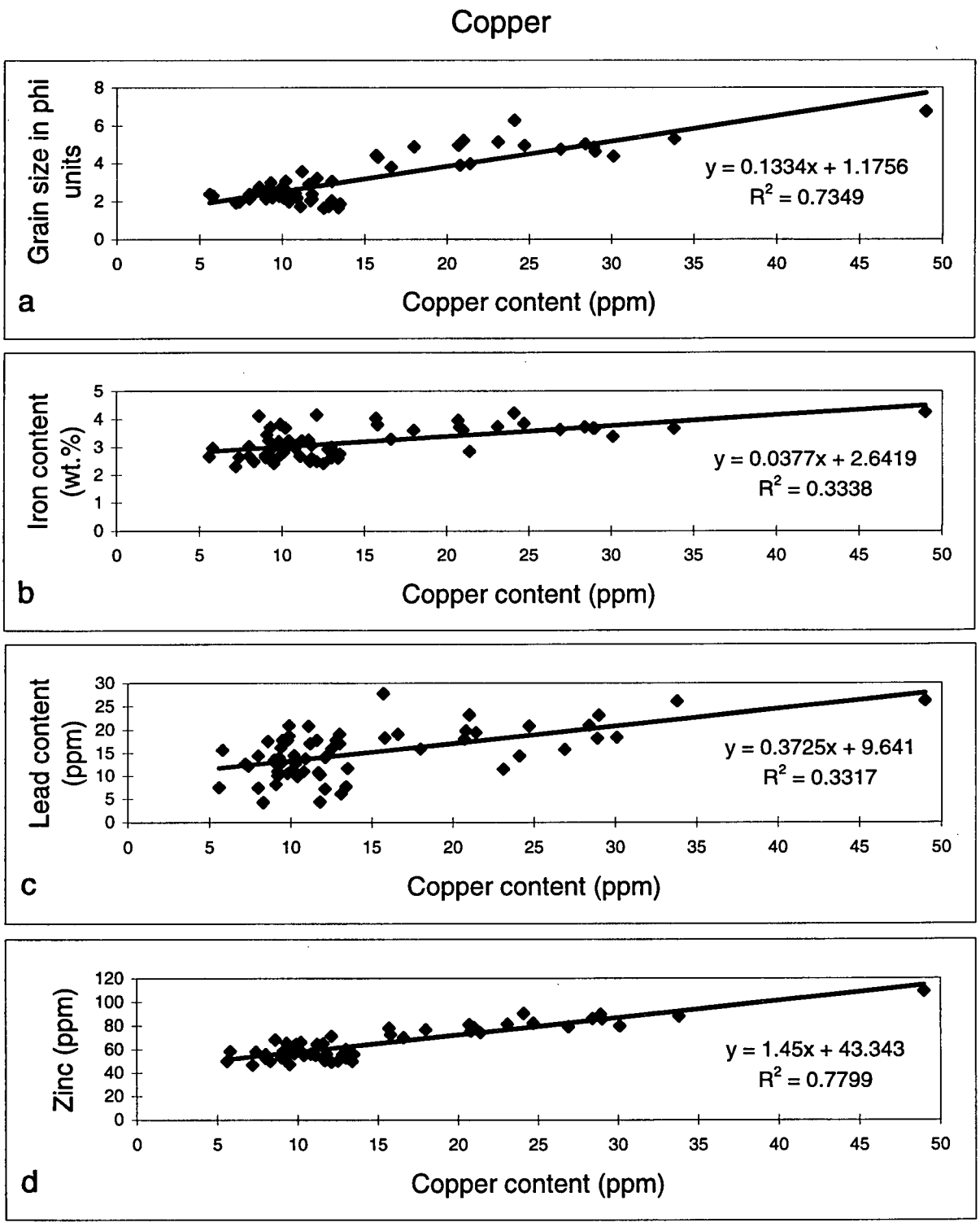

Figure 65: (a) Copper content versus grain size
(b) Copper content versus iron content
(c) Copper content versus lead content
(d) Copper content versus zinc content

rocks (Krauskopf, 1979). Because of its similarity in ionic size, Zn can substitute for Fe and Mg and therefore amphiboles, pyroxenes and biotite are the main zinc carriers in igneous rocks (Rankama and Sahama, 1950).

Zinc concentrations in surface sediments on Sturgeon Bank range from 46 to 109 ppm ± 3.1%, are highest at stations 21 and 40 in coarse silt sediments, and decrease seaward (Figure 66). These values are significantly lower that the lowest values found in Howe Sound sediments (Drysdale, 1990) and the values reported for marine clays, shales and sandstones (Mason and Moore, 1982). The zinc vs. aluminum distribution on Sturgeon Bank shows a consistent trend with Zn distribution with the highest value found at station 21 (Figure 67). The high Zn content in sediments from station 40 is not reflected in the Zn/Al ratio. Zinc and copper distributions in Sturgeon Bank surface sediments behave similarly with the sediments collected from station 21 containing higher Zn contents likely from the once active Iona sewage treatment outfall and the higher composition of organic material here.

Zinc correlates positively with grain size (Figure 68a), Fe (Figure 68b) and Pb (Figure 68c) ($r = +0.91$, $r = +0.71$, $r = +0.44$, respectively) and indicates the strong affinity for Zn in fine-grained sediments. Like Cu, the distribution of Zn on Sturgeon Bank reflects textural control and indicates that surface sediments are relatively uncontaminated with respect to zinc.

6.3.4.8. *Lead*

Lead exists as the independent mineral PbS (galena), $PbCO_3$ (cerrusite) and $PbSO_4$ (anglesite) and is often co-crystallized in apatite and titanite (Bowen, 1979). Lead has an ionic size similar to Fe and Mg and therefore substitutes for these elements in silicate lattices such as

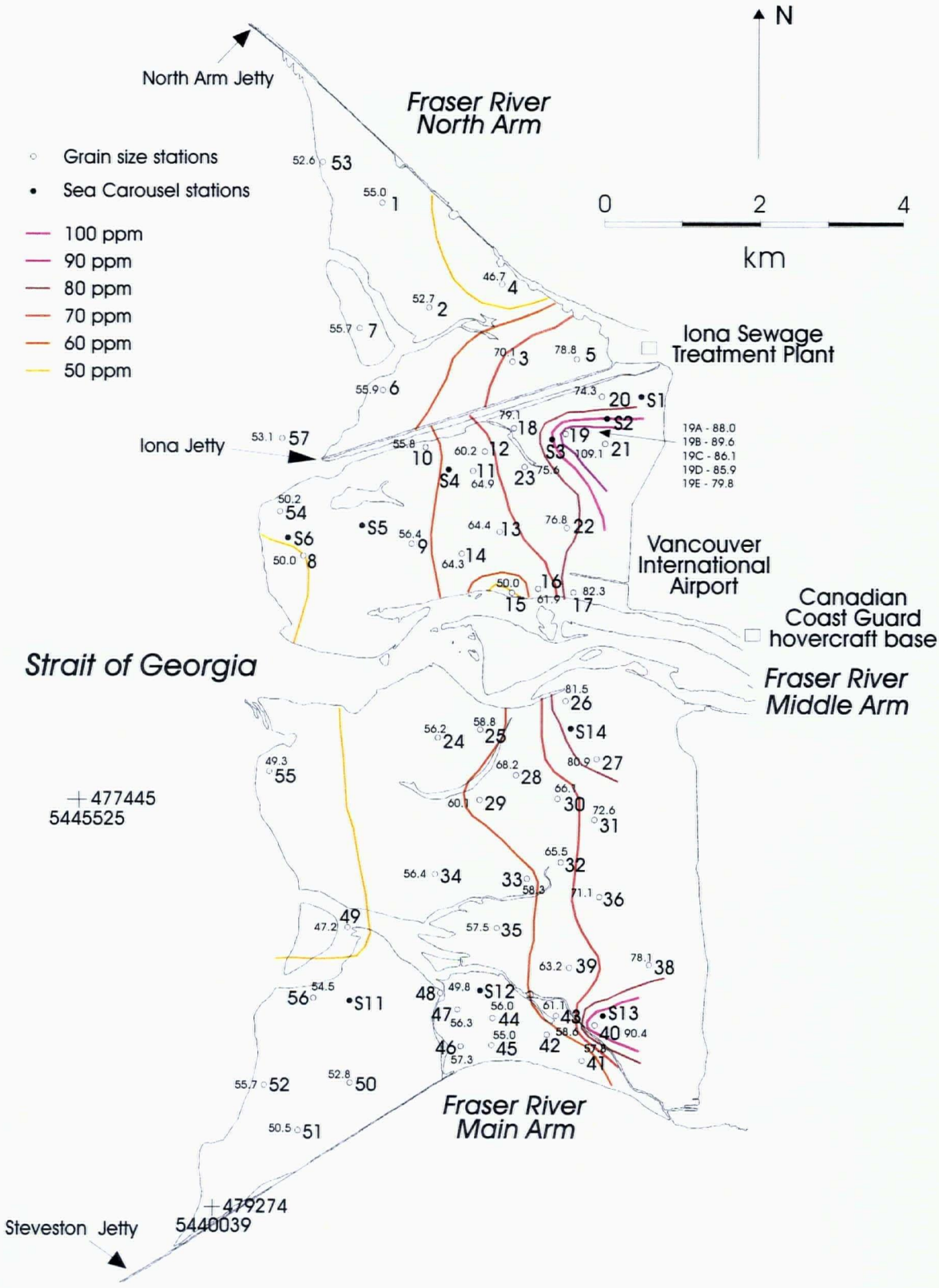

Figure 66: Areal distribution of zinc content on Sturgeon Bank

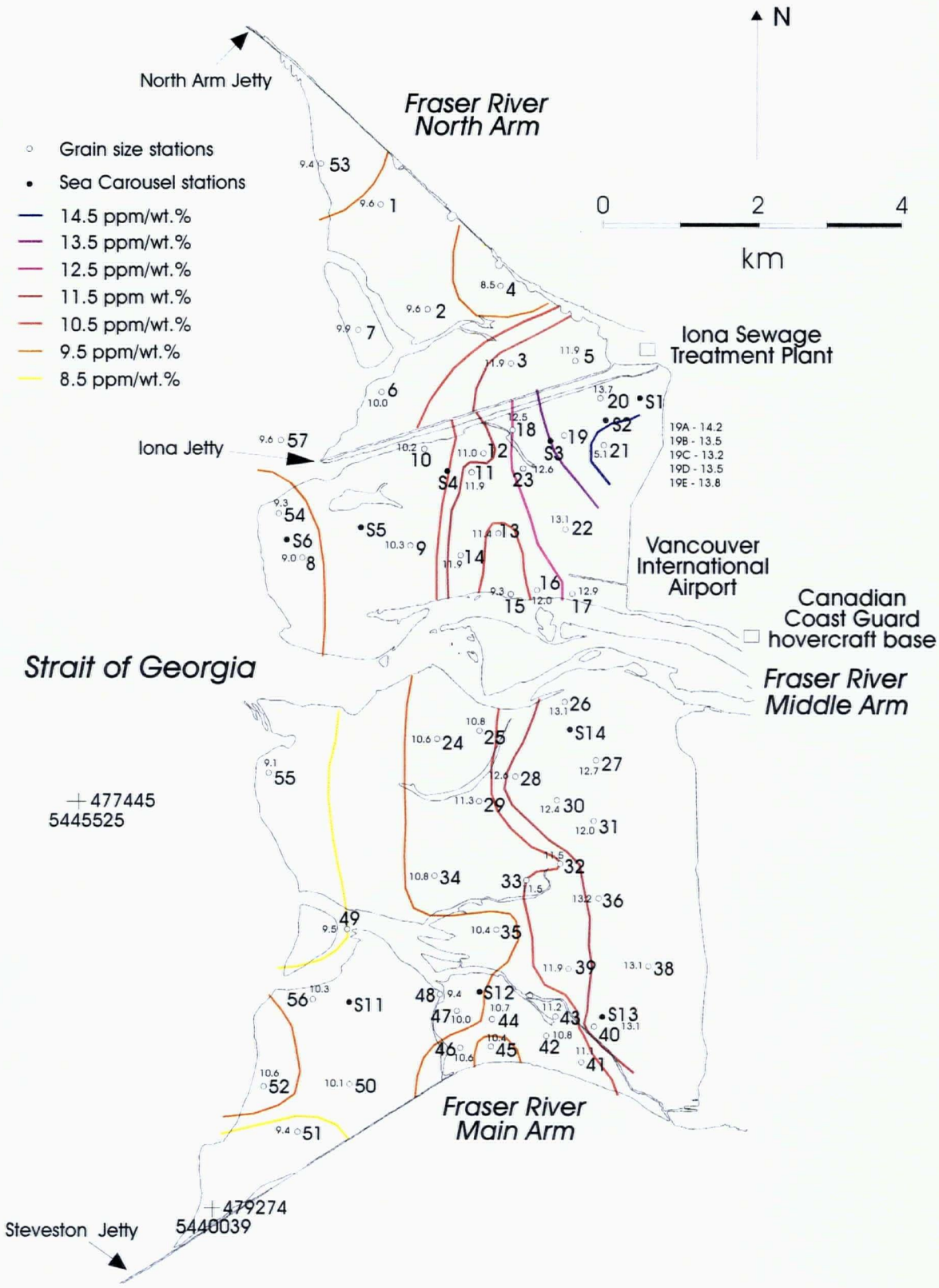

Figure 67: Areal distribution of Zn/Al on Sturgeon Bank

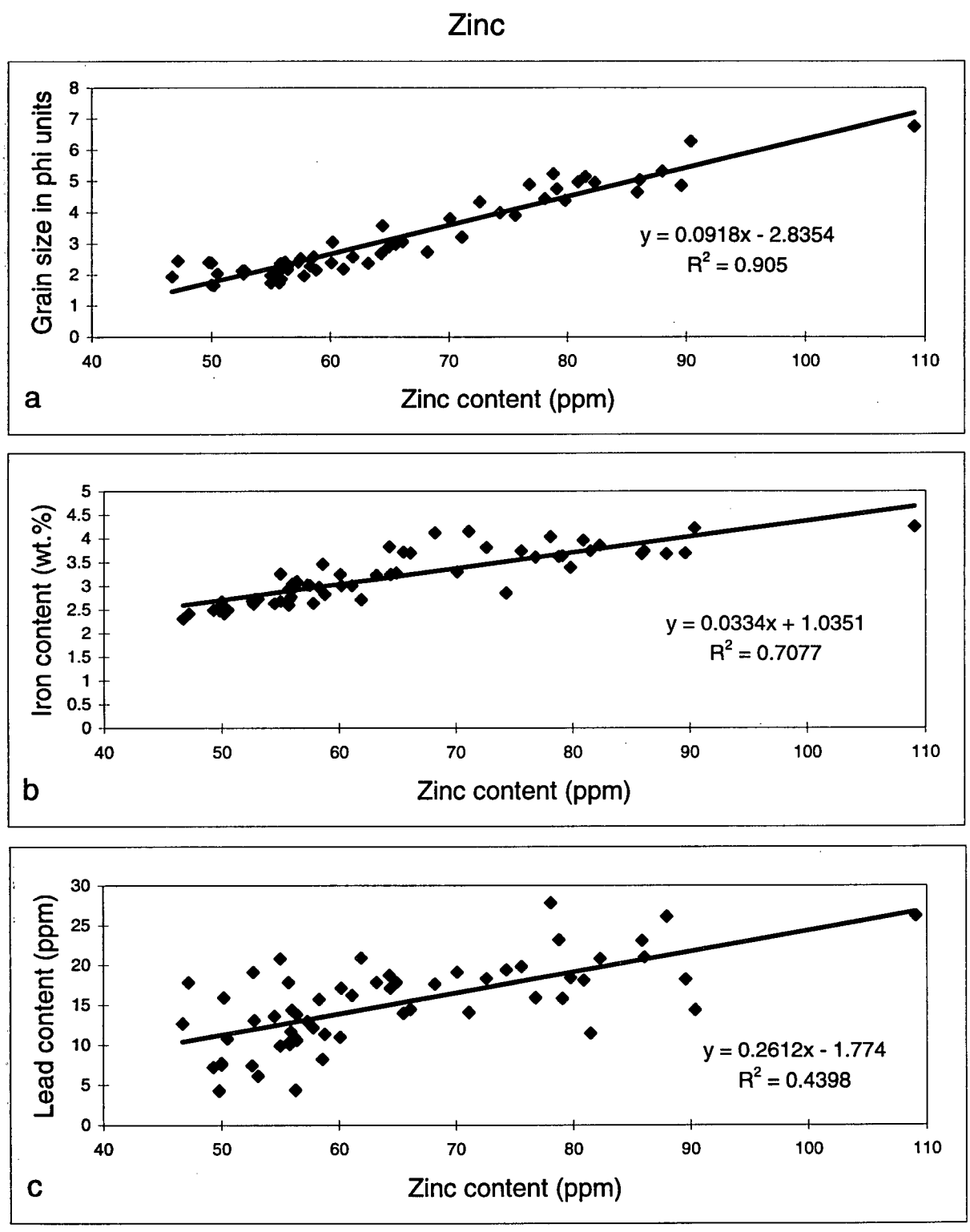

Figure 68: (a) Zinc content versus grain size
(b) Zinc content versus Iron content
(c) Zinc content versus Lead content

mica and chlorite. In addition, lead was present as a gasoline additive but effective January 1, 1987, the maximum allowable lead content in leaded gasoline in Canada was reduced from 0.77 grams per litre to 0.29 grams per litre. By December 1, 1990 leaded gasoline was effectively phased out (Poon, 1989). Therefore lead has also been introduced into marine sediments through the atmosphere via automobile exhaust.

Lead concentration in Sturgeon Bank sediments ranges from 4 to 28 ppm ± 58.4% with content generally decreasing seaward (Figure 69). The distribution of Pb/Al is very similar to that of Pb (Figure 70). Stations 1 and 2 show high Pb/Al values while Pb/Al values from sediments at stations 16, 38 and 49 are considerably higher than those from sediments at adjacent stations. Station 54 sediments are also noticeably higher in Pb/Al value while sediments from stations 15, 47 and 48 are markedly lower than other sediments from surrounding stations.

When Pb is plotted against grain size it shows positive correlation ($r = +0.39$) (Figure 71). Plots of Pb vs. Cu (Figure 65c) and Pb vs. Zn (Figure 68c) reveal that Pb has only a small association with copper ($r = +0.33$) and zinc ($r = +0.44$) hosted minerals. Lead values obtained using XRF analytical techniques show precision errors of more than 58% due to poor sensitivity by the XRF and low Pb concentrations. Although the values determined seem reasonable, conclusions made about lead abundance on Sturgeon Bank must be made cautiously. The low lead concentrations measured indicate that surface sediments on Sturgeon Bank are relatively uncontaminated with respect to lead.

6.3.4.9. *Zirconium*

Zirconium is too small to substitute in most silicate lattice positions so it tends to be

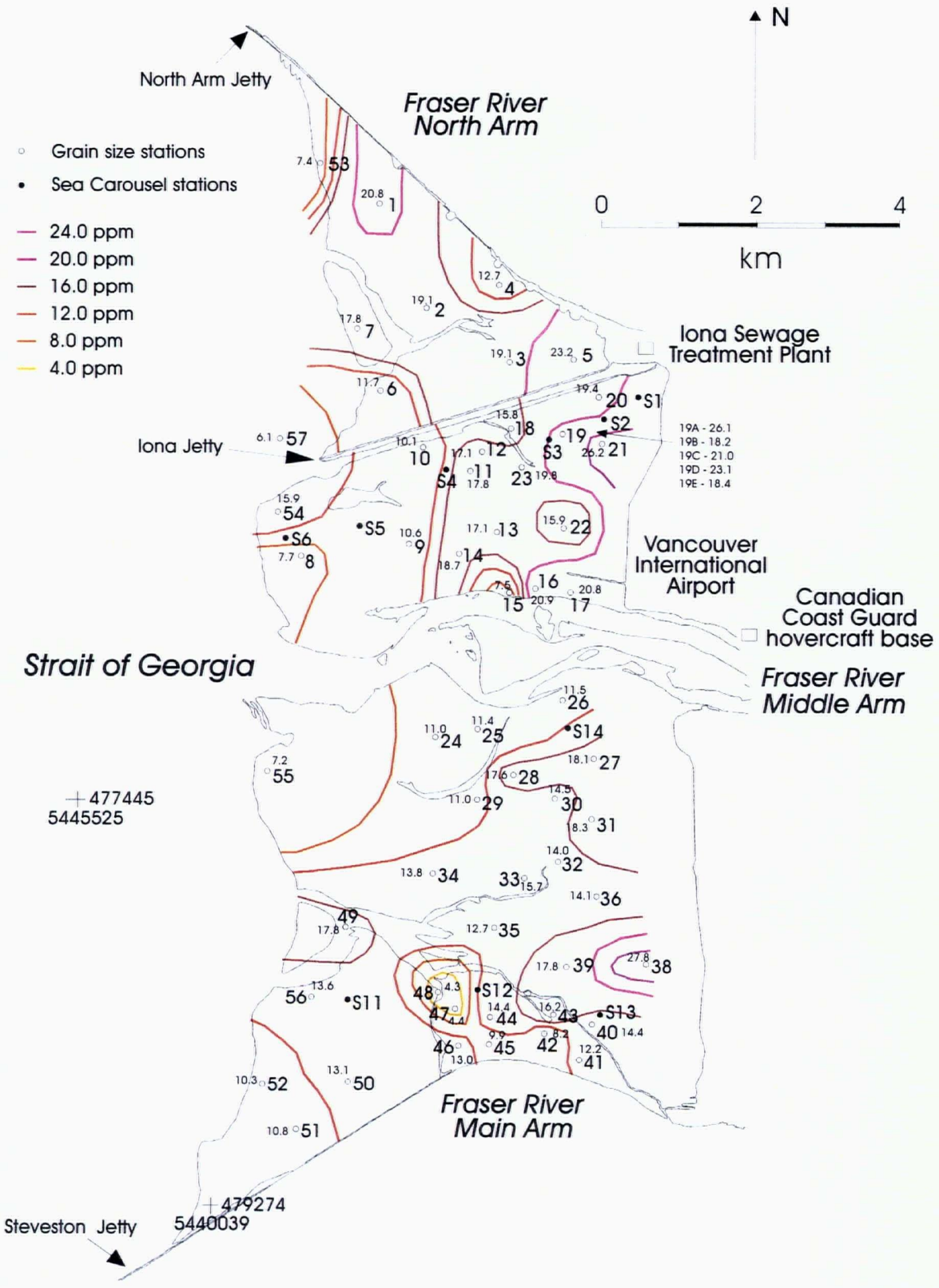

Figure 69: Areal distribution of lead content on Sturgeon Bank

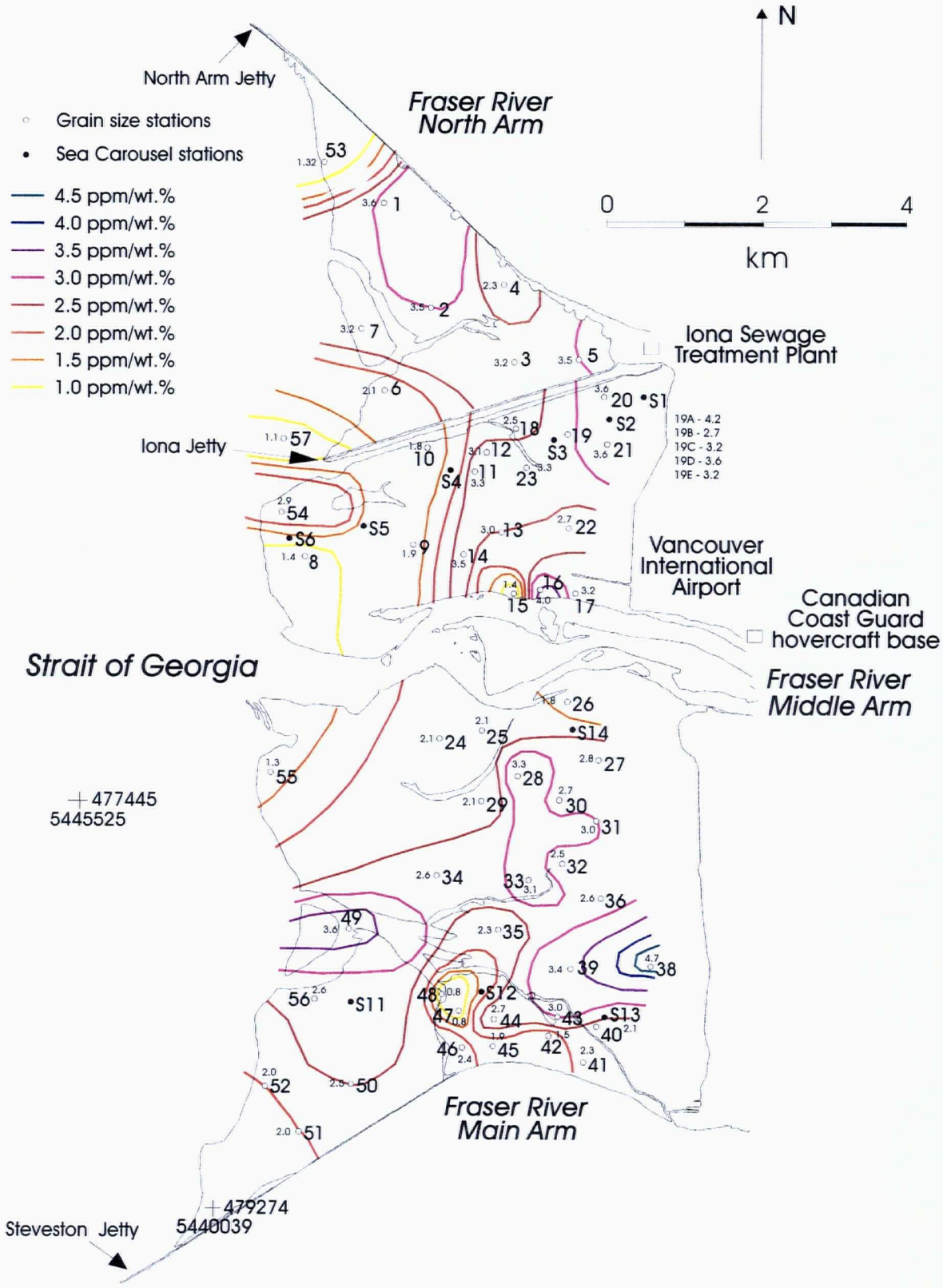

Figure 70: Areal distribution of Pb/Al on Sturgeon Bank

Figure 71: Lead content versus grain size

found in the felsic end of a rock series in residual solutions or largely found in the resistate mineral zircon (Krauskopf, 1979). Zirconium content is a good index for areas of heavy mineral accumulation. Zirconium content in shales is reported to be 160 ppm (Mason and Moore, 1982) and abundances over this value usually indicate that Zr is being hosted in the mineral zircon.

In Sturgeon Bank sediments zirconium is generally highest on the inner bank and ranges in concentration from 78 to 339 ppm ± 2.4% (Figure 72), considerably higher than values found in Howe Sound sediments (Drysdale, 1990). This contrast could be the result of the coarser grain sizes found in Sturgeon Bank compared to Howe Sound. Zr/Al distribution in sediments is very similar to Zr distribution with stations 14, 28, 30 and 36 showing the highest values (Figure 73).

It is evident that Zr does not preferentially accumulate in certain grain size fractions and therefore Zr does not correlate well with grain size ($r = +0.31$) (Figure 74). The highest Zr values are found in the very fine to fine sand and coarse silt size fractions which is consistent with results of Zr distribution in coarser grain sizes found by Bowen, 1979; Krauskopf, 1979; Wright, 1972; Calvert, 1983; Drysdale, 1990. Zr-accumulation is consistent with the distribution of Cr, Ti, Fe, V and to a lesser extent Ni in surface sediments on Sturgeon Bank and is indicative of areas of heavy-mineral accumulation.

6.3.5. SEDIMENT GEOCHEMICAL VARIABILITY

Station 19 was sampled 5 times in an east-west transect with a sample spacing of 2 metres. The major element concentrations measured at each of the 5 stations show only minor variation with sample 19E, the most seaward sample having the lowest Al, Ti, and Fe values. This is consistent with the increase in grain size within the station 19 transect in a seaward

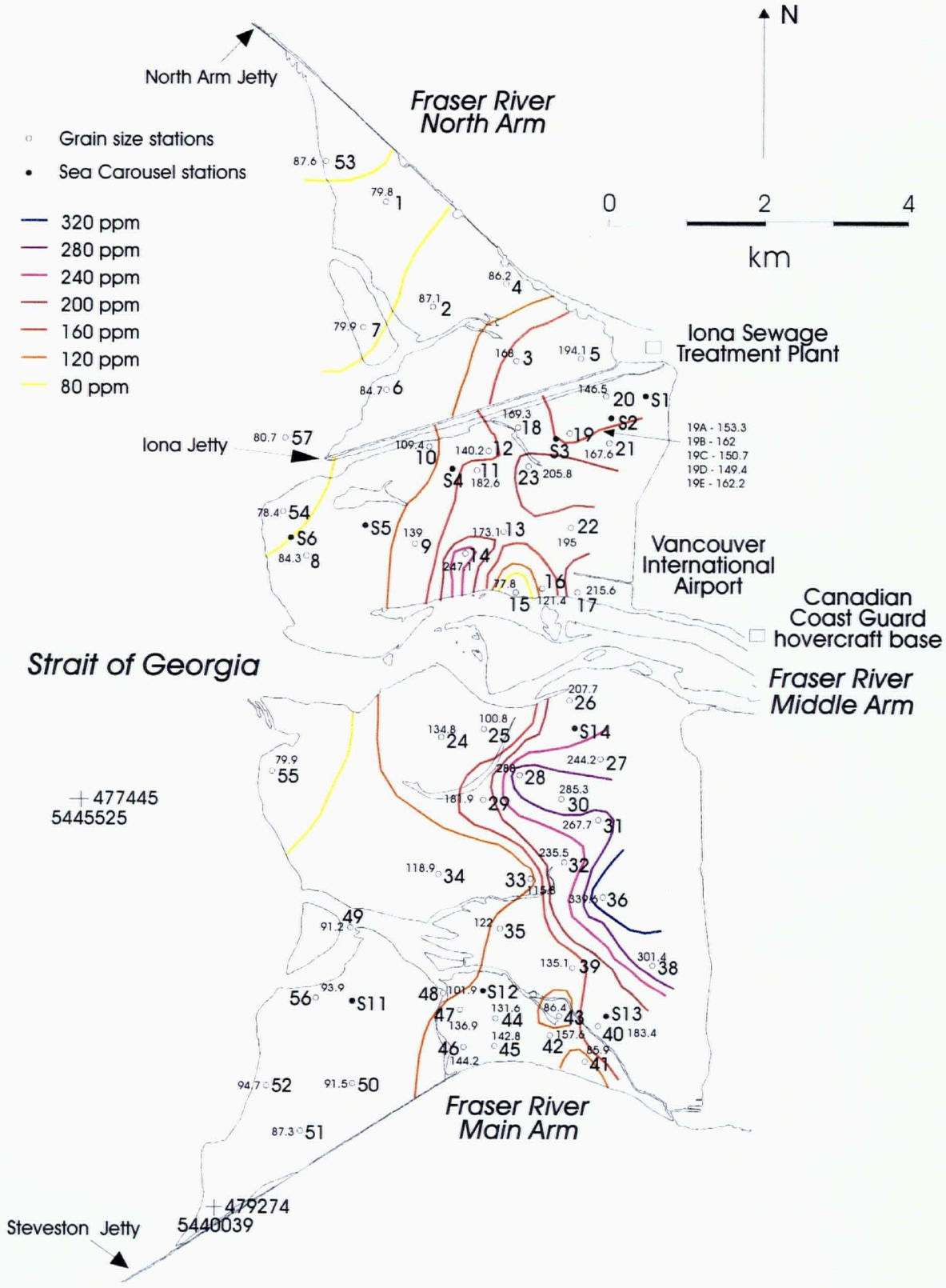

Figure 72: Areal distribution of zirconium content on Sturgeon Bank

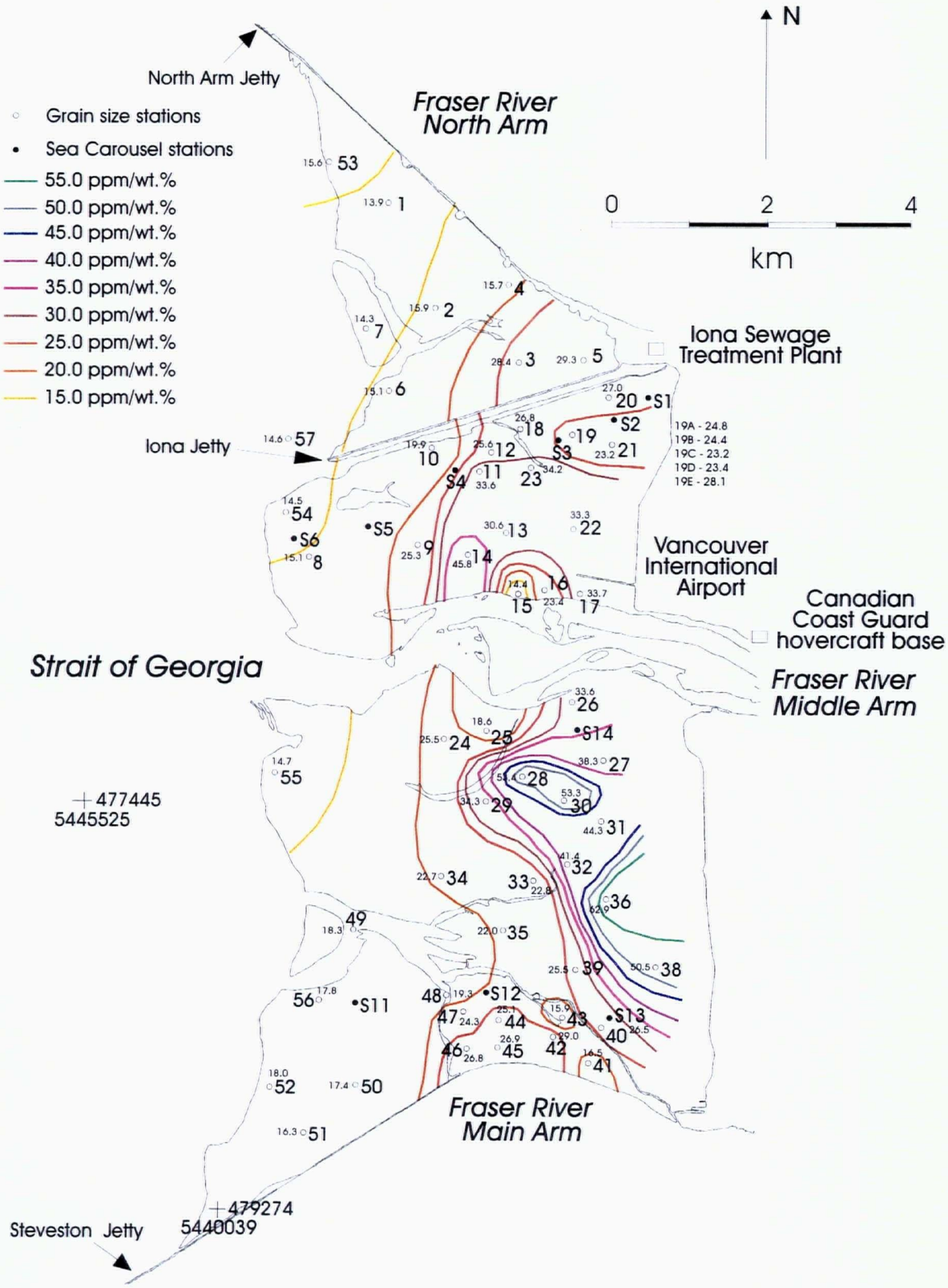

Figure 73: Areal distribution of Zr/Al on Sturgeon Bank

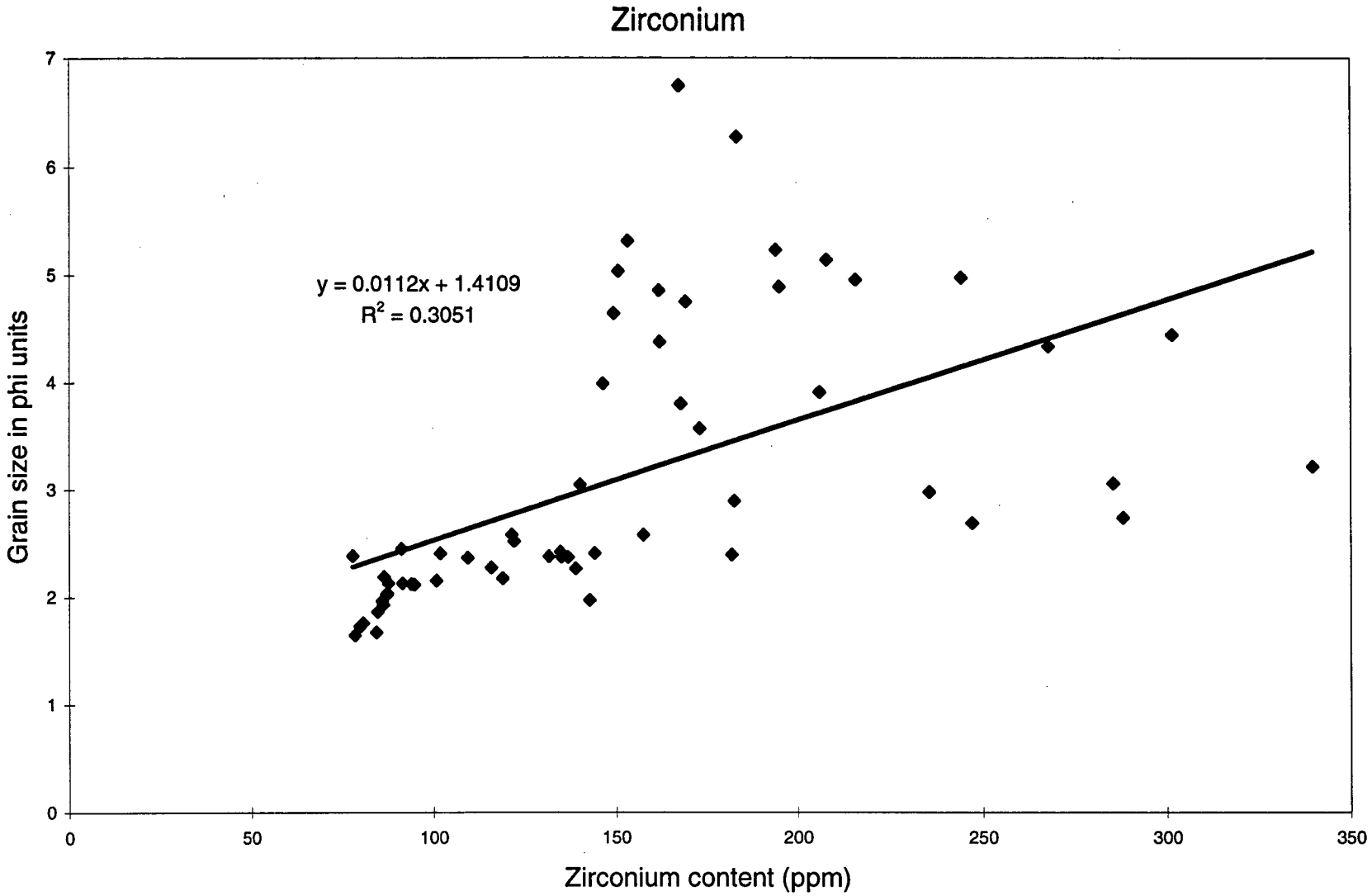

Figure 74: Zirconium content versus grain size

direction which was previously discussed.

The minor element concentrations measured at station 19 show a wider range in variation than the major elements. Cobalt content ranges from 32-82 ppm with no trend in concentration in any direction. Chromium concentrations show slight variation and are highest in a shoreward direction with the exception of sample 19E. Ni contents vary only slightly and decrease in a seaward direction, while V and Mn contents show no concentration trend in any direction. Cu content ranges from 28-34 ppm, zinc content ranges from 80-90 ppm and Pb content ranges from 18-26 ppm. All three elements show reasonably small variations between samples and no discernable trend in concentration in a seaward or shoreward direction. Zr behaves similar to Cu, Zn and Pb with only small sample variations and no Zr-concentration trends.

Organic carbon behaves similar to Ni and Cr in that it decreases in a seaward direction. The low C_{org} value measured in sample 19E is consistent with low Al, Ti, Fe, Ni, Zn and Pb contents measured at this station. The degree of variability and the lack of obvious trends in sediment geochemical results within a 10 metre spacing, especially in some of the minor element measurements, make it difficult to extrapolate values across the bank. Initially the 56 stations sampled for sediment geochemistry were thought to behave similarly to sediments collected from the 10 Sea Carousel sites and unfortunately geochemical analyses were not performed on the sediments collected from the Sea Carousel stations due to an inadequate sample supply. However, the degree of variability in sediment grain size results within a 10 metre spacing reveals how difficult it is to extrapolate values across the bank. Sediment geochemical results should therefore be assumed to be site specific.

6.3.6. GEOCHEMICAL SUMMARY OF STURGEON BANK SEDIMENTS

The fine silt sediments from stations 21 and 40 show the highest concentrations of Al, Fe, Cu, and Zn. These elements are generally more abundant in the finer grain size fraction on the inner bank and decrease in content in a seaward direction. The affinity for fine-grained sediments results in good correlation of these elements with grain size. High concentrations of these elements at station 40 can be explained by textural effects due to grain size, while at station 21 high concentrations indicate an additional host is contributing. This source is likely the now-inactive Iona sewage outfall which discharged onto this area of Sturgeon Bank from 1962-1988 causing contaminant deposition.

The iron present on the bank may be found in pyrite, mica, magnetite, chlorite, or ilmenite, with mica, magnetite and chlorite being the most likely phases. Sturgeon Bank surface sediments were found by Amos et al. (in prep.) to contain approximately 16% chlorite, 29% mica, 6% smectite, 39% quartz and 9% feldspar using X-ray diffraction which is consistent with the findings in this study. The Fe/Mg correlation suggests that there is an additional source of Fe than what is present as ferro-magnesian minerals, likely in the form of Fe-oxides. Fe-oxides may be responsible for the Cu and Zn enrichments at station 21. Manganese-oxides do not seem to be significant in surface sediments on Sturgeon Bank. Despite the higher concentrations of Cu, Zn and Fe in surface sediments at station 21, the values measured are relatively low and typical of uncontaminated estuaries in B.C. The enrichment of Cu and Zn in sediments collected from stations 21 and 40 is not reflected in the vanadium concentration, an element also released by sewage (Hall et al., 1974). The excellent vanadium correlation with iron indicates direct substitution of V for Fe probably in biotite, chlorite or magnetite and implies that V is not a

contaminant in surface sediments on Sturgeon Bank.

The coarse silts and very fine to fine sands, particulary at stations 14, 28, 30 and 36 tend to concentrate the heavier elements including Ti, Cr, Zr, Fe, V, and to a lesser extent Ni. This accumulation in the coarser-grained sediments results in poor correlation of these elements with grain size. Instead these elements are concentrated in areas of heavy-mineral accumulation where magnetite, zircon and ilmenite are probably more abundant. Silica and zirconium show concentrations in Sturgeon Bank surface sediments significantly higher than sediments from Howe Sound probably due to the coarse-grained nature of sediments deposited from the Fraser River. The high Co content on Sturgeon Bank can not be explained by textural effects, organic carbon content or element associations and therefore its distribution on the bank is unexplained.

The organic carbon content on Sturgeon Bank is low and representative of many nearshore estuaries, while the carbonate carbon content on the bank is extremely low. The excellent correlation between C_{org} and grain size indicates that hydraulic sorting plays a large role in the distribution of organic carbon on the bank.

The association of characteristics between specific stations is demonstrated using a principal components analysis (PCA). A PCA is a data reduction technique where the primary goal is to construct linear combinations (components) of the original data variables. The successive linear combinations are constructed in such a way that they are uncorrelated with each other and account for successively smaller amounts of the total data variation (Dillon and Goldstein, 1984). The elements Pb, Zn, Cu, Ni, Co, Cr and TiO_2 were used as data variables in a PCA. Examination of the first three components explained 90% of the variation in the data and therefore examination of additional components was not needed. The first component weights

Pb, Cu, and Cr positively; Zn, Ni and TiO_2 positively higher; and Co negatively. The second component weights Pb, Zn and Cu negatively, Ni slightly positively; Co and TiO_2 more positively; and Cr the most positively. The third component weights Pb, Zn, and Cu positively; Co considerably more positively; and Ni, Cr, and TiO_2 negatively.

Plotting the first two components results in a wide scatter of data points (Figure 75a). Stations 14, 28, 30 and 36 group together with stations 22 and 32 plotting close to these four stations; station 21 is plotted by itself; station 17, 19A-E, 26, and 40 plot towards station 1; and stations 5, 18, 23, 27, 31 and 38 group together towards the heavy-mineral accumulators at stations 14, 28, 30, and 36. Plotting the second and third components also results in a wide scatter of data points (Figure 75b). Stations 4 and 22 (the high cobalt stations) group together with stations 5 and 18 plotting close by; station 21 is once again plotted alone; and stations 14, 28, 30, 32, 36, and 42 are closely related. Station 19 samples A-E are not grouped tightly together in either plot and confirm the that the degree of variability between samples makes it difficult to extrapolate geochemical data to other areas of the bank.

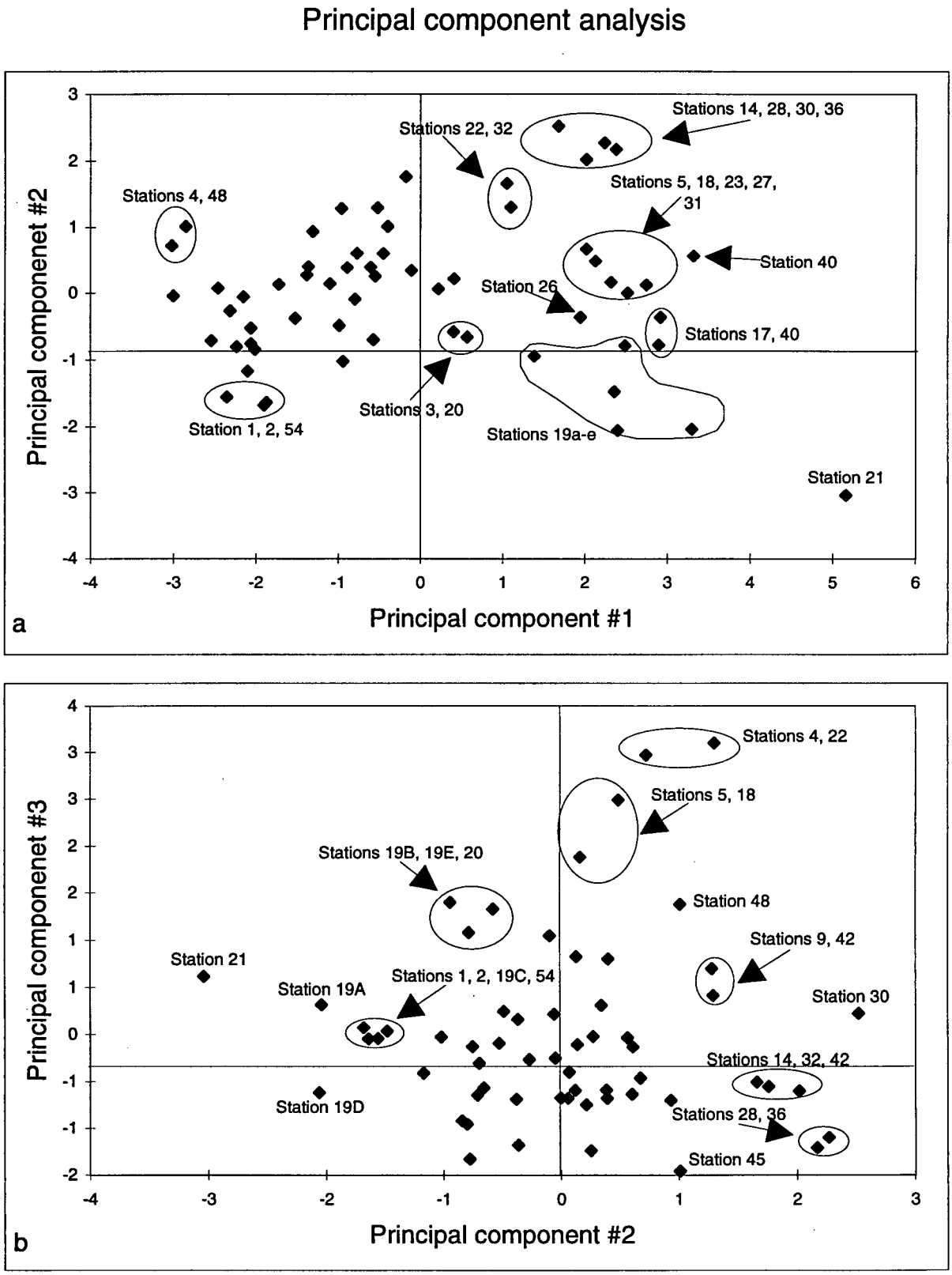

Figure 75: Principal componenet analysis using Pb, Zn, Cu, Ni, Co, Cr, TiO2

Chapter 7: SUMMARY AND CONCLUSIONS

7.1. SUMMARY

The fine-grained cohesive sediments from the inner bank require applied current velocities for sediment suspension greater than either wave particle or tidal velocities are known to reach on the bank. Therefore, sediments at these stations are not easily eroded. If the critical shear velocity for erosion is reached at stations 1, 2 and 14, sediments should erode very easily due to the presence of weak layers below the surface. It is for this reason that the entire failure envelope of a sediment rather than just its surface strength must be examined. Stations 3 and 13 do not show this weak layer below the surface and as a result erosion rates considerably lower than the other inner bank stations. It is expected that velocities capable of suspending sediments on the inner bank may be reached on the initial incoming or final outgoing tide especially in the presence of waves and therefore play a significant role in sediment transport. However these velocities could not be measured. The decrease in current velocities in a shoreward direction suggests that waves do not break but dissipate energy as they move across the bank as first suggested by Medley (1978).

High suspended sediment concentrations on the inner bank imply that sediments are being supplied from the outer bank diffusively resulting in overall sediment accumulation on the inner bank. This diffusive nature is responsible for the increase in SSC in a shoreward direction.

Non-cohesive sediments on Sturgeon Bank are suspended more easily because of their lack of cohesive strength, especially the fine-grained sands on the outer southern Sturgeon Bank. At all stations composed of non-cohesive sediments wave particle velocities (high-frequency

velocity fluctuations) capable of suspending sediments were reached. At station 11, where suspending velocities were reached several times, even tidal current velocities seemed capable of sediment erosion. A considerable amount of sediment is transported in a flooding direction from the outer southern bank implying advective movement of sediment in a shoreward direction. Sediment transported shoreward from the outer southern bank suggests erosion in this area and no evidence of sediment replenishment from the Fraser River is observed. The GPS-generated perspective of Sturgeon Bank (See Figure 3) shows lower elevations on the southern relative to the northern portion of Sturgeon Bank supporting this observation. The grain size, sorting, and geochemical data also support the transport of sediment shoreward with coarser-grained, better sorted, heavy-mineral-rich sediments occurring on the inner southern bank at stations 28, 30, 32, and 36.

Sediment transport rates in both flooding and ebbing directions on the outer southern bank are up to 8 times higher than on central Sturgeon Bank. On the outer central bank sediment transport in an ebbing direction is higher, however transport rates are low in both directions and therefore not considered significant. Sediment appears to be supplied from the Main Arm and to a lesser extent Middle Arm of the Fraser River on the outer central bank and elevations are high relative to the outer southern bank. Current velocities generated from fluvial discharge from the Middle Arm appear to play a minor role in sediment transport on the outer central bank. Despite the strong influence from the Middle Arm flow at station 14, discharge velocities capable of eroding sediments here are not reached even in freshet flows.

Recently GeoSea Consulting completed a report discussing sediment transport and its environmental implications in the lower Fraser River and Fraser delta (McLaren and Ren, 1995).

In this report the authors concluded that most of the intertidal flats are not receiving sand through normal deltaic processes and that there appears to be insufficient sand passing through the Middle Arm to have any impact on Sturgeon Bank. The report also suggests that intertidal sediments between the jetties no longer have any relationship with the Fraser River sediments. These findings are somewhat consistent with this study in that sediments are being eroded from the outer southern area of the bank and transported shoreward and these sediments are not being replenished from the Fraser River discharge. In contrast to the GeoSea report, this study concludes that sediments supplied from the Middle Arm, although minor, reach the outer central bank area and that sedimentation on the inner bank is taking place through not only advective but also diffusive processes which bring Fraser River sediment to the inner bank.

The generally high erosion thresholds, low erosion rates and low current velocities measured on the bank imply that a considerable amount of the sediment in suspension on the bank is derived from the Fraser River with a smaller amount derived from erosion of the bank itself. However waves can strongly influence the concentration of suspended sediments on Sturgeon Bank especially on the outer southern bank where sediments are more easily eroded as stated above. Winds from the west are most likely to increase current velocities, sediment erosion, suspended sediment concentration and sediment transport. Bioturbation by benthic organisms found on the bank will also contribute to increased sediment resuspension. In contrast, benthic diatoms may act as biostabilizers on the sediment surface especially on the inner bank, therefore decreasing the likelihood of sediment resuspension.

Geochemical analyses of surface sediments on Sturgeon Bank show little sign of contamination from anthropogenic Cu, Zn, Fe, V, Cr, Ti or Pb. The distribution of these

elements is more likely controlled by textural differences in grain size within the sediment. For this reason, the elemental composition of sediment samples should not be compared unless grain size effects are taken into consideration. Sturgeon Bank may contain lower concentrations of some anthropogenic tracers due to the general coarse-grained nature and relatively low clay contents of surface sediments.

Fe, V, Ti, Cr, and Zr are concentrated in areas of heavy mineral accumulation on the inner southern Sturgeon Bank and adjacent to the North Arm channel at station 14. The distribution of these elements is controlled not only by sediment texture but by the physical controls on sediment transport.

Cobalt behaves unlike any other minor element analyzed in this study. Co content is significantly higher than average values measured in igneous rocks and sediments from uncontaminated estuaries. Both the source and the host of the cobalt in Sturgeon Bank surface sediments is unknown and should be investigated.

Organic carbon content may contribute to the distribution of minor elements on the bank with potentially more reactive organic carbon found adjacent to the once active Iona sewage outfall. Organic carbon contents in Sturgeon Bank surface sediments however are low and thus only explain some of the minor element distribution. The higher Cu/Al, Pb/Al and Zn/Al ratios found at station 21 compared to station 40 in fine-silt sediments suggest that the distribution of these elements adjacent to the inactive outfall is due to controls in addition to grain size. Fe-oxides may be hosting some of the minor elements but Mn-oxides do not appear to be significant on the bank and therefore are unlikely hosts for metal accumulation.

7.2. CONCLUSIONS

Time, manpower and equipment limits the amount of data feasibly collected in any project. This study attempted to link together a multitude of aspects so that a more comprehensive view of the processes which control sediment and contaminant distribution on Sturgeon Bank could be understood. It was concluded from this study that 1) contamination on Sturgeon Bank from the sewage discharged there from 1962-1988 appears to have been greatly reduced in the surface sediments; 2) cobalt contents on the bank are high and need to be investigated; 3) minor element distribution appears to be controlled by both grain size and the physical processes responsible for sediment transport; 4) sediments from the outer southern bank appear to be easily eroded and transported shoreward, especially when waves are present, with no discernable sediment replenishment from the Fraser River; 5) currents measured on the inner bank are not capable of eroding sediments. However eroding velocities are expected to occur on the initial and final stages of the tide resulting in a high concentration of sediment suspended due to weak subsurface layers in sediments on the inner bank; 6) both advective and diffusive processes are responsible for supplying the inner bank with sediment; 7) the degree of variability in erosion thresholds, current velocities and directions, suspended sediment concentrations, grain size and sediment geochemistry restricts the extrapolation of specific results to other areas of the bank. The present results should therefore be considered both spatially and temporally specific.

7.2.1. RECOMMENDATIONS

Analyses of sediment cores would improve the understanding of surface sediments on Sturgeon Bank by providing a means to obtain sediment accumulation rates. A knowledge of the

subsurface geochemistry may also explain the resulting surface geochemistry. A detailed study to examine the variation in suspended sediment concentration over a tidal cycle and in the presence of waves as well as a more precise method of collecting a depth-integrated water sample would improve the understanding of suspended sediment dynamics. A more intensive look at erosion thresholds over more areas of the bank including within the Middle Arm channel and across the middle of the bank would greatly increase the knowledge of Sturgeon Bank sediment stability. Velocity fluctuation measurements in shallow-water conditions would provide information on currents generated on an initial rising and final falling tide. If sediments on the bank are being transported shoreward, a detailed look at the geochemistry and transport of sediments within the marsh may reveal the sink for contaminated sediments on the bank. These investigations would provide information needed to refine the conclusions of this study.

REFERENCES

Abbey, S., 1980. Studies in 'standard samples' of silicate rocks and minerals, 1969-1982. Geological Survey of Canada Paper 83-15, 114p.

Aitken, J.A. and T.D. Feeney, 1994. Two centimetre-level Global Positioning System surveys of intertidal habitat, Fraser River delta, British Columbia. *Geological Survey of Canada Current Research* **1994A**, 225-230.

Amos, C.L., 1995. Siliciclastic tidal flats. In *Geomorphology and Sedimentology of Estuaries: Developments in Sedimentology* **53,** G.M.E. Perillo (ed.). Elsevier Science, pp. 273-306.

Amos, C.L., G.R. Daborn, H.A. Christian, A. Atkinson, and A. Robertson, 1992b. *In situ* measurements of fine-grained intertidal sediments from the Bay of Fundy. *Marine Geology* **108,** 175-196.

Amos. C.L., J. Grant, G.R. Daborn, and K. Black. 1992a. Sea carousel - a benthic annular flume. *Estuarine, Coastal and Shelf Science* **34,** 557-577.

Amos, C.L, T.D. Feeney, and J.L. Luternauer, (in preparation). The stability and erodibility of fine-grained sediments from the Fraser River delta foreshore and upper foreslope.

Amos, C.L., N.A. van Wagonner, and G.R. Daborn, 1988. The influence of subaerial exposure on the bulk properties of fine-grained intertidal sediment from Minas Basin, Bay of Fundy. *Estuarine, Coastal and Shelf Science* **27,** 1-13.

Anderson, F.E. and B.A. Howell, 1984. Dewatering of an unvegetated muddy tidal flat during exposure - desiccation or drainage? *Estuaries* **7**, 225-232.

Armstrong, J.E., 1956. Surficial geology of the Vancouver area, British Columbia. *Geological Survey of Canada Paper* 55-40, 16p.

Bawden, C.A., W.A. Heath, and A.B. Norton, 1973. A preliminary baseline study of Roberts and Sturgeon Banks. *Westwater Research Centre* Technical Report No. 1., University of British Columbia, 54p.

B.C. Research, 1973. Environmental studies at Iona Island. Report 1 prepared for the Greater Vancouver Sewerage and Drainage District, 43p.

B.C. Research, 1975. Environmental studies at Iona Island. Report 2 prepared for the Greater Vancouver Sewerage and Drainage District, 162.

B.C. Research, 1977. Environmental studies at Iona Island. Report 3 prepared for the Greater Vancouver Sewerage and Drainage District, 23p.

Benedict, A.H., K.J. Hall, and F.A. Koch, 1973. A preliminary water quality survey of the lower Fraser River system. *Westwater Research Centre* Technical Report No. 2, University of British Columbia, 50p.

Birtwell, I.K., G.L. Greer, M.D. Nassichuk, and I.H. Rogers, 1983. Studies of the impact of municipal sewage discharged onto an intertidal area within the Fraser River Estuary, British Columbia. *Canadian Technical Reports of Fisheries and Aquatic Sciences* Number 1170, 55p.

Bogen, J., 1980. The hysteresis effect of sediment transport systems. *Norsk. Geogr. Tidsskr* **34,** 45-54.

Borodowskiy, O.K., 1965. Accumulation of organic matter in bottom sediments. *Marine Geology* **3**, 33-82.

Bowen, H.J.M., 1979. *Environmental Chemistry of the Elements*. Academic Press, London, 229p.

Brown, J., A. Colling, D. Park, J. Phillips, D. Rothery, and J. Wright, 1989. *Waves, Tides and Shallow-water Processes*. The Open University in Association with Pergamon Press, G. Bearman (ed.), 186p.

Burton, J.D. and Liss, P.S., 1976. *Estuarine Chemistry*. Academic Press, London, 229p.

Calvert, S.E. and N.B. Price, 1983. Geochemistry of Namibian Shelf sediments. In *Coastal Upwelling*, E. Suess and J. Thiede (eds.), Plenum Press, London, pp. 337-375.

Calvert, S.E., 1976. The mineralogy and geochemistry of nearshore sediments. In *Chemical Oceanography,* Volume 6, 2nd edition, J.P. Riley and R. Chester (eds.). Academic Press, London, pp. 187-280.

Cambell, P.G.C., A.G. Lewis, P.M. Chapman, A.A. Crowder, W.K. Fletcher, B.Imber, S.N. Luoma, P.M. Stokes, and M. Winfrey, 1988. Biologically available metals in sediments. *National Research Council of Canada Associate Committee on scientific criteria for environmental quality*. NRCC Publication Number 27694, 298p.

Canadian Hydrographic Service 1972. Tide and current tables. Volume 5 (Juan de Fuca and Georgia Strait), p14.

Carpenter, J.H., W.L. Bradford and V.E. Grant, 1975. Processes affecting the composition of estuarine waters. In *Estuarine Research*, L.E. Cronin (ed.), Volume 1. Academic Press, New York, pp. 188-214.

Church, M., D.G. McLean, R. Kostaschuk, S. McFarlane, B. Tassone, and D. Walton, 1990. Channel stability and management of lower Fraser River field excursion guide. Environment Canada, Inland Waters Directorate, Water Resources Branch, April, 1990.

Church, M. and R. Gilbert, 1975. Proglacial fluvial and lacustrine environments in glacifluvial and glaciolacustrine sedimentation, A.V. Jopling and B.C. McDonald (eds.). Special Publication of the *Society of econ. Paleont. Miner.* Tulsa. **23**, 22-100.

Clague, J.J., J.L. Luternauer, and R.J. Hebda, 1983. Sedimentary environments and postglacial history of the Fraser Delta and lower Fraser Valley, British Columbia. *Canadian Journal of Earth Science* **20,** 1314-1326.

Coastline Environmental Services Ltd., 1985. A field survey to determine the areal extent of sewage contamination on Sturgeon Bank in the vicinity of the Iona Island outfall. Consultant Report prepared for the Department of Fisheries and Oceans, Vancouver, 17p.

Davis, D.C., 1986. *Statistics and Data Analysis in Geology.* Wiley, New York, 646p.

Degens, E.T., 1965. *Geochemistry of sediments, a brief survey.* Prentice-Hall, Englewood Cliffs, N.J., 342p.

Dillon, W.R. and M. Goldstein, 1984. Multivariate analysis - Methods and applications. John Wiley and Sons, Toronto, Ontario, 587p.

Downing, J.P. and R.A. Beach, 1989. Laboratory apparatus for calibrating optical suspended solid sensors. *Marine Geology* **86**, 243-249.

Drysdale, K., 1990. Geochemistry of a buried marine mine tailings deposit, Howe Sound, British Columbia. Unpublished MSc thesis, University of British Columbia, 375p.

Dyer, K.R., 1986. *Coastal and Estuarine Sediment Dynamics.* John Wiley and Sons, Chichester, 342p.

Feeney, T.D., 1994. Preliminary studies of currents on Sturgeon Bank, Fraser River delta, British Columbia. *Geological Survey of Canada Current Research* **1994A**, 217-224.

Feeney, T.D., C.L. Amos, and J.L. Luternauer, 1994. Sediment pollution regime on the northern tidal flats, Fraser River delta, British Columbia, Canada. In *Coastal Zone Canada '94, "Cooperation in the coastal zone".* Conference Proceedings, No. 3, pp. 1273-1287.

Folk, R.L., 1968. *Petrology of Sedimentary Rocks*. Hemphills Book Store, Austin Texas, 170p.

Folk, R.L. and W.C. Ward, 1957. Brazos River bar: a study in the significance of grain size parameters. *Journal of Sedimentary Petrology*, **27**, 3-26.

Francois, R. 1987. Some aspects of the geochemistry of sulphur and iodine in marine humic substances and transition metal enrichment in anoxic sediments. Unpublised Ph.D. thesis, University of British Columbia, Canada, 462p.

Friedman, G.M., 1967. Dynamic processes and statistical parameters compared for size frequency distribution of beach and river sands. *Journal of Sedimentary Petrology*, **37**, 327-354.

Gibbs, R.J., 1972. The accuracy of particle size analyses utilizing settling tubes. *Journal of Sedimentary Petrology* **42**, No. 1, 141-145.

Grant, J., U.V. Bathmann, and E.L. Mills, 1986. The interaction between benthic diatom films and sediment transport. *Estuarine and Coastal Shelf Sciences*, **23**, 225-238.

Gregory, K.J., and D.E. Walling, 1973. *Drainage Basin Form and Process. A Geomorphological Approach*. Edward Arnold, London, 456 p.

Grieve, D.A., 1977. Behaviour of some trace metals in sediments of the Fraser River delta-front, southwestern British Columbia. Unpuplished M.Sc. thesis, University of British Columbia, Canada.

Grieve, D.A. and W.K. Fletcher, 1976. Heavy metals in deltaic sediments of the Fraser River, British Columbia. *Canadian Journal of Earth Science*, **13**, 1683-1693

Hall, K.J., F.A. Koch, I. Yesaki. 1974. Further investigations into water quality conditions in the lower Fraser River system. *Westwater Research Centre* Technical Report No. 4., University of British Columbia, 104 p.

Hall, K.J. and W.K. Fletcher, 1974. Trace metal pollution from a metropolitan area: sources and accumulation in the lower Fraser River and estuary. In *Proceedings for the International Conference on Transport of Persistent Chemicals in Aquatic Ecosystems*, Ottawa, Ontario, May 1974, pp. 183-187.

Harding, L. and D. Goyette, 1989. Metals in northeast Pacific coastal sediments and fish, shrimp, and prawn tissues. *Marine Pollution Bulletin* **20,** No. 4, 187-189.

Harrison, P.J., 1981. The biological determinants of the structure of harpacticoid copepod communities on an estuarine intertidal flat (Fraser River delta, B.C.). Unpublished Ph.D. thesis, University of British Columbia, Canada, 350p.

Hodgins, D.O., T.R. Osborn and M.C. Quick, 1977. Numerical model of stratified estuary flows. American Society of Civil Engineers, *Journal of Waterways, Ports, Coastal and Ocean Division*, WW1, pp. 25-42.

Hoos, L.M. and Packman, G.A. 1974. The Fraser River estuary: status of environmental knowledge to 1974. Canada Department of the Environment Regional Board, Pacific Region, *Special Estuary Series*, No. 1, 518 p.

Johnston, W.A., 1921. Sedimentation of the Fraser River delta. *Geological Survey of Canada, Memoir* 125, 46p.

Jumars, P.A., A.R.M. Nowell, and R.F.L. Self, 1981. A simple model of flow-sediment-organism interaction. *Marine Geology*, **42**, No. 1, 155-172.

Klein, C. and C.S. Hurlbut Jr., 1977. *Manual of Mineralogy*, 20th edition. John Wiley and Sons, 596 p.

Kostaschuk, R.A., M.A. Church and J.L. Luternauer, 1989. Bedforms, bed-material and bed load transport in a salt-wedge estuary: Fraser River, British Columbia. *Canadian Journal of Earth Sciences*, **27**, 1440-1452.

Kostaschuk, R.A., B.A. Stephan and J.L. Luternauer, 1993. Suspended sediment concentration in a buoyant plume; Fraser River, Canada. *Geo-marine letters*, **13**, 165-171

Krauskopf, K.B., 1979. *Introduction to Geochemistry*, 2nd ed. McGraw-Hill, 617p.

Krom, M.D. and E.R. Sholokovitz, 1977. Nature and reactions of dissolved organic matter in the interstitial waters of marine sediments. *Geochimica Cosmochimica Acta*, **41**, 1565-1573.

Krumbein, W.C., 1934. Size frequency distribution of sediments. *Journal of Sedimentary Petrology*, **4**, 65-77.

Kuenen, P.H., 1965. Primary sedimentary structures formed by turbidity currents and related resedimentation mechanisms. In *Primary sedimentary structures and their hydrodynamic interpretation - A symposium for the Society of Economic Geologists and Mineralogists*, Special Publication, pp. 217-218.

Leick, A., 1990. *GPS Satellite Surveying*. Wiley, New York, 352p.

Levings, C.D., R.E. Foreman and V.J. Tunnicliffe, 1983. Review of the benthos of the Strait of Georgia and contiguous fjords. *Canadian Journal of Fisheries and Aquatic Sciences*, **40**, 1120-1141.

Loring, D.H. and R.T.T. Rantala, 1992. Manual for the geochemical analyses of marine sediments and suspended particulate matter. *Earth-Science Reviews*, **32**, 235-283.

Luternauer, J.L., 1975. Fraser Delta sedimentation, Vancouver, British Columbia. *Geological Survey of Cananda Paper*, **75-1(B)**, 171-172.

Luternauer, J.L. and J.W. Murray. 1973. Sedimentation on the western delta-front of the Fraser River, British Columbia. *Canadian Journal of Earth Science,* **10**, 1642-1663.

Mason, B. and C.B. Moore, 1982. *Principles of Geochemistry*, 4th ed. Wiley and Sons, N.Y., 344p.

Mathews, W.H. and F.P. Shepard. 1962. Sedimentation of the Fraser River Delta, British Columbia. *American Association of Petroleum Geologists,* **46**, 1416-1443.

McGreer, E.R. 1982. Factors affecting the distribution of Macoma balthica on a mudflat receiving sewage effluents, Fraser River estuary, B.C. *Marine Environmental Research,* **7**, 131-149.

McLaren, P. and P. Ren. 1995. Sediment transport and its environmental implications in the lower Fraser River and Fraser delta. Environment Canada, Environemental Conservation, DOE FRAP 1995-03.

McLean, D.G., and M.A. Church, 1986. A re-examination of sediment transport observations in the lower Fraser River; Environment Canada, Water Resources Branch, Inland Waters Directorate, Sediment Survey Section, IWD-HQ-WRB-SS-86-6.

McLean, D.G., and B.L. Tassone, 1991. A sediment budget of the lower Fraser River. In *Proceedings of the 5th Federal Interagency Sedimentation Conference*, March 18-21, Las Vegas, Nevada, pp. 2-33 to 2-40.

McNichol, A.P., C. Lee and E.R.M. Druffel, 1988. Carbon cycling in coastal sediments: 1. A quantitative estimate of the remineralization of organic carbon in the sediments of Buzzards Bay, MA. *Geochimica Cosmochimica Acta*, **52**, 1531-1534.

Medley, E., 1978. Dendritic channels and tidal flat erosion, west of Steveston, Fraser River delta, British Columbia. Unpublished B.A.Sc. thesis, University of British Columbia, Canada, 70p.

Medley, E. and J.L. Luternauer. 1976. Use of aerial photographs to map sediment distribution and to identify historical changes on a tidal flat. *Geological Survey of Cananad Report of Activities,* **76-1C**, 293-204.

Milliman, J.D. 1980. Sedimentation in the Fraser River and its Estuary, Southwestern British Columbia (Canada). *Estuarine and Coastal Marine Science,* **10**, 609-633.

Morton, R.A. and M.P. Leach, 1993. Monitoring beach changes using GPS surveying techniques. *Journal of Coastal Research,* **9**, No. 3, 701-720.

Müller, P.J., 1977. C/N ratios in Pacific deep-sea sediments: Effect of inorganic ammonium and organic nitrogen compounds sorbed by clays. *Geochimica Cosmochimica Acta*, **41**, 765-776.

Nesse, W.D., 1986. *Introduction to Optical Mineralogy.* Oxford University Press, Oxford, 325p.

Norrish, K. and J.T. Hutton, 1969. An accurate X-ray spectrographic method for the analysis of a wide range of geochemical samples. *Geochimica Cosmochimica Acta*, **33**, 431-453.

Nowell, A.R.M., P.A. Jumars, and J.E. Eckman, 1981. Effects of biological activity on the entrainment of marine sediments. *Marine Geology*, **42**, No. 1, 133-153.

Otte, G. and C.D. Levings, 1975. Distribution of macroinvertebrate communities on a mudflat influenced by sewage. Fraser River Estuary, British Columbia. *Fisheries Marine Series* Technical Report No. 476, 78p.

Parsons, T.R., C.A. Bawden, and W.A. Heath. 1973. A preliminary survey of mercury and other metals contained in animals from the Fraser River mudflats. *Journal of Fisheries Research Board,* **30**, 1014-1016.

Paterson, D.M., 1989. Short-term changes in the erodibility of intertidal cohesive sediments related to the migratory behavior of epipelic diatoms. *Limnology and Oceanography*, **34**, No. 1, 223-234.

Paterson, D.M., R.M. Crawford, and C. Little, 1990. Subaerial exposure and changes in the stability of intertidal estuarine sediments. *Estuarine and Coastal Shelf Science*, **30**, 541-556.

Pettijohn, F.J., P.E. Potter, and R. Siever, 1973. *Sand and Sandstone.* Springer-Verlag, New York, 618 p.

Pharo, C.H., 1972. Sediments of the central and southern Strait of Georgia, B.C. Unpublished Ph.D. thesis, University of British Columbia, Canada, 265p.

Poon, D., 1989. Leaded and lead-free gas regulations monitoring program. *Environment Canada Conservation and Protection; Environmental Protection Pacific and Yukon Region*, Program Report 88-04.

Postma, H., 1961. Transport and accumulation of suspended matter in the Dutch Wadden Sea. Netherlands Journal of Sea Research, **1**, 148-190.

Postma, H., 1967. Sediment transport and sedimentation in the estuarine environment. *Estuaries*, **83**, 158-179.

Premuzic, E.T., C.M. Benkovitz, J.S. Gaffney, and J.J. Walsh, 1982. The nature and distribution of organic matter in the surface sediments of world oceans and seas. *Organic Geochemistry*, **4**, 63-77.

Rankama, K. and T. Sahama, 1950. *Geochemistry*. Chicago University Press, Chicago, 919p.

Rawn, A.M., C.G. Hyde and J. Oliver, 1953. Sewerage and drainage of the Greater Vancouver area, British Columbia. *Vancouver and Districts Sewerage and Drainage Board.*

Remondi, B.W., 1985. Performing centimetre-level surveys in seconds with GPS carrier phase: Initial results. *Journal of the Institute of Navigation*, **32**, 194-208.

Richardson, S.M. and H.Y. Jr. McSween, 1989. *Geochemistry*. Prentice-Hall, New Jersey, 488p.

Rosenfeld, J.K., 1979. Amino acid diagenesis and adsorption in nearshore anoxic sediments. *Limnology and Oceanography*, **24**, No. 6, 1014-1021.

S & S Consultants, 1983. Iona deep sea outfall feasibility study, Volume I and II. *Greater Vancouver Sewerage and Drainage District*, 159 p.

Statham, I., 1977. *Earth Surface Sediment Transport.* Clarendon press, Oxford, 184 p.

Swan, D., J.J. Clague, and J.L. Luternauer, 1978. Grain-size statistics I: Evaluation of the Folk and Ward graphic measures. *Journal of Sedimentary Petrology*, **48**, No. 3, 863-878.

Swan, D., J.J. Clague, and J.L. Luternauer, 1979. Grain size statistics II: Evaluation of grouped moment measures. *Journal of Sedimentary Petrology*, **49**, No. 2, 487-500.

Tabata, S., 1972. The movement of Fraser River-influenced surface water in the Strait of Georgia as deduced from a series of aerial photographs. *Marine Sciences Branch, Pacific Region, Pacific Marine Science* Report 72-6, 69p.

Tabata, S., Giovando, L.F., and Devlin, D. 1971. Current velocities in the vicinity of the Greater Vancouver Sewerage and Drainage District's Iona Island Outfall, 1968. *Fisheries Research Board of Canada* Technical Report 263, 110 p.

Thomson, R.E., 1975. Longshore current generation by internal waves in the Strait of Georgia. *Canadian Journal of Earth Science*, **12**, 472-488.

Thomson, R.E. 1977. The oceanographic setting of the Fraser River delta front. Unpublished manuscript, Institute of Ocean Sciences, Patricia Bay.

Troup, B.N. and O.P. Bricker, 1975. Processes affecting the transport of materials from continents to oceans. In *Marine Chemistry of the Coastal Environment.* T.M. Church (ed.), ACS Symposium Series 18, Washington, D.C., Ch. 8.

Udden, J.A., 1898. *Mechanical composition of wind deposits.* Augustana Library Publications, Volume 1, 69p.

Underwood, G.J.C. and D.M. Paterson, 1993. Seasonal changes in diatom biomass, sediment stability and biogenic stabilization in the Severn Estuary. *Journal of the Marine Biology Association*, **73**, 871-887.

van Straaten, L.M.J.U. and Kuenen, P.D., 1957. Accumulation of fine-grained sediments in the Dutch Wadden Sea. *Geol. Mijnb.*, **19**, 329-354.

Walling, D.E., 1974. Suspended sediment and solute yields from a small catchment prior to urbanization in Fluvial Processes. In *Instrumental Watersheds.* K.J. Gregory and D.E. Walling (eds.), Institute of British Geography, Special publication, No. 6, pp. 169-192.

Wells, D.E., N. Beck, D. Delikaraoglou, A. Kleusberg, E.J. Krakiwsky, G. Lachapelle, R.B. Langley, M. Nakiboglu, K.P. Schwarz, J.M. Tranquilla, and P. Vanicek, 1987. *Guide to GPS Positioning.* Canadian GPS Associates, Fredericton, New Brunswick.

Wentworth, C.K., 1922. A scale of grade and class terms for clastic sediments. *Journal of Geology*, **30**, 377-392.

Wright, 1972. The geochemistry of Recent sediments of the Barents Sea. Unpublished Ph.D. thesis, University of Edinburgh, Scotland.

Appendix I: GPS BATHYMETRIC SURVEY ON STURGEON BANK

The purpose of this study was to establish a highly accurate surveying method suited to delta habitats. A two day survey on Sturgeon Bank employed Global Positioning System (GPS) survey techniques and the Canadian Coast Guard Search and Rescue hovercraft. Elevation data was obtained in twelve transects between Iona and Steveston jetties, with the post-processed data being accurate to 10 cm or less in three dimensions relative to known reference point. A more detailed description of the study is found in Aitken and Feeney (1993). This approach is suited for surveying intertidal areas which are difficult to access and are not represented on bathymetric and topographic maps in detail.

Differential GPS involves the use of two receivers collecting data simultaneously; one receiver over a known reference point and one receiver on an unknown point (static) or on a moving platform (kinematic). The GPS solution is affected by error in the satellite orbits, satellite clocks, receiver clocks, and deliberate signal degradation by the U.S. Department of Defense (Selective Availability, or SA) (Wells et al., 1987). When the reference receiver is over a known reference point the receiver determines the error in signals and in post-processing these corrections are applied to the second receiver, provided the second receiver is within a given range (in this application < 50 km). Differential kinematic GPS allows position determination at the centimetre level (post-processed) with accuracies of 0.5 cm ± 1 to 2 ppm of the baseline (Remondi, 1985). A full overview of the Global Positioning System is available in Leick (1990) or Wells et al. (1987). Morton and Leach (1993) provide an introduction for a kinematic GPS survey on beach sediments.

Two geodetic quality GPS receivers and two GPS antennas (one specifically for mobile data collection) were used. Prior to mobile data collection an accessible reference point was established at the Canadian Coast Guard hovercraft base, Vancouver International Airport. The reference point co-ordinates were determined via a static differential survey tied to a first-order survey marker in Steveston, approximately 9 km away. The reference position is accurate relative to the Steveston marker at the sub-centimetre level and has the co-ordinates 49°10'51.8371, 123°11'4.9314 and a height of 3.406 m. The accuracy of all mobile GPS solutions are relative to the established reference co-ordinates. In order to solve for the unknown variables (latitude, longitude and height) with the GPS solution in post processing, both GPS receivers must maintain continuous phase lock with at least four common satellites throughout the survey.

The GPS survey was conducted at spring low tides on July 29 and 30, 1993, to obtain ground elevations of the bank. The GPS solution provides a position for the antenna. To obtain the ground position, the height of the antenna mounted on the hovercraft was measured before and after the survey and this height subtracted from the position data. Height was fixed by keeping the hovercraft at full inflation during height measurement and while collecting transect positions. The hovercraft traversed twelve transects between the Iona and Steveston jetties, spaced approximately 500 m apart while the mobile receiver recorded position data once every second. Speed of the hovercraft averaged 25 knots and each transect took an average of 10 minutes, providing close to 600 data points for each of the twelve transects. The antenna height variations before and after the survey were -4.9 cm and +6.4 cm for July 29 and July 30, repsectively.

Kinematic data were processed with the U.S. National Geodetic Survey OMNI processing software. The solution files contain the starting index position for the mobile antenna and an independent position solution for each second of data collection. The position solutions are expressed as delta values from the starting position. All positions were then transformed to latitude, longitude and height (WGS 84) using the known reference station co-ordinates. Data points at the end of each transect were removed because the hovercraft loses height when it slows to make a turn. Each position data point was plotted in ARC/Info, a commercial GIS program, and a contour map created. The contours were then overlayed on the station location map of Sturgeon Bank where the elevations of each station could be observed directly from the map (Figure 76). The contours were then used to develop a three-dimensional perspective of the Sturgeon Bank area using ARC/Info (Figure 77). While collecting the position data, the locations of "wetted" areas of the bank were also being recorded by visual examination and verbal indication. These positions were then plotted on the traverse map and the approximate location of channels on the bank were drawn in and the channel locations overlayed on the perspectives map (Figure 78). This was subject to some human interpretation due to the fact that wetted areas on the bank may not be the result of tidal channels but simply the product of areas which remain wet (with as little as 1or 2 cm of water over them) even when the bank is completely exposed. It should therefore be interpreted as the "wetted" areas in some places rather than the position of channels.

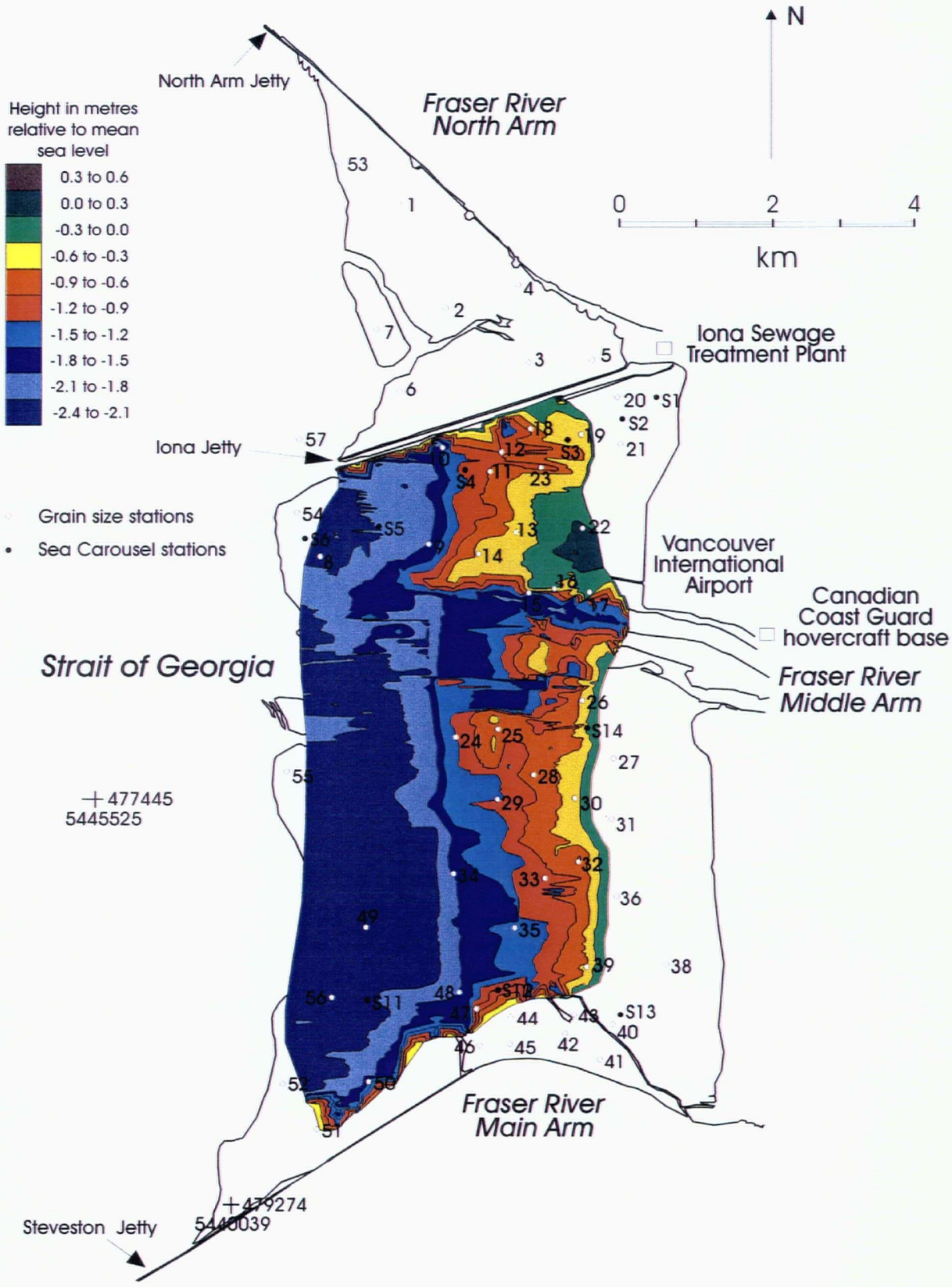

Figure 76: Sturgeon Bank contours constructed from GPS kinematic survey data

Figure 77: Three-dimensional perpective of Sturgeon Bank

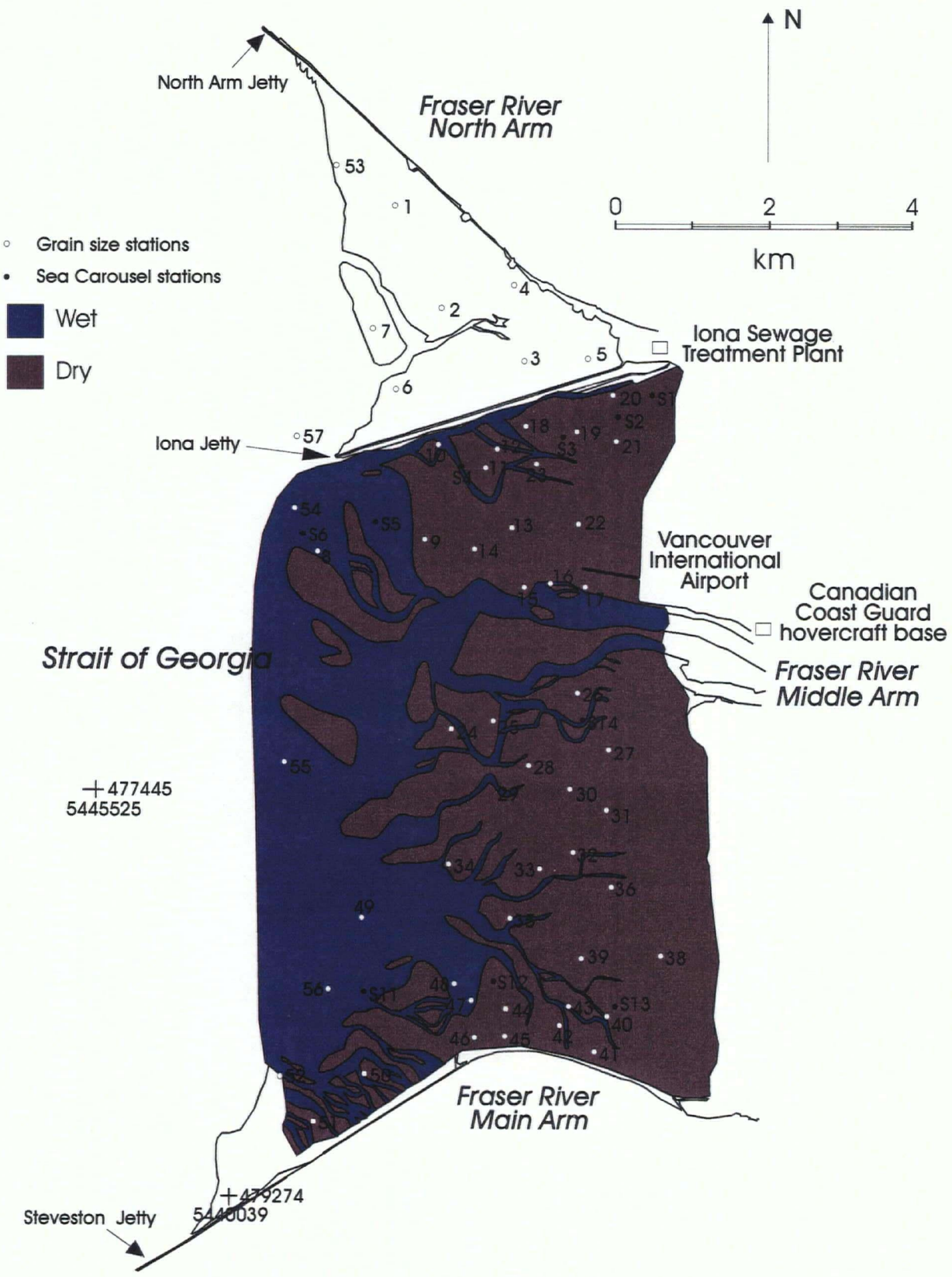

Figure 78: Approximate channel locations constructed using GPS kinemeatic survey

Appendix II: GEOGRAPHICAL STATION LOCATIONS ON STURGEON BANK

Station	Latitude	Longitude	Easting	Northing
1	49 14.12	123 15.25	481497	5453429
2	49 13.42	123 14.83	482002	5452130
3	49 13.02	123 13.87	483165	5451386
4	49 13.58	123 14.01	482998	5452424
5	49 13.04	123 12.89	496201	5451398
6	49 12.81	123 15.32	481404	5451002
7	49 13.26	123 15.59	481079	5451837
8	49 11.61	123 16.19	480340	5448783
9	49 11.71	123 15.03	481749	5448963
10	49 12.40	123 14.85	481972	5450241
11	49 12.21	123 14.28	482663	5449886
12	49 12.36	123 14.21	482748	5450164
13	49 11.79	123 14.03	482964	5449107
14	49 11.63	123 14.41	482501	5448812
15	49 11.37	123 13.86	483168	5448328
16	49 11.36	123 13.60	483483	5448309
17	49 11.36	123 13.21	483957	5448308
18	49 12.54	123 13.86	483174	5450496
19	49 12.49	123 13.35	483793	5450402
20	49 12.79	123 12.94	484293	5450956
21	49 12.42	123 12.83	484424	5450270
22	49 11.82	123 13.27	483887	5449160
23	49 12.26	123 13.74	483318	5449977
24	49 10.31	123 14.73	482105	5446368
25	49 10.37	123 14.22	482725	5446477
26	49 10.58	123 13.27	483880	5446863
27	49 10.15	123 12.92	484303	5446065
28	49 10.03	123 13.80	483233	5445846
29	49 9.86	123 14.23	482710	5445532
30	49 9.88	123 13.38	483743	5445566
31	49 9.70	123 12.93	484288	5445231
32	49 9.40	123 13.31	483825	5444676
33	49 9.27	123 13.69	483362	5444437
34	49 9.31	123 14.70	482135	5444515
35	49 8.91	123 14.02	482959	5443771
36	49 9.16	123 12.88	484346	5444230
38	49 8.76	123 12.88	484344	5443489
39	49 8.63	123 13.23	483918	5443250
40	49 8.20	123 12.92	484293	5442452
41	49 7.96	123 13.09	484085	5442008
42	49 8.14	123 13.45	483648	5442342
43	49 8.28	123 13.35	483770	5442601
44	49 8.26	123 14.05	482919	5442567
45	49 8.06	123 14.06	482906	5442196
46	49 8.05	123 14.40	482492	5442179
47	49 8.32	123 14.44	482445	5442680
48	49 8.43	123 14.64	482203	5442884
49	49 8.92	123 15.67	480954	5443796
50	49 7.78	123 15.63	480995	5441684
51	49 7.43	123 16.22	480276	5441038
52	49 7.76	123 16.58	479840	5441651
53	49 14.23	123 16.12	480442	5453637
54	49 11.93	123 16.46	480014	5449377
55	49 10.05	123 16.56	479880	5445894
56	49 8.40	123 16.05	480489	5442834
57	49 12.47	123 16.45	480030	5450377

Appendix II cont'd:

Station	Latitude	Longitude	Easting	Northing
S1	49 12.78	123 12.35	485009	5450936
S2	49 12.62	123 12.73	484547	5450641
S3	49 12.47	123 13.34	483805	5450365
S4	49 12.25	123 14.48	482420	5449961
S4a	49 12.51	123 14.74	482106	5450444
S5	49 11.84	123 15.44	481252	5449206
S6	49 11.75	123 16.26	480256	5449042
S11	49 08.39	123 15.54	481109	5442814
S12	49 08.47	123 14.09	482872	5442956
S13	49 08.29	123 12.73	484524	5442618
S14	49 10.38	113 13.11	484073	5446492

Appendix III: TIME SERIES PLOTS FOR SEA CAROUSEL ERODIBILITY DATA

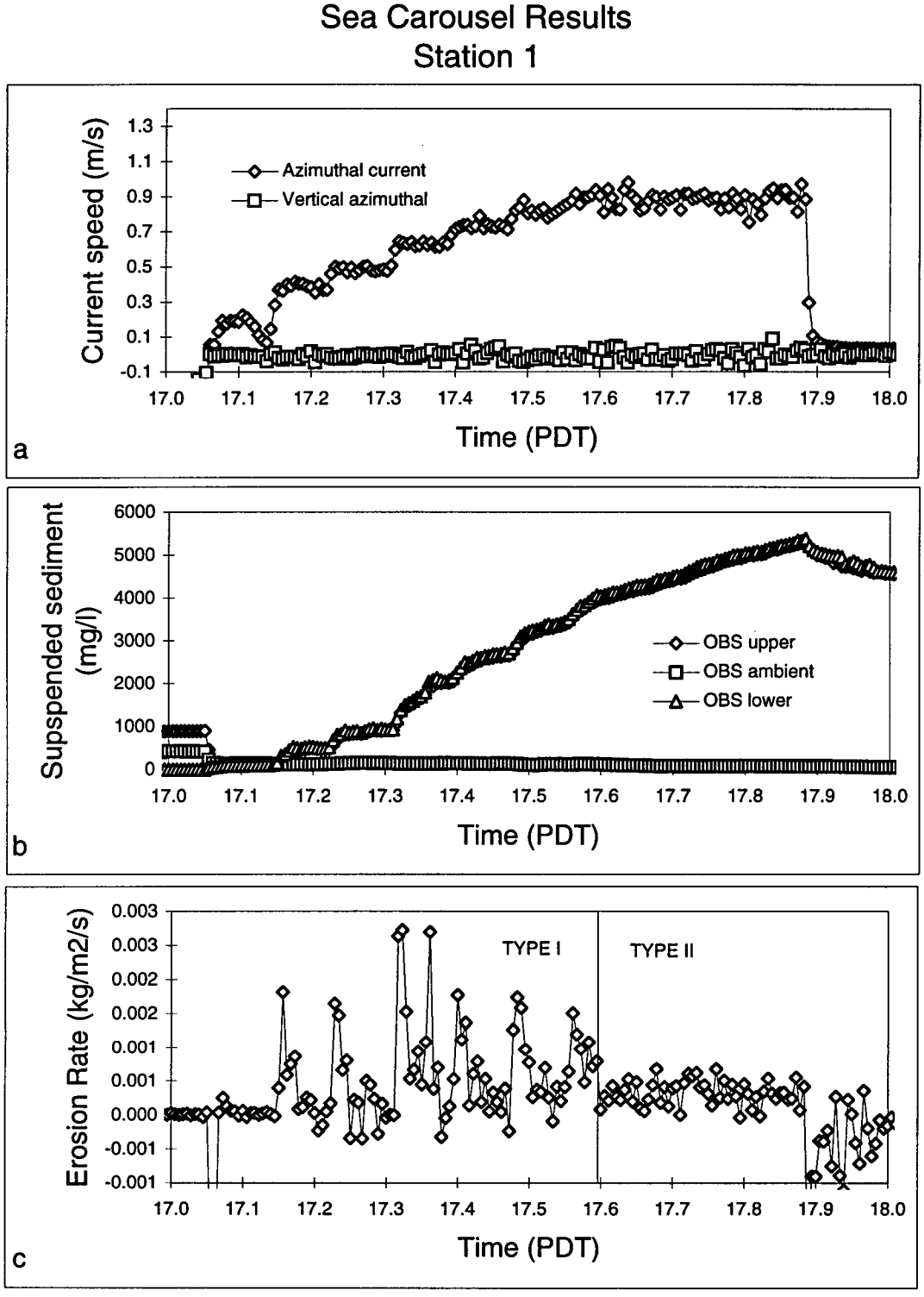

Figure 79: Time series plots of Sea Carousel Results at station 1

(a) Current speed versus time

(b) Suspended sediment concentration versus time

(c) Ersosion rate versus time

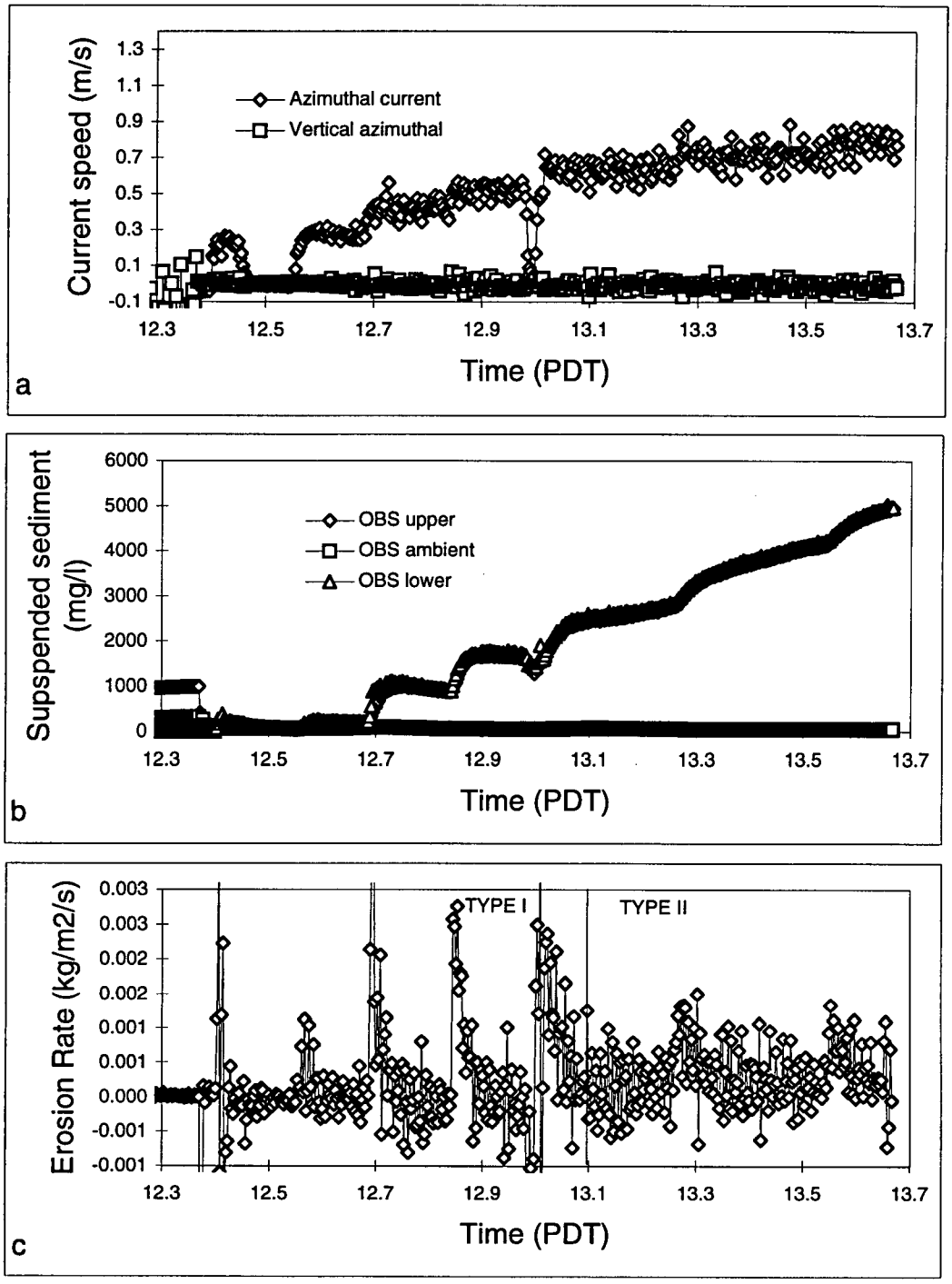

Figure 80: Time series plots of Sea Carousel Results at station 2

(a) Current speed versus time

(b) Suspended sediment concentration versus time

(c) Ersosion rate versus time

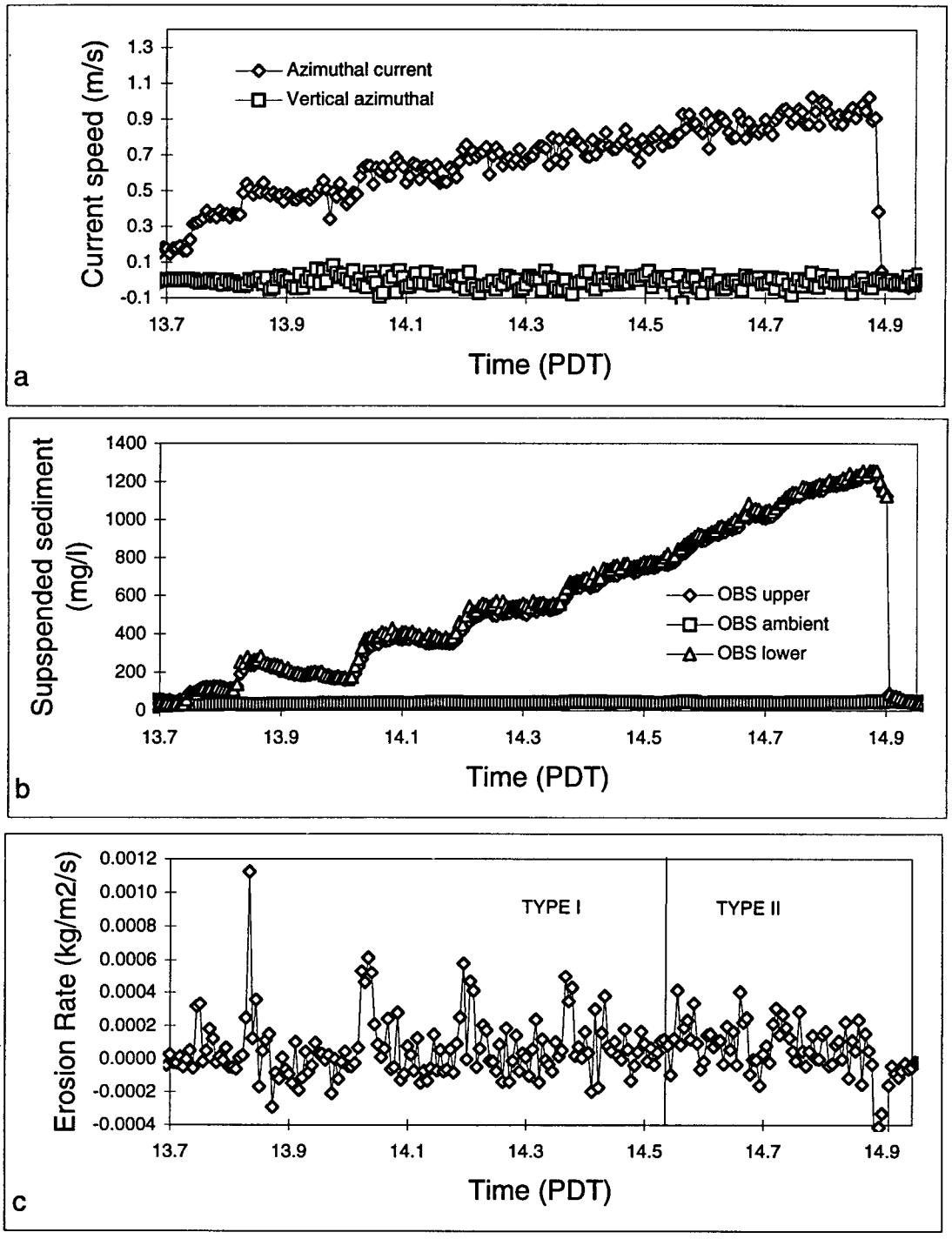

Figure 81: Time series plots of Sea Carousel Results at station 3

(a) Current speed versus time

(b) Suspended sediment concentration versus time

(c) Ersosion rate versus time

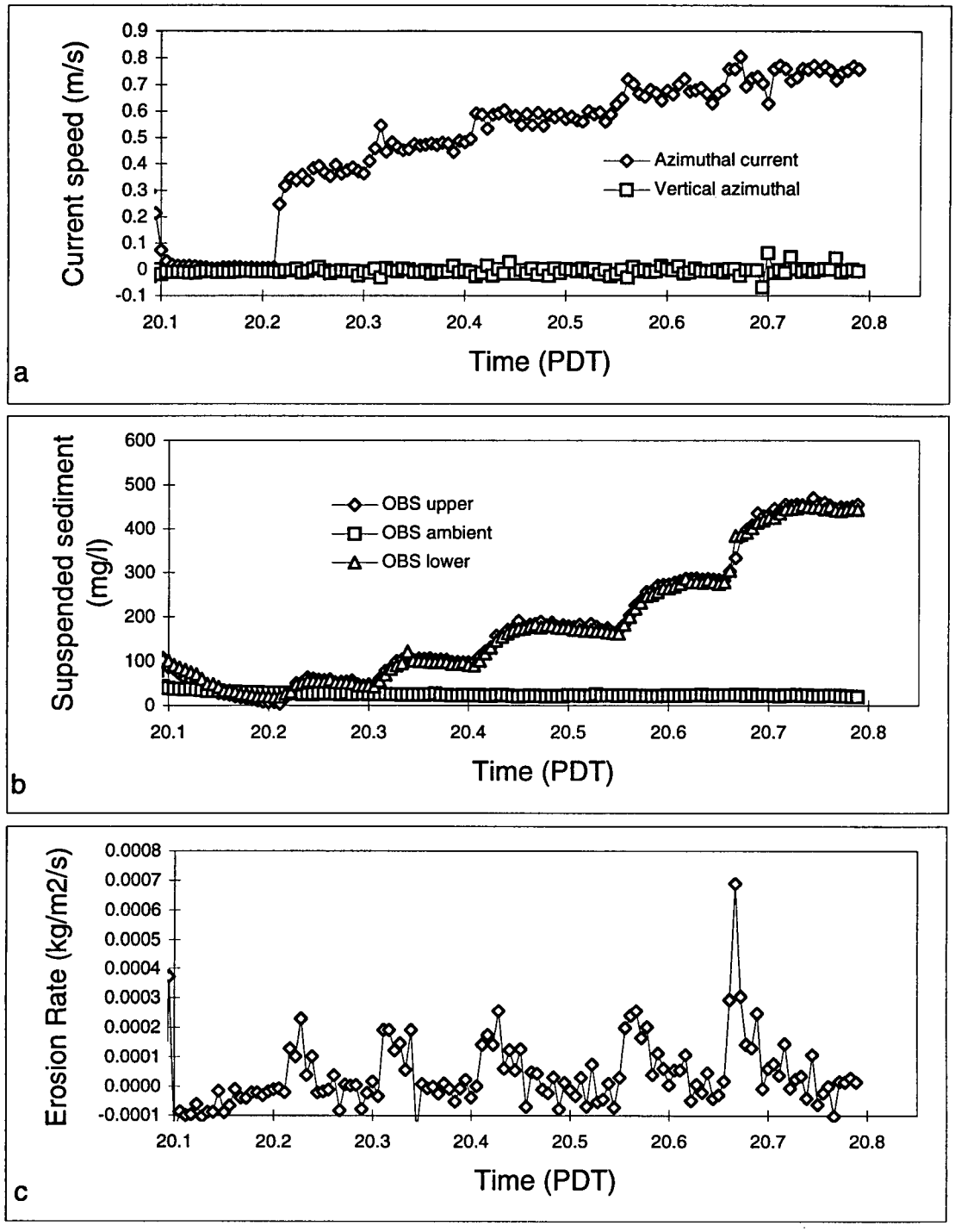

Figure 82: Time series plots of Sea Carousel Results at station 13

(a) Current speed versus time

(b) Suspended sediment concentration versus time

(c) Ersosion rate versus time

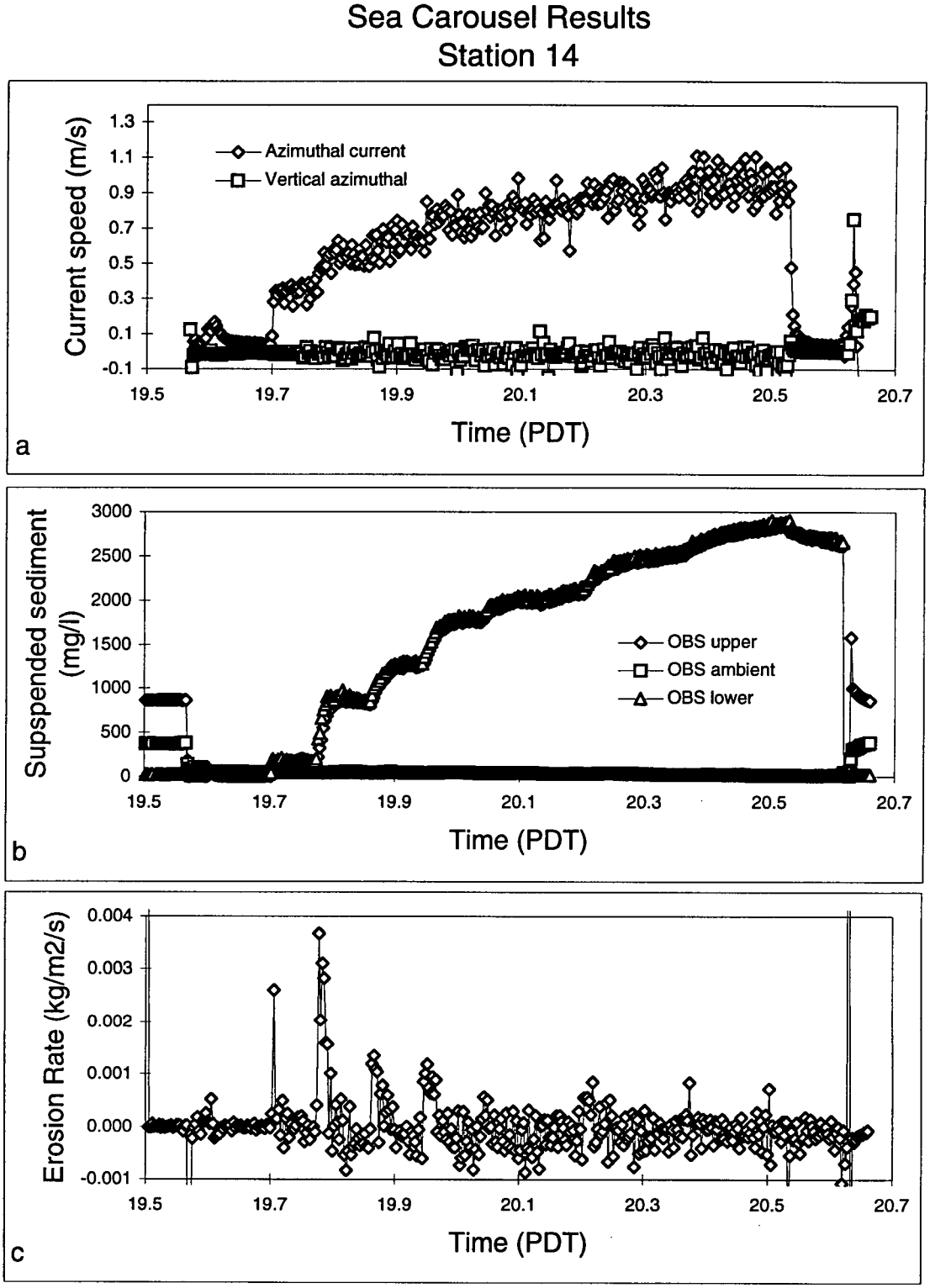

Figure 83: Time series plots of Sea Carousel Results at station 14

(a) Current speed versus time

(b) Suspended sediment concentration versus time

(c) Ersosion rate versus time

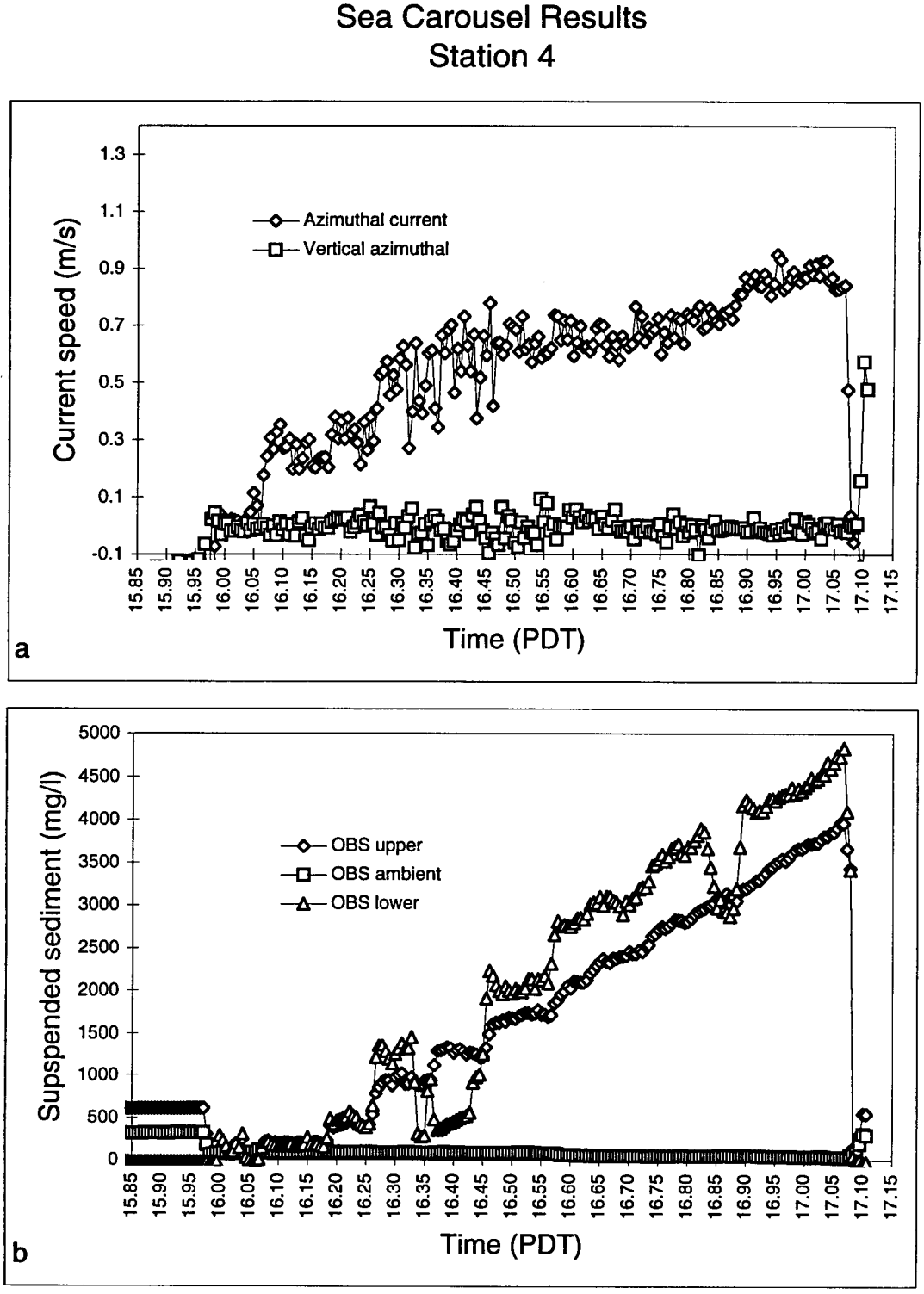

Figure 84: Time series plots of Sea Carousel Results at station 4
(a) Current speed versus time
(b) Suspended sediment concentration versus time

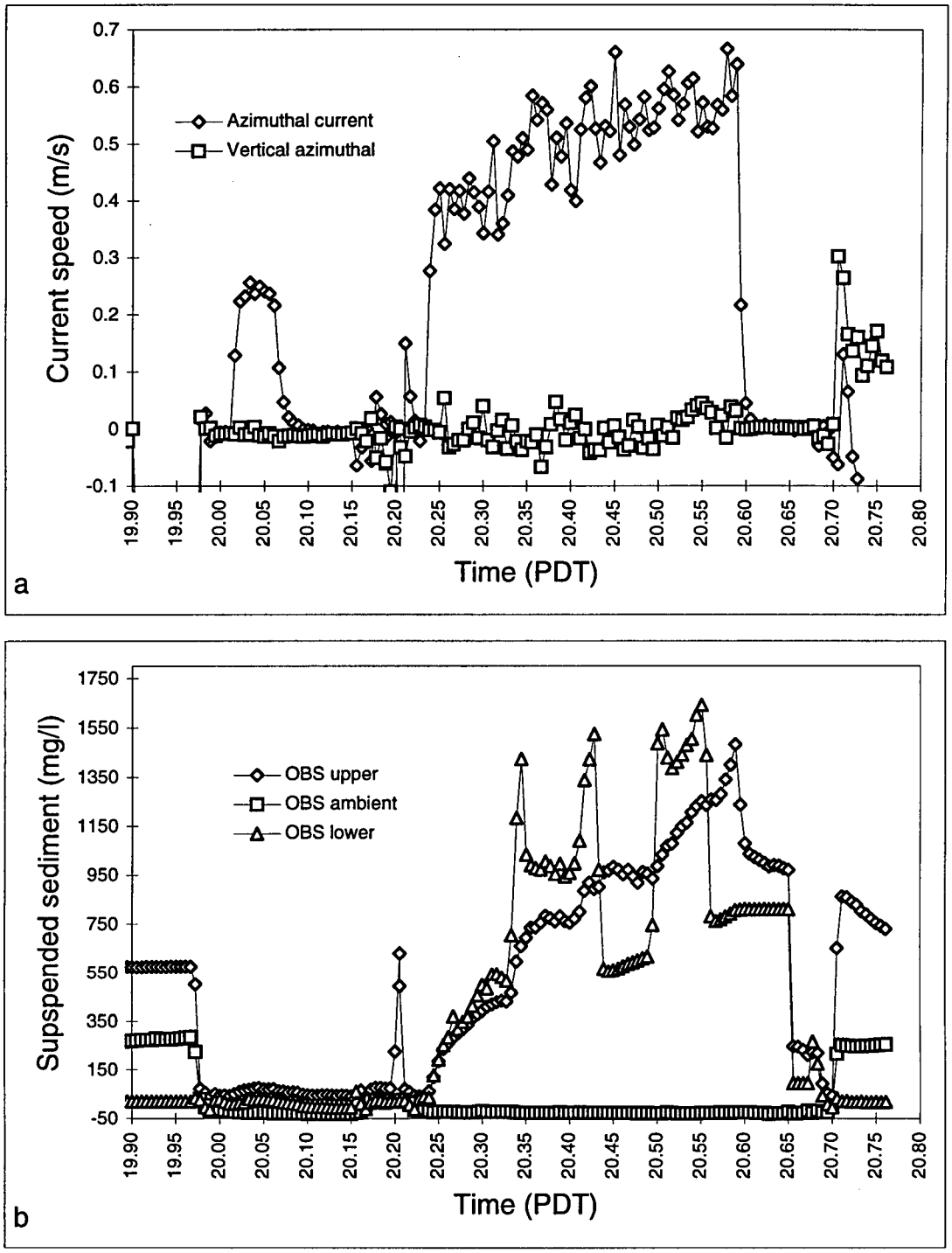

Figure 85: Time series plots of Sea Carousel Results at station 5
(a) Current speed versus time
(b) Suspended sediment concentration versus time

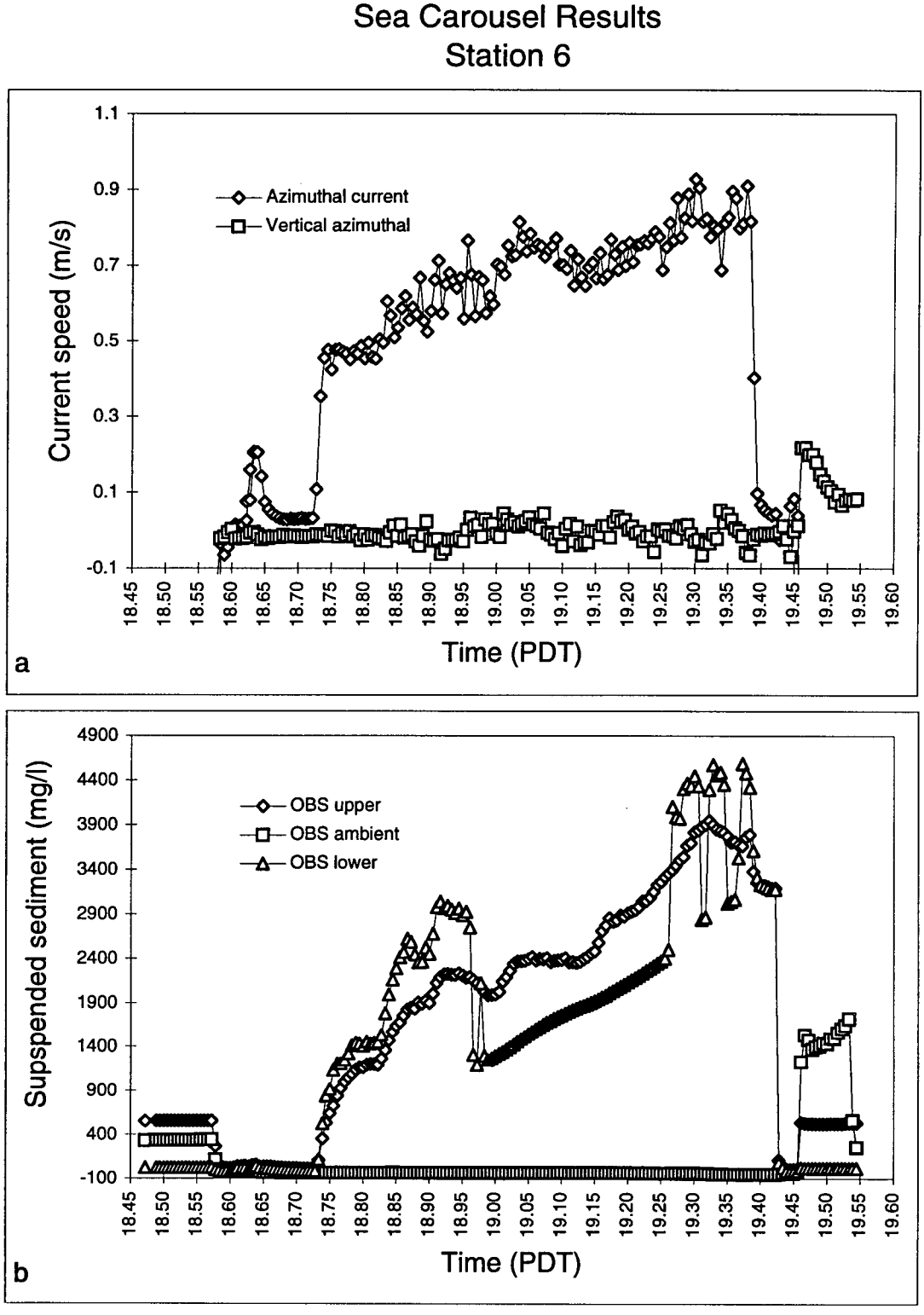

Figure 86: Time series plots of Sea Carousel Results at station 6
(a) Current speed versus time
(b) Suspended sediment concentration versus time

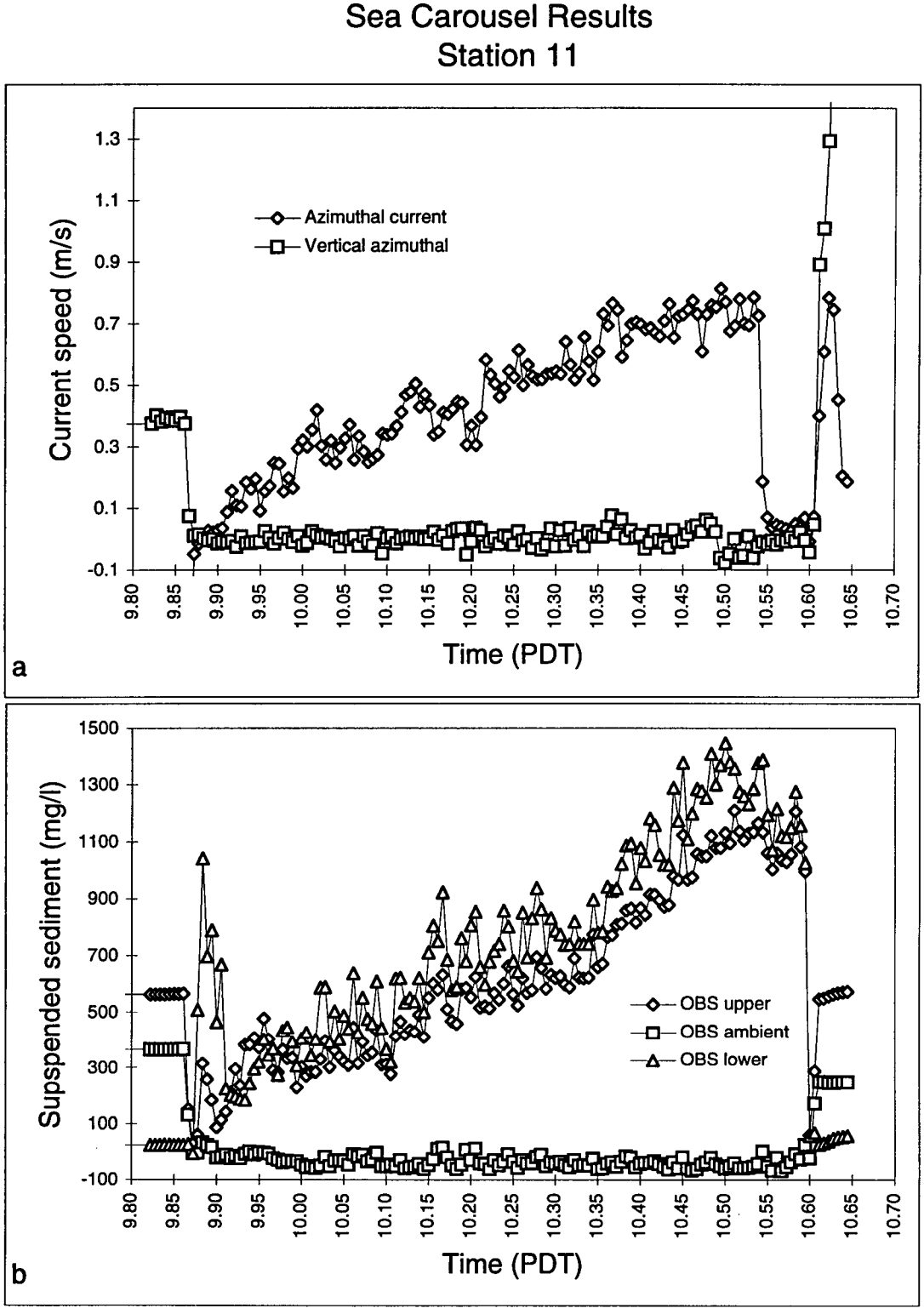

Figure 87: Time series plots of Sea Carousel Results at station 11
(a) Current speed versus time
(b) Suspended sediment concentration versus time

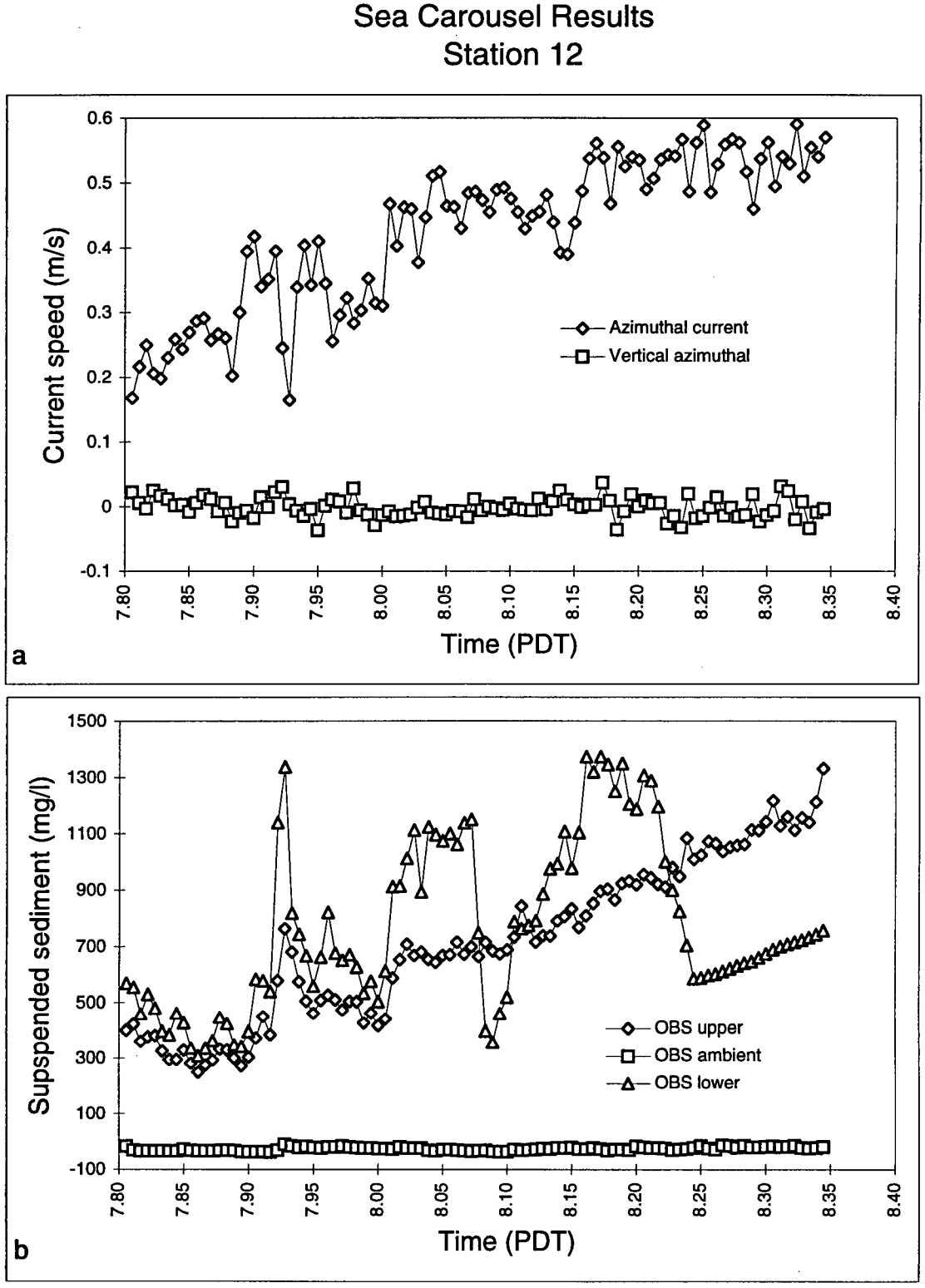

Figure 88: Time series plots of Sea Carousel Results at station 12

(a) Current speed versus time

(b) Suspended sediment concentration versus time

Appendix IV: PHYSICAL OCEANOGRAPHIC DATA ON STURGEON BANK

IV-1. Station S1

The current meter deployed at station S1 was only inundated for 18% of the time usually for 3 to 4 hours per submersion interval. One-minute-averaged velocities for the time of inundation range from 2.19 to 13.18 cm/s with a mean value of 5.68 cm/s (Figure 89). The tidal curve for the month of June, 1993 was superimposed on the measured current values to determine trends in velocity measurements over the spring and neap tides. The two peaks in velocity measured at station 1 coincide approximately with the time of the highest (spring) tidal ranges. Values are highest through sampling periods June 9 (2100-2400 h) and June 21 (1900-2200), with velocities of 12.91 and 13.18 cm/s, respectively.

Wave particle velocities reach 38 cm/s on June 21 between 1900 and 2200 hours in directions ranging from 260° to 290°, approximately an ebbing direction (Figure 90). Currents at station S1 only exceed 30 cm/s 10 times for the entire length of the survey with most of these values occurring on the June 21 inundation mentioned above. Currents over 30 cm/s occur more often in a flooding direction, however the high currents found on June 21 are in an ebbing direction. Current velocities never reach 73 cm/s, the critical shear velocity for erosion, at any time during the sampling period.

Plots of average speeds and directions over 10° increments show no preferred orientation (Figure 91). This averaging effectively filters out wave effects similar to the one minute averaging described above. Average velocities range from approximately 4.2 to 7.8 cm/s. Although the frequency of occurrence of currents in any direction shows no trend, the velocity

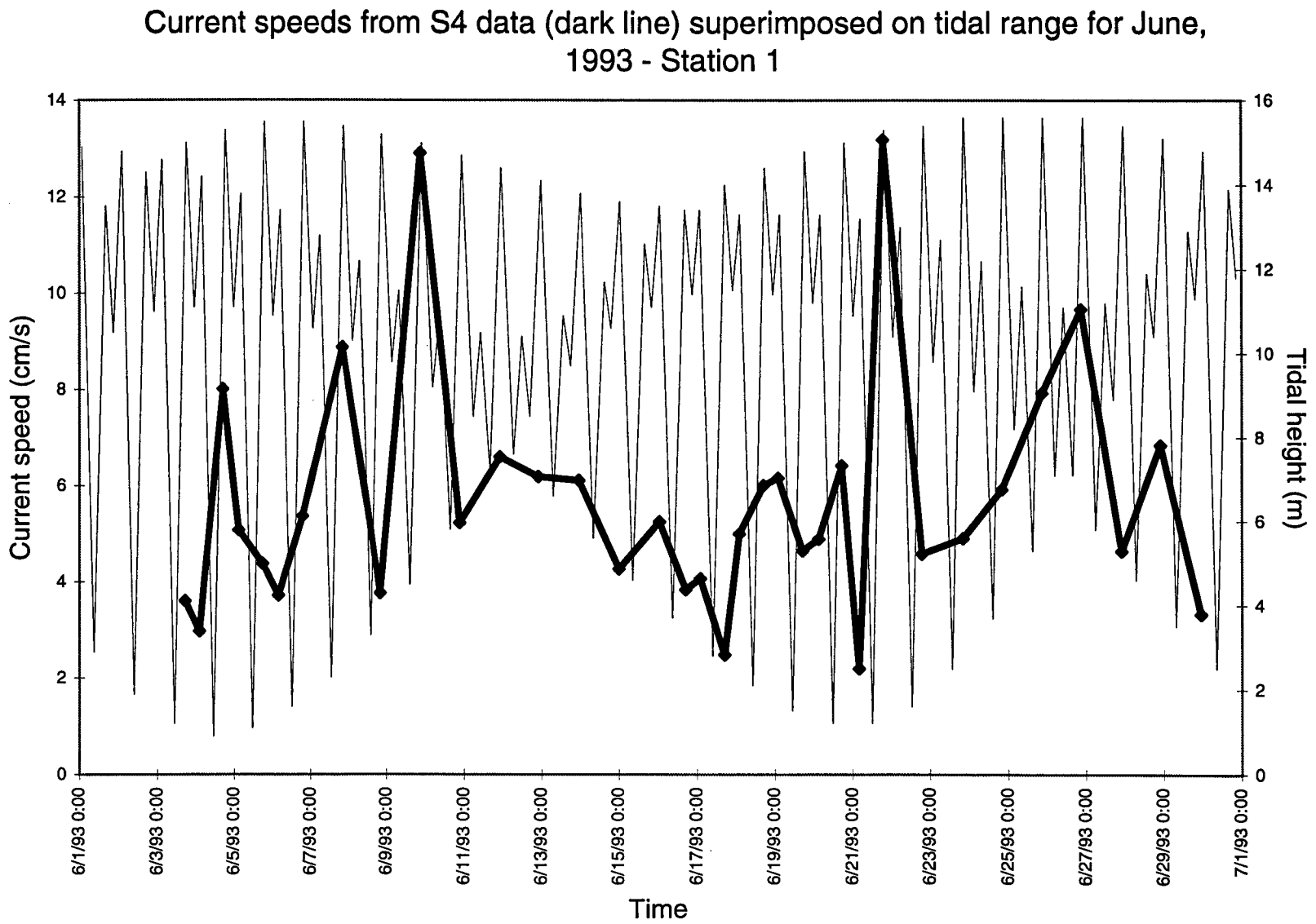

Figure 89: One-minute-averaged velocities for the month of June, 1993 at station 1

Figure 90: Wave particle velocities for the June21, 1900-2200 h sampling interval at station 1

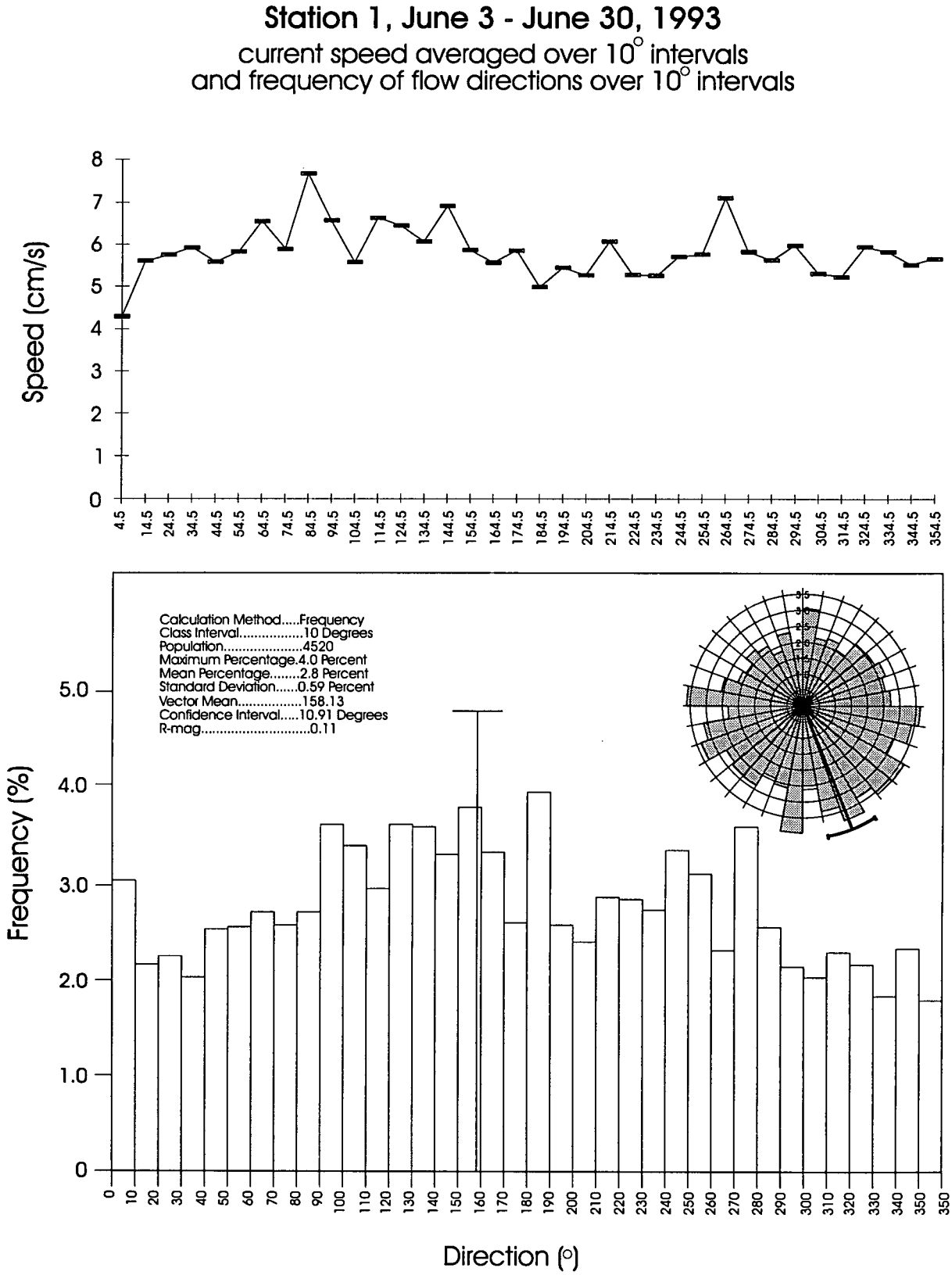

Figure 91: Average speed and direction plotted over 10 degree-averaged increments at station 1

does peak slightly in ebbing and flooding directions (approximately 250-260° and 70-80°, respectively) with the flood currents averaging slightly higher than the ebbs. The population of the data used in the generation is given in the legend of the 10° averaged increment plots. Data collected from current meters situated on the inner tidal flat will have a smaller population because of the shorter period of inundation. The maximum percentage in one 10° class interval is also given in the legend and the mean percentage is based on the percentage values in each petal or cell. This value should not be viewed as a dominant direction as currents at most stations are bidirectional in nature. Standard statistics of deviation and trend were calculated using methods of Davis (1986). A confidence interval of 95% was used throughout the calculations.

Water temperatures at the beginning of June are approximately 19°C and drop to 15°C on June 9 (Figure 92). Temperatures begin increasing until June 17 where they reach 26°C and then decrease to 19°C again by the end of the month. Temperatures within an inundation interval vary up to 3°C but typically only 1.5 to 2°C. Both temperatures and salinities are measured 4 times during a one minute current meter sampling interval however the variation within the minute is not significant at station S1.

Salinity measurements at station S1 shows two peaks through the month of June (Figure 93). Measurements at the beginning of June are approximately 6‰ and then increase to 12.5‰ on June 8 and 9 before dropping to 2‰ on June 29. The variation in salinity and temperature measurements over the 4 week sampling period shows a good relationship with the tidal cycle and therefore is assumed to be partially the result of spring and neap tidal effects. Salinity can vary from 4.5‰ to 12‰ over a sampling inundation period. Typically salinity varies 0.5 to 2‰ over an inundation interval.

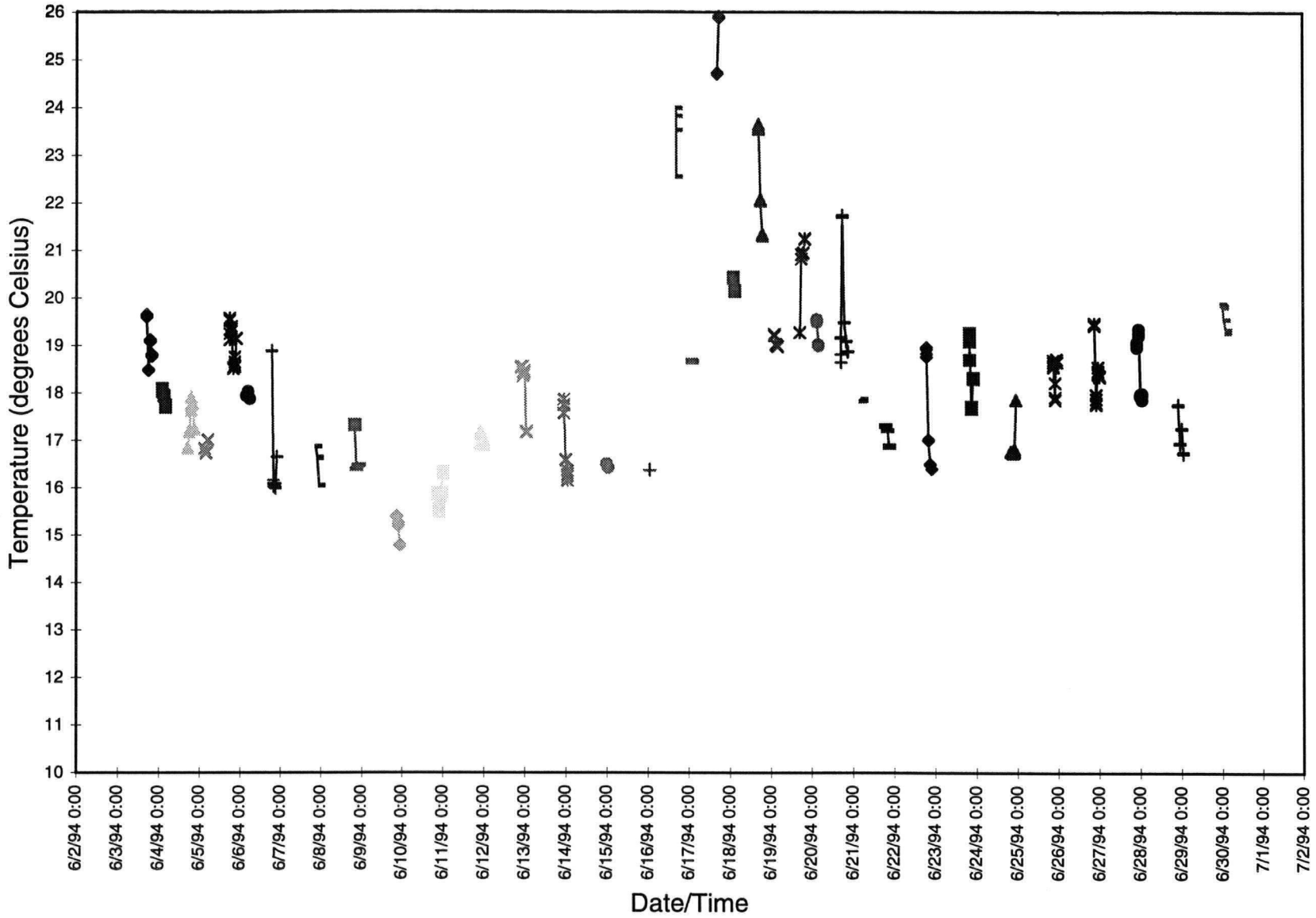

Figure 92: Water temperature variations for the month of June, 1993 at station 1

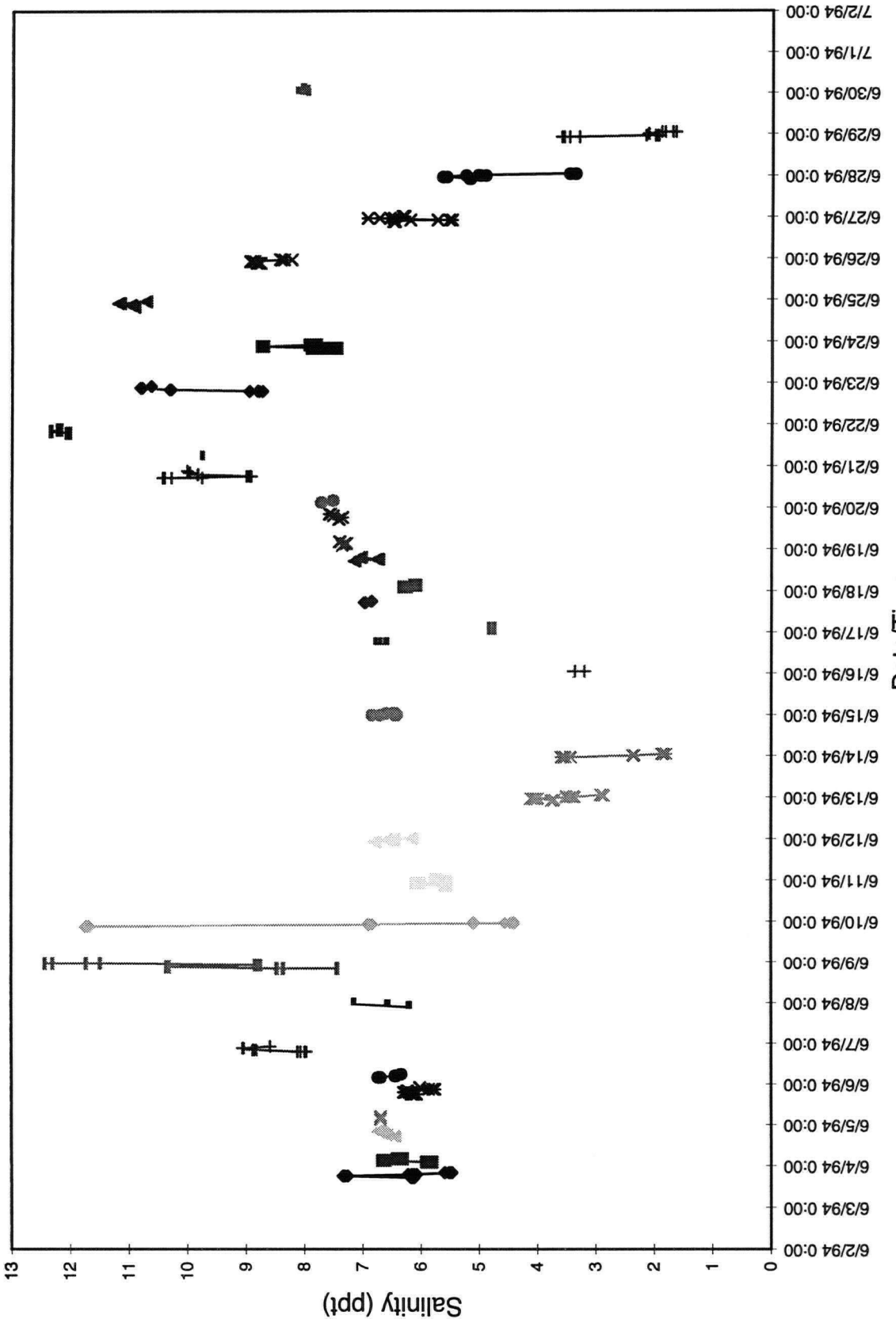

Figure 93: Salinity variations for the month of June, 1993 at station 1

IV-2. Station S2

The current meter deployed at station S2 was submersed for 44% of the total sampling time for 3 to 15 hours per sampling interval. One-minute-averaged velocities range from 3.01 to 13.82 cm/s with a mean value of 6.39 cm/s (Figure 94). Values are highest through the sampling interval May 11 (2000 h) to May 12 (0200 h). Superimposing the tidal range curve over the measured velocities shows little association and suggests that velocity measurements at station S2 for the month of May, 1993 are unrelated to spring and neap tidal currents.

Wave particle velocities at station S2 exceed 30 cm/s only 7 times, less than station 1, and all in the sampling interval on May 11 mentioned above (Figure 95). Currents in a flooding direction (~50-110°) of this interval reach 37 cm/s, the only velocity over 30 cm/s, while the ebbing direction (~260-320°) shows values over 30 cm/s 6 times, with a peak obtaining 43 cm/s. In general, flood tide current velocities exceed ebb tide current velocities, however the high currents found on May 11 occur in an ebbing direction. Currents at station S2 never reach the critical shear velocity for erosion of 86 cm/s at any time during the sampling period.

Current plots averaged over 10° increments show no strongly preferred orientation (Figure 96). Average velocities range from 4.8 to 8.3 cm/s with several peaks in random directions. The highest peak lies between 30 and 50° however an additional peak exists between 120 and 130° and three peaks lie between 210 and 320°. Although two distinct peaks in velocity due to flooding and ebbing currents are not evident, currents in the general flooding direction are slightly higher than those in the ebbing direction.

Water temperatures at the beginning of May are ~11°C and climb to 25°C on May 16

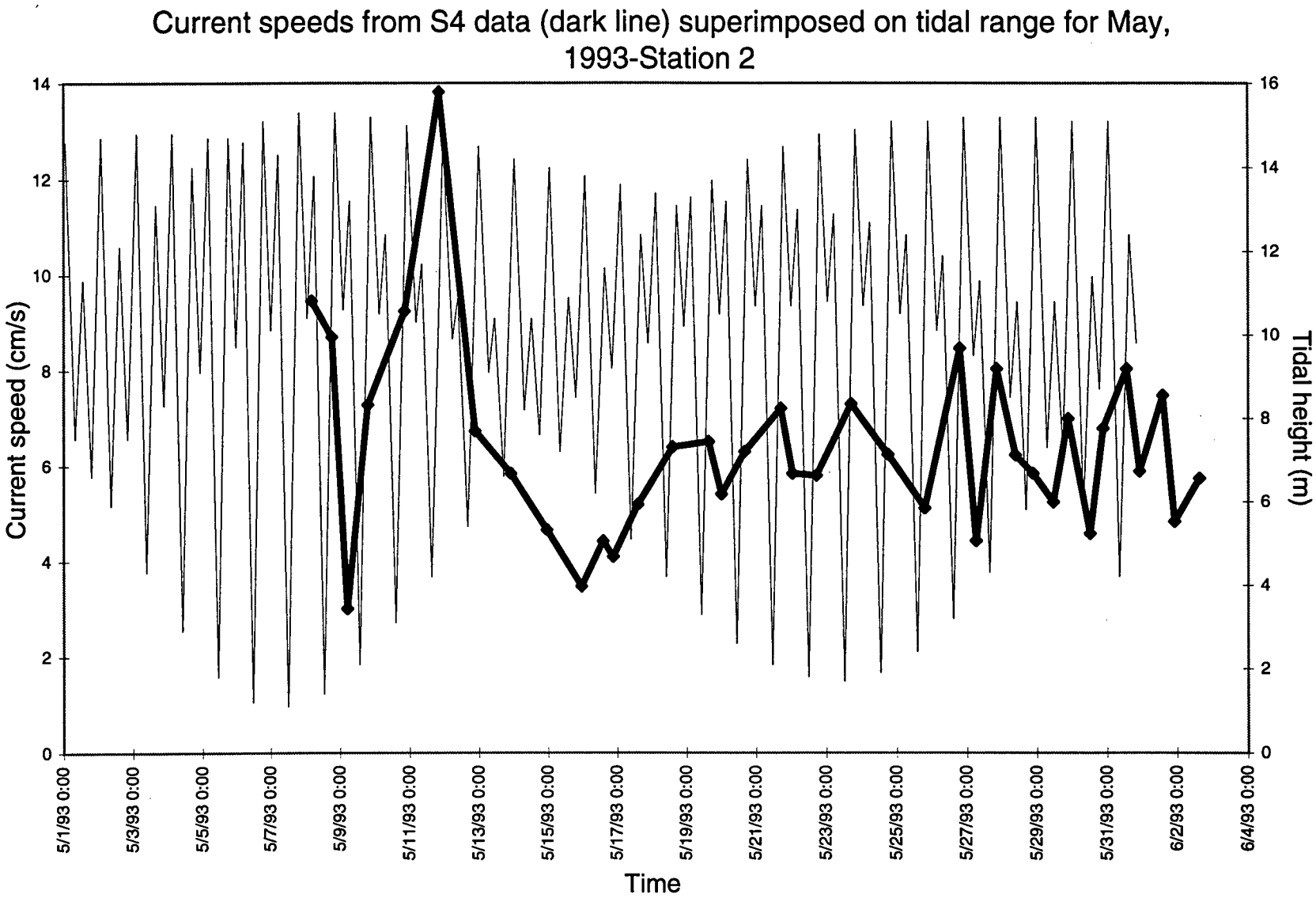

Figure 94: One-minute-averaged-velocities for the month of May, 1993 at station 2

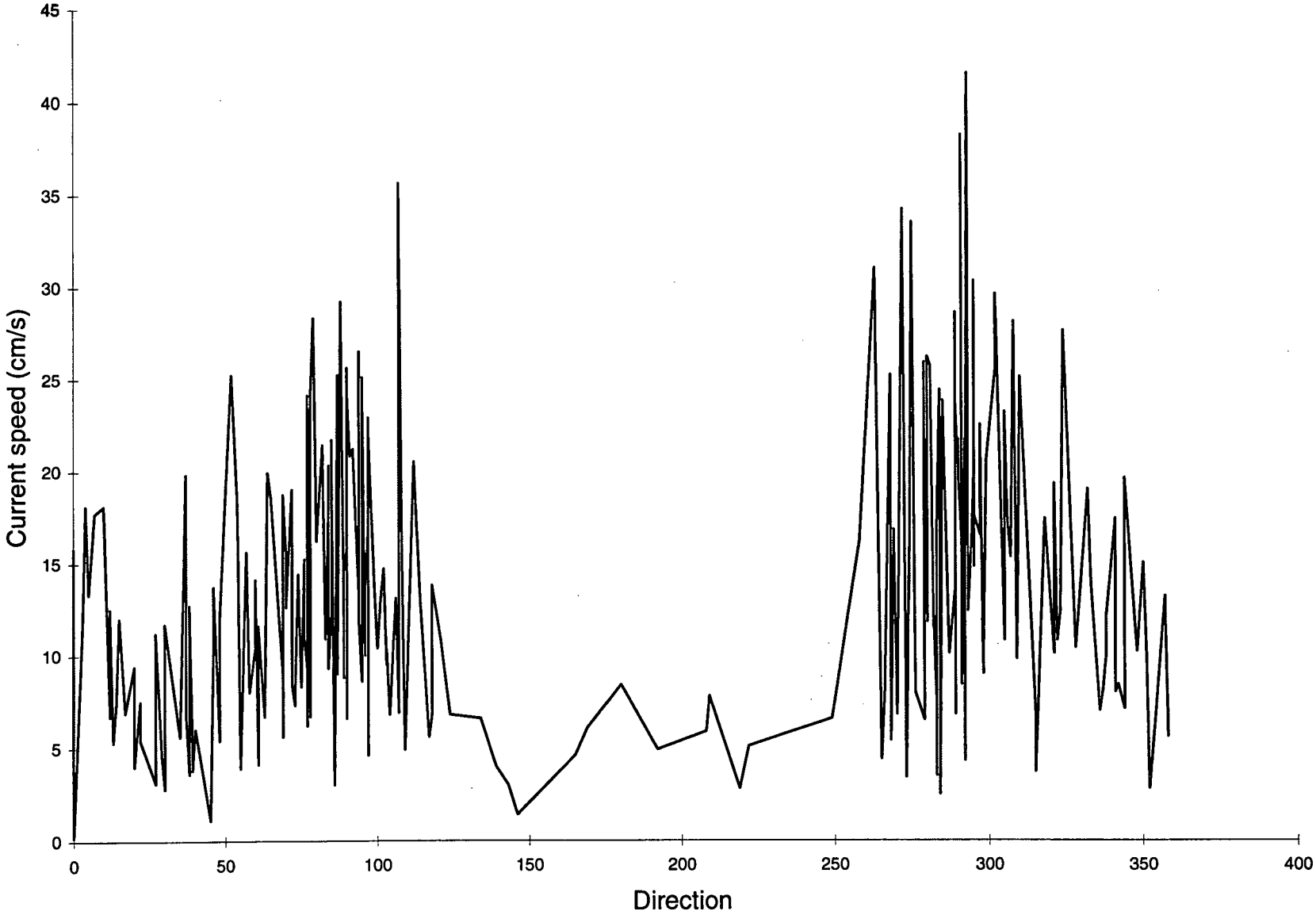

Figure 95: Wave particle velocities for the May 11, 2000 to May 12, 0200 h sampling interval

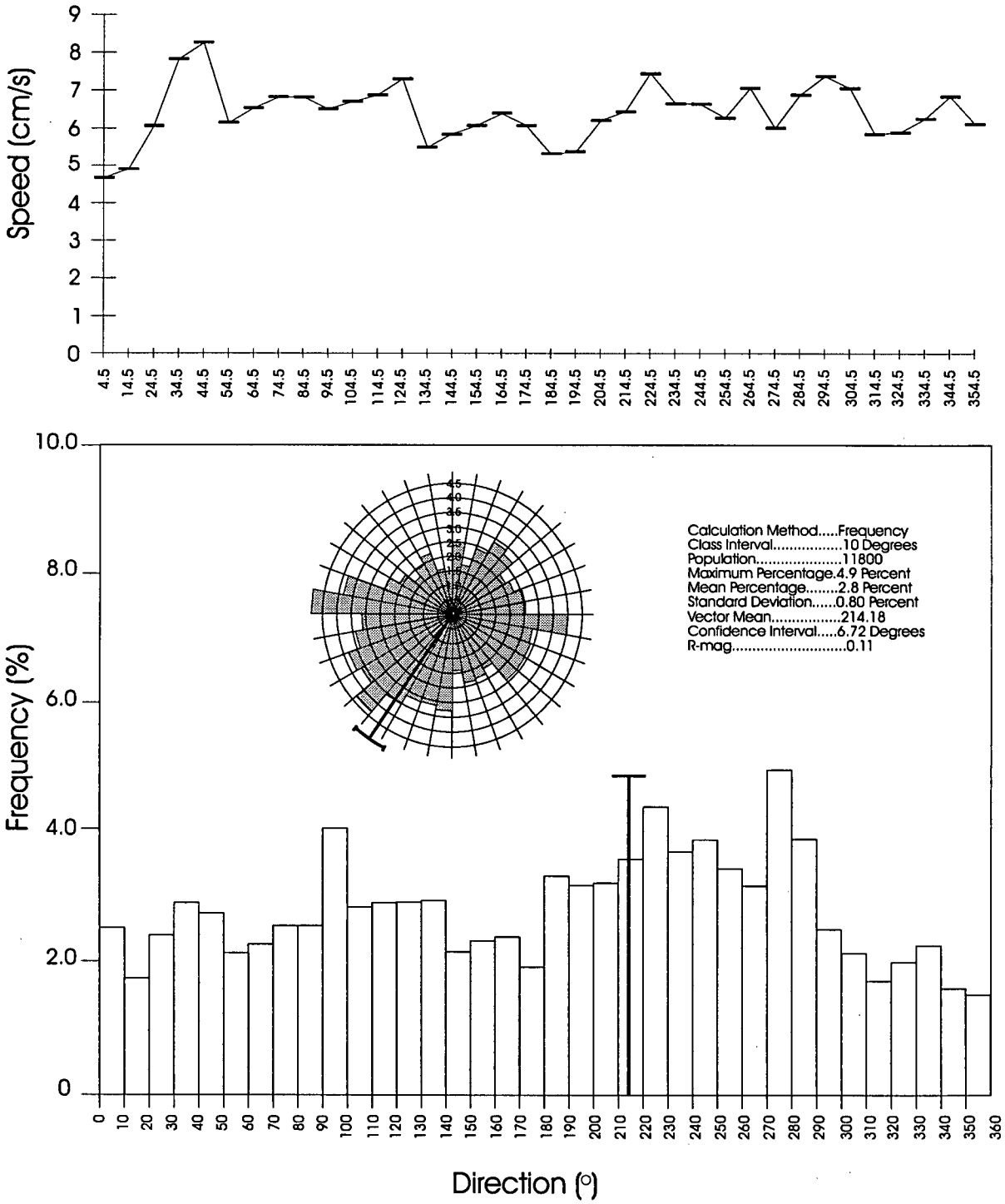

Figure 96: Average speed and direction plotted over 10 degree-averaged increments at station 2

(Figure 97). Temperatures decrease to 14°C by May 22 before increasing to 21°C on May 27 where they remain stable until May 31 and then begin a slow decline to 16°C by the end of the survey. This trend follows the tidal curve where warmer waters seem to be associated with the neap tidal time and cooler temperatures coincide with the spring tides. This observation is not unexpected as neap tides are considerably shallower than the spring tidal heights and therefore carry warmer surface water with them. The Fraser River discharge also peaks on May 16 and may bring warmer fresh water to the bank. Temperatures within a sampling inundation vary by as much a 7°C over the 15 hour current meter submersion. Generally temperatures decrease over the submersion period as expected because deeper water moves over the sampling instrument. Temperatures often remain low until the end of the inundation, however, in some cases they increase as the water shallows again.

The salinity measured at station S2 is 24‰ at the beginning of May and decreases to 2‰ by May 18 (Figure 98). Salinity increases slowly until May 26 to 13‰ and then decreases to 7‰ for the remainder of the sampling period. This trend is similar but in reverse to that described by the temperature measurements at this station. The spring tides effectively bring more saline (deeper) water to the bank and the neap tides carry the fresher surface water. The effect of the Fraser River discharge may enhance this effect by bringing more fresh water to the bank at the peak of the freshet. Salinity varies over a sampling inundation by as much as 10‰ but typically 2 to 6‰. Salinity values are generally low at the start of an inundation and increase rapidly as the more saline deeper water encroaches. Salinity often stays high as the tide ebbs suggesting that the water becomes more mixed as it moves up the bank but in many cases it decreases again as the water shallows.

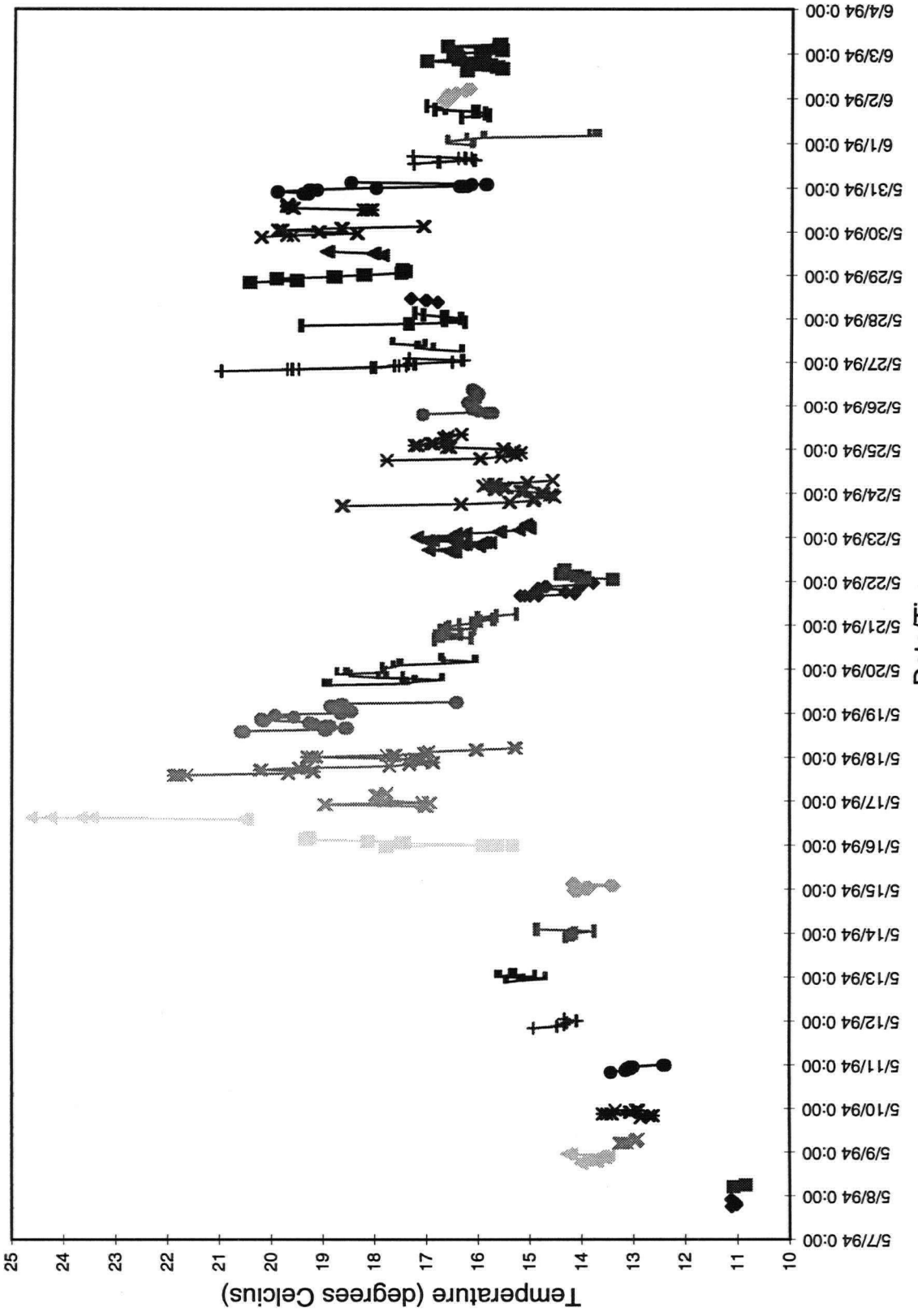

Figure 97: Water temperture variations for the month of May, 1993 at station 2

Figure 98: Salinity variations for the month of May, 1993 at station 2

IV-3. Station S3

Submersion of the current meter at station S3 occurred 56% of the total sampling time usually for 8 to 16 hours per inundation. One-minute-averaged velocities range from 5.86 to 15.37 cm/s with a mean value of 10.32 cm/s (Figure 99). Values are highest through the sampling intervals June 9 (1900 h) to June 10 (0200 h) and June 26 (1900 h) to June 27 (0300 h) with currents averaging 13.86 and 15.37 cm/s, respectively. In addition, one-minute-averaged currents are high (above 12 cm/s) in 6 other intervals throughout the survey. Measured velocities coincide well with the tidal range curve with the highest velocities recorded in the spring tides.

Wave particle velocities at station S3 exceed 35 cm/s 71 times in the study period with 61 of these values recorded in a flooding direction (~50-100°). Currents over 40 cm/s are reached 22 times with only 1 of these values recorded in an ebbing direction (~260-320°). Currents exceed 40 cm/s on June 6 (1700 h) to June 7 (0900 h), June 8 (1800-2000 h), June 19 (0500-0700 h), June 19 (1500 h) to June 20 (0700 h), June 20 (1600-1700 h), and June 23 (1800-1900). The maximum wave particle velocity was recorded in the interval on June 20 (1600-1700 h) and reached a value of 47 cm/s. Wave particle velocity measurements for the June 6 interval are shown in Figure 100 and represent a typical inundation period where current velocities are high. In general, flooding current velocities exceed ebbing velocities, however, high ebbing velocities are observed when velocities over the inundation period are lower. The peak for the flooding velocities are not only higher but the velocities are more focussed in one direction. The ebbing velocities are lower and occur over a wider range of directions. Current velocities of 80 cm/s, the critical shear velocity for erosion at station S3, are never reached at any time in the sampling period.

Figure 99: One-minute-averaged velocities for the month of June, 1993 at station 3

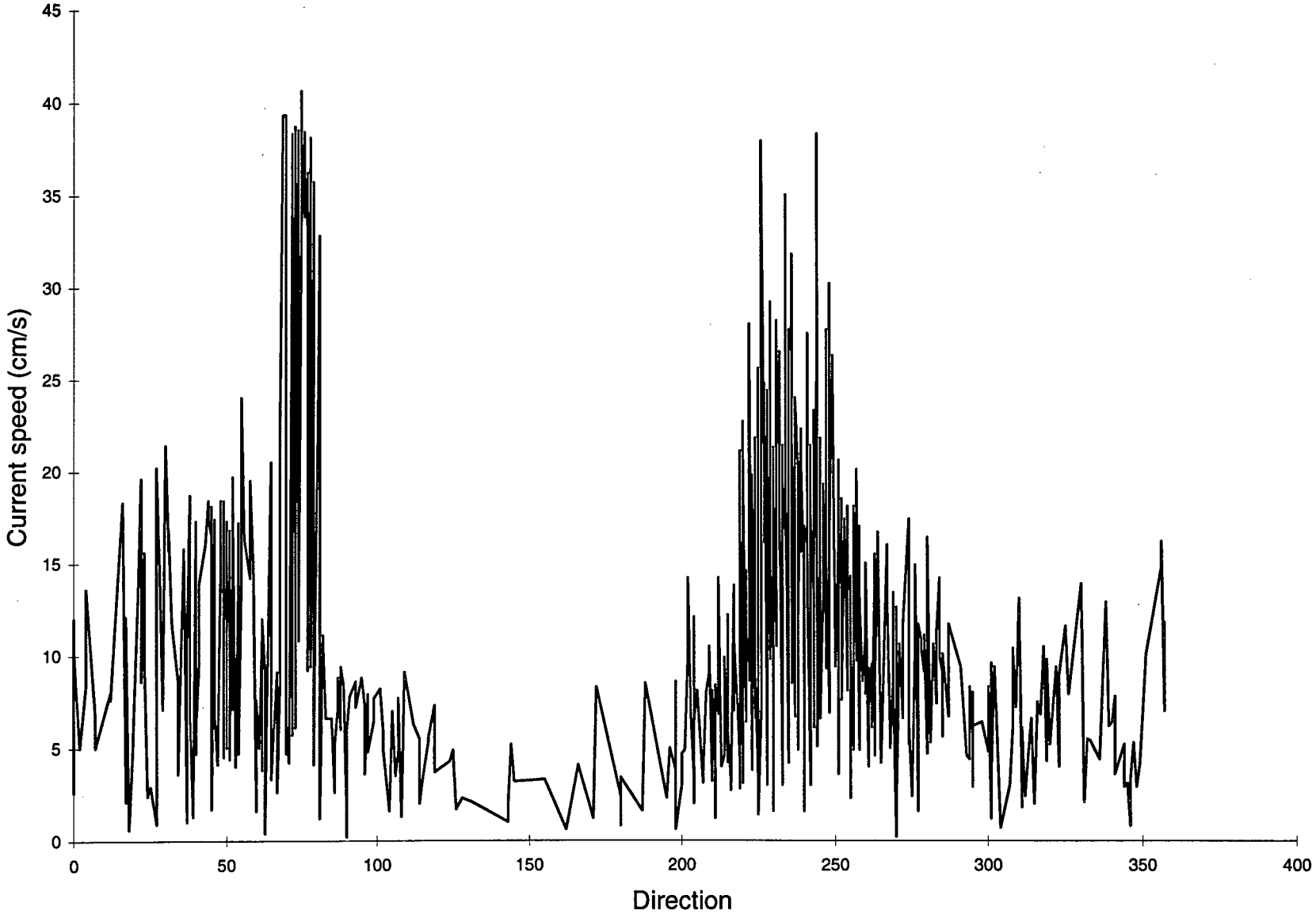

Figure 100: Wave particle velocities for the June 6, 1700 to June 7, 0900 h sampling interval at station 2

The plot of currents averaged over 10° increments shows a strong bidirectional flow towards ~70-90° (flooding) and ~230-250° (ebbing) (Figure 101). Currents in a flooding direction not only occur more often but display higher average velocities (~17.5 cm/s) than currents in an ebbing direction (~13 cm/s) which is consistent with the wave particle velocity observations. Like the wave data, the flooding peak is more focussed towards high velocities in a consistent direction whereas, the ebbing peak is more broad with lower speeds over a wider range of directions. Currents in directions other than the flood and ebb generally average 4-6 cm/s.

Water temperatures vary less throughout the survey than at stations S1 and S2, ranging from 14.5° on June 6 to 20.5°C on June 19 (Figure 102). Temperatures start at 18°C and fall to 4°C by June 10. They increase until June 19 and then decrease to 17°C by June 22 where they increase slightly until the end of the month. Temperatures within a sampling inundation only vary slightly with a maximum variation of 3.5°C.

Like temperature, salinity does not vary as markedly as stations S1 and S2. Values at station S3 range from 2.5‰ to 15.5‰ (Figure 103). The trend in salinity values follows that found at station 1 with an increase from the beginning of June to a peak on June 9 and a drop in value to June 13. A second increase occurs until June 22 and then salinities fall until the end of the survey. The pattern is indicative of spring/neap tidal effects. The largest degree of variation in salinity over a single inundation period occurs on the falling limbs of the salinity peaks. The valleys and the rising limbs show the lowest degree of variability over a single current meter submersion because the instrument is inundated for less time in lower high tides and therefore is more likely to experience well mixed water with less variation throughout the inundation.

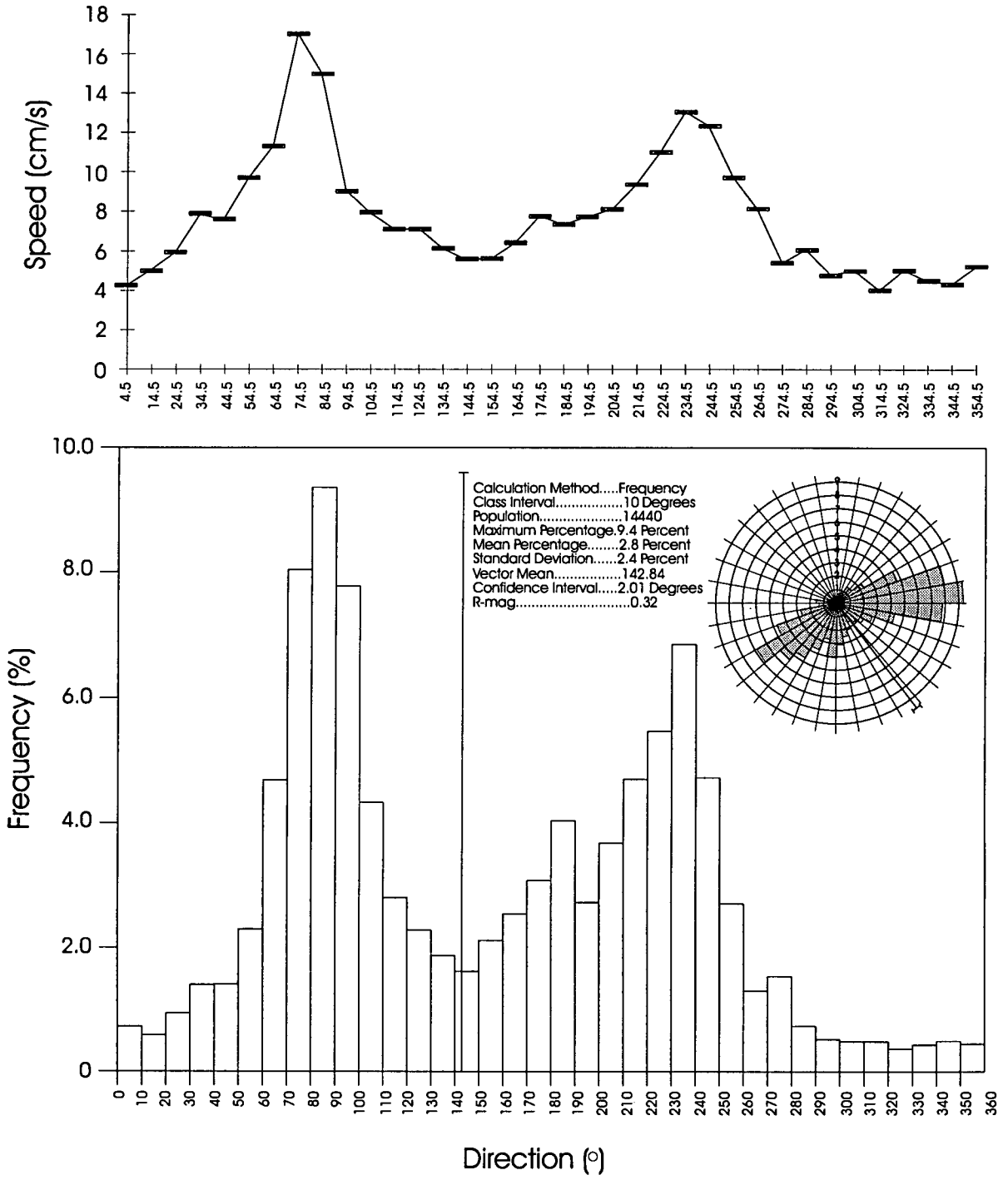

Figure 101: Average speed and direction plotted over 10 degree-averaged increments at station 3

Figure 102: Water temperature variations for the month of June, 1993 at station 3

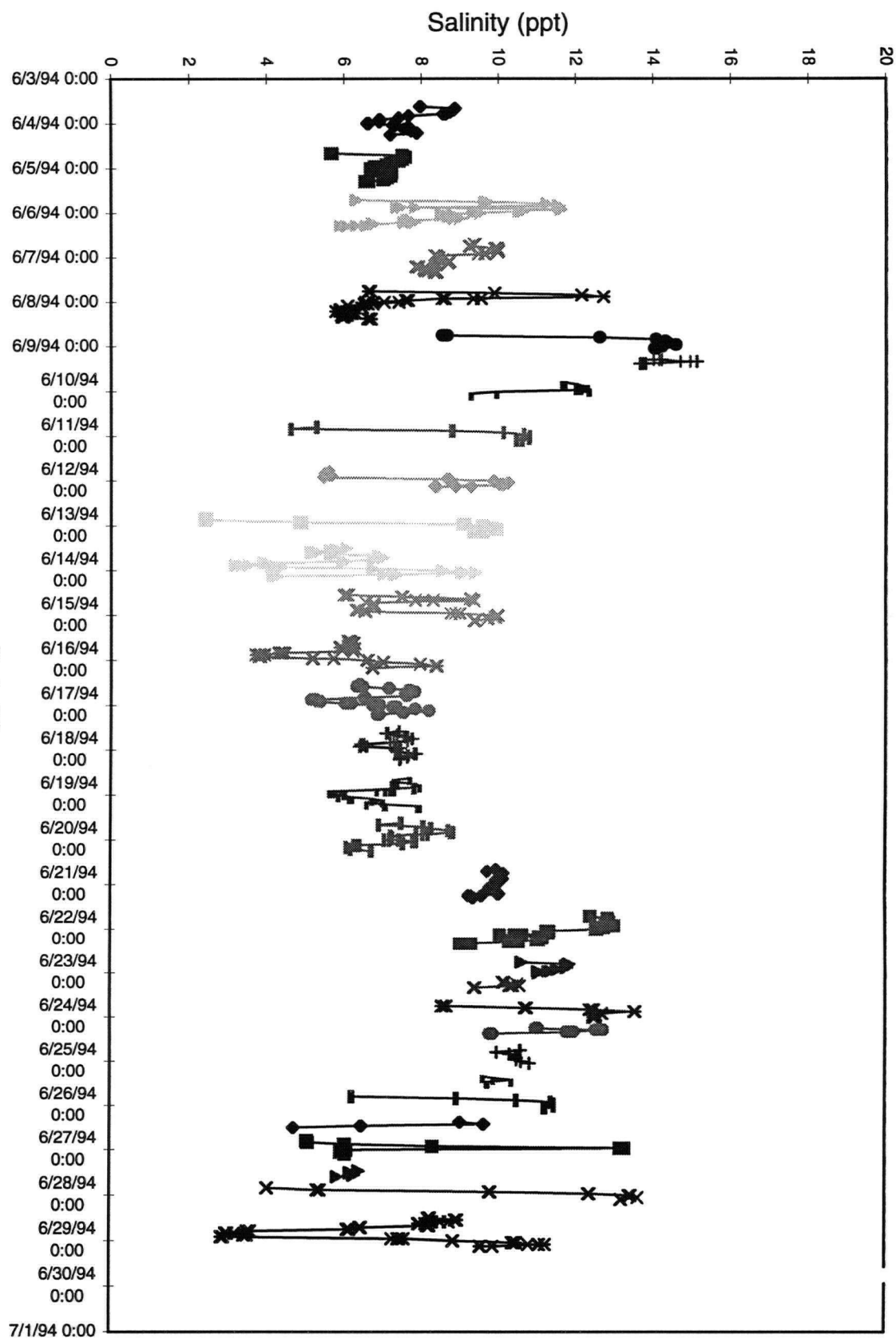

Figure 103: Salinity variations for the month of June, 1993 at station 3

Salinity varies on a single submersion period by up to 10‰ but typically varies between 0.5 and 1.5‰.

IV-4. Station S4

The current meter deployed at station S4 in the month of May experienced full submersion 72% of the sampling period usually for 18 hours per interval. The one-minute-averaged velocities measured at station S4 for this month ranged from 10.45 to 17.78 cm/s and were highest on sampling intervals May 23 (1600 h) to May 24 (1000 h) and May 28 (1800 h) to May 29 (0600 h) (Figure 104). Superimposing the tidal range curve on this figure demonstrates that there is little relation between the tidal cycle and the current velocities measured at station S4 in May. For the deployment in the month of June the current meter was submersed for 76% of the time and again for usually 18 hours per interval. The highest one-minute-averaged velocity was 19.89 cm/s with the lowest being 9.17 cm/s and the average being 13.52 cm/s (Figure 105). The highest values occurred through sampling intervals June 24 (1700 h) to June 25 (0300 h) and June 25 (1700 h) to June 26 (0300 h) with values of 18.86 and 19.89 cm/s, respectively. Superimposing the tidal range curve on the measured velocities shows slightly better consistency than the May curve, with the highest velocities occurring on the spring tides as expected.

Wave particle velocities in the month of May exceed 40 cm/s 47 times with 44 of these values recorded in a flooding direction (~30-60°). The critical shear velocity for erosion at station S4 is 49 cm/s and it is reached only once in May in an ebbing direction. The highest single velocity reached was ~50 cm/s on May 11 (2000 h) to May 12 (1100 h) in and ebbing

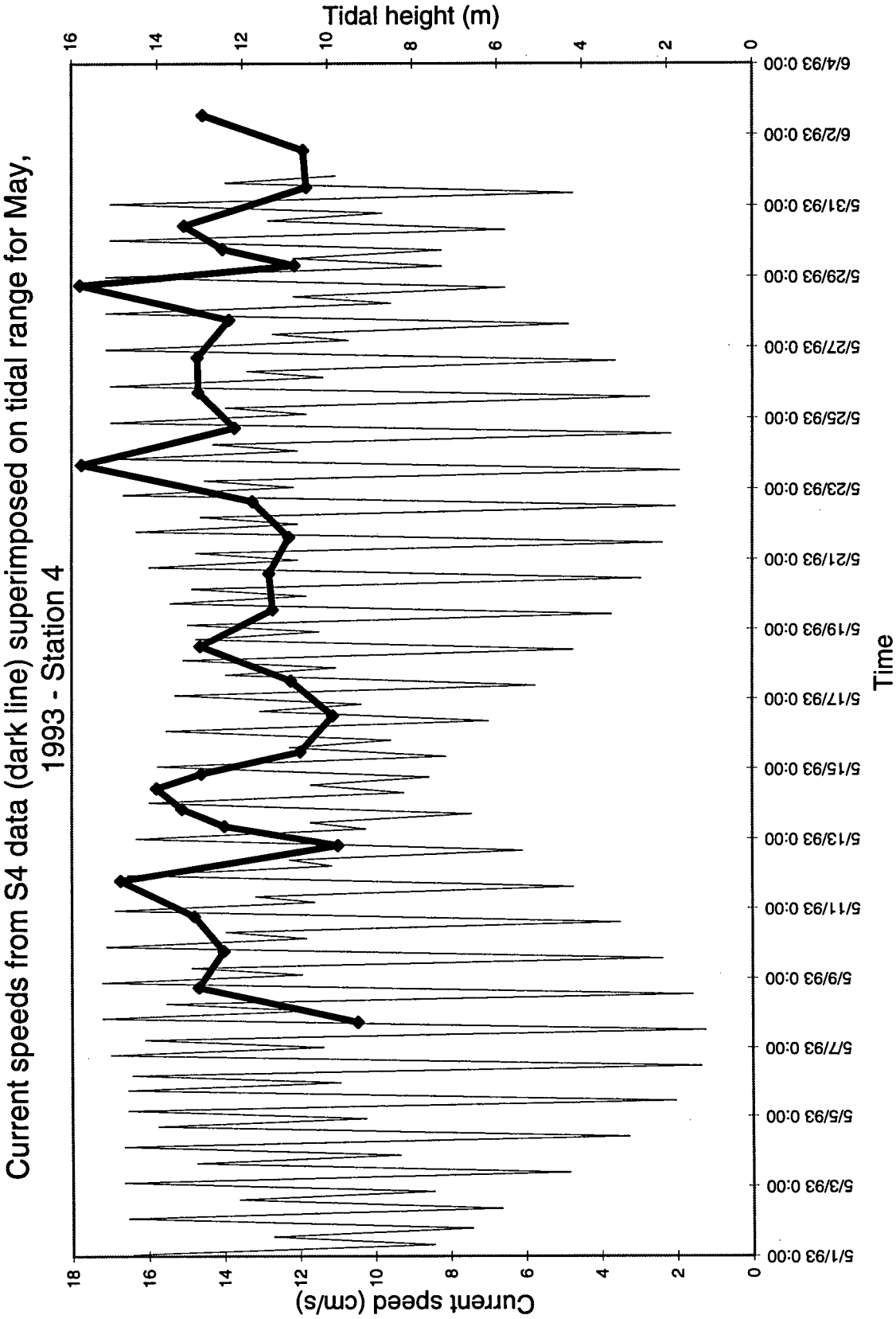

Figure 104: One-minute-averaged velocities for the month of May, 1993 at station 4

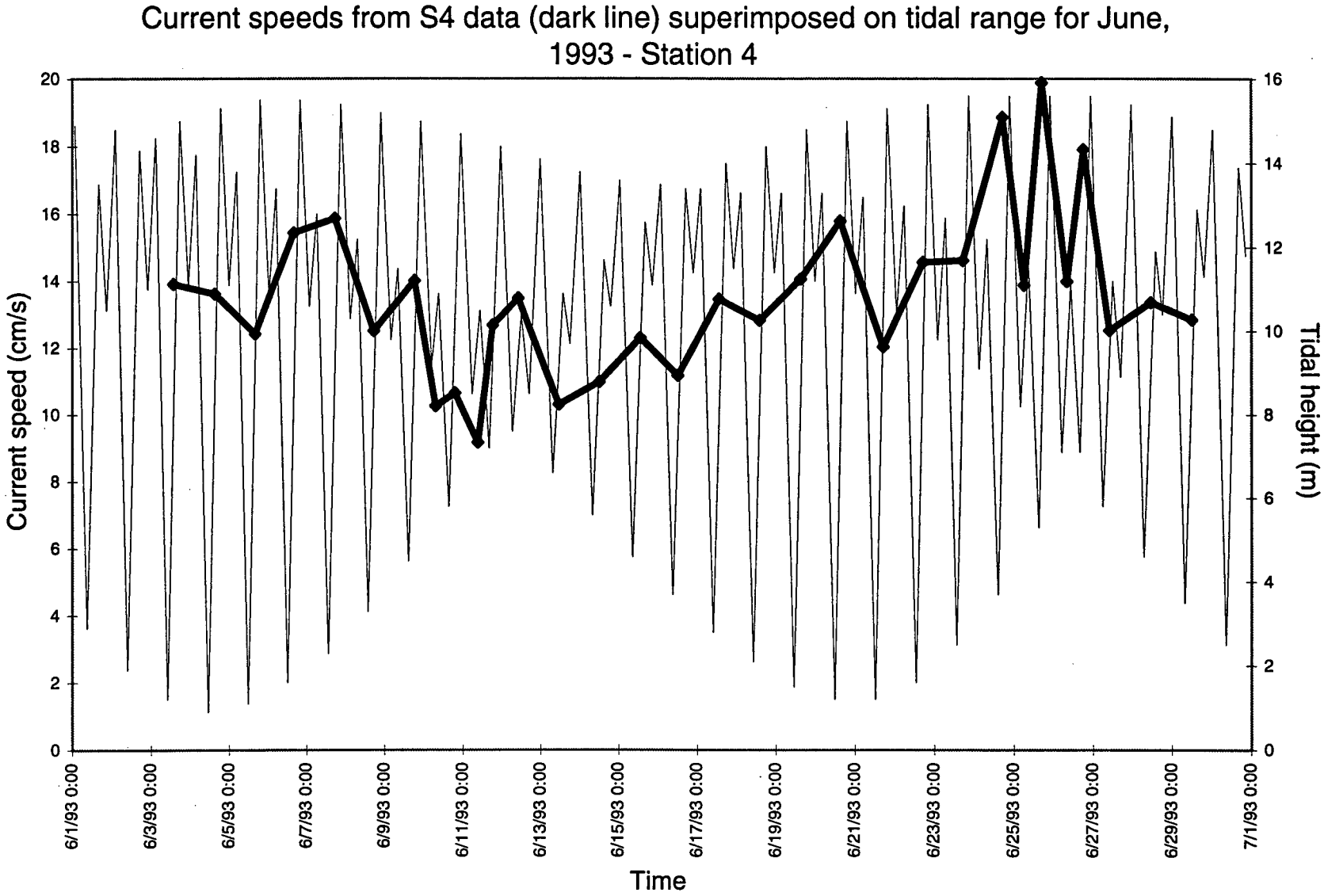

Figure 105: One-minute-averaged velocities for the month of June, 1993 at station 4

direction (Figure 106). Currents in a flooding direction in this interval are also high. Typically the flooding current velocities exceed the ebb, however, in some cases the ebbing velocities may be higher. Wave particle velocities for the month of June are significantly higher than the month of May at station S4. Velocities exceed 40 cm/s 125 times with 110 of these values recorded in a flooding direction. The maximum single velocity recorded occurred on the interval of June 4 (1500 h) to June 5 (0800 h) with a value of 53 cm/s in flooding direction (Figure 107). The critical shear velocity for erosion of 49 cm/s is reached 12 times in June, always in a flooding direction. Only 4 of the sampling intervals recorded show ebbing velocities greater than flooding velocities.

Current plots averaged over 10° increments for the month of May confirm this observation as flooding currents are higher (22 cm/s) and more concentrated in one direction than ebbing currents (~190-250°) which are lower (18 cm/s) and spread out in a wider range of directions (Figure 108). Velocities in other directions are typically 7 cm/s. The frequency of occurrence of directions shows that ebbing currents occur more often than flooding currents suggesting that on a flooding tide the water moves onto the bank quickly resulting in higher velocities for shorter durations, while on an ebbing tide, the water moves off the bank at a slower rate resulting in lower velocities for longer durations. Current plots averaged over 10° increments for June show a similar distribution pattern to the month of May (Figure 109). Flooding currents (~30-60°) are higher (24 cm/s) and more focussed in one direction than ebbing currents (~210-250°) which are lower (18 cm/s). Velocities in other directions are consistent with the May results of 7 cm/s. However, unlike the May results, the frequency of occurrence of both the flooding and ebbing directions is approximately equal. This is supported by the

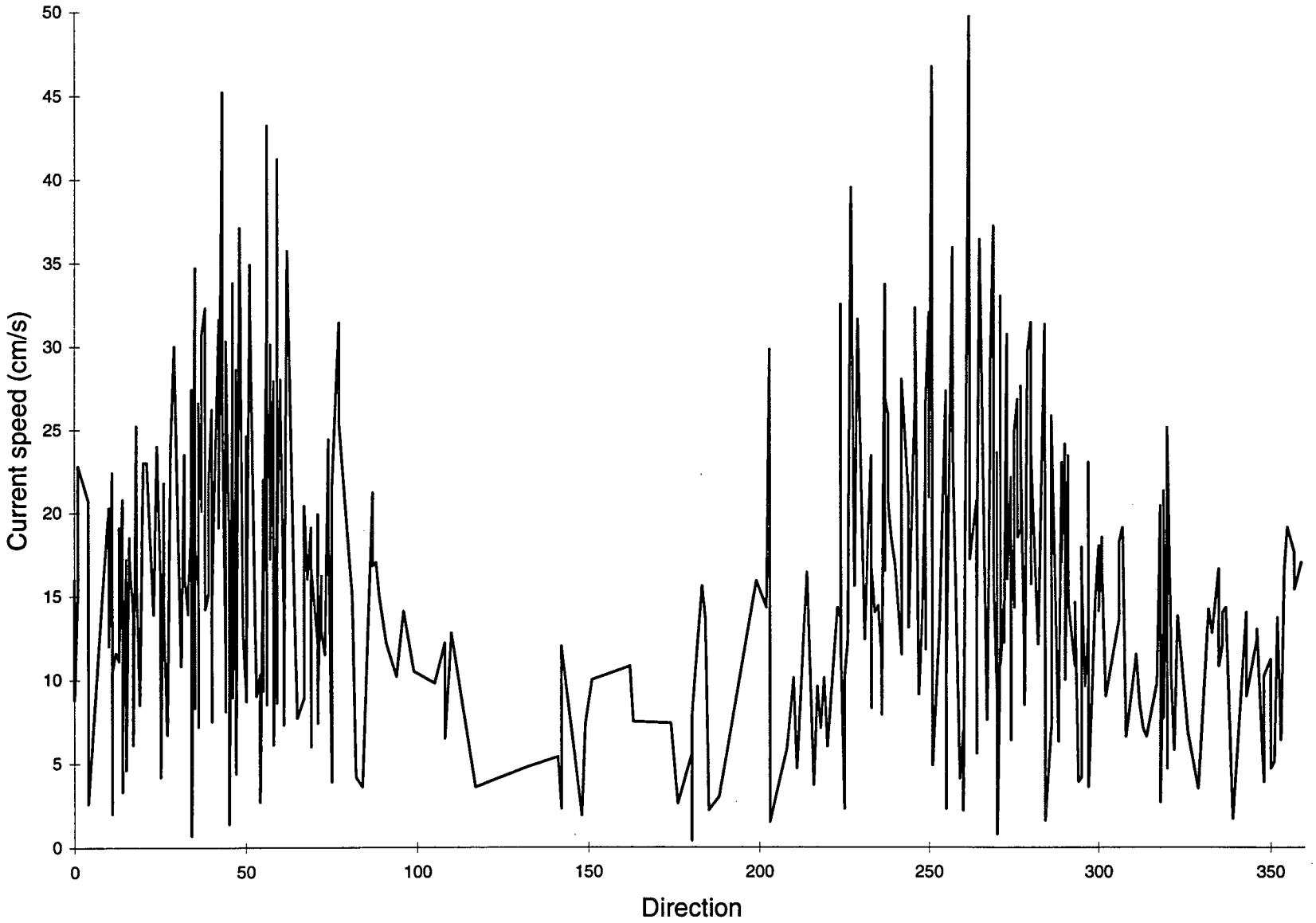

Figure 106: Wave particle velocities for the May 11, 2000 to May 12, 1100 h sampling interval at station 4

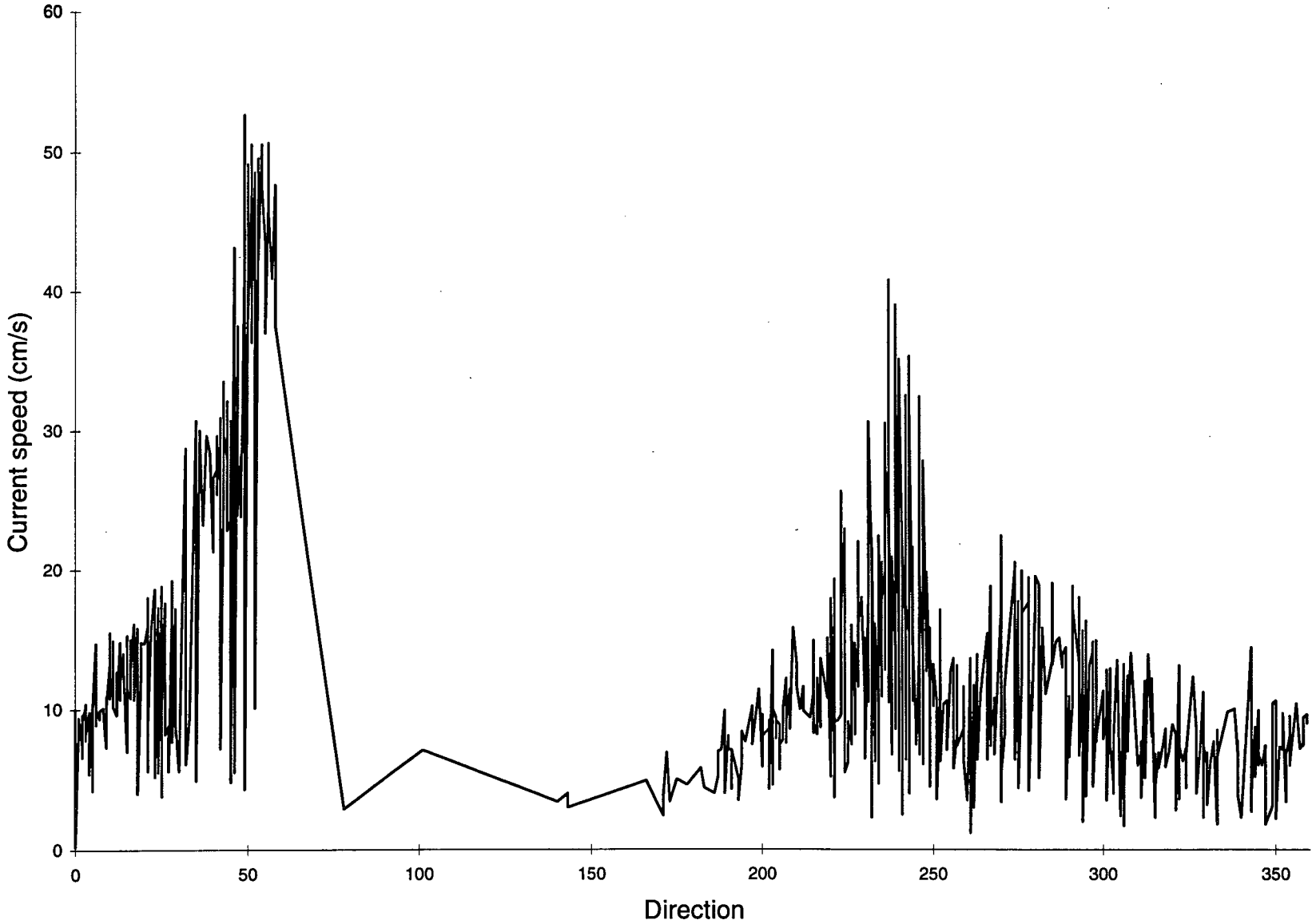

Figure 107: Wave particle velocities for the June 4, 1500 to June 5, 0800 h sampling interval at station 4

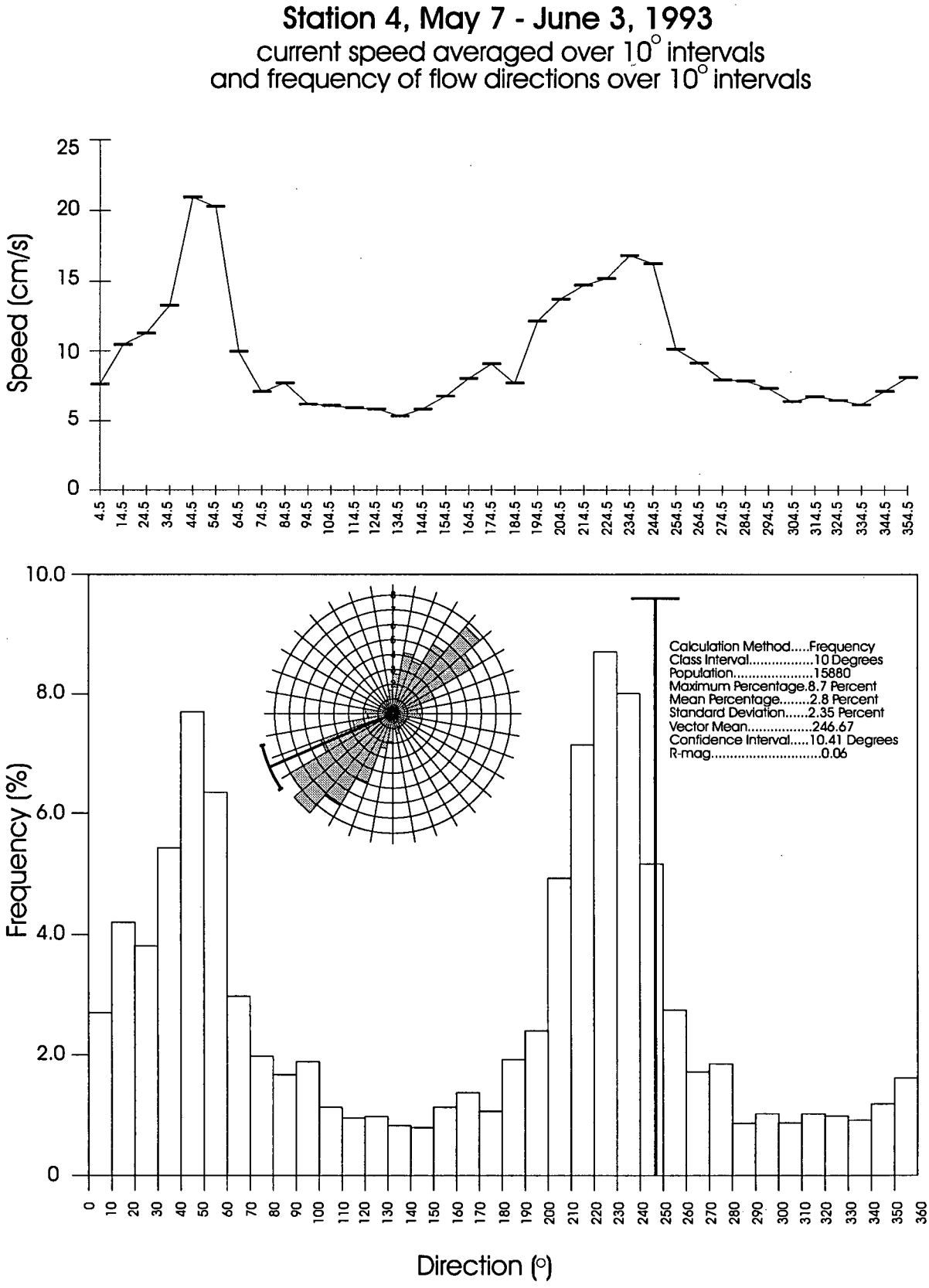

Figure 108: Average speed and direction plotted over 10 degree-averaged increments at station 4 in May

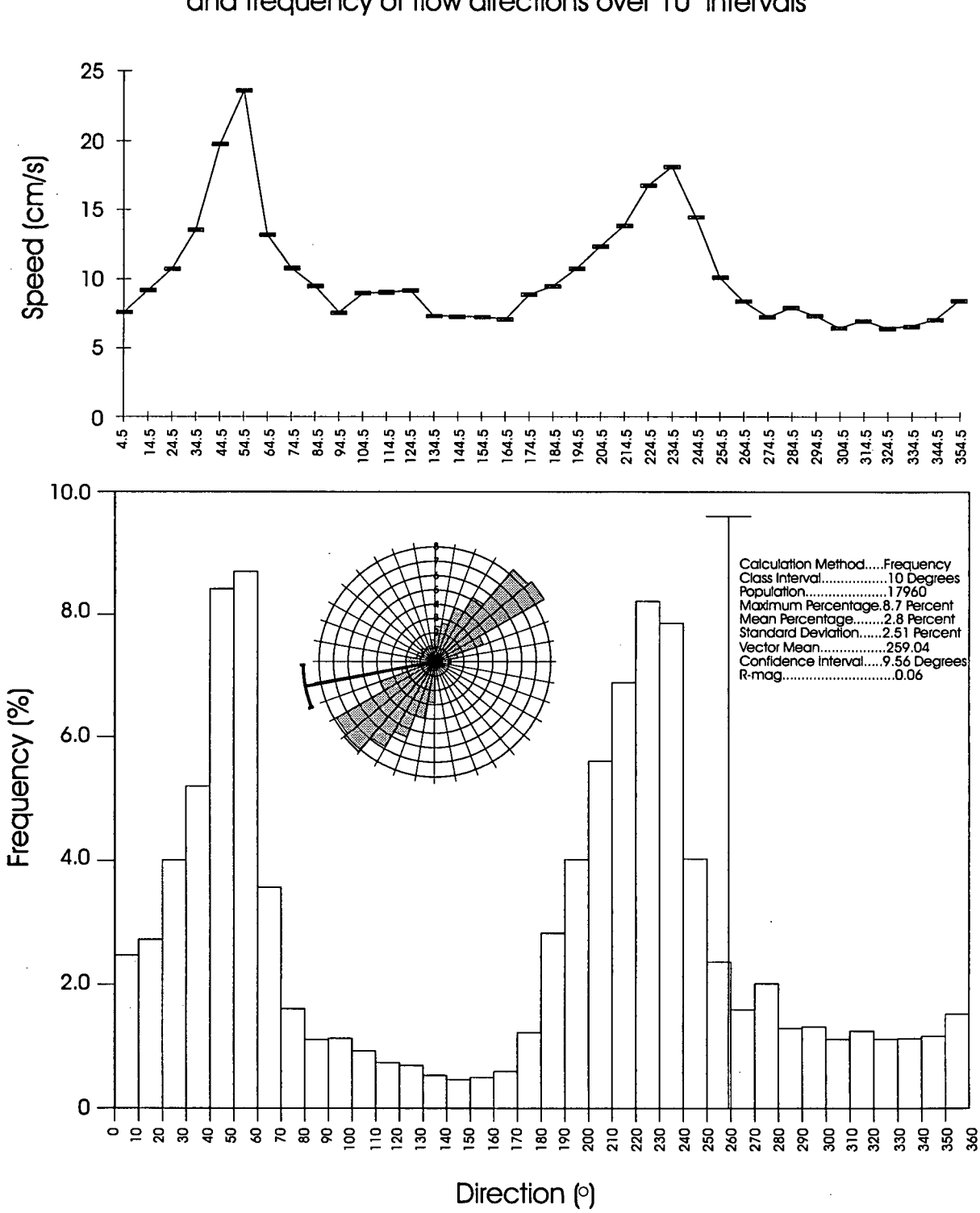

Figure 109: Average speed and direction plotted over 10 degree-averaged increments at station 4 in June

observation that the velocity peak in the ebbing direction is sharper for the month of June than for the month of May.

Temperature measurements recorded in the month of May range from 10°C on May 13 to 19°C on May 30 (Figure 110). Temperatures at the beginning of May are 12°C and increase to 18.5°C by May 19, decrease to 13°C by May 22, gradually increase to 19°C by May 30 and fall to 16° until the end of the survey. This temperature trend follows very closely to that observed at station 1 and represents the spring and neap tidal influences. Temperatures within a single sampling inundation show a maximum variation of 4.5°C but typically vary 1 to 2°C. Temperature variation for the month of June is significantly less than the month of May ranging from 14.5 to 20.5°C (Figure 111). Temperatures at the beginning of June are approximately 16°C, fall to 14.5°C by June 10 before rising to 20°C on June 12 and falling to 16°C by June 14. A slow increase in temperature takes place until June 20 when values reach 20°C again before falling to 16°C on June 23. A gradual increase in temperature occurs until the end of the month. Within interval temperature variation is minimal in June with typical values of less than 1°C in an inundation. The maximum variation in a single submersion was 5°C.

Salinity measurements at station S4 in May are 22‰ at the beginning of the survey and increase to 28.5‰ by May 13 before falling to 3‰ by May 19 (Figure 112). From May 15 to the end of the survey salinities vary over each inundation interval by an average of 9‰ over a range of 3‰ to 19‰ so any peaks in salinity after this date are being obscured by the large variation within each sampling interval. Not only is the pattern indicative of spring and neap tidal influences but also of Fraser River freshet influence. Salinity values vary over a tidal inundation by as much as 16‰ and generally show an increase as deeper, more saline water approaches

Figure 110: Water temperature variations for the month of May, 1993 at station 4

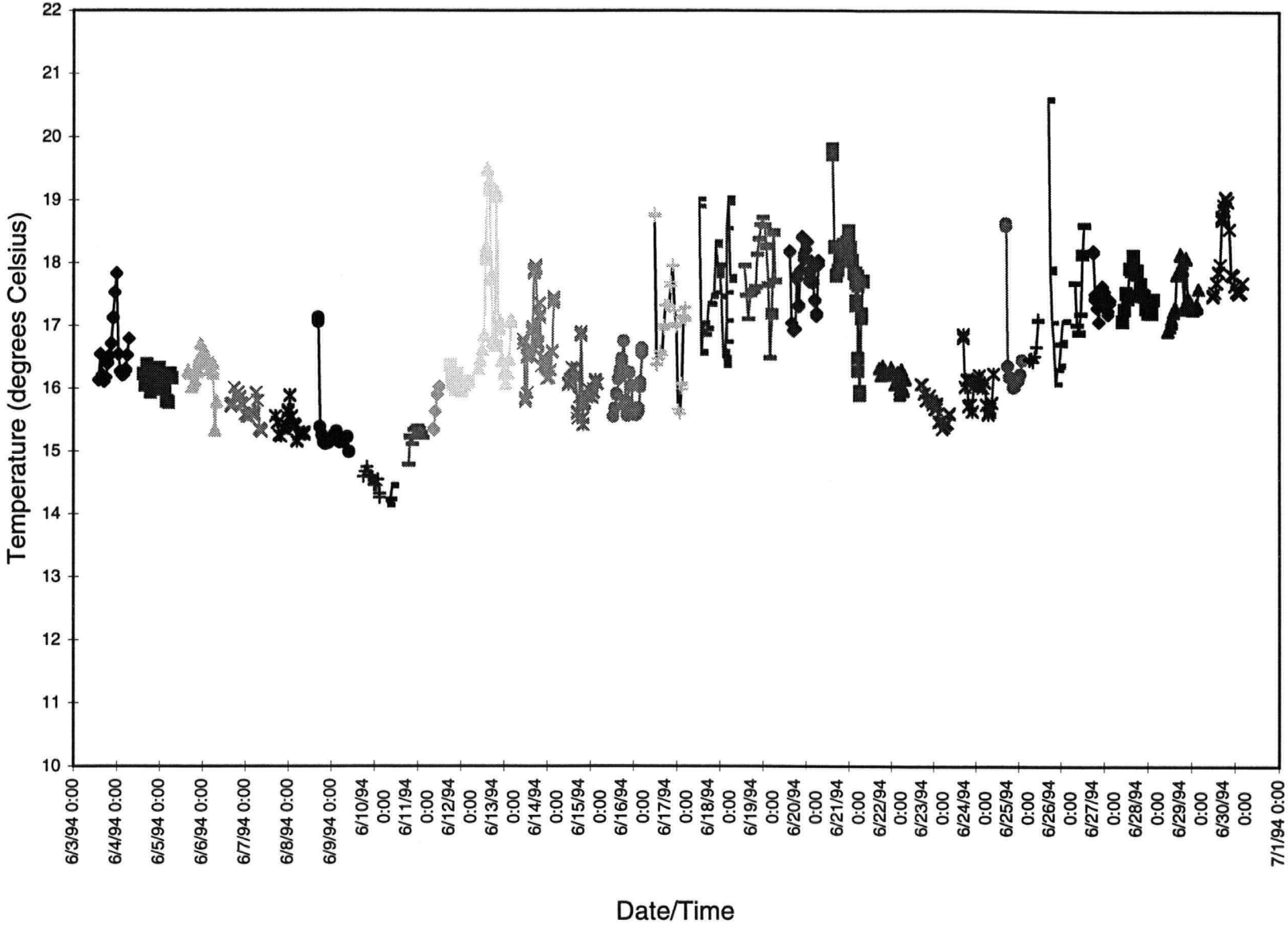

Figure 111: Water temperature variations for the month of June, 1993 at station 4

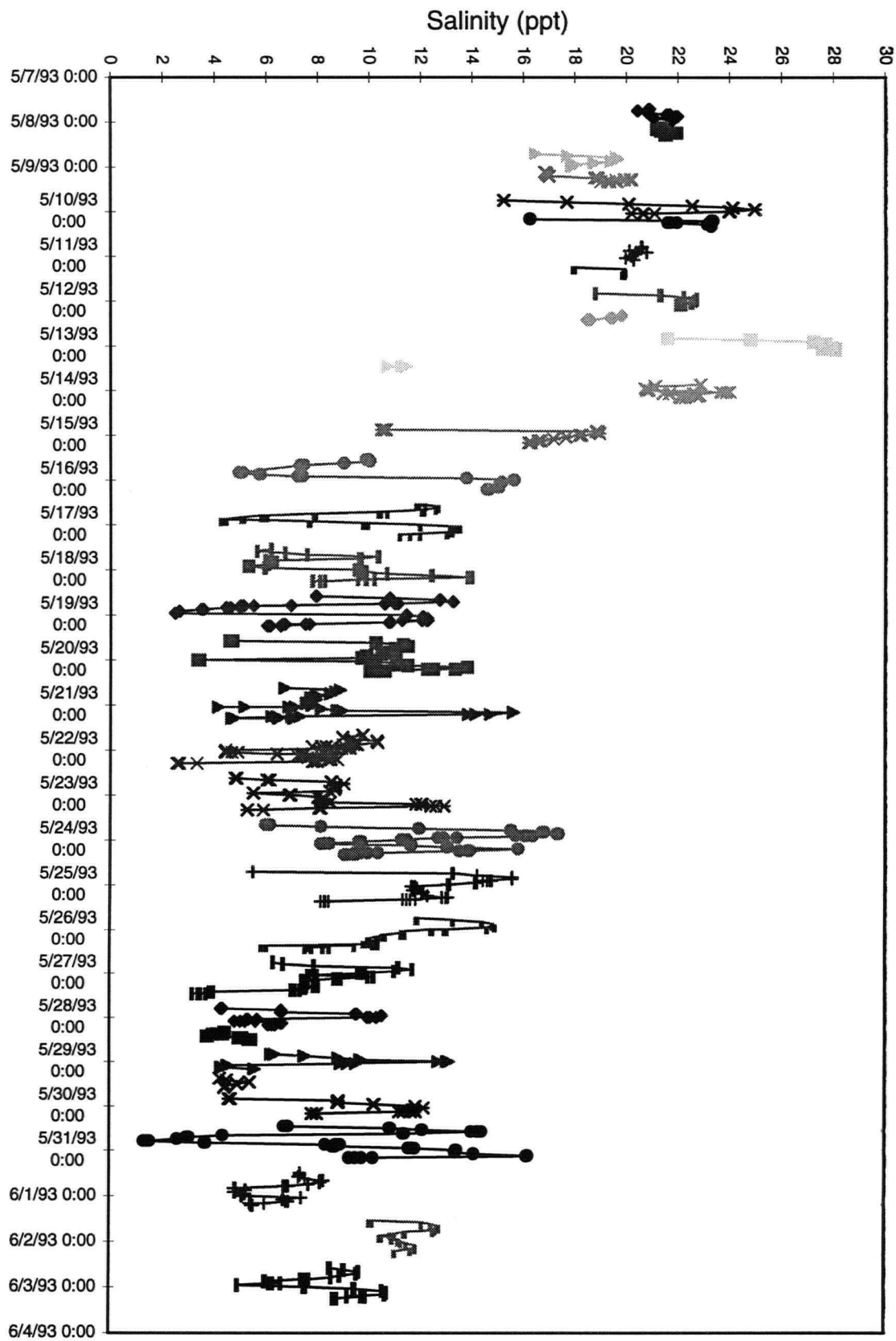

Figure 112: Salinity variations for the month of May, 1993 at station 4

followed by a decrease as the water shallows. The depth at station S4 allowed the current meter to be submersed for two flooding tides without exposure during the high-low tide between them on many occasions. Like temperature, salinity measurements recorded in June, are much less variable than in May, ranging from 1.5 to 17.5‰ (Figure 113). A slight peak in salinity occurs on June 9 to 17.5‰ followed by a drop to 1.5‰ on June 12. A gradual increase to 17.5‰ by June 21 precedes a slight decrease to 16‰ to the end of the survey. Similar to May results, salinity varies over a submersion period significantly and therefore masks the effects of salinity variation over the spring and neap tides. The maximum salinity variation over a single inundation was 14‰.

The current meter at station S4 was equipped with a pressure sensor which recorded depth. Depth measurements demonstrate the effect of spring and neap tides in the month of May (Figure 114) as depth during a spring tide varies more significantly than depth during a neap tide. Depth ranged from 0.6 m above the sensor, located at the midpoint of the current meter with the speed and direction electrodes (~50 cm from the seabed), to 2.75 m. Depth measurements recorded in June at station S4 show the spring and neap tidal cycle but also display a larger depth range than in May (Figure 115). The maximum depth over the sensor for the month of June was ~2.75 m, similar to May, however, this depth is recorded on both spring tides in June but only one spring tide in May. Prior to May 19, depths do not exceed 2 m over the sensor. This may be the result of the increase in the volume of water arriving from the mouth of the Fraser and/or the slight increase in spring tidal height in the month of June.

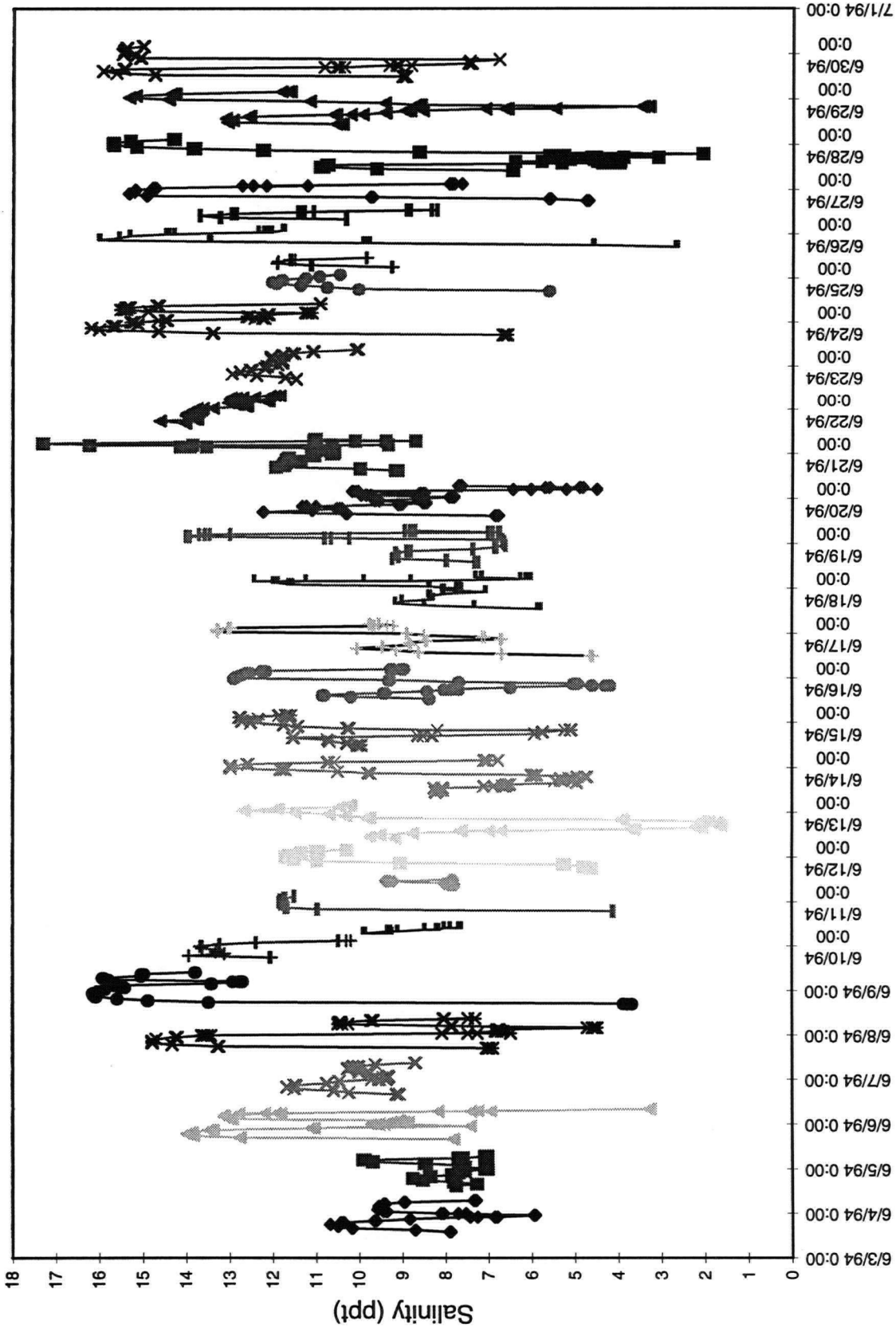

Figure 113: Salinity variations for the month of June, 1993 at station 4

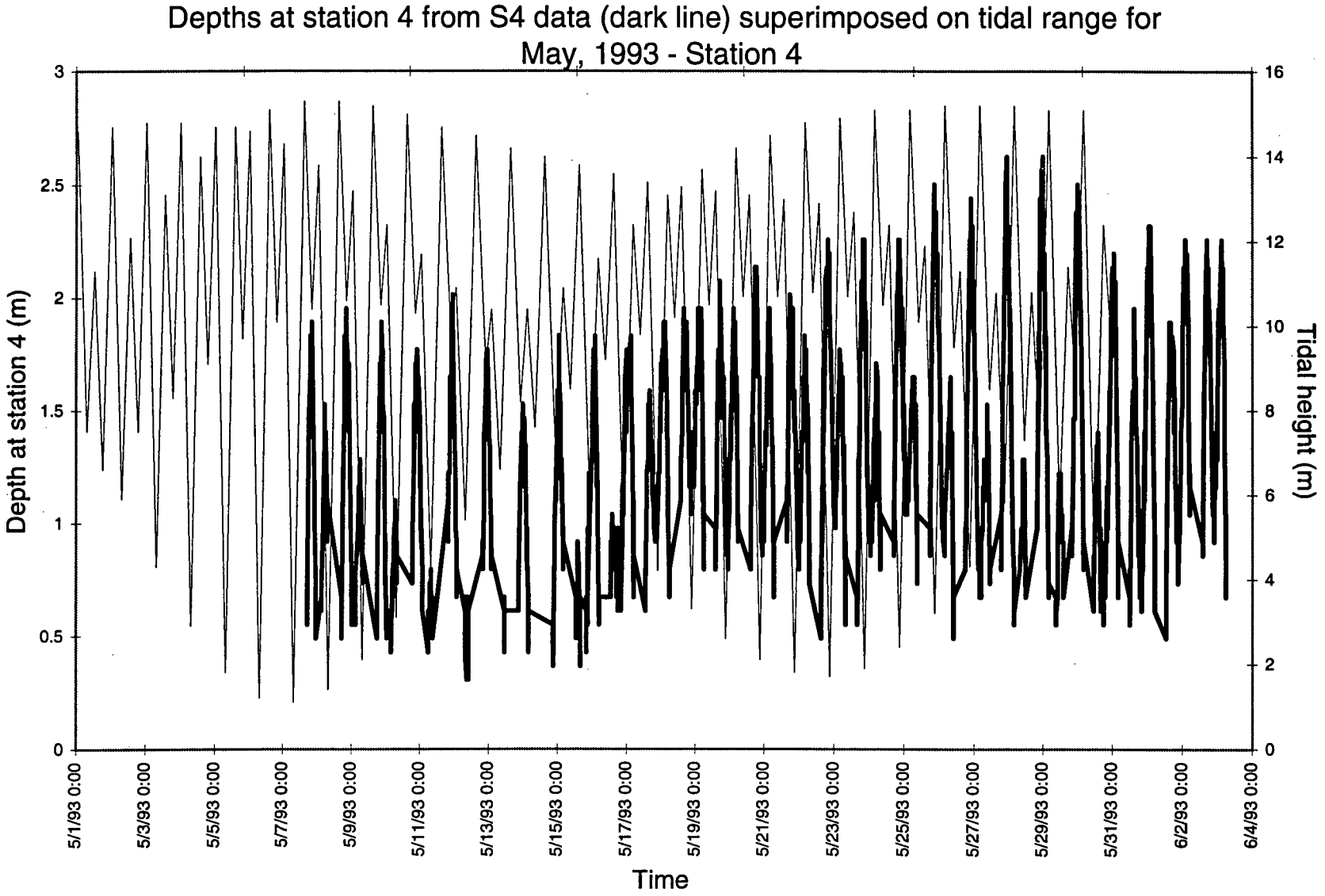

Figure 114: Depth variations for the month of May, 1993 at station 4

Figure 115: Depth variations for the month of June, 1993 at station 4

IV-5. Station S5

The current meter deployed at station S5 through the month of June was inundated 77% of the time, similar to the submersion time of the current meter deployed at station S4 through June. Inundation intervals were usually for 19 hours. One-minute-averaged velocities ranged from a low of 10.81 cm/s to a high of 18.12 cm/s with an average value of 14.01 cm/s (Figure 116). The highest velocities were recorded in sampling intervals June 3 (1400 h) to June 4 (0900 h), June 4 (1400 h) to June 5 (0900 h), and June 24 (1600 h) to June 25 (1300 h) with values of 18.12, 17.47 and 17.90 cm/s, respectively. Superimposing the tidal range curve on the measured velocities reveals a good relationship with peaking velocities in spring tides.

Wave particle velocity measurements at station S5 exceed 50 cm/s 32 times throughout the survey with 28 of these values recorded in a flooding direction. The maximum velocity recorded at this station was 62 cm/s in an ebbing direction in both sampling intervals June 6 (2300 h) to June 7 (1000 h) (Figure 117) and June 19 (0400-0800 h) (Figure 118). Typically the flooding velocities are higher than the ebb with some exceptions. The critical shear velocity for erosion at station S5 is 58 cm/s and it is reached 6 times in the sampling period. Although the critical shear velocity is reached an equal number of times in a flooding and ebbing direction, the ebbing velocities are 4 cm/s higher than the flooding velocities.

Averaging speed and direction measurements over 10° increments shows that current velocities in flooding directions exceed these in ebbing directions with peak values of 23 cm/s and 18 cm/s, respectively (Figure 119). As seen previously, the peak in velocity in the flooding direction (70-100°) is more focussed in one direction whereas the peak in the ebb direction (220-270°) is broader, encompassing a wider range of directions. In contrast to measurements made

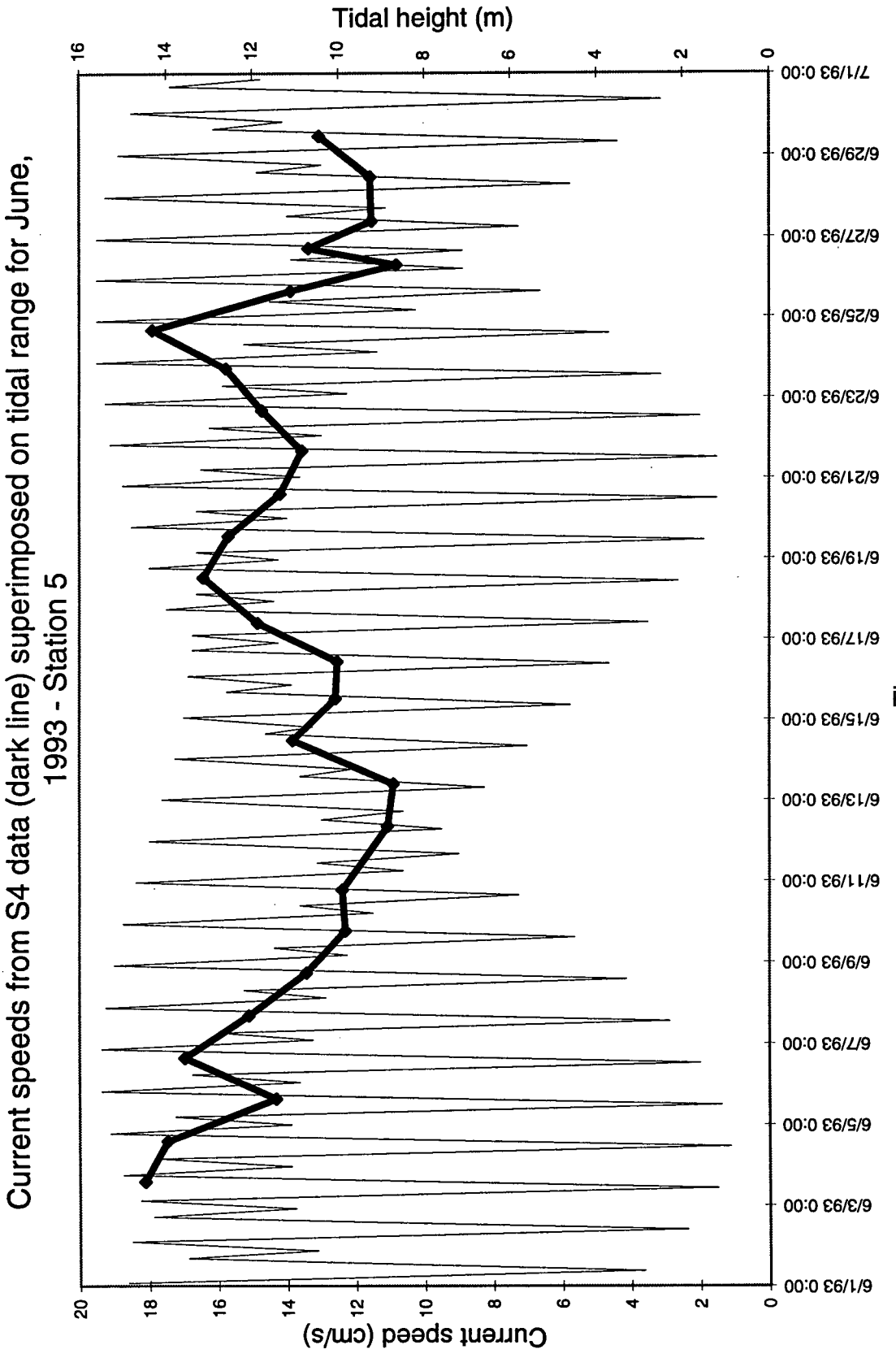

Figure 116: One-minute-averaged velocities for the month of June, 1993 at station 5

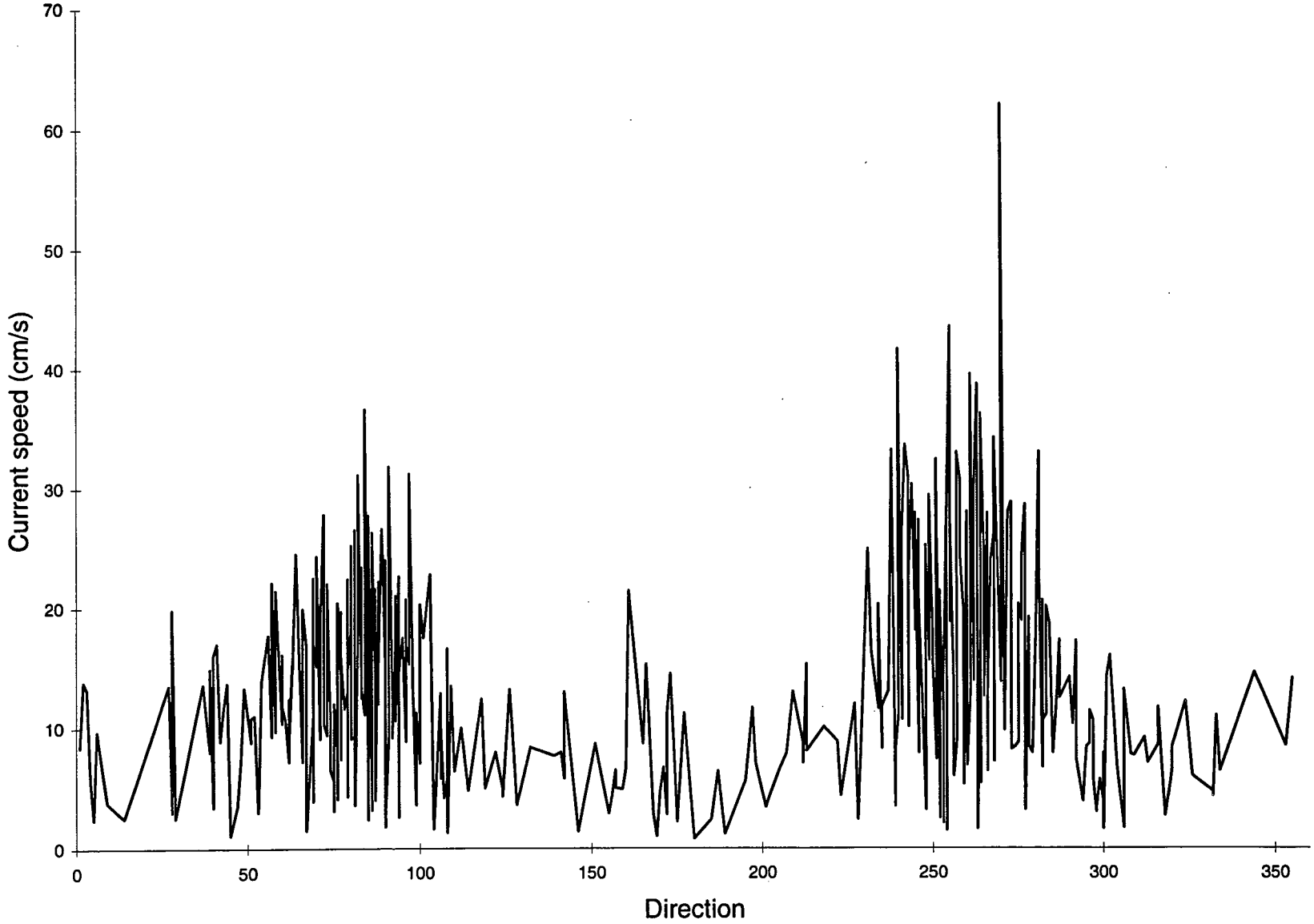

Figure 117: Wave particle velocities for the June 6, 2300 to June7, 1000 h sampling interval at station 5

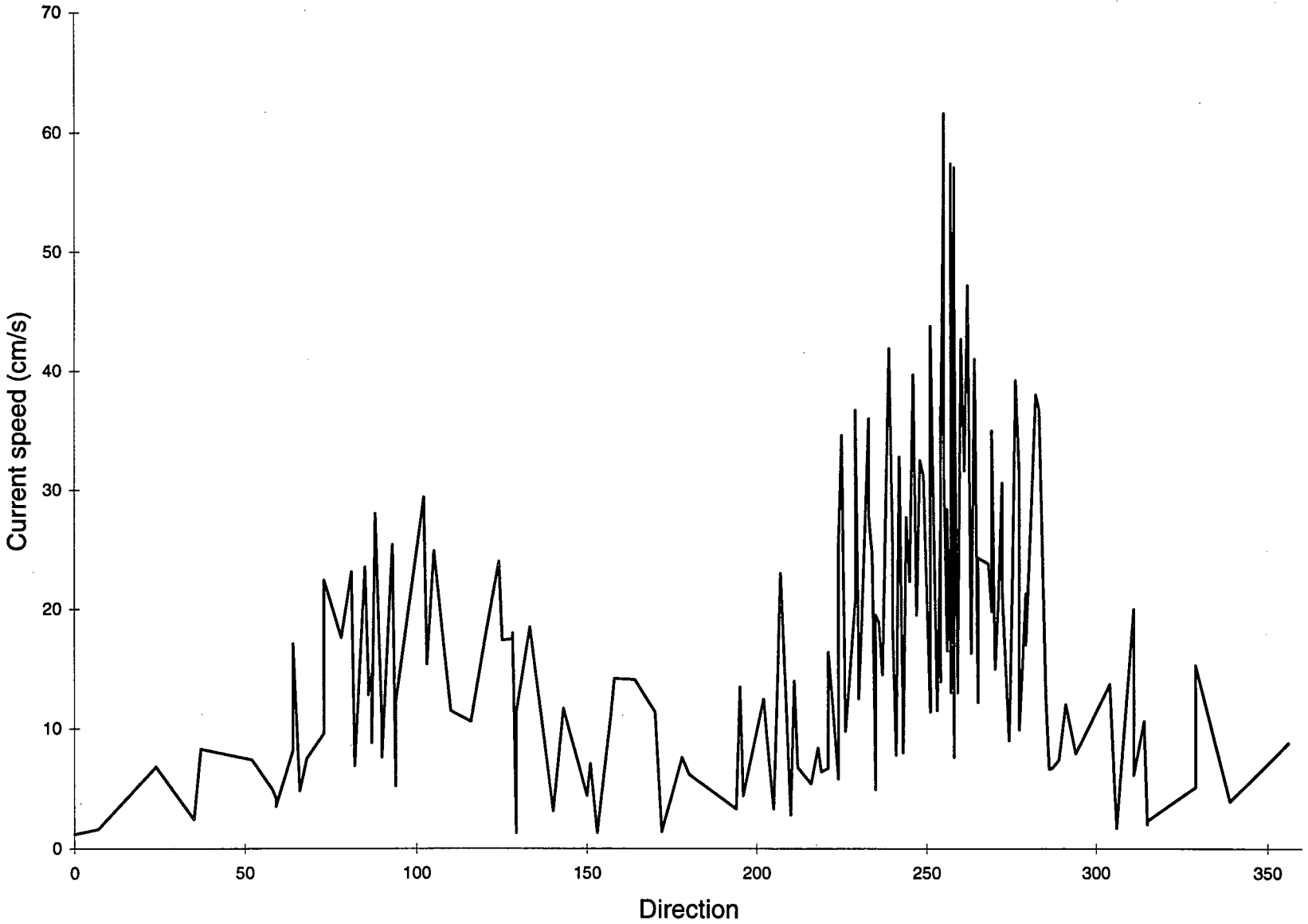

Figure 118: Wave particle velocities for the June 19, 0400-0800 h sampling interval at station 5

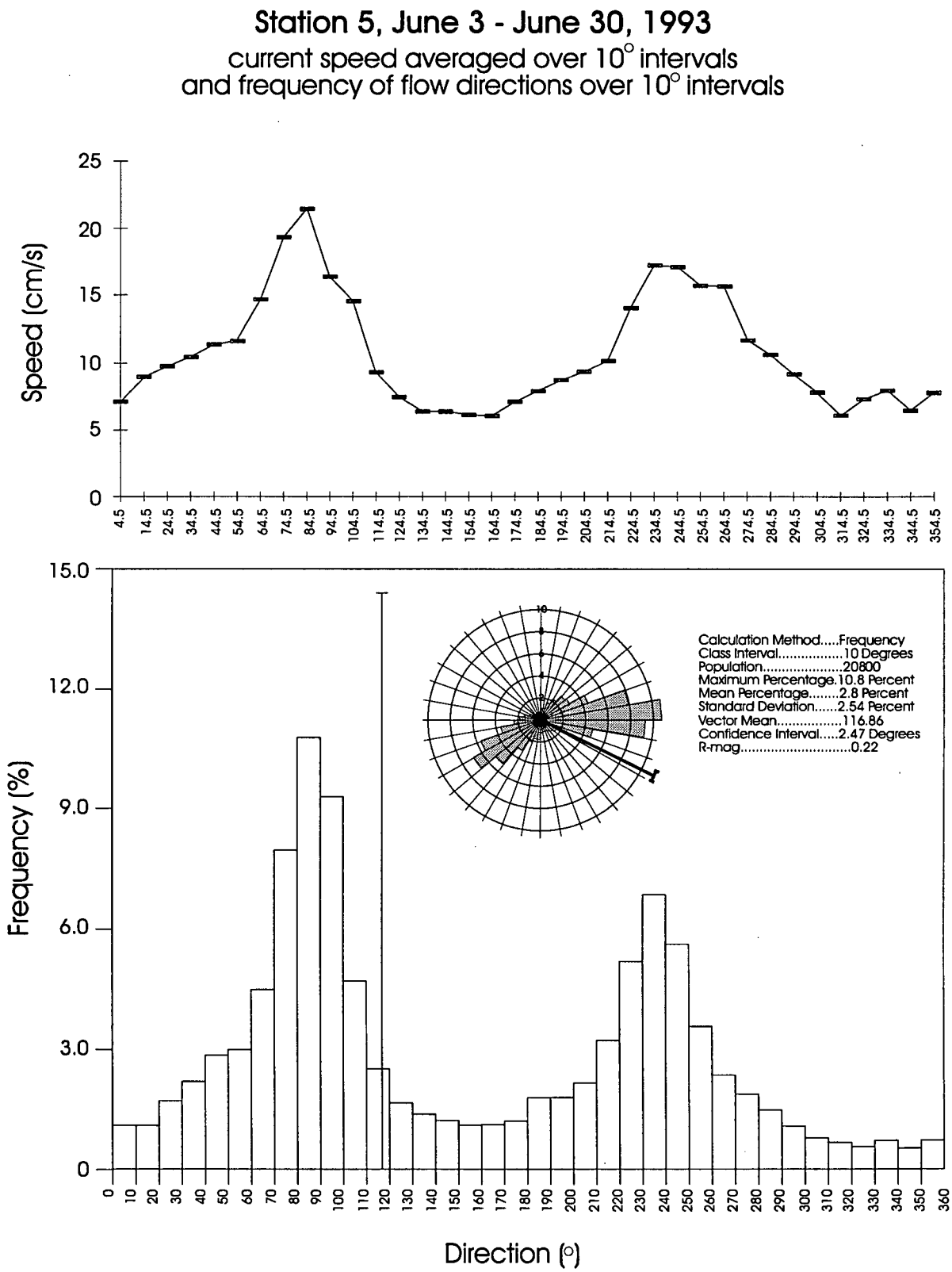

Figure 119: Average speed and direction plotted over 10 degree-averaged increments at station 5

in May at station S4, the frequency of occurrence of flooding directions is much greater than ebbing directions, likely due to the shape of the bank. Like station S4, currents in directions other than ebb and flood, have velocities of ~7 cm/s.

Temperature varies from 12.5 to 19.5°C over the whole sampling period and in a single sampling interval (Figure 120). This 7° interval variation was also found at station S2 and is the largest temperature variation recorded in one interval. Temperatures are 16°C at the beginning of June, fall to less than 13°C on June 9, rise slowly and with minor fluctuations to 19.5°C on June 20 and fall in the same sampling interval to 12.5°C by June 21. Temperature rises steadily to 18°C until the end of the survey.

Salinity varies from 2 to 25.5‰ with little evidence of salinity peaks because of the large variations in salinity values within sampling intervals (Figure 121). Slight peaks near June 5 and June 21 are evident with salinity lows near June 10 and June 27. This corresponds roughly with the spring/neap tidal cycle. The maximum salinity variation in one current meter submersion is 19‰.

IV-6. Station S6

The deployment of the current meter situated at station S6 resulted in inundation for 75% of the sampling time, similar to stations S4 and S5 submersion for the month of May and June. However, averaged velocities at station S6 are considerably higher, reaching values of 27.8 cm/s in the interval recorded on May 11 (1900 h) to May 12 (0100 h) (Figure 122). Average velocities are lowest on the interval recorded on May 14 (1000-1500 h) with a value of 9.63 cm/s but are above 20 cm/s on 6 other sampling intervals. Velocities measured at station S6 show only a

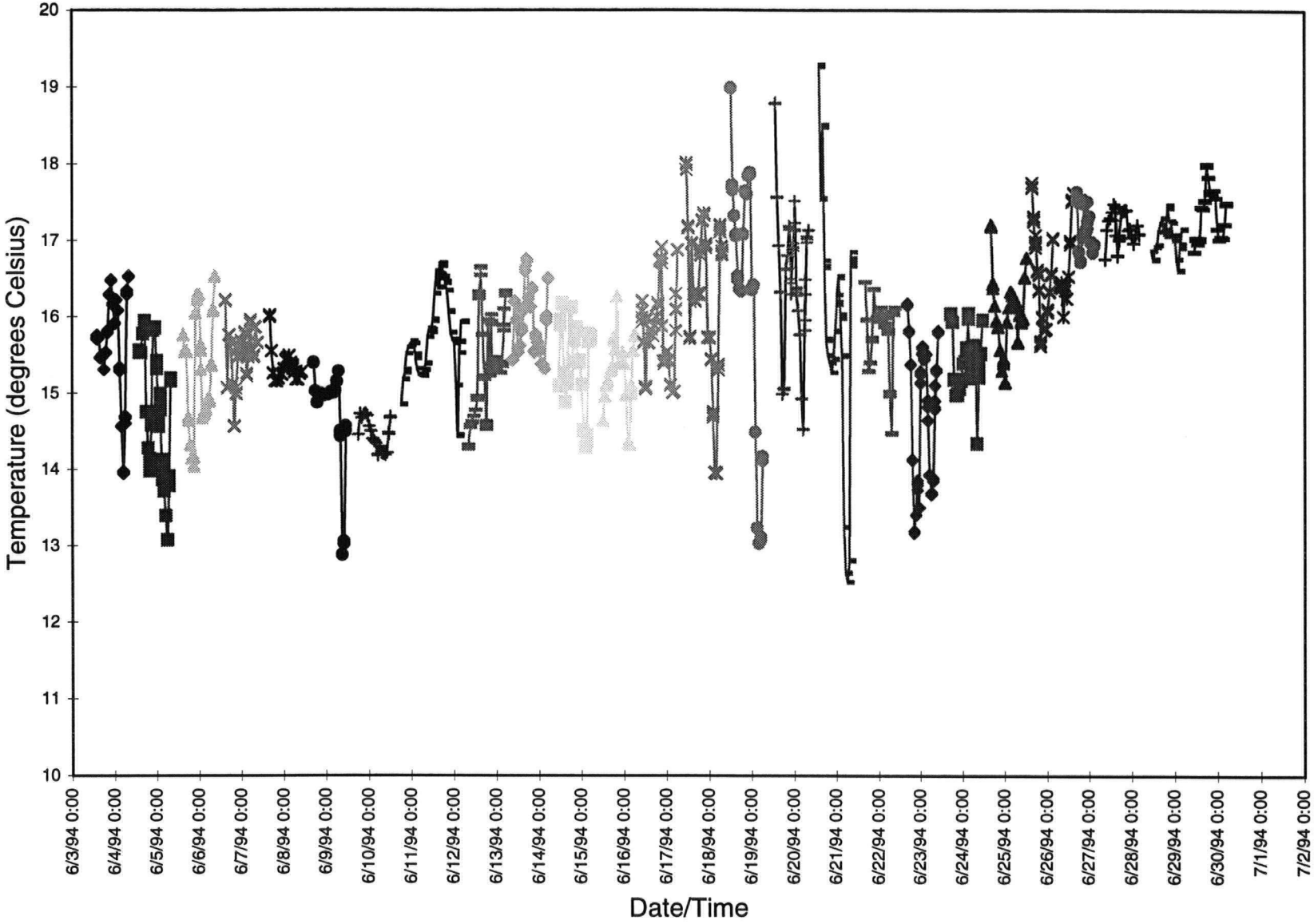

Figure 120: Water temperature variations for the month of June, 1993 at station 5

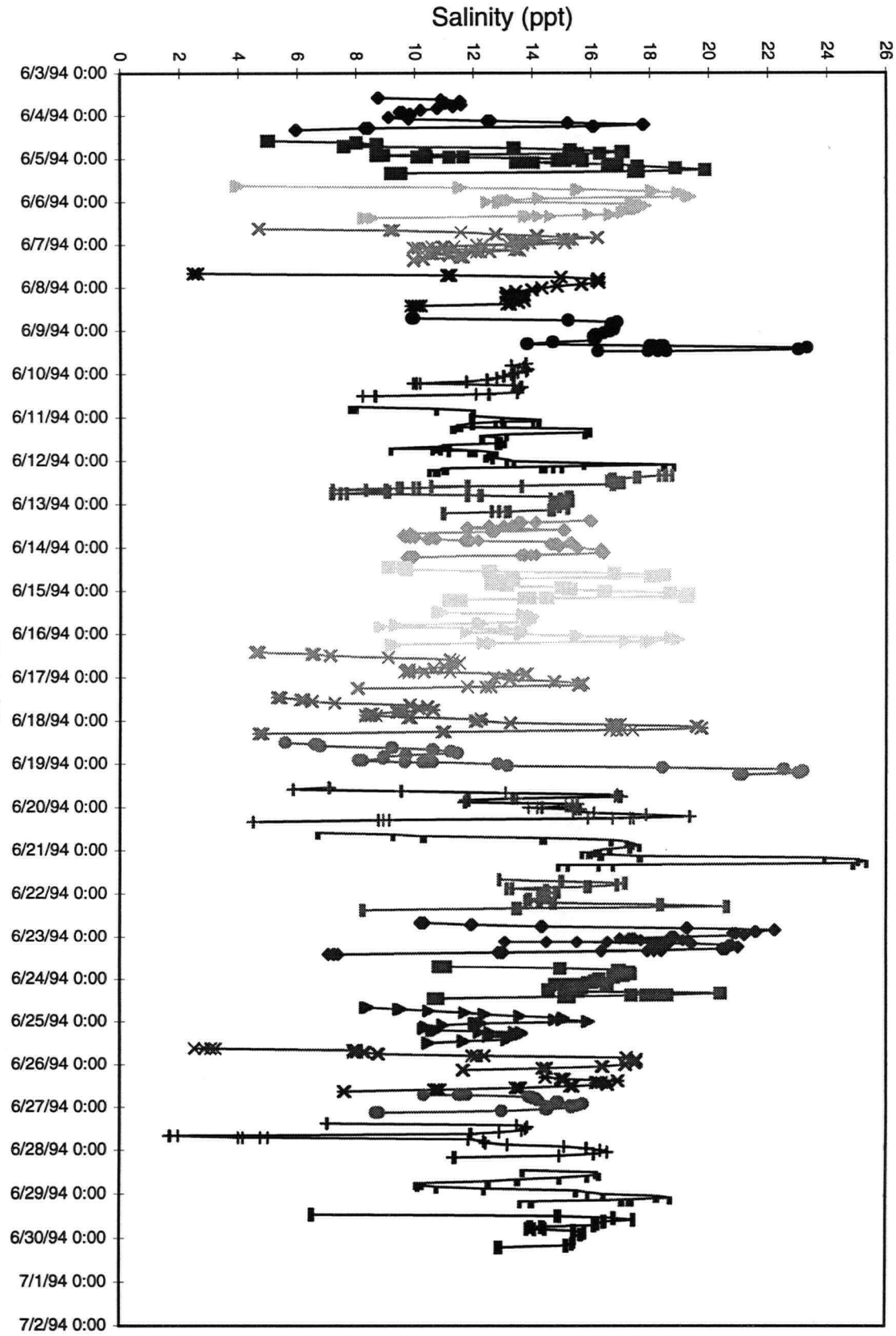

Figure 121: Salinity variations for the month of June, 1993 at station 5

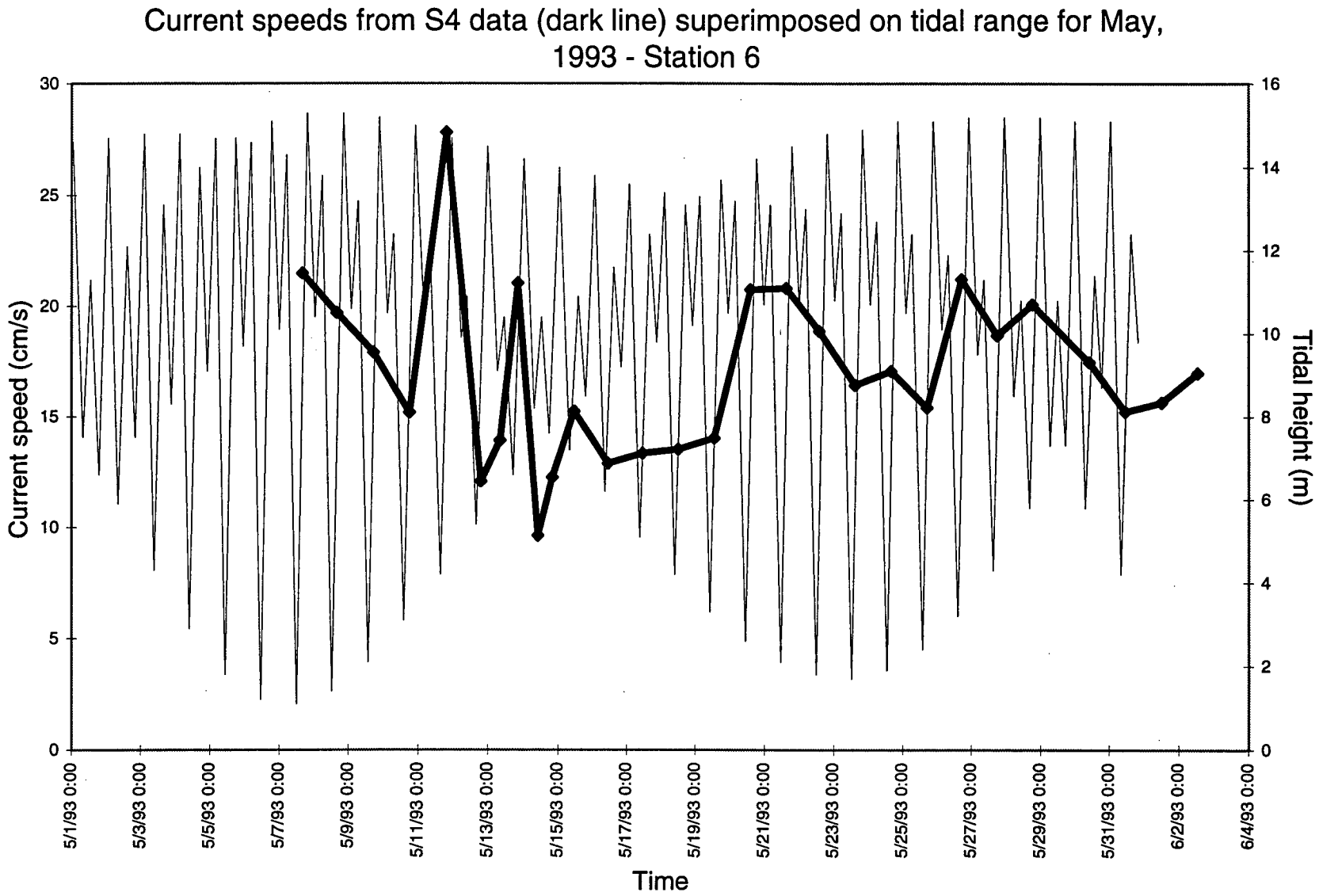

Figure 122: One-minute-averaged velocities for the month of May, 1993 at station 6

minor relation to the tidal cycle, however higher values are generally found in the spring tides.

Wave particle velocities at station S6 exceed 50 cm/s 96 times with 56 of these values recorded in a flooding direction (~60-110°) with ebbing velocities (230-290°) maintaining a higher influence than at the stations previously discussed. Several sampling intervals show higher ebbing than flooding velocities at station S6. The highest single velocity recorded at station S6 was 90 cm/s in the sampling interval of May 11 (1900 h) to May 12 (1300 h) (Figure 123). Velocity measurements on the ebbing tide show currents over 60 cm/s 11 times while on the flooding tide these velocities are only reached 6 times. Currents reach 56 cm/s, the critical shear velocity for erosion of sediments at this station, 56 times during the sampling period with 32 of these occurrences in flooding directions. Despite the more frequent occurrence of eroding currents in the flooding direction, the eroding ebbing currents are typically 10 to 20 cm/s higher than the flooding currents.

The greater influence of ebbing directions is evident when examining the plot of speed and direction averaged over 10° increments (Figure 124). Ebbing currents are slightly higher (24 cm/s) than flooding currents (23 cm/s), however flooding currents ar longer in duration than ebbing currents. Current velocities in directions other than the ebb and flood, measure 12 cm/s, significantly higher than the other stations on the bank.

Temperature measurements show a variation from 9°C on May 13 to 17.5°C by May 19 (Figure 125). Temperatures decrease after May 19 to 11.5°C by May 20 and then increase slowly to 16.5°C by May 28 where they remain stable until the end of the survey. This is consistent with other measurements recorded in May and demonstrate the influence of both the Fraser River freshet and the spring/neap tidal cycle. Temperature variations over one inundation interval are

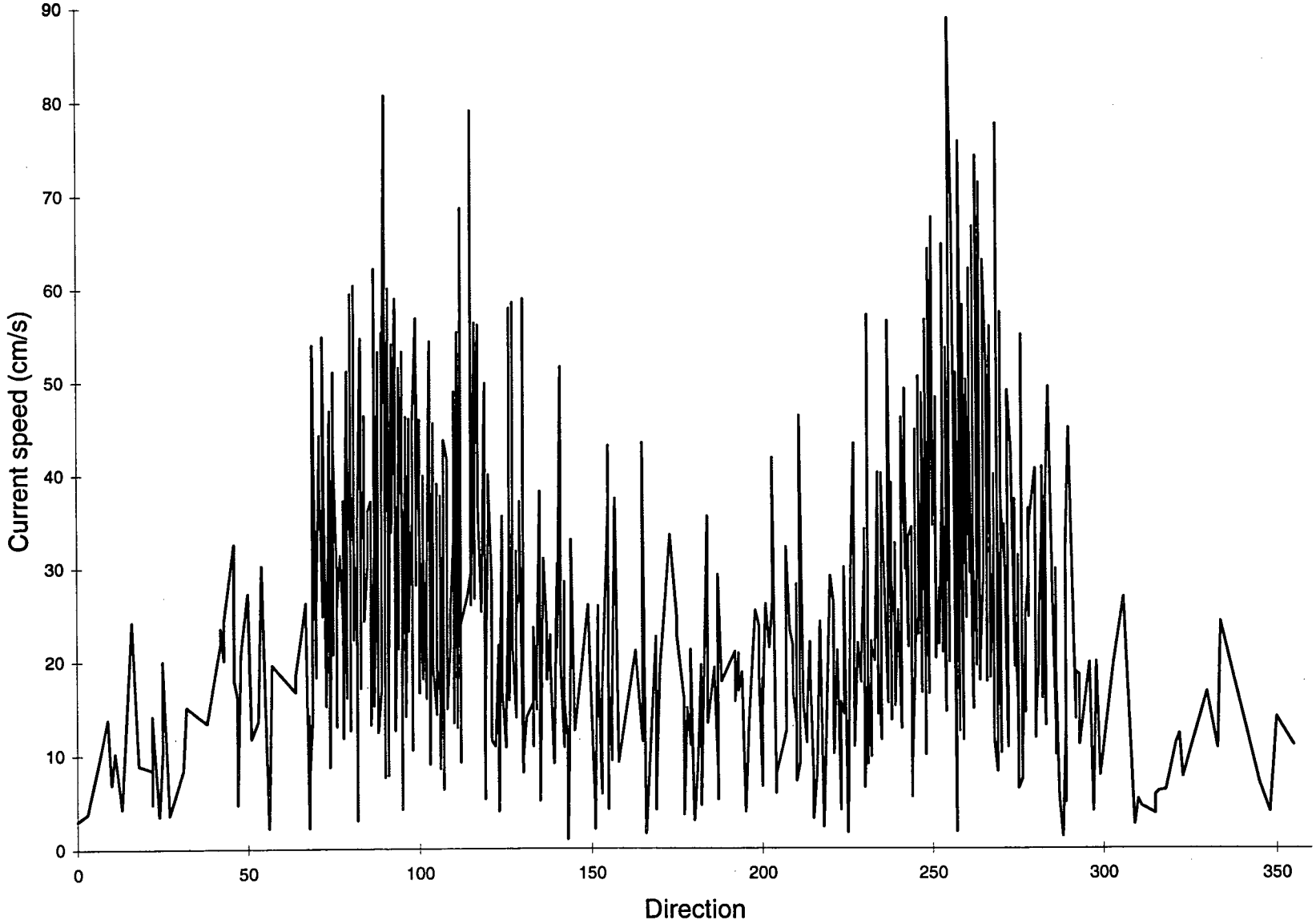

Figure 123: Wave particle velocities for the May 11, 1900 to May 12, 1300 h sampling interval at station 6

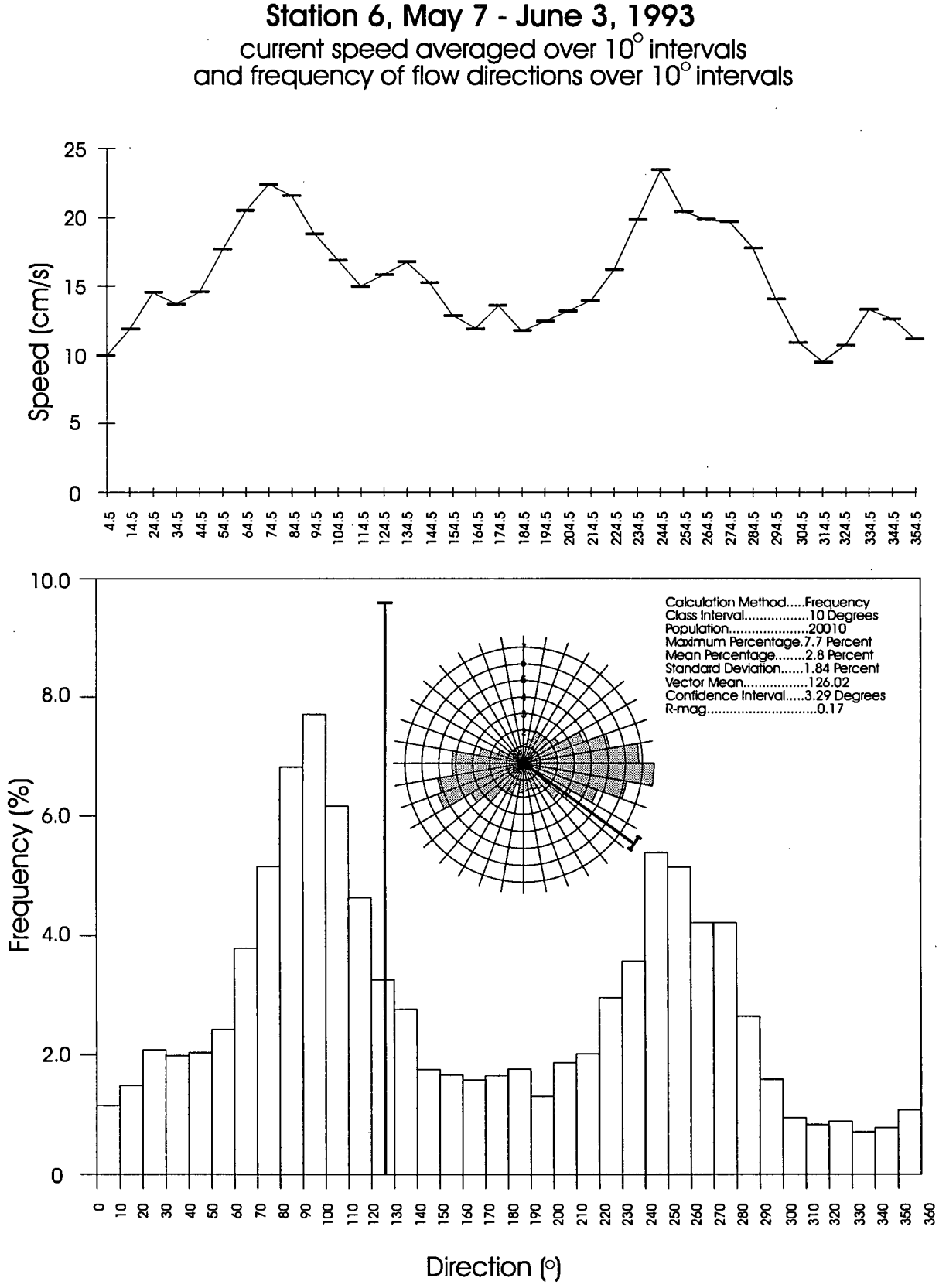

Figure 124: Average speed and direction plotted over 10 degree-averaged increments at station 6

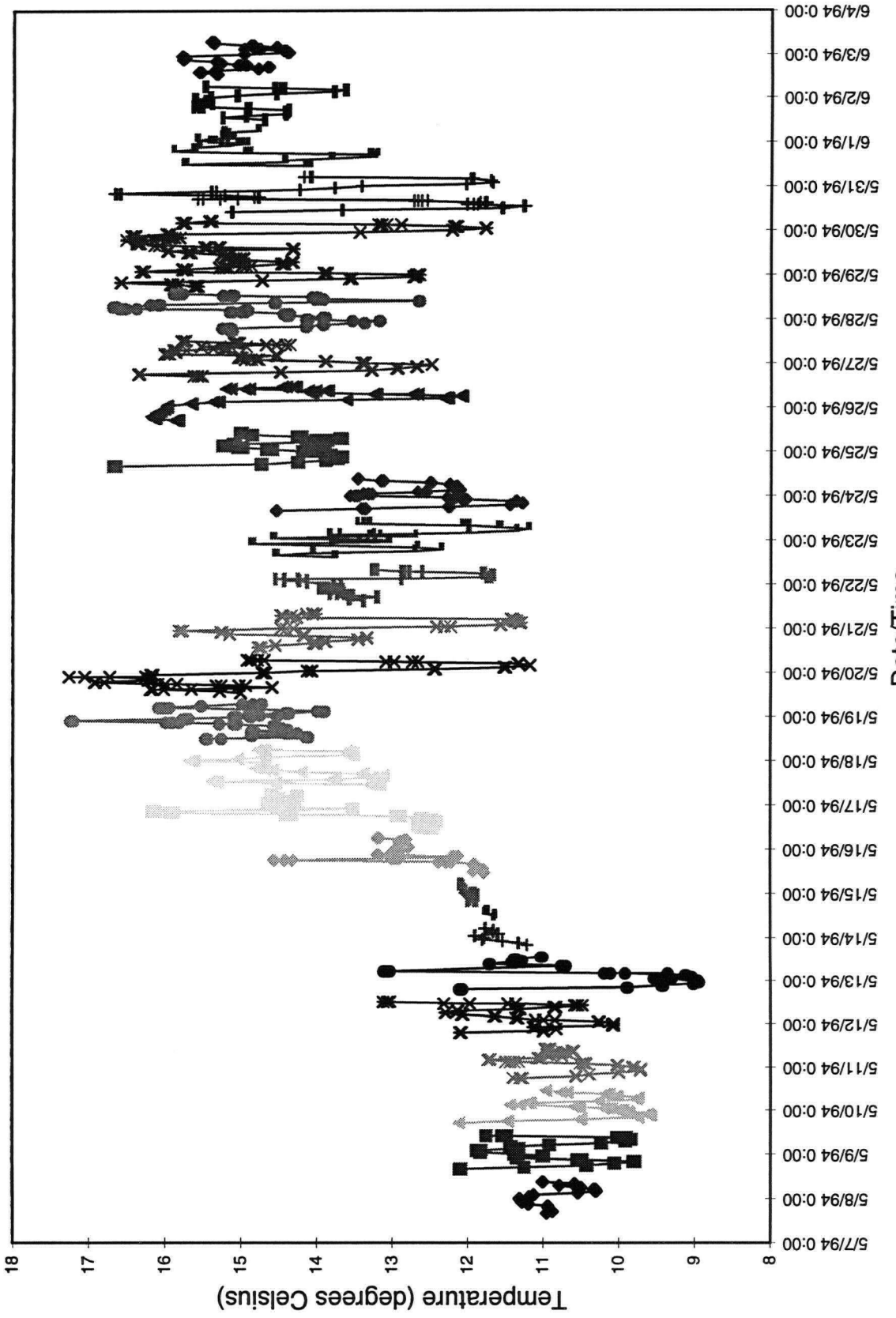

Figure 125: Water temperature variations for the month of May, 1993 at station 6

generally low until May 19, averaging 2°C, and then increase with a maximum variation of 6.5°C.

Salinity varies similarly to temperature but reciprocated. Salinities are up to 30‰ at the beginning of May and decrease until May 18 (Figure 126). From May 18, salinity values through single sampling intervals show a high degree of variation and therefore obscure the effects of the flood/neap tides. Variations within sampling intervals before May 18 range from 1‰ to 13‰ while after May 18, salinity variations are commonly 18‰ and higher with a maximum variation of 21‰.

IV-7. Station S11

The current meter deployed at station S11 was submersed 82% of the total sampling period, the most of any in the study, and was usually covered for 19 hours per interval. The one-minute-averaged velocities at station S11 range from 9.68 to 17.76 cm/s with an average of 13.46 cm/s (Figure 127). The highest velocity was recorded in the sampling intervals June 4 (1400 h) to June 5 (0900 h), June 6 (1500 h) to June 7 (1100 h), and June 24 (1600 h) to June 25 (0400 h) with values of 16.26, 16.80, and 17.76 cm/s, respectively. The tidal range curve shows a good relationship with measured velocity values with the highest velocities on the spring tides and an obvious low on the neap tide.

Wave particle velocity measurements at station S11 exceed 40 cm/s 57 times and occur evenly in the flooding and ebbing directions. The maximum velocity measurement was 53 cm/s in ebbing and flooding directions in the sampling intervals on June 4 (1400 h) to June 5 (0900 h) and June 5 (1500-1700 h) (Figure 128). Slightly higher velocity values occur in the flood

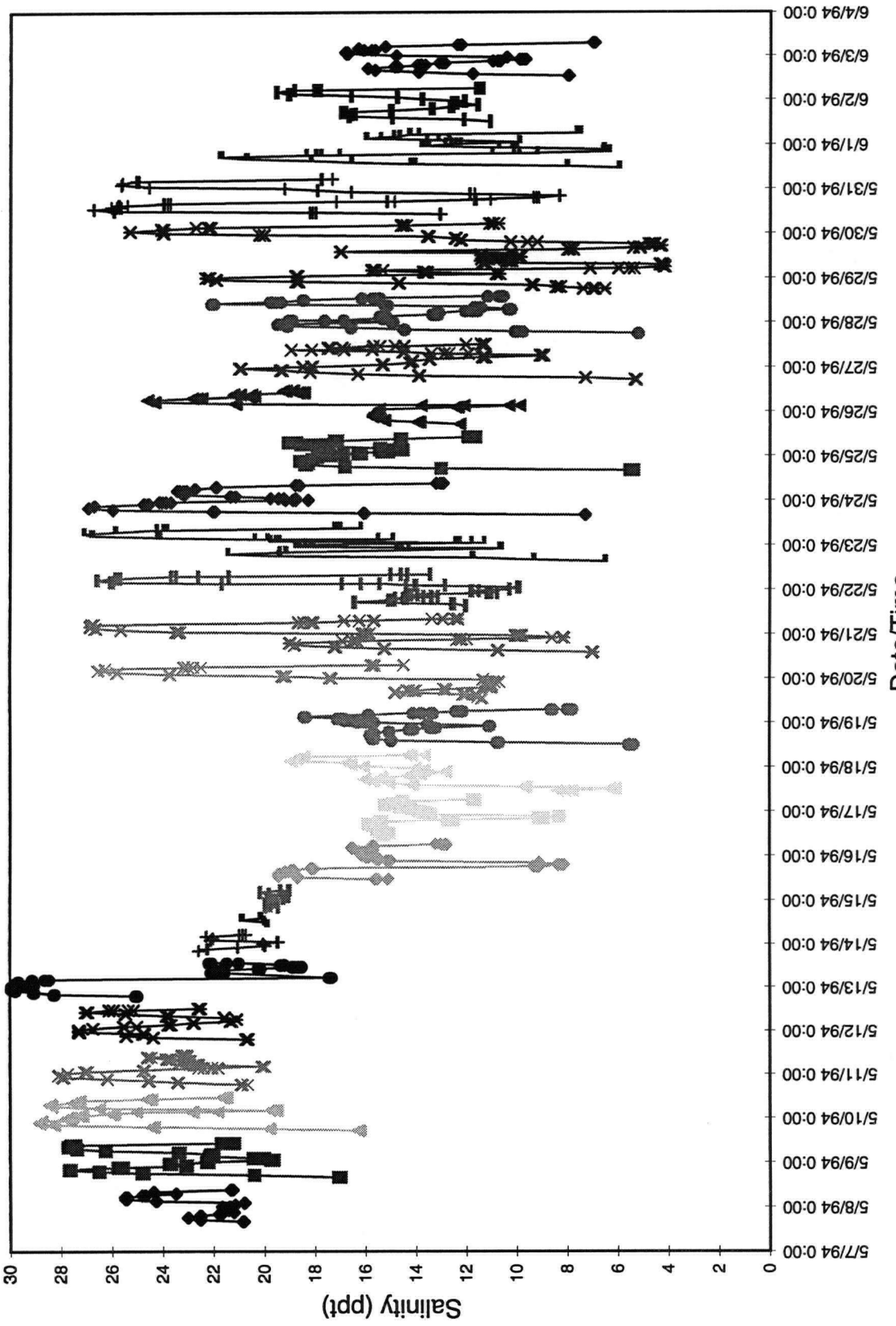

Figure 126: Salinity variations for the month of May, 1993 at station 6

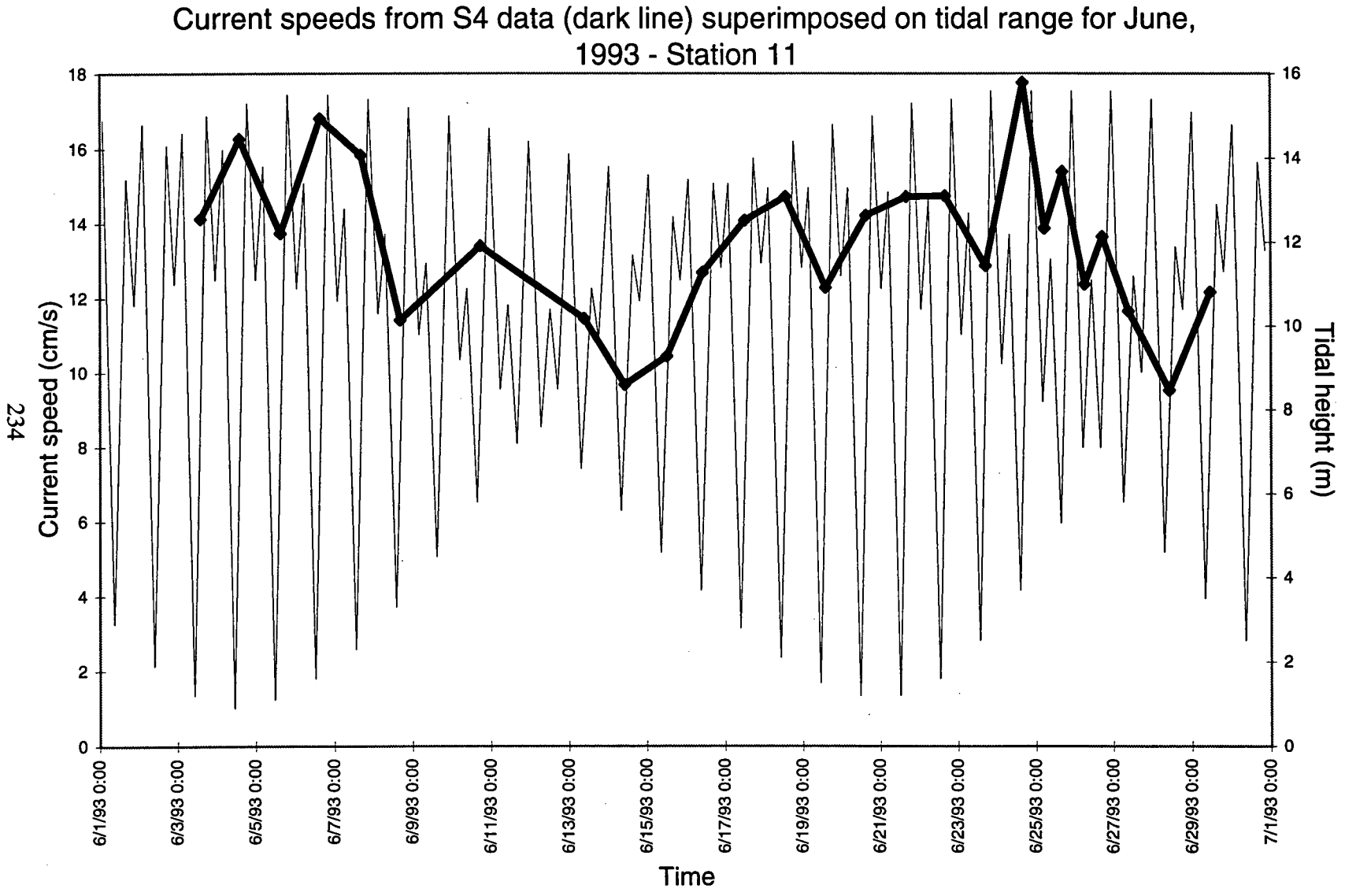

Figure 127: One-minute-averaged velocities for the month of June, 1993 at station 11

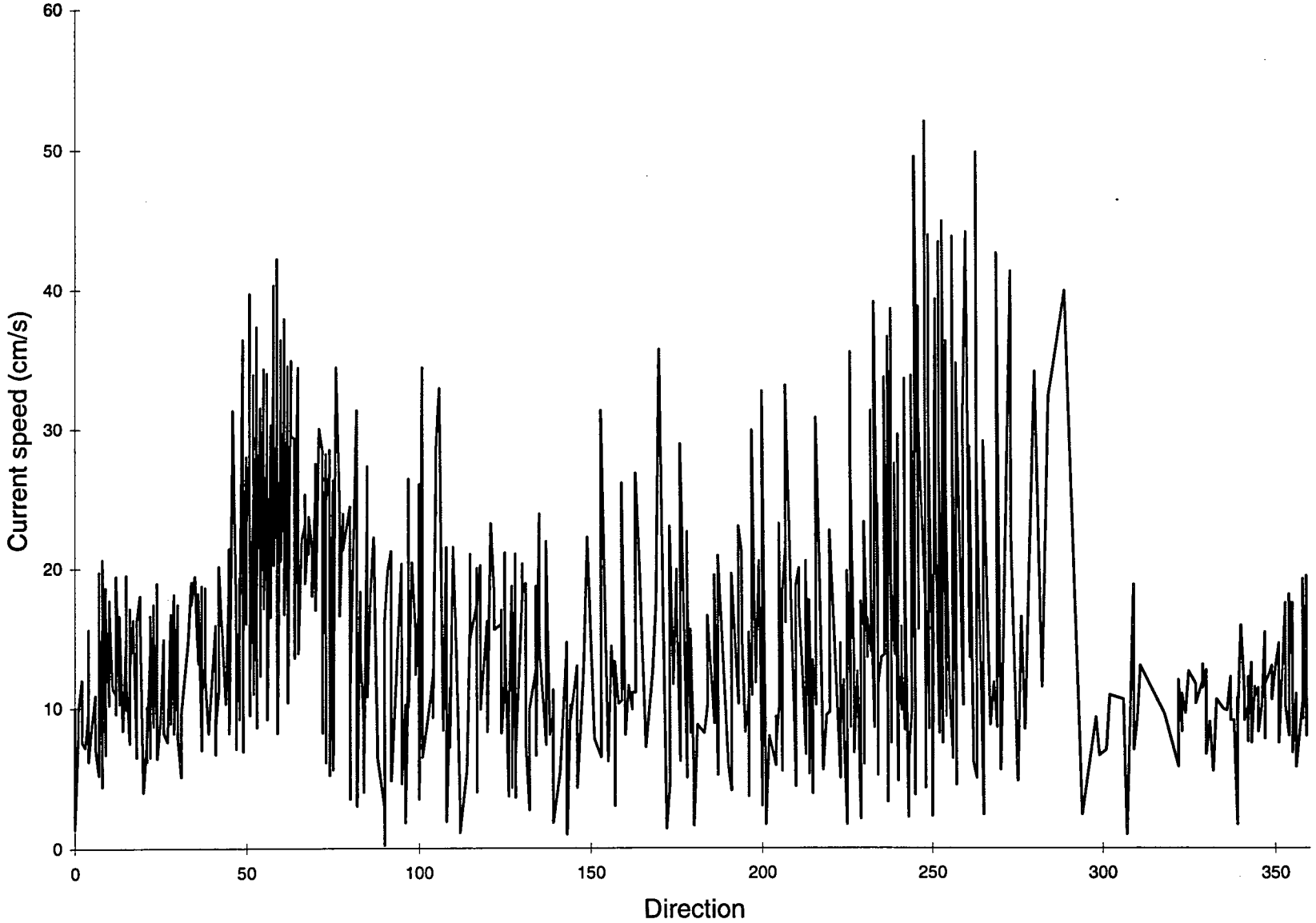

Figure 128: Wave particle velocities for the June 4, 1400 to June 5, 0900 h sampling interval at station 11

direction. Sediments at station S11 likely begin eroding at critical shear velocity values near 26 cm/s. Eroding currents occur more frequently in a flooding direction (1163 times out of 1735) and obtain approximately the same velocity in both flooding and ebbing directions.

Currents in the flooding direction, averaged over 10° increments, measured 21 cm/s and were concentrated in a small range of directions (40-70°), while the ebbing currents measured 17 cm/s and occurred over a broader range of directions (200-270°) (Figure 129). Currents in other directions average 9 cm/s. The frequency of occurrence of currents in the flooding and ebbing directions is essentially equal.

Temperature variations over the period of sampling at station S11 show only minor variations ranging from 12 to 19.5°C (Figure 130). Variations within a single sampling period are large, ranging from 0.5 to 5°C. In general, temperatures variations within a sampling interval are low with some exceptions.

Salinity measurements do not vary significantly over the entire sampling period, however, within interval variations are high (Figure 131). The influence of the spring/neap tidal cycle is obscured by the variation within sampling intervals with a maximum range of 19‰.

IV-8. Station S12

The current meter deployed at station S12 was inundated for 67% of the total sampling period, usually for 17 hours per interval. The one-minute averaged velocities had a minimum value of 7.52 cm/s, a maximum value of 24.92 cm/s and an average value of 11.27 cm/s (Figure 132). The highest average velocity values at station S12 occur in the intervals May 11 (1900 h) to May 12 (0400 h) and May 12 (0600-1300 h) and reach 24.20 and 24.92 cm/s, respectively.

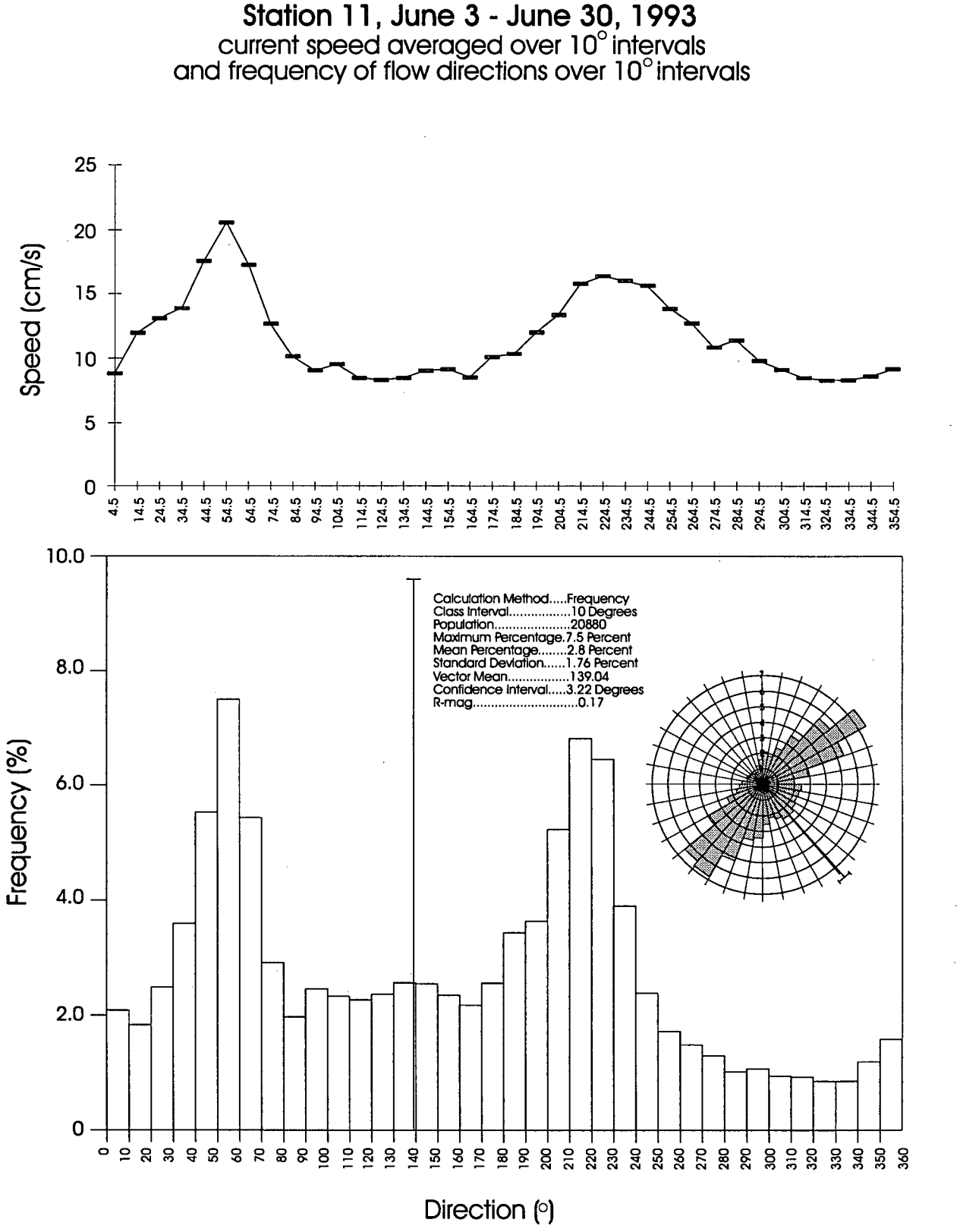

Figure 129: Average speed and direction plotted over 10 degree-averaged increments at station 11

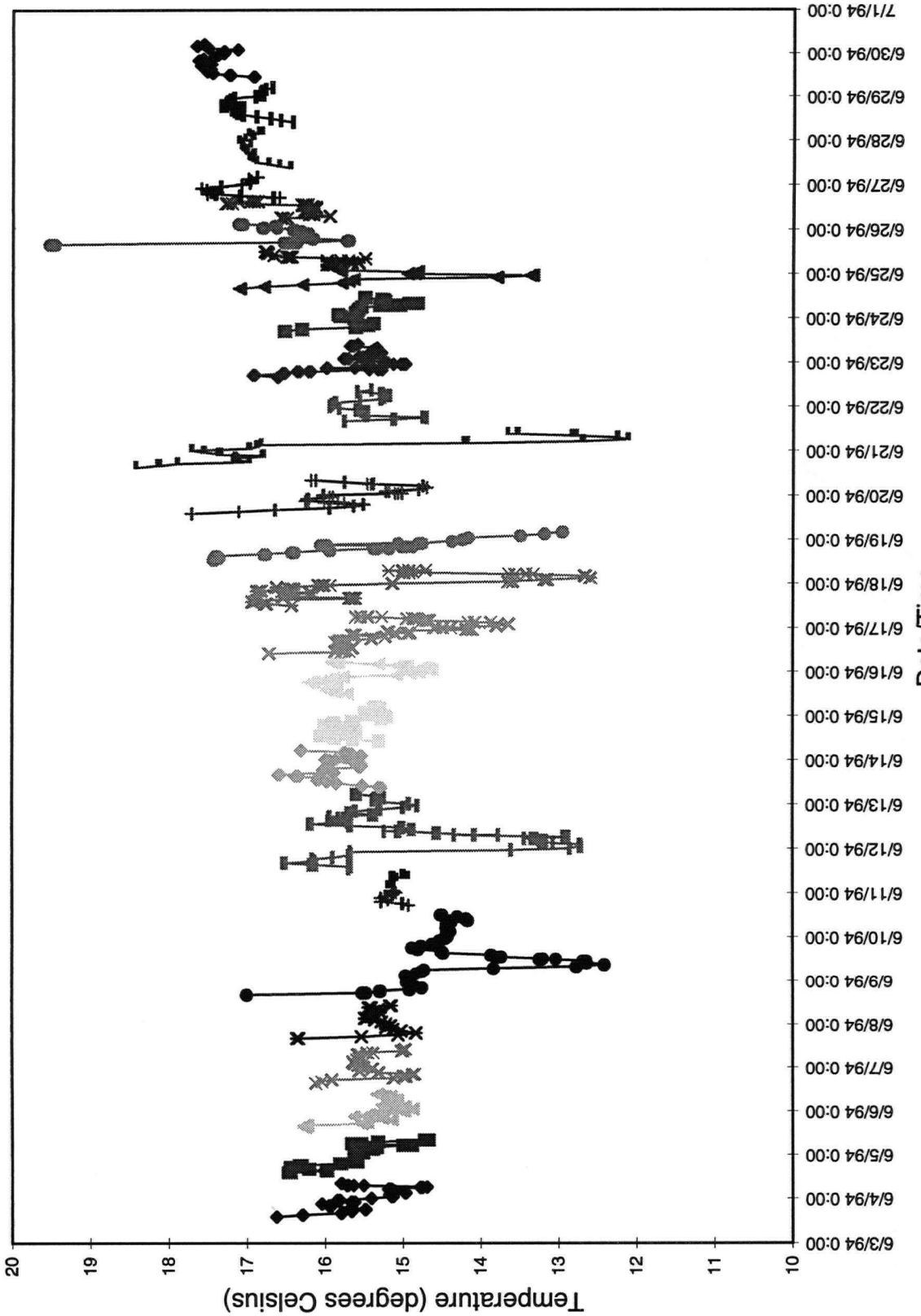

Figure 130: Water temperature variations for the month of June, 1993 at station 11

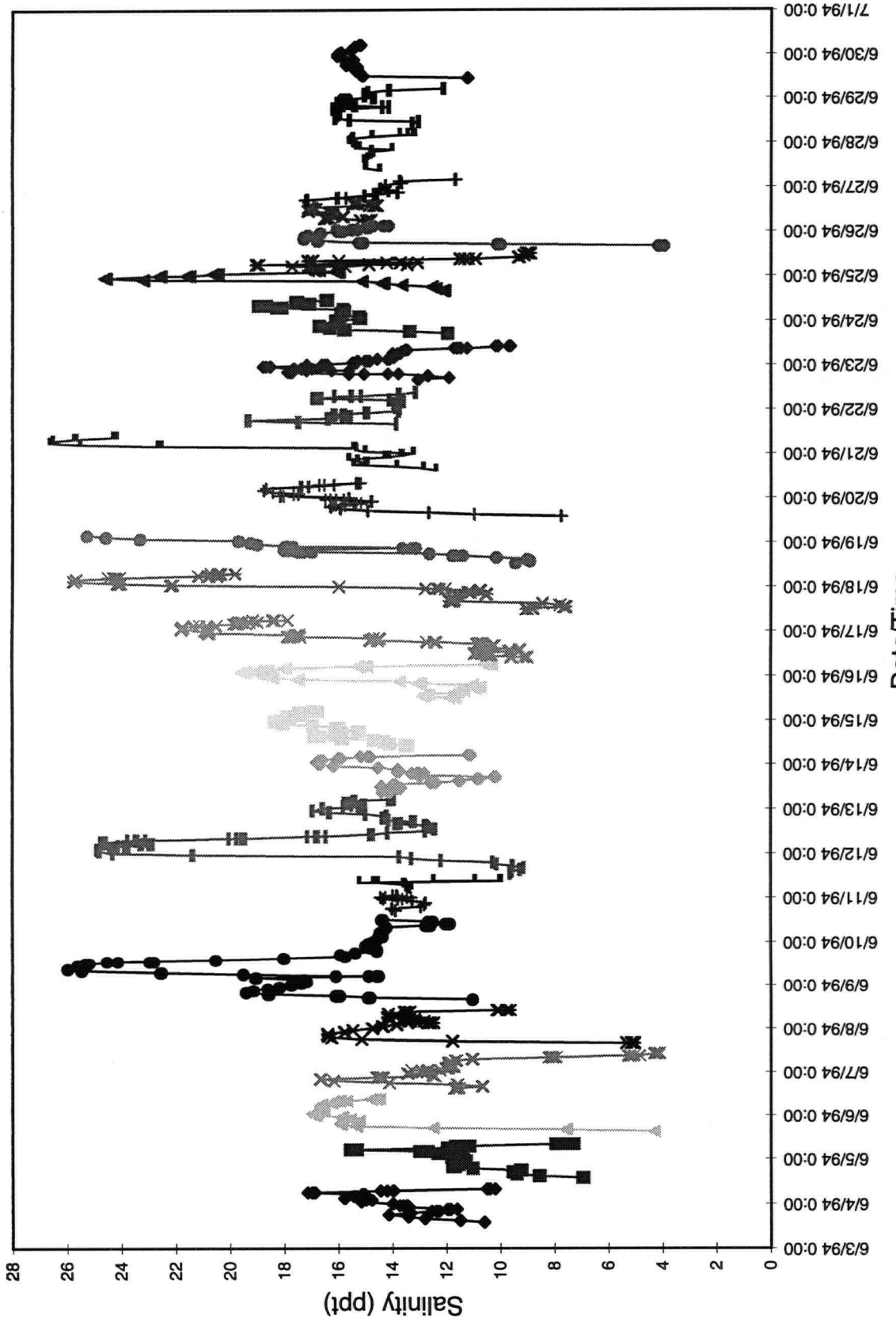

Figure 131: Salinity variations for the month of June, 1993 at station 11

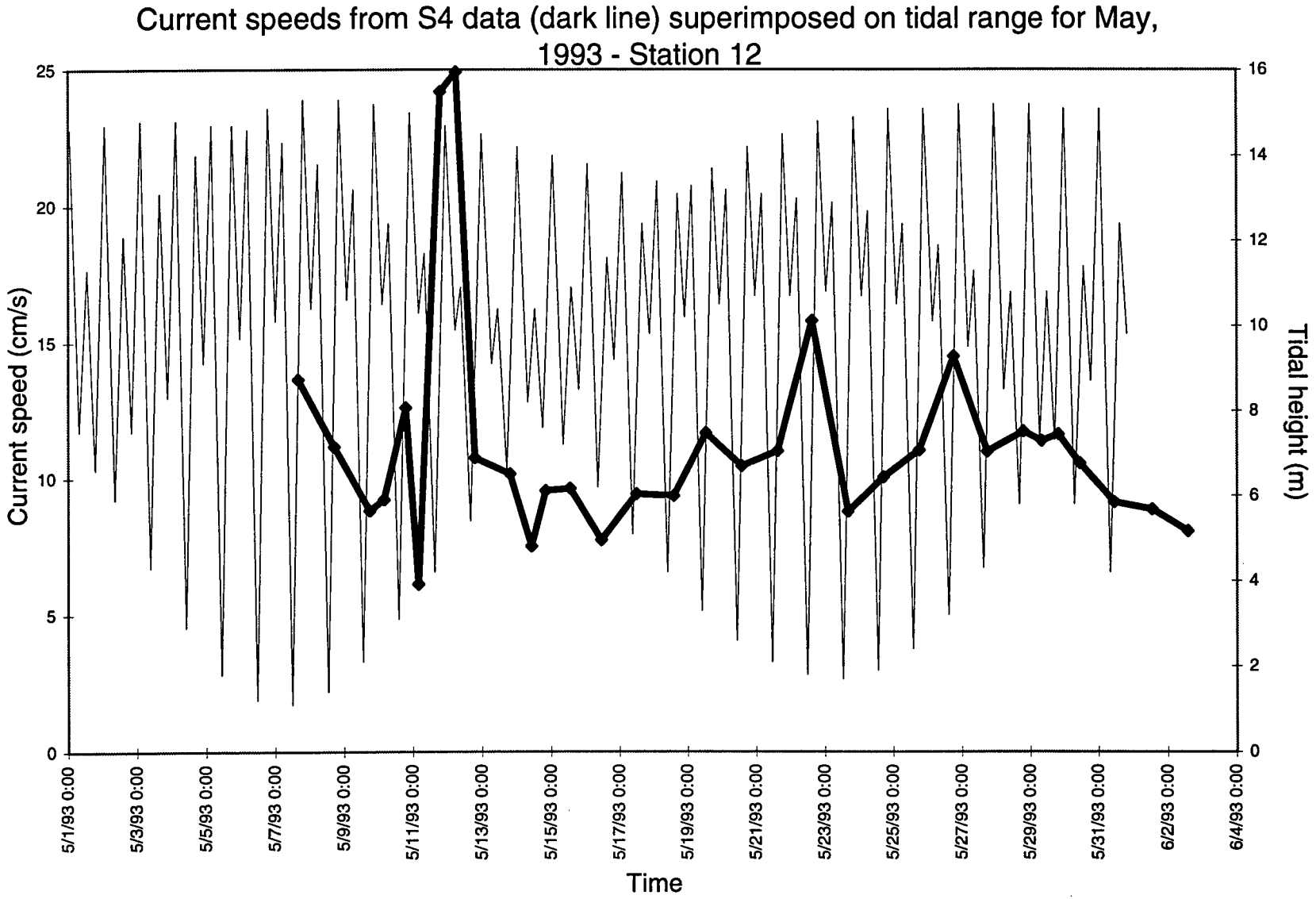

Figure 132: One-minute-averaged-velocities for the month of May, 1993 at station 12

The tidal range curve superimposed on the measured current velocities show little relation but velocity peaks are generally found in the spring tides, with the exception of the large peak on May 11 and 12.

Wave particle velocity measurements at station S12 are significantly higher than at more seaward station S11, however this observation is made cautiously because the data were collected in different months. Wave particle velocities at station S12 exceed 40 cm/s 97 times with 56 of these values occurring in an ebbing direction. The highest velocities recorded at station S12 were reached on May 11 (1900 h) to May 12 (0400 h) (Figure 133), May 12 (0600-1300 h) (Figure 134) and May 23 (0500-0900 h) (Figure 135) with values reaching 83 cm/s on May 23 in an ebbing direction. In general, velocities in the flooding direction exceed those in the ebbing direction, however on the maximum velocity intervals described above, ebbing velocities exceed flooding velocities. The low critical shear velocity for erosion at station S12 of 33 cm/s results in sediment being eroded in both flooding and ebbing directions frequently, similar to station S11. Eroding currents in ebbing directions reach velocities up to 20 cm/s higher than eroding currents in flooding directions although eroding flooding currents occur more often.

In contrast to wave particle velocity trends, when speed and direction are plotted as averages over 10° increments, flooding velocities exceed ebbing velocities with values of 18 and 15 cm/s, respectively (Figure 136). Velocities in the flood direction (~60-100°) are focussed toward a smaller range of directions while velocities in the ebb direction (230-300°) occur in a wider range of directions. Current velocities in other directions range between 5 and 8 cm/s. The frequency of occurrence of the flooding velocities is slightly greater than the ebbing velocities, however there is strong component of flow southwards at station S12, in addition to the

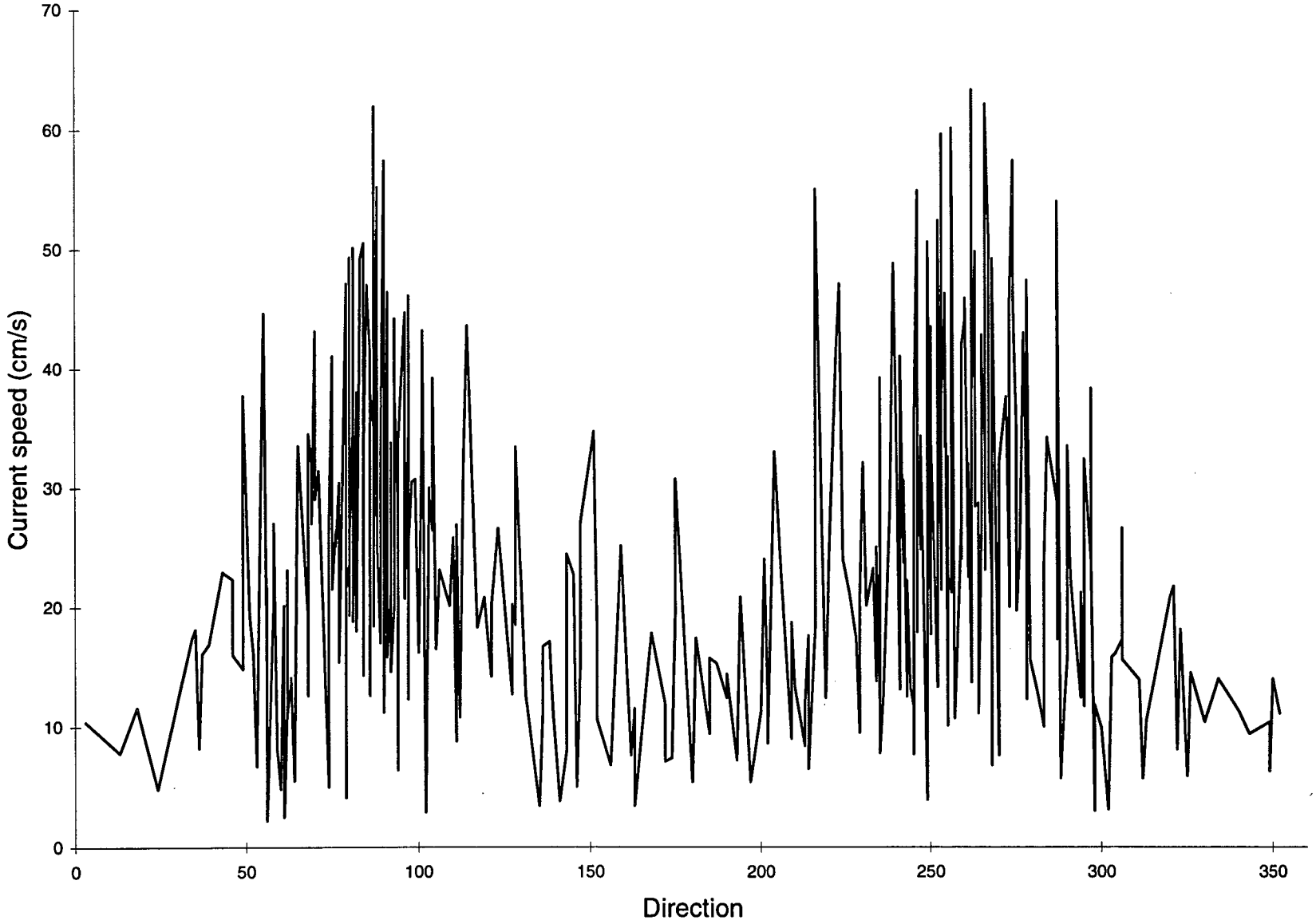

Figure 133: Wave particle velocities for the May 11, 1900 to May 12, 0400 h sampling interval at station 12

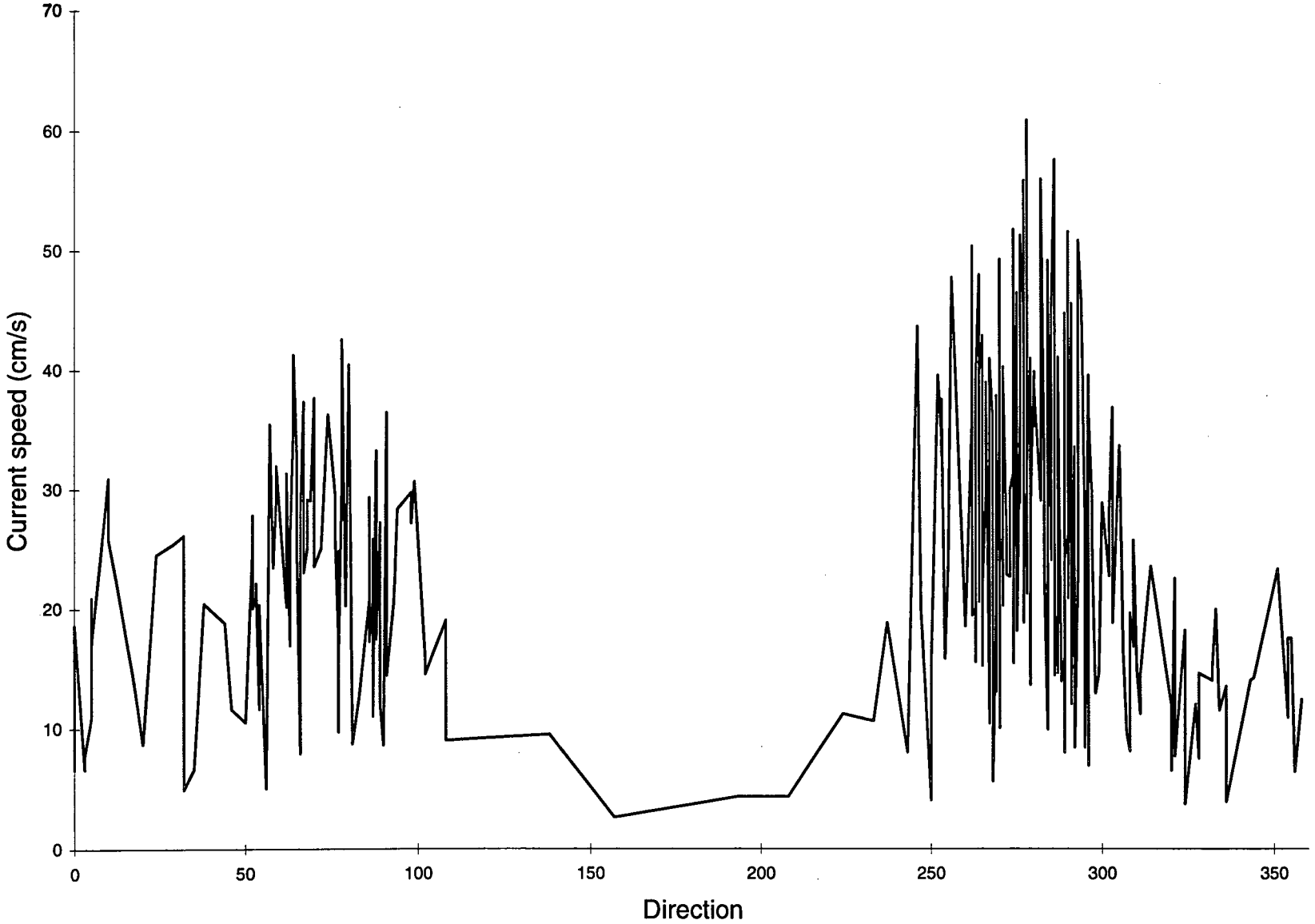

Figure 134: Wave particle velocities for the May 12, 0600-1300 h, sampling interval at station 12

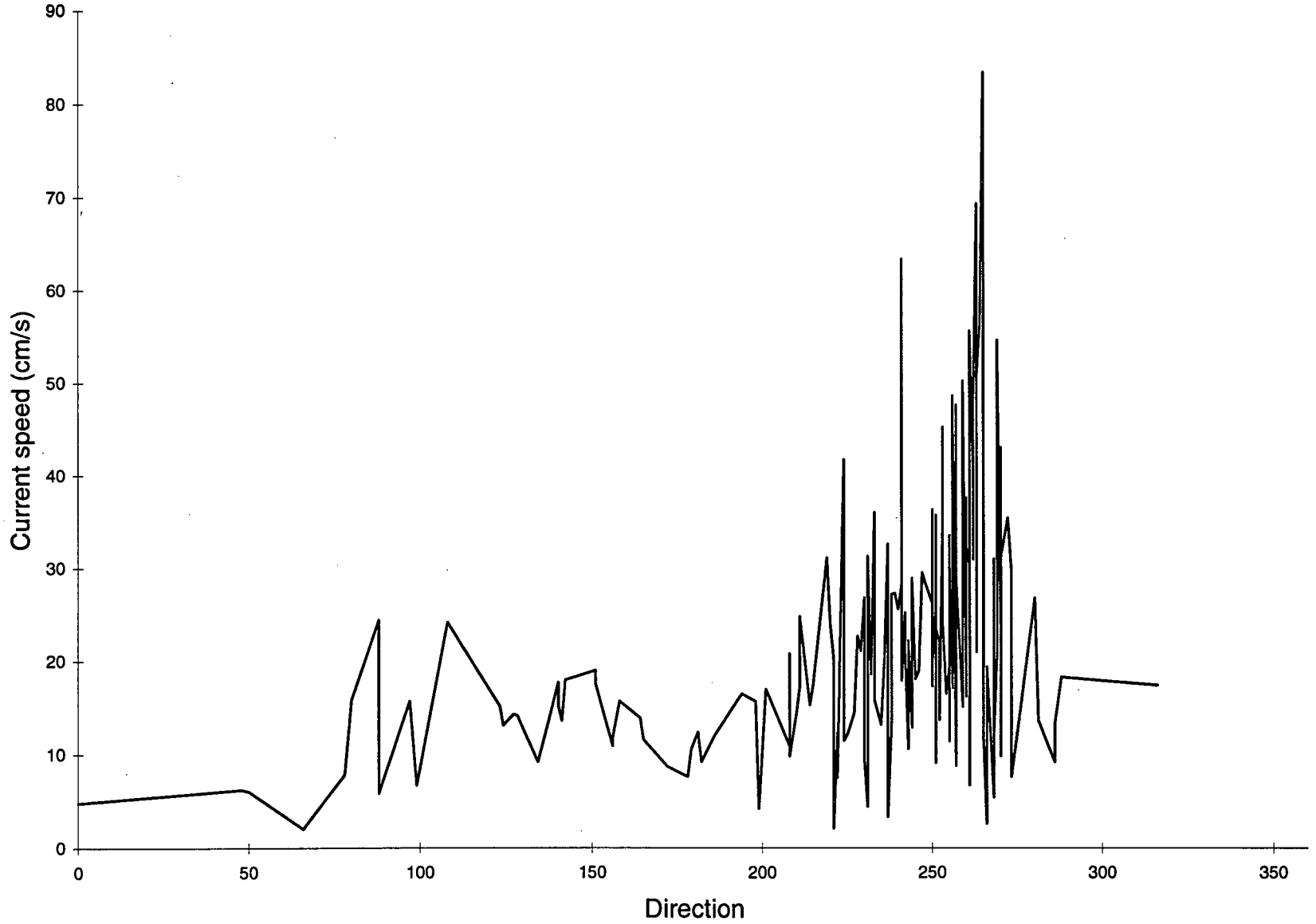

Figure 135: Wave particle velocities for the May 23, 0500-0900 h sampling interval at station 12

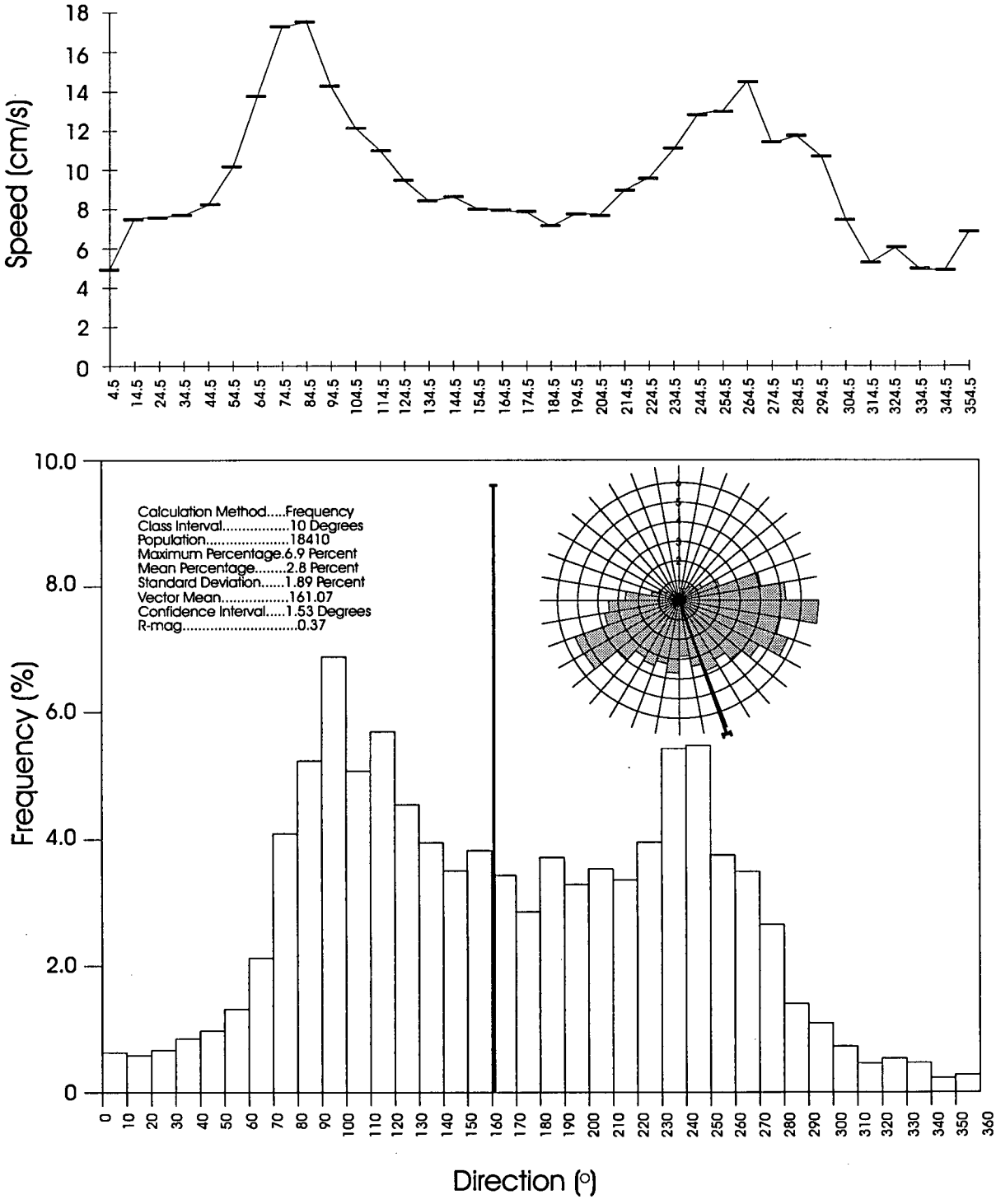

Figure 136: Average speed and direction plotted over 10 degree-averaged increments at station 12

bidirectional flooding and ebbing currents, which occurs with significant frequency.

Temperature varies from 9.5°C at the beginning of the month to 17.5°C by May 24 (Figure 137). Values recorded after May 19 show a higher degree of variability within sampling intervals with the exception of the maximum variation of 6°C which occurs on May 12. Temperature trends suggest the influence of a warmer water mass by May 18 which is consistent with peak Fraser River flow. The spring/neap tidal cycle is only slightly observed through the temperature values recorded at station S12.

Salinity shows the opposite trend to temperature, with values of up to 29‰ at the beginning of the survey and dropping to values less than 1‰ by May 23 (Figure 138) with the exception of the maximum salinity variation of 19‰ on May 12. Variations within sampling intervals are lower before May 19, similar to the temperature behavior. This reinforces the influence of the Fraser freshet as both a warmer and fresher water source moving onto the bank.

IV-9. Station S13

Inundation of the current meter deployed at station S13 occurred 55% of the total sampling time for 7 to 15 hours per interval. One-minute-averaged velocities for each sampling interval ranged from 4.22 to 11.07 cm/s with a mean value of 7.39 cm/s (Figure 139). The highest velocities were recorded through sampling intervals June 9 (1900 h) to June 10 (0300 h) and June 23 (1800 h) to June 24 (0100 h) with values of 11.07 and 11.03 cm/s, respectively. The tidal range curve was superimposed on the measured velocities and a good relationship between peak velocities and spring tides was observed.

Wave particle velocities exceed 30 cm/s 18 times throughout the sampling period, with

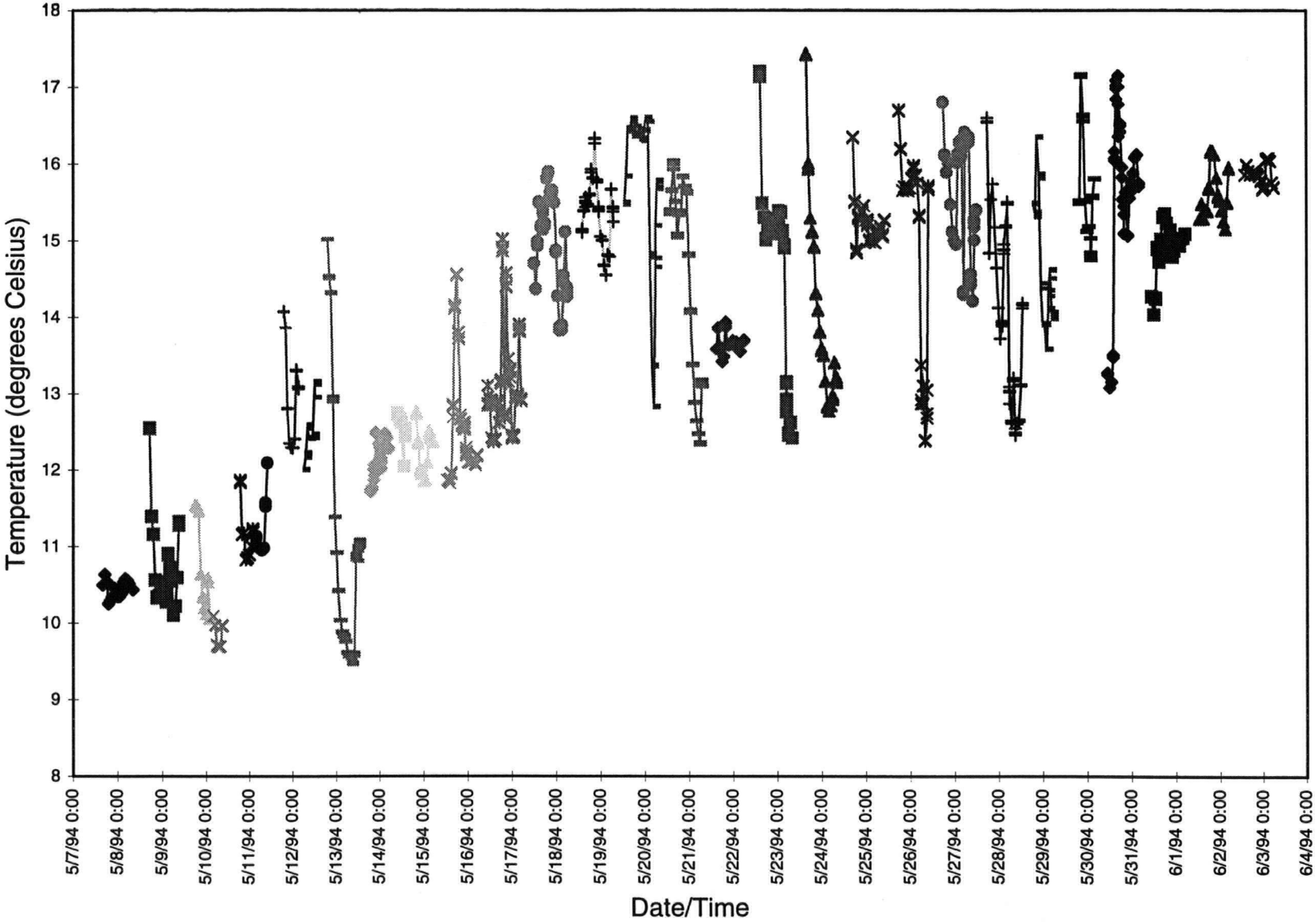

Figure 137: Water temperature variations for the month of May, 1993 at station 12

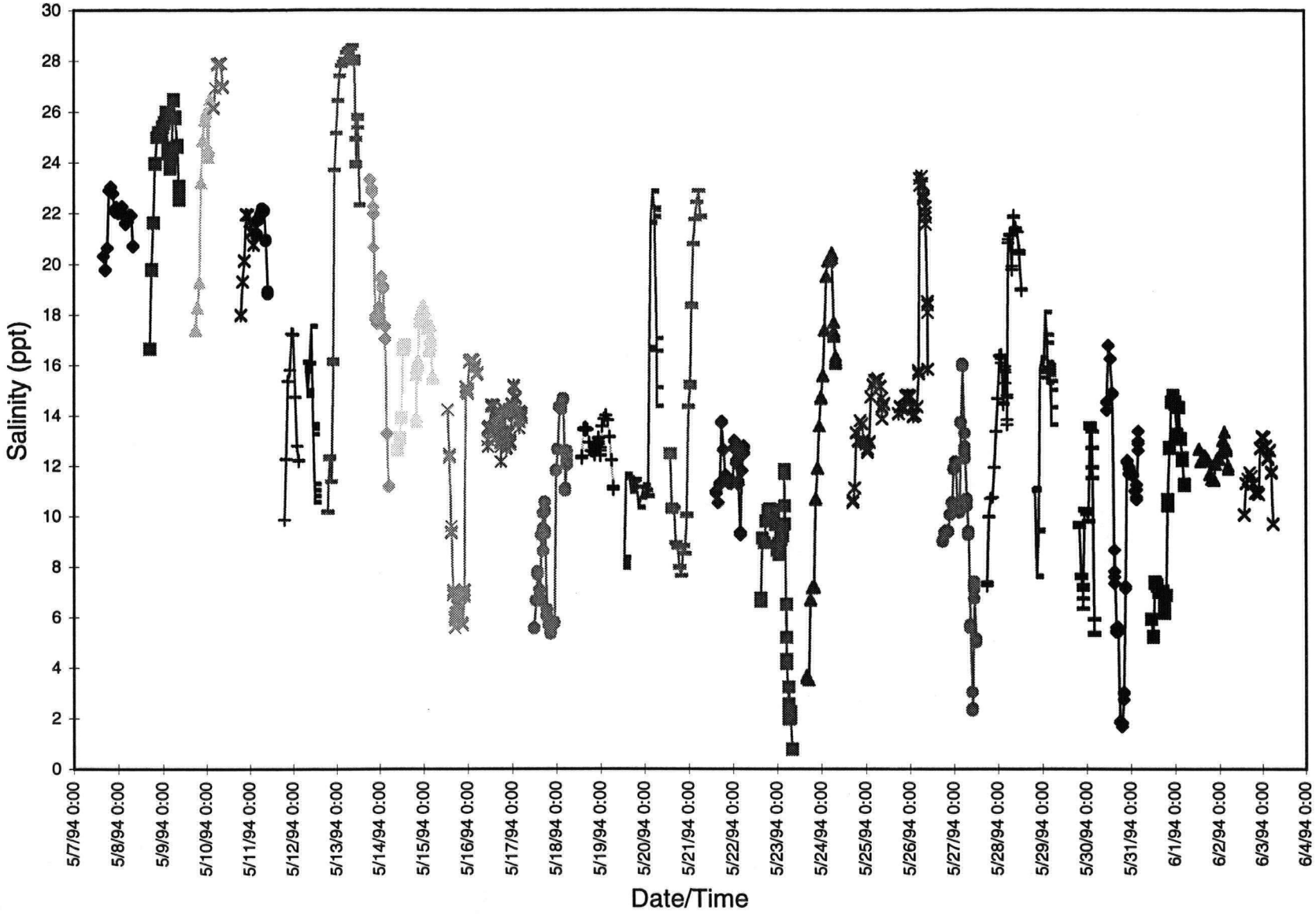

Figure 138: Salinity variations for the month of May, 1993 at station 12

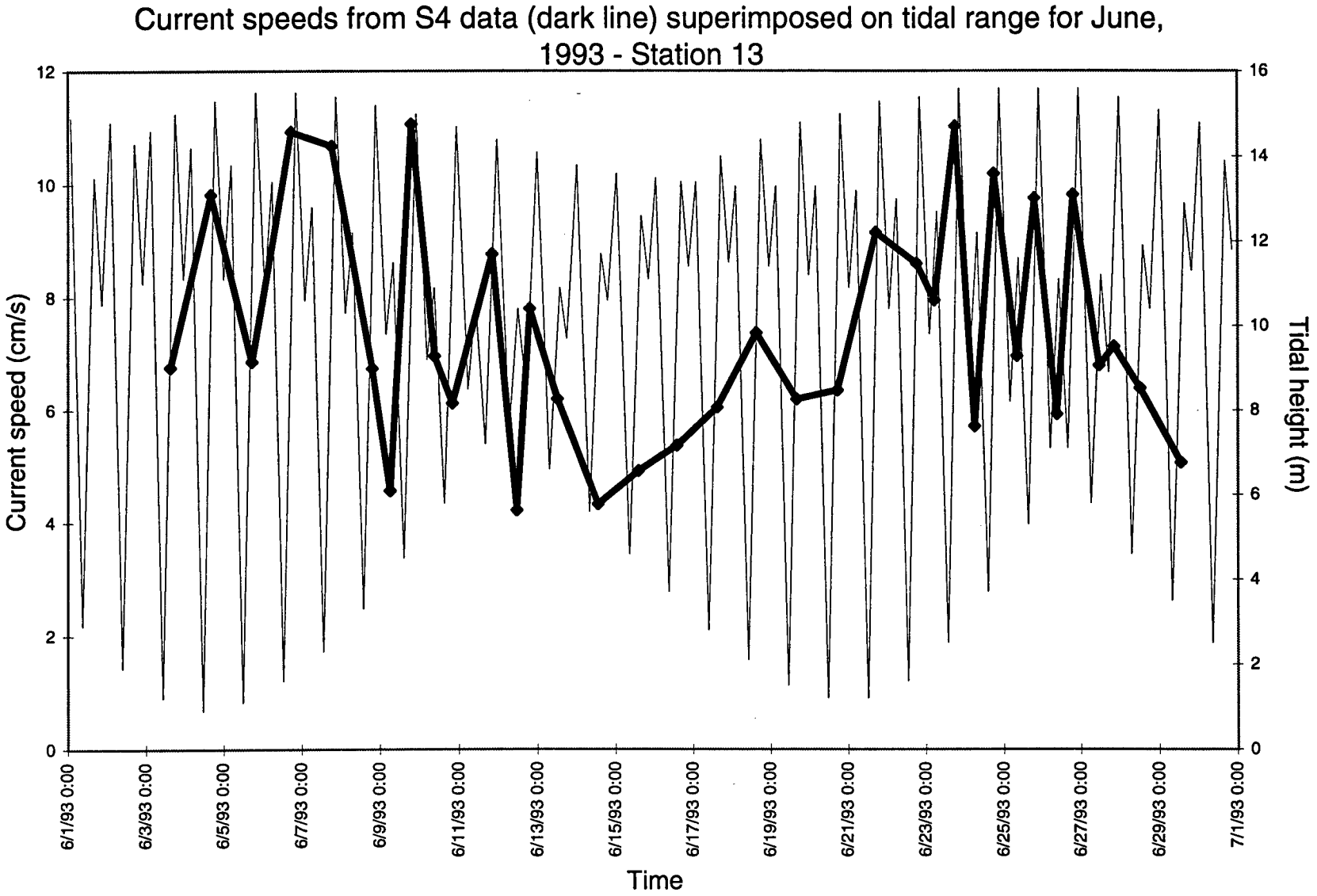

Figure 139: One-minute-averaged velocities for the month of June, 1993 at station 13

15 of these values occurring in an ebbing direction and those occurring in the flooding direction occurring all on the same day. The maximum velocity recorded at station S13 occurred in the interval June 6 (2200 h) to June 7 (0900 h) and reached a value of 42 cm/s in an ebbing direction (Figure 140). Typically flooding velocities exceed ebbing velocities, however, many of the maximum velocity days have higher velocities in an ebbing direction. The critical shear velocity of 57 cm/s is not reached at any time during the sampling period at station S13.

When a plot of the data averaged over 10° increments is examined, the increased role of currents in the ebbing direction can be seen. Ebbing velocities average 11 cm/s in directions toward 250-300°, while flooding velocities average 10 cm/s in directions toward 50-100° (Figure 141). Velocities toward southerly directions average 6 cm/s, while velocities towards northern directions average 4 cm/s. The frequency of occurrence plot reveals ebbing velocities occur more often than flooding velocities but only to a minor extent.

Temperature measurements at station 13 show values of 18°C at the beginning of June, a drop to 14°C by June 10 and a slow increase to 20°C by June 20 (Figure 142). Temperatures decrease suddenly on June 21 to 15.5°C and begin a slow increase to 18°C by the end of the survey. This pattern coincides, to a greater extent, with the spring/neap tidal cycle with the exception of the sharp temperature drop on June 21. Temperature variations within a sampling interval are small, averaging less than 2°, with the maximum variation within an interval measuring 4°C.

The salinity measurements plotted over the length of the survey are much more scattered than temperature (Figure 143). Within interval-variation is large and effectively obscures salinity trends over the 4 week period, with maximum variations of 11‰. Salinity at station S13 ranges

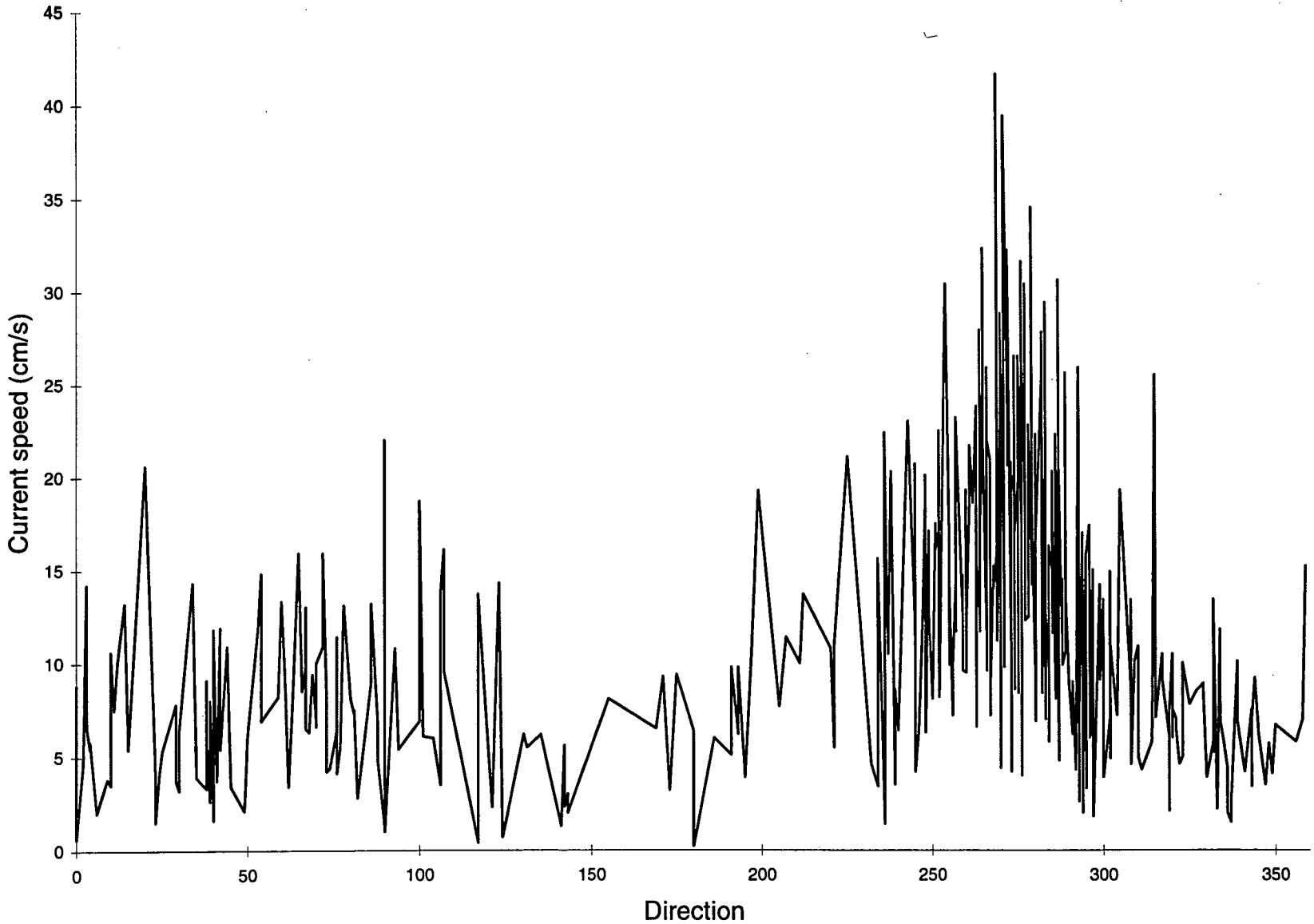

Figure 140: Wave particle velocities for the June 6, 2200 to June 7, 0900 h sampling interval at station 13

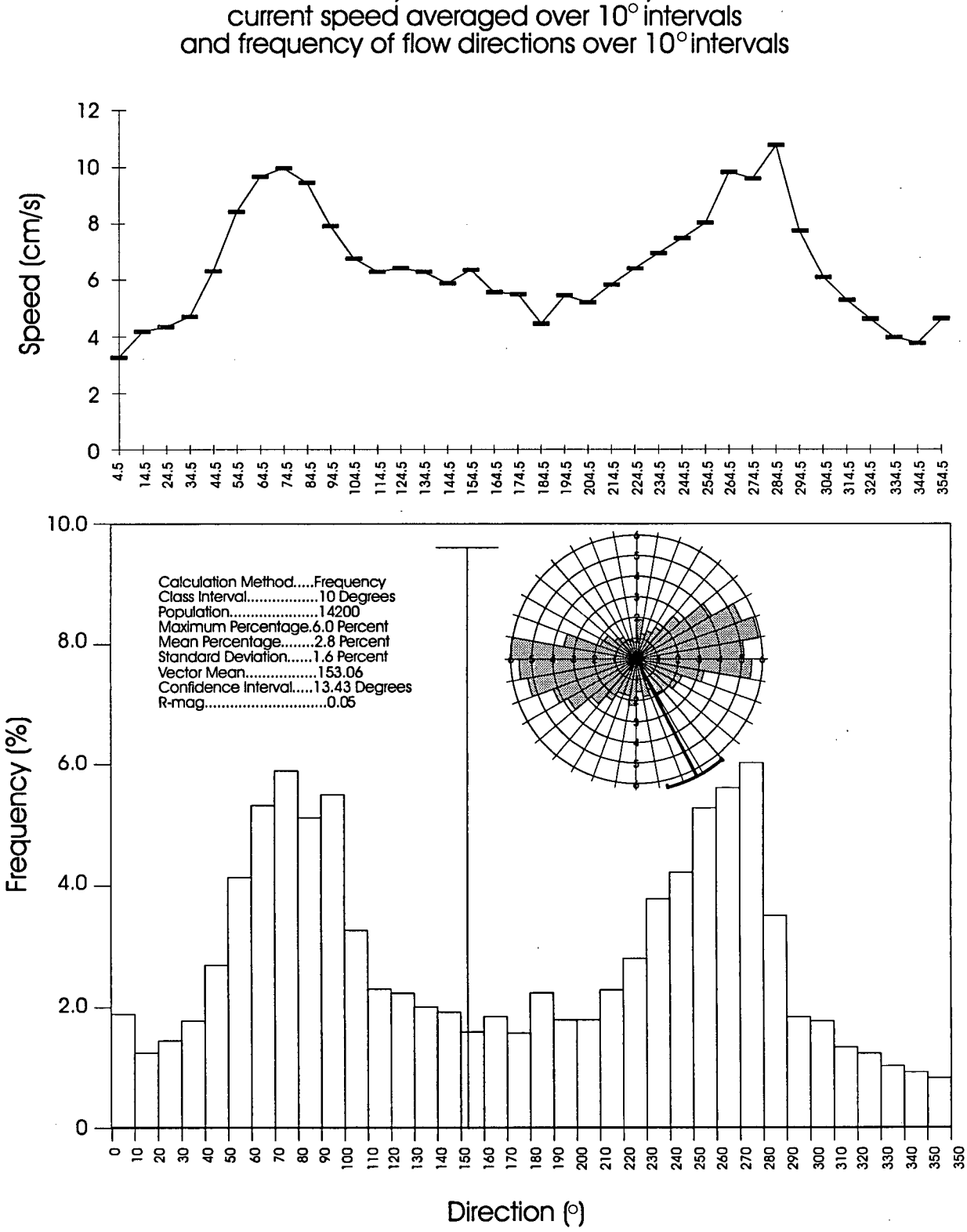

Figure 141: Average speed and direction plotted over 10 degree-averaged increments at station 13

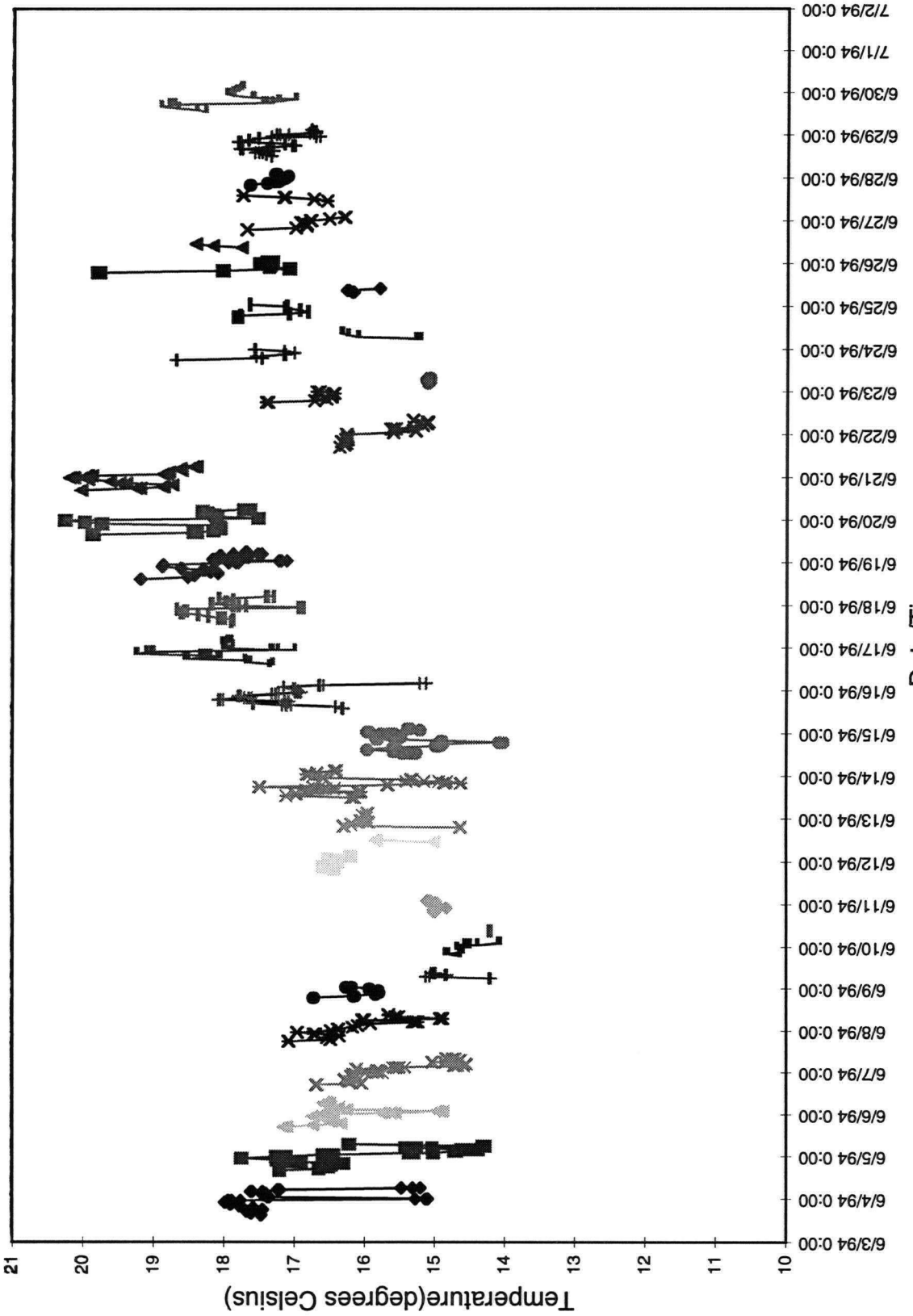

Figure 142: Water temperature variations for the month of June, 1993 at station 13

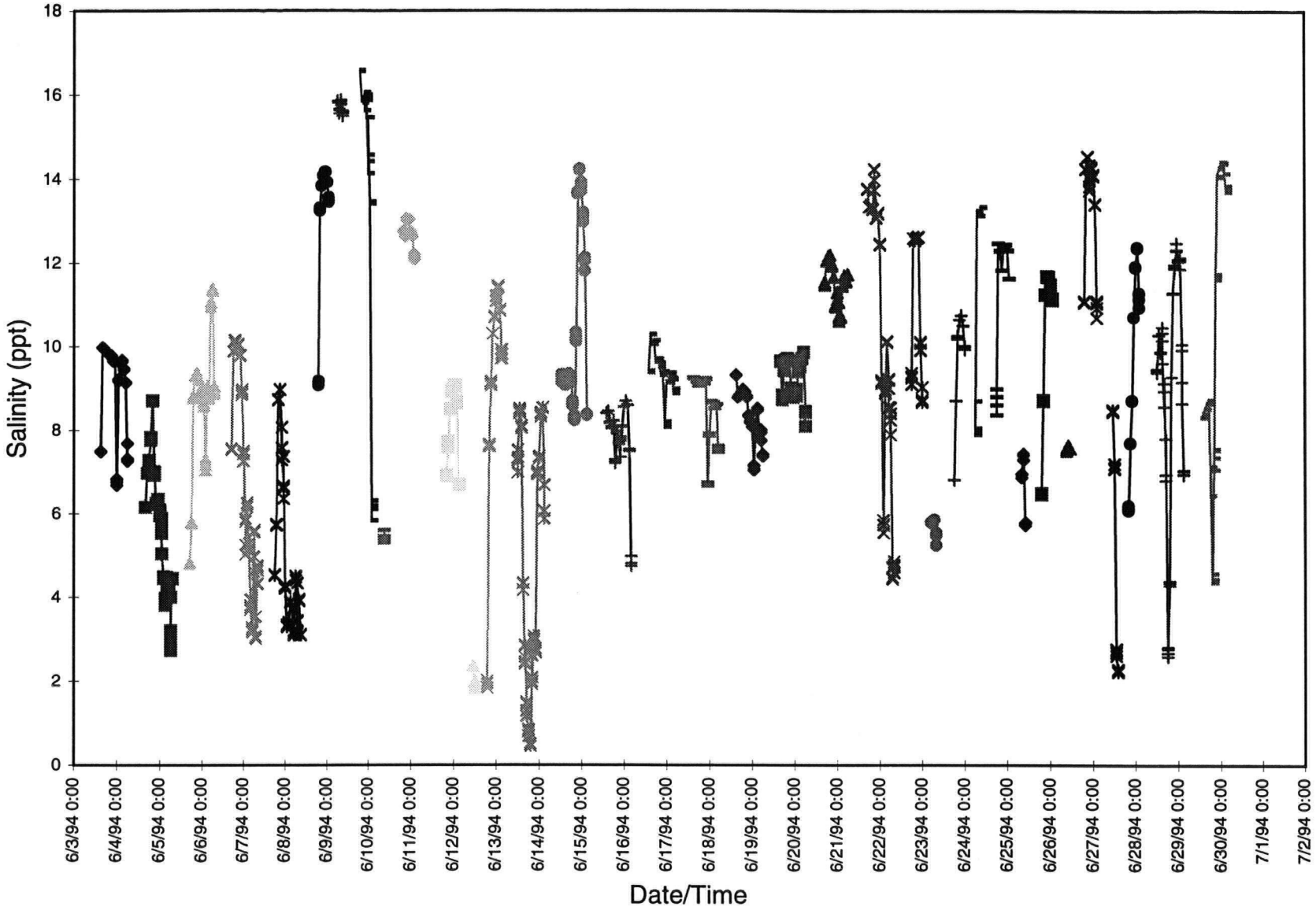

Figure 143: Salinity variations for the month of June, 1993 at station 13

from a low of 0‰ to a high of 17‰. Generally there is a drop in salinity from 10‰ to 3‰ by June 8 before a sharp rise to 16‰ by June 10. Another drop to 0‰ by June 14 is followed by a gradual increase to 14‰ and then values which range from 2 to 14‰ without a discernable pattern to the end of the survey.

IV-10. Station S14

The current meter deployed at station S14 was fully submersed for 43% of the sampling period usually for 5 to 15 hours at a time. One-minute-averaged velocities at station S14 are slightly higher than station S13 and range from 5.66 to 20.4 cm/s with an average of 9.3 cm/s (Figure 144). The highest velocity was recorded through the sampling interval May 11 (2100 h) to May 12 (0200 h). Velocities this high are more likely to be encountered on the outer bank rather than adjacent to shore. There was a slight relationship between the tidal cycle and velocity measurements, however, slightly higher values were seen in spring tides with the value recorded on May 11 being an exception.

Wave particle velocity measurements exceed 30 cm/s 72 times throughout the survey and consistently in an ebbing direction except on May 11 where wave particle velocities in the flooding direction exceed 30 cm/s 12 times. The maximum velocity recorded at station S14 was in the May 11 sampling interval with values reaching 60 cm/s (Figure 145). Current velocities in an ebbing direction dominate the wave measurements in both speed and direction at station S14. Currents at station S14 never reach the critical shear velocity for erosion value of 69 cm/s at any time in the sampling period.

Plots of current speeds and directions averaged over 10° increments show a similar trend

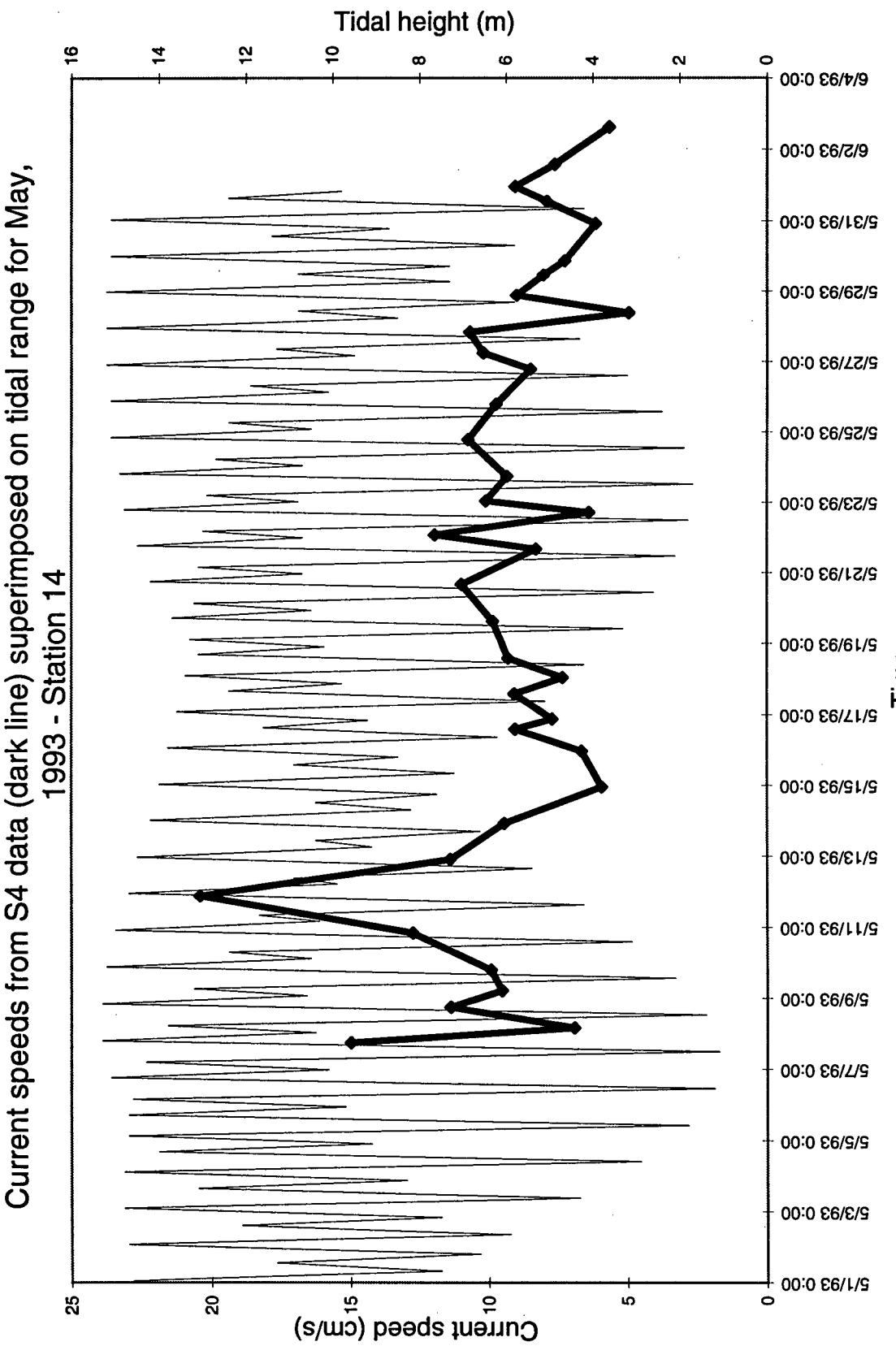

Figure 144: One-minute-averaged velocities for the month of May, 1993 at station 14

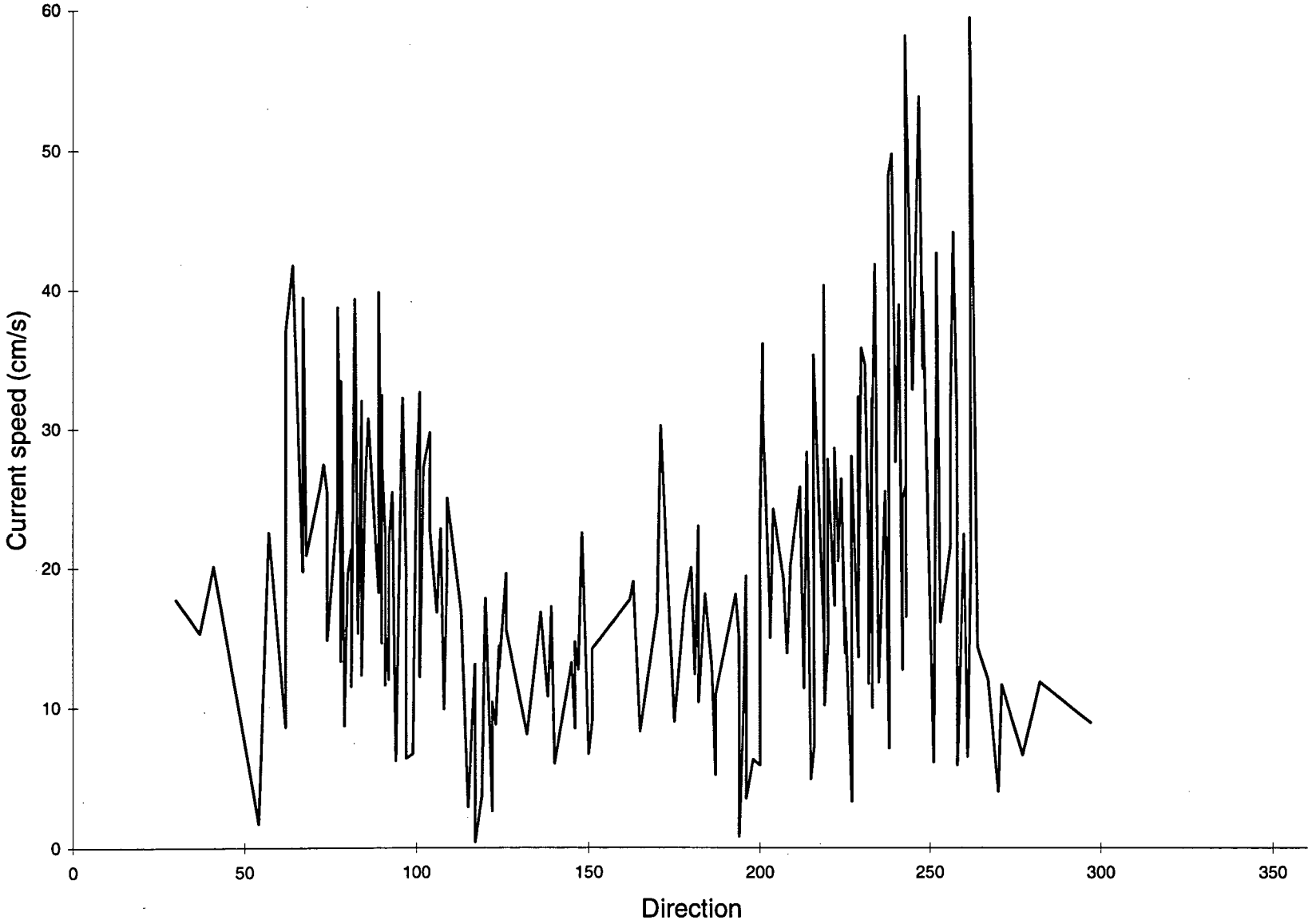

Figure 145: Wave particle velocities for the May 11, 2100 to May 12, 0200 h sampling interval at station 14

to wave patterns with currents in an ebbing direction (~200-270°) reaching 15 cm/s, while currents in a flooding direction (~40-90°) reach only 10 cm/s (Figure 146). Both flooding and ebbing current velocity peaks are broad and encompass a wide range of directions, however, the peak associated with flooding directions is so broad, it is difficult to place boundaries on its limits. Currents in other directions are typically 8 cm/s. Despite higher velocities in the ebbing direction, flooding velocities occur significantly more often. In addition, currents in directions other than flood and ebb, dominate a considerable frequency of occurrence.

Temperature varies from 11 to 19°C with temperatures starting at the lowest values at the beginning of the month and increasing slowly until the highest value is reached on May 21 (Figure 147). Temperatures fall to 13°C by May 22 and then increase to 18.5°C until May 28 where they fall until the end of the month to 15.5°C. Temperatures within sampling intervals vary from less than 0.5°C to 7°C with typical variations of 3°C. Maximum temperature variations within a sampling interval reach the same value as stations 2 and 5, the highest recorded in the survey.

Salinity measurements recorded at station 14 show an obvious trend of decreasing values from 20‰ at the beginning of the month to an average of 6‰ and a low of 0‰ by May 17 until the end of the survey (Figure 148). There is little evidence of the spring/neap tidal cycle influence, however there is support for the addition of a significant source of fresh water by May 17 suggesting that the Fraser freshet is playing a large role in dictating salinity values found at this station. Within interval salinity variation is 10‰, with the highest value reaching 16‰.

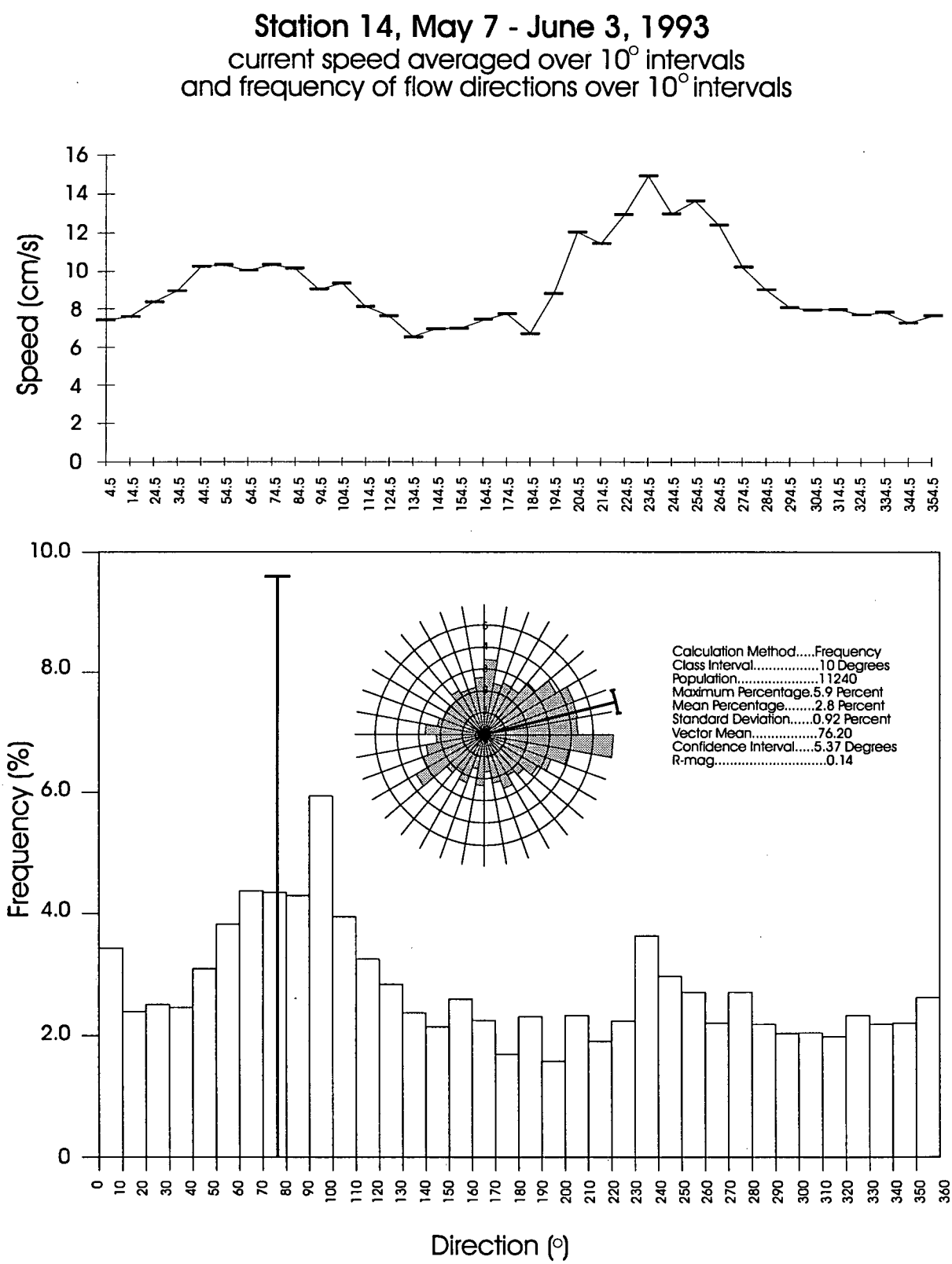

Figure 146: Average speed and direction plotted over 10 degree-averaged increments at station 14

Figure 147: Water temperature variations for the month of May, 1993 at station 14

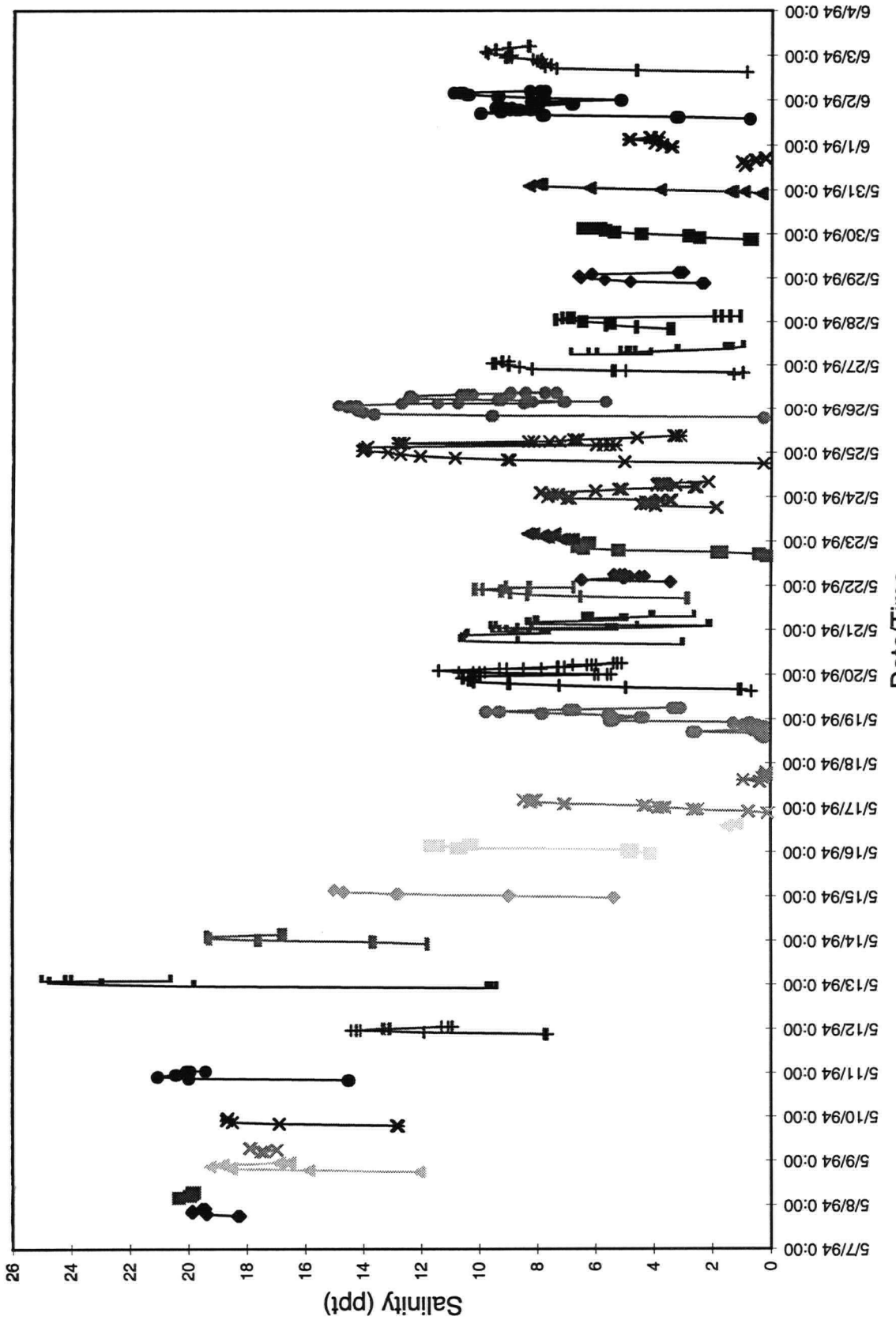

Figure 148: Salinity variations for the month of May, 1993 at station 14

Appendix V: SUSPENDED SEDIMENT RESULTS

date	station	sample #	filter weight (grams)	volume (ml)	dry weight (grams)	weight of sediment	concentration (mg/l)	Average
05/14	1	1	0.09163	480	0.7227	0.63107	1314.729167	
05/14	1	2	0.09135	480	0.4534	0.36205	754.2708333	1178.11
05/14	1	3	0.09257	480	0.79593	0.70336	1465.333333	
05/14	2	1	0.09323	480	0.1165	0.02327	48.47916667	
05/14	2	2	0.09376	480	0.11566	0.0219	45.625	47.0521
05/14	2	3	0.0931	480				
05/14	3	1	0.09084	480	0.10682	0.01598	33.29166667	
05/14	3	2	0.08965	480	0.10353	0.01388	28.91666667	33.8333
05/14	3	3	0.0925	480	0.11136	0.01886	39.29166667	
05/14	4	1	0.09238	360	0.10223	0.00985	27.36111111	
05/14	4	2	0.09217	480	0.10157	0.0094	19.58333333	22.8009
05/14	4	3	0.09009	480	0.10039	0.0103	21.45833333	
05/14	4a	1	0.09222	480	0.11248	0.02026	42.20833333	
05/14	4a	2	0.09308	480	0.12036	0.02728	56.83333333	51.4821
05/14	4a	3	0.09034	420	0.11361	0.02327	55.4047619	
05/14	5	1	0.09134	480	0.10395	0.01261	26.27083333	
05/14	5	2	0.09108	480	0.10377	0.01269	26.4375	25.1597
05/14	5	3	0.09029	480	0.10122	0.01093	22.77083333	
05/14	6	1	0.09264	345	0.10271	0.01007	29.1884058	
05/14	6	2	0.09064	480	0.10134	0.0107	22.29166667	24.5975
05/14	6	3	0.08959	480	0.1003	0.01071	22.3125	
05/14	11	1	0.0922	480	0.11214	0.01994	41.54166667	
05/14	11	2	0.09252	480	0.11125	0.01873	39.02083333	41.8264
05/14	11	3	0.09263	480	0.11419	0.02156	44.91666667	
05/14	12	1	0.09213	480	0.10536	0.01323	27.5625	
05/14	12	2	0.09129	480	0.10218	0.01089	22.6875	22.2222
05/14	12	3	0.09088	480	0.09876	0.00788	16.41666667	
05/14	13	1	0.08904	480	0.10451	0.01547	32.22916667	
05/14	13	2	0.08988	480	0.10538	0.0155	32.29166667	32.7708
05/14	13	3	0.09073	480	0.10695	0.01622	33.79166667	
05/14	14	1	0.08932	480	0.10836	0.01904	39.66666667	
05/14	14	2	0.0913	480	0.11456	0.02326	48.45833333	75.1498
05/14	14	3	0.09208	370	0.14289	0.05081	137.3243243	
05/18	1	1	0.09202	480	0.12759	0.03557	74.10416667	
05/18	1	2	0.09184	480	0.11677	0.02493	51.9375	59.375
05/18	1	3	0.09382	480	0.11882	0.025	52.08333333	
05/18	2	1	0.09362	480	0.10641	0.01279	26.64583333	
05/18	2	2	0.09357	448	0.10733	0.01376	30.71428571	27.3839
05/18	2	3	0.09336	480	0.10526	0.0119	24.79166667	
05/18	3	1	0.09267	480	0.10626	0.01359	28.3125	
05/18	3	2	0.09336	480	0.10728	0.01392	29	31.4449
05/18	3	3	0.09312	450	0.10978	0.01666	37.02222222	
05/18	4	1	0.08125	480	0.08595	0.0047	9.791666667	
05/18	4	2	0.08162	480	0.08616	0.00454	9.458333333	9.83333
05/18	4	3	0.08053	480	0.08545	0.00492	10.25	

Appendix V: cont'd.

05/18	4a	1	0.09368	353	0.09726	0.00358	10.14164306	
05/18	4a	2	0.09326	480	0.09877	0.00551	11.47916667	12.1167
05/18	4a	3	0.0936	480	0.10067	0.00707	14.72916667	
05/18	5	1	0.08138	370	0.0844	0.00302	8.162162162	
05/18	5	2	0.08159	480	0.08713	0.00554	11.54166667	9.19989
05/18	5	3	0.08194	480	0.08573	0.00379	7.895833333	
05/18	6	1	0.09365	480	0.09932	0.00567	11.8125	
05/18	6	2	0.09323	480	0.09744	0.00421	8.770833333	9.84028
05/18	6	3	0.09304	480	0.09733	0.00429	8.9375	
05/18	11	1	0.08101	480	0.09722	0.01621	33.77083333	
05/18	11	2	0.08064	480	0.10111	0.02047	42.64583333	37.123
05/18	11	3	0.08102	420	0.0957	0.01468	34.95238095	
05/18	12	1	0.09276	480	0.10496	0.0122	25.41666667	
05/18	12	2	0.09316	480	0.10752	0.01436	29.91666667	27.4375
05/18	12	3	0.0917	480	0.10465	0.01295	26.97916667	
05/18	13	1	0.0936	480	0.11395	0.02035	42.39583333	
05/18	13	2	0.09358	373	0.11617	0.02259	60.56300268	52.6738
05/18	13	3	0.09352	480	0.11995	0.02643	55.0625	
05/18	14	1	0.09415	480	0.12772	0.03357	69.9375	
05/18	14	2	0.09299	480	0.12745	0.03446	71.79166667	54.5833
05/18	14	3	0.09269	480	0.10326	0.01057	22.02083333	
05/19	4a	1	0.0809	480	0.08434	0.00344	7.166666667	
05/19	4a	2	0.08092	460	0.08555	0.00463	10.06521739	9.18841
05/19	4a	3	0.08438	480	0.08934	0.00496	10.33333333	
05/21	1	1	0.08222	480	0.10274	0.02052	42.75	
05/21	1	2	0.08113	480	0.09875	0.01762	36.70833333	38.5486
05/21	1	3	0.08067	480	0.09804	0.01737	36.1875	
05/21	2	1	0.08111	480	0.09623	0.01512	31.5	
05/21	2	2	0.08132	480	0.09701	0.01569	32.6875	34.4653
05/21	2	3	0.08128	480	0.1001	0.01882	39.20833333	
05/21	3	1	0.09308	480	0.10758	0.0145	30.20833333	
05/21	3	2	0.09404	480	0.10952	0.01548	32.25	30.5556
05/21	3	3	0.09372	480	0.10774	0.01402	29.20833333	
05/21	4	1	0.08471	480	0.09325	0.00854	17.79166667	
05/21	4	2	0.0847	480	0.09249	0.00779	16.22916667	16.8056
05/21	4	3	0.08431	480	0.09218	0.00787	16.39583333	
05/21	4a	1	0.08466	480	0.09541	0.01075	22.39583333	
05/21	4a	2	0.08476	480	0.09265	0.00789	16.4375	20.0833
05/21	4a	3	0.08502	480	0.0953	0.01028	21.41666667	
05/21	5	1	0.08444	480	0.09183	0.00739	15.39583333	
05/21	5	2	0.08454	480	0.09199	0.00745	15.52083333	15.3333
05/21	5	3	0.08459	480	0.09183	0.00724	15.08333333	
05/21	6	1	0.08447	480	0.08847	0.004	8.333333333	
05/21	6	2	0.08459	480	0.08828	0.00369	7.6875	8.34722
05/21	6	3	0.08434	480	0.08867	0.00433	9.020833333	
05/21	11	1	0.08098	480	0.08511	0.00413	8.604166667	
05/21	11	2	0.08104	480	0.08497	0.00393	8.1875	8.20833
05/21	11	3	0.08131	480	0.08507	0.00376	7.833333333	

Appendix V: cont'd.

05/21	12	1	0.08123	480	0.08529	0.00406	8.458333333	
05/21	12	2	0.08173	480	0.086	0.00427	8.895833333	8.86111
05/21	12	3	0.08137	480	0.0858	0.00443	9.229166667	
05/21	13	1	0.08197	480	0.09244	0.01047	21.8125	
05/21	13	2	0.08095	480	0.08974	0.00879	18.3125	19.2917
05/21	13	3	0.08229	480	0.09081	0.00852	17.75	
05/21	14	1	0.09351	480	0.12288	0.02937	61.1875	
05/21	14	2	0.09284	480	0.1265	0.03366	70.125	62.782
05/21	14	3	0.08092	418	0.10476	0.02384	57.03349282	
05/25	1	1	0.08494	480	0.11621	0.03127	65.14583333	
05/25	1	2	0.08485	480	0.11444	0.02959	61.64583333	60.2569
05/25	1	3	0.08472	480	0.11063	0.02591	53.97916667	
05/25	2	1	0.08162	480	0.09913	0.01751	36.47916667	
05/25	2	2	0.08184	480	0.10294	0.0211	43.95833333	43.1806
05/25	2	3	0.08204	480	0.10561	0.02357	49.10416667	
05/25	3	1	0.08269	480	0.09199	0.0093	19.375	
05/25	3	2	0.08208	480	0.09584	0.01376	28.66666667	22.3819
05/25	3	3	0.0818	480	0.09097	0.00917	19.10416667	
05/25	4	1	0.08153	480	0.08724	0.00571	11.89583333	
05/25	4	2	0.08164	480	0.08871	0.00707	14.72916667	13.2569
05/25	4	3	0.08164	480	0.08795	0.00631	13.14583333	
05/25	4a	1	0.08122	480	0.09175	0.01053	21.9375	
05/25	4a	2	0.08135	480	0.09355	0.0122	25.41666667	22.9514
05/25	4a	3	0.08167	480	0.09199	0.01032	21.5	
05/25	5	1	0.08154	480	0.08624	0.0047	9.791666667	
05/25	5	2	0.08099	480	0.08538	0.00439	9.145833333	9.63194
05/25	5	3	0.08089	480	0.08567	0.00478	9.958333333	
05/25	6	1	0.08176	480	0.08355	0.00179	3.729166667	
05/25	6	2	0.08137	480	0.08302	0.00165	3.4375	3.71528
05/25	6	3	0.08136	480	0.08327	0.00191	3.979166667	
05/25	11	1	0.08503	480	0.08681	0.00178	3.708333333	
05/25	11	2	0.08496	480	0.08669	0.00173	3.604166667	3.40972
05/25	11	3	0.08144	480	0.08284	0.0014	2.916666667	
05/25	12	1	0.08472	480	0.08861	0.00389	8.104166667	
05/25	12	2	0.08485	480	0.08921	0.00436	9.083333333	8.38194
05/25	12	3	0.08465	480	0.08847	0.00382	7.958333333	
05/25	13	1	0.08476	480	0.09318	0.00842	17.54166667	
05/25	13	2	0.0849	480	0.09217	0.00727	15.14583333	15.4167
05/25	13	3	0.08477	480	0.09128	0.00651	13.5625	
05/25	14	1	0.08427	480	0.10386	0.01959	40.8125	
05/25	14	2	0.0844	480	0.10127	0.01687	35.14583333	36.3819
05/25	14	3	0.0845	480	0.10043	0.01593	33.1875	
05/27	4a	1	0.08282	480	0.0918	0.00898	18.70833333	
05/27	4a	2	0.08334	480	0.09195	0.00861	17.9375	18.8056
05/27	4a	3	0.08158	480	0.09107	0.00949	19.77083333	
05/28	1	1	0.08165	480	0.15246	0.07081	147.5208333	
05/28	1	2	0.08141	480	0.14702	0.06561	136.6875	151.417
05/28	1	3	0.08135	480	0.16297	0.08162	170.0416667	

Appendix V: cont'd.

05/28	2	1	0.0827	470	0.10413	0.02143	45.59574468	
05/28	2	2	0.0817	480	0.1413	0.0596	124.1666667	103.136
05/28	2	3	0.08192	480	0.14895	0.06703	139.6458333	
05/28	3	1	0.08234	480	0.0953	0.01296	27	
05/28	3	2	0.08256	426	0.09567	0.01311	30.77464789	28.4225
05/28	3	3	0.08231	355	0.09207	0.00976	27.49295775	
05/28	4	1	0.08152	480	0.0918	0.01028	21.41666667	
05/28	4	2	0.0817	445	0.09106	0.00936	21.03370787	21.2473
05/28	4	3	0.08114	480	0.09136	0.01022	21.29166667	
05/28	4a	1	0.08222	480	0.11419	0.03197	66.60416667	
05/28	4a	2	0.08224	480	0.11482	0.03258	67.875	52.3472
05/28	4a	3	0.08224	480	0.09307	0.01083	22.5625	
05/28	5	1	0.08176	480	0.08565	0.00389	8.104166667	
05/28	5	2	0.08169	480	0.08644	0.00475	9.895833333	9.04167
05/28	5	3	0.08218	480	0.08656	0.00438	9.125	
05/28	6	1	0.08096	480	0.08362	0.00266	5.541666667	
05/28	6	2	0.08095	480	0.0837	0.00275	5.729166667	5.74306
05/28	6	3	0.08094	480	0.0838	0.00286	5.958333333	
05/28	11	1	0.08154	480	0.08745	0.00591	12.3125	
05/28	11	2	0.08181	480	0.08785	0.00604	12.58333333	12.4792
05/28	11	3	0.08205	480	0.08807	0.00602	12.54166667	
05/28	12	1	0.0822	480	0.08847	0.00627	13.0625	
05/28	12	2	0.08286	480	0.08787	0.00501	10.4375	11.5556
05/28	12	3	0.08192	480	0.08728	0.00536	11.16666667	
05/28	13	1	0.08214	480	0.10443	0.02229	46.4375	
05/28	13	2	0.08148	480	0.09916	0.01768	36.83333333	39.8472
05/28	13	3	0.08144	480	0.09885	0.01741	36.27083333	
05/28	14	1	0.08176	480	0.10136	0.0196	40.83333333	
05/28	14	2	0.08149	480	0.10012	0.01863	38.8125	38.9861
05/28	14	3	0.08153	480	0.09944	0.01791	37.3125	
05/31	1	1	0.08129	480	0.15808	0.07679	159.9791667	
05/31	1	2	0.0839	480	0.16334	0.07944	165.5	315.201
05/31	1	3	0.08397	480	0.38163	0.29766	620.125	
05/31	2	1	0.08237	480	0.12185	0.03948	82.25	
05/31	2	2	0.0827	460	0.13628	0.05358	116.4782609	111.979
05/31	2	3	0.08262	480	0.14848	0.06586	137.2083333	
05/31	3	1	0.08273	480	0.09928	0.01655	34.47916667	
05/31	3	2	0.08289	480	0.0967	0.01381	28.77083333	31.0977
05/31	3	3	0.08282	463	0.09673	0.01391	30.04319654	
05/31	4	1	0.08295	480	0.09177	0.00882	18.375	
05/31	4	2	0.08276	480	0.09208	0.00932	19.41666667	18.5903
05/31	4	3	0.08274	480	0.09137	0.00863	17.97916667	
05/31	4a	1	0.0833	480	0.09109	0.00779	16.22916667	
05/31	4a	2	0.08256	480	0.09016	0.0076	15.83333333	16.3056
05/31	4a	3	0.08267	480	0.09076	0.00809	16.85416667	
05/31	5	1	0.08294	480	0.09095	0.00801	16.6875	
05/31	5	2	0.08268	480	0.08962	0.00694	14.45833333	15.2917
05/31	5	3	0.0828	480	0.08987	0.00707	14.72916667	

Appendix V: cont'd.

05/31	6	1	0.0832	480	0.09291	0.00971	20.22916667	
05/31	6	2	0.08299	409	0.08987	0.00688	16.82151589	18.1488
05/31	6	3	0.08138	480	0.08973	0.00835	17.39583333	
05/31	11	1	0.08165	480	0.08765	0.006	12.5	
05/31	11	2	0.08283	480	0.08742	0.00459	9.5625	10.0694
05/31	11	3	0.0828	480	0.08671	0.00391	8.145833333	
05/31	12	1	0.08302	480	0.09224	0.00922	19.20833333	
05/31	12	2	0.08245	480	0.09171	0.00926	19.29166667	19.25
05/31	12	3	0.08286	480	0.0921	0.00924	19.25	
05/31	13	1	0.08443	480	0.10293	0.0185	38.54166667	
05/31	13	2	0.08424	480	0.10262	0.01838	38.29166667	39.125
05/31	13	3	0.08467	480	0.10413	0.01946	40.54166667	
05/31	14	1	0.08424	480	0.11135	0.02711	56.47916667	
05/31	14	2	0.08423	480	0.11165	0.02742	57.125	57.7778
05/31	14	3	0.08457	480	0.11324	0.02867	59.72916667	
06/02	4a	1	0.08433	480	0.0939	0.00957	19.9375	
06/02	4a	2	0.08435	480	0.09321	0.00886	18.45833333	19.3403
06/02	4a	3	0.08467	480	0.09409	0.00942	19.625	
06/07	1	1	0.08284	480	0.11384	0.031	64.58333333	
06/07	1	2	0.0831	480	0.11065	0.02755	57.39583333	59.2986
06/07	1	3	0.08277	480	0.10961	0.02684	55.91666667	
06/07	2	1	0.08112	480	0.1187	0.03758	78.29166667	
06/07	2	2	0.08121	480	0.1259	0.04469	93.10416667	86.3333
06/07	2	3	0.08124	480	0.12329	0.04205	87.60416667	
06/07	3	1	0.08334	480	0.09915	0.01581	32.9375	
06/07	3	2	0.08337	480	0.10394	0.02057	42.85416667	39.0972
06/07	3	3	0.08344	480	0.10336	0.01992	41.5	
06/07	4	1	0.08281	480	0.09041	0.0076	15.83333333	
06/07	4	2	0.08283	480	0.09052	0.00769	16.02083333	15.7292
06/07	4	3	0.08272	480	0.09008	0.00736	15.33333333	
06/07	4a	1	0.08324	480	0.09992	0.01668	34.75	
06/07	4a	2	0.08258	480	0.09961	0.01703	35.47916667	35.1389
06/07	4a	3	0.08241	480	0.0993	0.01689	35.1875	
06/07	5	1	0.08306	480	0.08673	0.00367	7.645833333	
06/07	5	2	0.08293	480	0.08731	0.00438	9.125	8.03472
06/07	5	3	0.0833	480	0.08682	0.00352	7.333333333	
06/07	6	1	0.08325	480	0.08559	0.00234	4.875	
06/07	6	2	0.08294	480	0.08533	0.00239	4.979166667	5.1875
06/07	6	3	0.08291	480	0.08565	0.00274	5.708333333	
06/07	11	1	0.08317	480	0.08502	0.00185	3.854166667	
06/07	11	2	0.08304	480	0.08469	0.00165	3.4375	3.84722
06/07	11	3	0.08129	480	0.08333	0.00204	4.25	
06/07	12	1	0.08129	480	0.08563	0.00434	9.041666667	
06/07	12	2	0.08144	480	0.08507	0.00363	7.5625	8.47222
06/07	12	3	0.08102	480	0.08525	0.00423	8.8125	
06/07	13	1	0.08392	480	0.09449	0.01057	22.02083333	
06/07	13	2	0.08343	480	0.09143	0.008	16.66666667	18.2222
06/07	13	3	0.08372	480	0.09139	0.00767	15.97916667	

Appendix V: cont'd.

06/07	14	1	0.08305	480	0.10265	0.0196	40.83333333	
06/07	14	2	0.08294	480	0.10268	0.01974	41.125	41.5139
06/07	14	3	0.08304	480	0.10348	0.02044	42.58333333	
06/09	4a	1	0.08096	480	0.08986	0.0089	18.54166667	
06/09	4a	2	0.08109	480	0.0899	0.00881	18.35416667	18.6111
06/09	4a	3	0.08101	480	0.0901	0.00909	18.9375	
06/11	2	1	0.08145	480	0.20601	0.12456	259.5	
06/11	2	2	0.08159	480	0.24038	0.15879	330.8125	399.958
06/11	2	3	0.08139	480	0.37398	0.29259	609.5625	
06/11	3	1	0.08138	480	0.13706	0.05568	116	
06/11	3	2	0.08147	480	0.16994	0.08847	184.3125	147.05
06/11	3	3	0.08142	465	0.14691	0.06549	140.8387097	
06/11	4	1	0.08149	480	0.09969	0.0182	37.91666667	
06/11	4	2	0.08139	480	0.10889	0.0275	57.29166667	44.7292
06/11	4	3	0.08125	480	0.09996	0.01871	38.97916667	
06/11	4a	1	0.08116	480	0.09587	0.01471	30.64583333	
06/11	4a	2	0.08117	480	0.09913	0.01796	37.41666667	28.5556
06/11	4a	3	0.08134	480	0.08979	0.00845	17.60416667	
06/11	5	1	0.08101	480	0.10454	0.02353	49.02083333	
06/11	5	2	0.08106	480	0.10671	0.02565	53.4375	50.4097
06/11	5	3	0.08118	480	0.10459	0.02341	48.77083333	
06/11	6	1	0.08128	480	0.09837	0.01709	35.60416667	
06/11	6	2	0.08095	480	0.09845	0.0175	36.45833333	34.5086
06/11	6	3	0.08118	410	0.09408	0.0129	31.46341463	
06/11	11	1	0.08145	480	0.09106	0.00961	20.02083333	
06/11	11	2	0.0814	480	0.09355	0.01215	25.3125	20.1389
06/11	11	3	0.08127	480	0.08851	0.00724	15.08333333	
06/11	12	1	0.08119	480	0.10775	0.02656	55.33333333	
06/11	12	2	0.08131	455	0.11057	0.02926	64.30769231	56.1598
06/11	12	3	0.08154	396	0.10088	0.01934	48.83838384	
06/11	13	1	0.08144	480	0.20932	0.12788	266.4166667	
06/11	13	2	0.08116	480	0.17136	0.0902	187.9166667	189.965
06/11	13	3	0.08132	480	0.13679	0.05547	115.5625	
06/11	14	1	0.08148	480	0.19371	0.11223	233.8125	
06/11	14	2	0.08152	480	0.22421	0.14269	297.2708333	223.757
06/11	14	3	0.08127	480	0.14856	0.06729	140.1875	
06/14	1	1	0.08111	480	0.08494	0.00383	7.979166667	
06/14	1	2	0.08112	480	0.08971	0.00859	17.89583333	25.9583
06/14	1	3	0.08086	480	0.10582	0.02496	52	
06/14	2	1	0.08097	480	0.0986	0.01763	36.72916667	
06/14	2	2	0.08094	480	0.10481	0.02387	49.72916667	53.6319
06/14	2	3	0.08047	480	0.1162	0.03573	74.4375	
06/14	3	1	0.08456	480	0.08855	0.00399	8.3125	
06/14	3	2	0.08478	480	0.08865	0.00387	8.0625	8.32639
06/14	3	3	0.08472	480	0.08885	0.00413	8.604166667	
06/14	4	1	0.08517	480	0.08673	0.00156	3.25	
06/14	4	2	0.08458	480	0.08613	0.00155	3.229166667	3.34722
06/14	4	3	0.08493	480	0.08664	0.00171	3.5625	

Appendix V: cont'd.

06/14	4a	1	0.08469	480	0.09414	0.00945	19.6875	
06/14	4a	2	0.08465	480	0.09595	0.0113	23.54166667	21.7431
06/14	4a	3	0.0848	480	0.09536	0.01056	22	
06/14	5	1	0.08473	480	0.08646	0.00173	3.604166667	
06/14	5	2	0.08499	480	0.08659	0.0016	3.333333333	3.6875
06/14	5	3	0.08501	480	0.08699	0.00198	4.125	
06/14	6	1	0.08475	480	0.08597	0.00122	2.541666667	
06/14	6	2	0.08253	480	0.08377	0.00124	2.583333333	2.54861
06/14	6	3	0.08243	480	0.08364	0.00121	2.520833333	
06/14	11	1	0.0813	480	0.08221	0.00091	1.895833333	
06/14	11	2	0.08118	480	0.0824	0.00122	2.541666667	2.47917
06/14	11	3	0.08089	480	0.08233	0.00144	3	
06/14	12	1	0.08107	480	0.0828	0.00173	3.604166667	
06/14	12	2	0.08469	460	0.08649	0.0018	3.913043478	3.64463
06/14	12	3	0.08489	480	0.08653	0.00164	3.416666667	
06/14	13	1	0.08501	480	0.09296	0.00795	16.5625	
06/14	13	2	0.08489	480	0.09568	0.01079	22.47916667	28.9931
06/14	13	3	0.08469	480	0.1077	0.02301	47.9375	
06/14	14	1	0.08103	480	0.09256	0.01153	24.02083333	
06/14	14	2	0.08098	480	0.09153	0.01055	21.97916667	22.5417
06/14	14	3	0.08102	480	0.0914	0.01038	21.625	
06/16	4a	1	0.08255	480	0.08708	0.00453	9.4375	
06/16	4a	2	0.08251	413	0.08763	0.00512	12.39709443	10.2435
06/16	4a	3	0.08242	480	0.08669	0.00427	8.895833333	
06/18	1	1	0.08199	480	0.1721	0.09011	187.7291667	
06/18	1	2	0.08182	480	0.18427	0.10245	213.4375	200.583
06/18	2	1	0.08205	480	0.09924	0.01719	35.8125	
06/18	2	2	0.08207	480	0.10196	0.01989	41.4375	39.6528
06/18	2	3	0.08212	480	0.10214	0.02002	41.70833333	
06/18	3	1	0.08058	457	0.0886	0.00802	17.54923414	
06/18	3	2	0.08053	480	0.08841	0.00788	16.41666667	17.0997
06/18	3	3	0.08077	480	0.08909	0.00832	17.33333333	
06/18	4	1	0.08065	480	0.08406	0.00341	7.104166667	
06/18	4	2	0.08037	480	0.08368	0.00331	6.895833333	7.0625
06/18	4	3	0.08072	480	0.08417	0.00345	7.1875	
06/18	4a	1	0.08196	480	0.0881	0.00614	12.79166667	
06/18	4a	2	0.0822	480	0.08797	0.00577	12.02083333	13.0347
06/18	4a	3	0.08209	480	0.08895	0.00686	14.29166667	
06/18	5	1	0.08216	480	0.08411	0.00195	4.0625	
06/18	5	2	0.0807	480	0.08298	0.00228	4.75	4.56457
06/18	5	3	0.08073	463	0.08299	0.00226	4.881209503	
06/18	6	1	0.0807	480	0.08262	0.00192	4	
06/18	6	2	0.08073	480	0.08264	0.00191	3.979166667	4.09722
06/18	6	3	0.08235	480	0.08442	0.00207	4.3125	
06/18	11	1	0.08246	480	0.08411	0.00165	3.4375	
06/18	11	2	0.08231	480	0.08428	0.00197	4.104166667	3.59028
06/18	11	3	0.08226	480	0.08381	0.00155	3.229166667	

Appendix V: cont'd.

06/18	12	1	0.08213	480	0.08401	0.00188	3.916666667	
06/18	12	2	0.08206	480	0.08395	0.00189	3.9375	4.11111
06/18	12	3	0.08226	480	0.08441	0.00215	4.479166667	
06/18	13	1	0.08228	480	0.08612	0.00384	8	
06/18	13	2	0.08215	480	0.08549	0.00334	6.958333333	7.80556
06/18	13	3	0.08181	480	0.08587	0.00406	8.458333333	
06/18	14	1	0.08213	480	0.08492	0.00279	5.8125	
06/18	14	2	0.08216	480	0.08529	0.00313	6.520833333	5.95833
06/18	14	3	0.08235	480	0.08501	0.00266	5.541666667	
06/23	1	1	0.08245	480	0.2474	0.16495	343.6458333	
06/23	1	2	0.08233	480	0.24358	0.16125	335.9375	344.104
06/23	1	3	0.08233	480	0.25164	0.16931	352.7291667	
06/23	2	1	0.08256	480	0.12182	0.03926	81.79166667	
06/23	2	2	0.08255	480	0.13234	0.04979	103.7291667	84.2431
06/23	2	3	0.08278	480	0.11504	0.03226	67.20833333	
06/23	3	1	0.08252	480	0.09909	0.01657	34.52083333	
06/23	3	2	0.08238	480	0.09557	0.01319	27.47916667	35.876
06/23	3	3	0.08256	398	0.10072	0.01816	45.6281407	
06/23	4	1	0.08097	480	0.08865	0.00768	16	
06/23	4	2	0.081	480	0.08794	0.00694	14.45833333	17.2014
06/23	4	3	0.08066	480	0.09081	0.01015	21.14583333	
06/23	4a	1	0.08055	480	0.08474	0.00419	8.729166667	
06/23	4a	2	0.08068	480	0.08528	0.0046	9.583333333	8.52778
06/23	4a	3	0.08087	480	0.08436	0.00349	7.270833333	
06/23	5	1	0.08062	480	0.08456	0.00394	8.208333333	
06/23	5	2	0.08054	480	0.08356	0.00302	6.291666667	7.45139
06/23	5	3	0.08065	480	0.08442	0.00377	7.854166667	
06/23	6	1	0.08071	480	0.08527	0.00456	9.5	
06/23	6	2	0.08055	480	0.08392	0.00337	7.020833333	7.77083
06/23	6	3	0.08059	480	0.08385	0.00326	6.791666667	
06/23	11	1	0.08082	480	0.0853	0.00448	9.333333333	
06/23	11	2	0.08195	465	0.08461	0.00266	5.720430108	7.08042
06/23	11	3	0.08247	480	0.08544	0.00297	6.1875	
06/23	12	1	0.08266	480	0.09524	0.01258	26.20833333	
06/23	12	2	0.08224	480	0.09826	0.01602	33.375	31.0417
06/23	12	3	0.08242	480	0.09852	0.0161	33.54166667	
06/23	13	1	0.08237	480	0.11692	0.03455	71.97916667	
06/23	13	2	0.08248	480	0.14417	0.06169	128.5208333	93.1319
06/23	13	3	0.08259	480	0.12046	0.03787	78.89583333	
06/23	14	1	0.08255	480	0.11619	0.03364	70.08333333	
06/23	14	2	0.08239	480	0.10821	0.02582	53.79166667	55.567
06/23	14	3	0.08247	368	0.09823	0.01576	42.82608696	
06/25	1	1	0.08043	480	0.12456	0.04413	91.9375	
06/25	1	2	0.08051	480	0.1203	0.03979	82.89583333	87.4167
06/25	2	1	0.08238	480	0.09342	0.01104	23	
06/25	2	2	0.08232	480	0.09346	0.01114	23.20833333	24.75
06/25	2	3	0.08029	480	0.09375	0.01346	28.04166667	

Appendix V: cont'd.

06/25	3	1	0.08063	480	0.08626	0.00563	11.72916667	
06/25	3	2	0.08079	480	0.0862	0.00541	11.27083333	11.0903
06/25	3	3	0.08049	480	0.08542	0.00493	10.27083333	
06/25	4	1	0.08021	480	0.0824	0.00219	4.5625	
06/25	4	2	0.08006	480	0.08214	0.00208	4.333333333	4.53472
06/25	4	3	0.08025	480	0.08251	0.00226	4.708333333	
06/25	4a	1	0.08037	480	0.08703	0.00666	13.875	
06/25	4a	2	0.08048	480	0.08624	0.00576	12	12.2986
06/25	4a	3	0.08037	480	0.08566	0.00529	11.02083333	
06/25	5	1	0.08125	480	0.08351	0.00226	4.708333333	
06/25	5	2	0.08095	480	0.08329	0.00234	4.875	4.78472
06/25	5	3	0.08083	480	0.08312	0.00229	4.770833333	
06/25	6	1	0.0809	480	0.08244	0.00154	3.208333333	
06/25	6	2	0.08099	480	0.08274	0.00175	3.645833333	3.40972
06/25	6	3	0.0811	480	0.08272	0.00162	3.375	
06/25	11	1	0.08043	480	0.08259	0.00216	4.5	
06/25	11	2	0.08036	480	0.0827	0.00234	4.875	5.03472
06/25	11	3	0.0801	480	0.08285	0.00275	5.729166667	
06/25	12	1	0.08283	480	0.08578	0.00295	6.145833333	
06/25	12	2	0.0827	480	0.08556	0.00286	5.958333333	5.94444
06/25	12	3	0.08251	480	0.08526	0.00275	5.729166667	
06/25	13	1	0.08247	480	0.08686	0.00439	9.145833333	
06/25	13	2	0.0825	480	0.08791	0.00541	11.27083333	10.0556
06/25	13	3	0.08253	480	0.08721	0.00468	9.75	
06/25	14	1	0.08067	480	0.08933	0.00866	18.04166667	
06/25	14	2	0.08092	480	0.08931	0.00839	17.47916667	19.1667
06/25	14	3	0.08067	480	0.09122	0.01055	21.97916667	
06/28	1	1	0.08042	480	0.22227	0.14185	295.5208333	
06/28	1	2	0.08069	480	0.22975	0.14906	310.5416667	294.361
06/28	1	3	0.08137	480	0.21434	0.13297	277.0208333	
06/28	2	1	0.08074	480	0.09572	0.01498	31.20833333	
06/28	2	2	0.08061	480	0.09108	0.01047	21.8125	28.1944
06/28	2	3	0.08076	480	0.09591	0.01515	31.5625	
06/28	3	1	0.0807	464	0.08785	0.00715	15.40948276	
06/28	3	2	0.08064	480	0.08641	0.00577	12.02083333	13.3865
06/28	3	3	0.08077	480	0.08688	0.00611	12.72916667	
06/28	4	1	0.08049	480	0.08389	0.0034	7.083333333	
06/28	4	2	0.08067	480	0.08401	0.00334	6.958333333	7.01389
06/28	4	3	0.08058	480	0.08394	0.00336	7	
06/28	4a	1	0.08053	480	0.08644	0.00591	12.3125	
06/28	4a	2	0.08042	480	0.0963	0.01588	33.08333333	19.0694
06/28	4a	3	0.08088	480	0.08655	0.00567	11.8125	
06/28	5	1	0.08047	480	0.08236	0.00189	3.9375	
06/28	5	2	0.08073	480	0.0825	0.00177	3.6875	3.86111
06/28	5	3	0.08024	480	0.08214	0.0019	3.958333333	
06/28	6	1	0.08066	480	0.08198	0.00132	2.75	
06/28	6	2	0.0806	480	0.08167	0.00107	2.229166667	2.63889
06/28	6	3	0.08064	480	0.08205	0.00141	2.9375	

Appendix V: cont'd.

06/28	11	1	0.0814	480	0.08295	0.00155	3.229166667	
06/28	11	2	0.08129	480	0.08366	0.00237	4.9375	4.19444
06/28	11	3	0.08157	480	0.08369	0.00212	4.416666667	
06/28	12	1	0.08096	480	0.08466	0.0037	7.708333333	
06/28	12	2	0.08081	480	0.08448	0.00367	7.645833333	7.70139
06/28	12	3	0.08066	480	0.08438	0.00372	7.75	
06/28	13	1	0.08087	480	0.08991	0.00904	18.83333333	
06/28	13	2	0.08148	480	0.09415	0.01267	26.39583333	20.8681
06/28	13	3	0.08124	480	0.08958	0.00834	17.375	
06/28	14	1	0.081	480	0.09362	0.01262	26.29166667	
06/28	14	2	0.08094	480	0.09318	0.01224	25.5	26.1319
06/28	14	3	0.08085	480	0.09362	0.01277	26.60416667	

Appendix VI: RESULTS AND STATISTICAL ANALYSES OF GRAIN SIZE MEASUREMENTS

VI-1. STATISTICAL ANALYSES

Mean grain size is a function of (1) the size range of available materials and (2) the amount of energy imparted to the sediment which depends on current velocity or turbulence of the transporting medium. The grain size scale was devised by Udden (1898) and is based on a constant ratio of 2 between successive size classes. The names of the class intervals were proposed by Wentworth (1922) and modern grain size data is nearly always stated in terms of phi units $\phi = -\log_2 S$ (where S is size in millimetres), a logarithmic transformation of the Wentworth scale devised by Krumbein (1934).

Grain size parameters are calculated generally by either graphical techniques using percentiles read from a cumulative curve (Folk and Ward, 1957) or by the method of moments using grouped size weight-frequency data (Friedman, 1967). The method of moments is a computational (not graphical) method of obtaining values, in which every grain in the sediment affects the measure. Thus it probably gives a truer picture than the graphic methods, which rely on only a few selected percentage lines (Folk, 1968). Swan et al. (1978, 1979) found that graphical measures were relatively insensitive to significant deviations from normality in grain-size distributions and therefore classification schemes of sediment types should make use of graphic parameters only if the range in values of statistical parameters is sufficiently large such that the limitations of the graphic technique do not significantly affect the classification units. Although the grouping of grain size data into class intervals permits a reduction in the amount of data to be examined there is obviously information lost in the grouping procedure. The

authors also found that the accuracy of grouped moment measures improves as the class interval sizes decrease and that the errors due to grouping grain-size data into size classes are small and can be ignored for most sediment types. They concluded that the use of grouped moment measures will lead to environmental interpretations consistent with the actual characteristics of the size weight-frequency distributions of the samples and therefore the method of moments has been used to describe the statistical parameters of sediments on Sturgeon Bank. The first moment describes the mean and is defined as:

$$\bar{x}_\phi = \sum_{i=1}^{n} f_i m_{i\phi}$$

The second moment describes the standard deviation or sorting and is defined as:

$$s_\phi = [\sum_{i=1}^{n} f_i (M_{i\phi} - \bar{x}_\phi)^2]^{1/2}$$

where f_i = fraction of the total weight in each class interval; $m_{i\phi}$ = the midpoint of each class interval in phi units; and $M_{i\phi} = 1 + \frac{(\phi_f - \phi_c)}{2\phi}$ where ϕ_f is the midpoint of the finest mode and ϕ_c is the midpoint of the coarsest mode. Examination of the results shows that the moment method of analysis gives values which are 0.08ϕ higher (coarser) in grain size and 0.17ϕ higher (poorer sorted) in standard deviation on average than the values calculated using the graphical method.

VI-2. GRAIN SIZE RESULTS

Station	Grain size moment (phi)	Grain size Folk (phi)	Wentworth Size class	% sand	% silt	% clay	% mud	sand/mud	clay/silt	silt/mud	std. dev. moment	std. dev phi (Folk)	sorting Pettijohn
1A	1.72521	1.67471	medium sand	98.83	1.17		1.16	84.77		1.0086	0.50197	0.31743	well
2A	2.02121	1.96372	fine sand	97.51	2.49		2.49	39.16		1	0.66968	0.50432	moderate
3A	3.79885	3.55775	very fine sand	58.78	37.37	3.85	41.22	1.43	0.103	0.9066	1.93456	1.6659	poor
4A	1.92928	1.88997	medium sand	99.24	0.76		0.76	130.78		1	0.38764	0.26007	well
5A	5.23265	5.08571	medium silt	8.69	86.33	4.98	91.31	0.1	0.0577	0.9455	1.42569	1.16174	poor
6A	1.86152	1.78922	medium sand	98.13	1.87		1.87	52.51		1	0.62834	0.45495	moderate
7A	1.725	1.69004	medium sand	99.19	0.81		0.81	122.76		1	0.44292	0.31148	well
8A	1.67072	1.63638	medium sand	99.14	0.86		0.86	115.66		1	0.44331	0.3067	well
9A	2.26421	2.22107	fine sand	98.18	1.82		1.82	53.84		1	0.59993	0.49902	moderate
10A	2.36425	2.32548	fine sand	96.78	3.22		3.22	30.02		1	0.74705	0.61652	moderate
11A	2.89102	2.81981	fine sand	94.33	5.67		5.67	16.63		1	0.61117	0.48133	moderate
12A	3.04437	2.66074	very fine sand	88.14	7.25	4.61	11.86	7.43	0.6359	0.6113	1.87893	1.31221	poor
13A	3.56792	3.27142	very fine sand	83.53	11.8	4.67	16.47	5.07	0.3958	0.7165	1.7306	1.16858	poor
14A	2.706085	2.69664	fine sand	98.05	1.95		1.95	50.22		1	0.50796	0.34779	moderate
15A	2.38174	2.36028	fine sand	99.1	0.9		0.91	109.53		0.989	0.35434	0.25052	well
16A	2.5787	2.50782	fine sand	96.23	3.77		3.77	25.5		1	0.56999	0.33421	moderate
17A	4.95664	4.87447	coarse silt	46.72	40.27	13.01	53.28	0.88	0.3231	0.7558	2.4213	2.29171	very poor
18A	4.75236	4.62927	coarse silt	53.65	34.29	12.06	46.35	1.16	0.3517	0.7398	2.30315	2.1866	very poor
19A	5.31535	5.25894	medium silt	42.47	38.6	18.93	57.53	0.74	0.4904	0.671	2.65323	2.59092	very poor
19B	4.85412	4.71002	coarse silt	52.23	32.56	15.2	47.77	1.09	0.4668	0.6816	2.57768	2.47042	very poor
19C	5.03542	4.94467	medium silt	47.17	36.4	16.43	52.83	0.89	0.4514	0.689	2.58032	2.51395	very poor
19D	4.64287	4.5244	coarse silt	51.75	36.7	11.55	48.25	1.07	0.3147	0.7606	2.3808	2.29761	very poor
19E	4.3768	4.27605	coarse silt	61.21	26.85	11.94	38.79	1.58	0.4447	0.6922	2.49202	2.33848	very poor
20A	3.98674	4.01547	very fine sand	70.53	20.84	8.62	29.47	2.39	0.4136	0.7072	2.20817	2.02859	very poor
21A	6.74339	6.71932	fine silt	3.25	74.62	22.13	96.75	0.03	0.2966	0.7713	1.88574	1.90212	poor
22A	4.89037	4.72382	coarse silt	56.58	28.42	14.99	43.42	1.3	0.5274	0.6545	2.54181	2.34389	very poor
23A	3.899885	3.877005	very fine sand	74.27	17.2	8.53	25.73	2.89	0.4959	0.6685	2.22606	1.966425	very poor
24A	2.41946	2.33639	fine sand	96.41	3.59		3.59	26.82		1	0.65324	0.47715	moderate
25A	2.15317	2.11661	fine sand	98.68	1.32		1.32	74.59		1	0.57796	0.49142	moderate
26A	5.14016	5.00321	medium silt	38.73	48.65	12.62	61.27	0.63	0.2594	0.794	2.32068	2.20417	very poor
27A	4.9445	4.84165	coarse silt	43.84	44.08	12.08	56.16	0.78	0.274	0.7849	2.29048	2.183755	very poor
28A	2.73779	2.67757	fine sand	95.85	4.15		4.15	23.09		1	0.60974	0.45175	moderate
29A	2.39052	2.33615	fine sand	97.27	2.73		2.73	35.64		1	0.61246	0.46478	moderate
30A	3.05861	2.90576	very fine sand	93.1	5.18	1.72	6.9	13.5	0.332	0.7507	1.17826	0.62199	poor
31A	4.33347	4.12368	coarse silt	58.02	35.5	6.49	41.98	1.38	0.1828	0.8456	1.89391	1.69385	poor

VI-2. CONT'D.

Station	Grain size moment (phi)	Grain size Folk (phi)	Wentworth Size class	% sand	% silt	% clay	% mud	sand/mud	clay/silt	silt/mud	std. dev. moment	td. dev (Folk phi	sorting Pettijohn
32A	2.97692	2.88624	fine sand	93.51	6.49		6.49	14.41		1	0.61998	0.49356	moderate
33A	2.27421	2.24806	fine sand	98.99	1.01		1.01	97.6		1	0.50634	0.43657	moderate
34A	2.17117	2.15316	fine sand	99.04	0.96		0.96	103		1	0.48829	0.41014	well
35A	2.52037	2.42158	fine sand	94.89	5.11		5.11	18.57		1	0.71701	0.58904	moderate
36A	3.21369	2.96786	very fine sand	91.26	6.06	2.68	8.74	10.44	0.4422	0.6934	1.33326	0.63034	poor
38A	4.44024	4.38316	coarse silt	62.5	26.81	10.68	37.5	1.67	0.3984	0.7149	2.21418	2.00852	very poor
39A	2.37118	2.31729	fine sand	98.33	1.67		1.67	58.89		1	0.55626	0.45659	moderate
40A	6.27506	6.23336	fine silt	10.29	69.22	20.49	89.72	0.11	0.296	0.7715	2.19007	2.18732	very poor
41A	1.96256	1.91935	medium sand	98.26	1.74		1.74	56.46		1	0.46608	0.22404	well
42A	2.57723	2.51833	fine sand	97.36	2.64		2.64	36.91		1	0.505	0.32829	moderate
43A	2.18812	2.0948	fine sand	96.51	3.49		3.49	27.68		1	0.61589	0.36403	moderate
44A	2.35456	2.318255	fine sand	97.42	2.58		2.58	37.76		1	0.54488	0.346475	moderate
45A	1.96998	1.94568	medium sand	99.71	0.29		0.29	341.07		1	0.37454	0.34087	well
46A	2.40691	2.33533	fine sand	96.7	3.3		3.3	29.31		1	0.65558	0.52476	moderate
47A	2.37006	2.28763	fine sand	96.31	3.69		3.69	26.06		1	0.63663	0.44068	moderate
48A	2.40637	2.3599	fine sand	97.84	2.16		2.16	45.23		1	0.48901	0.32746	well
49A	2.44876	2.43495	fine sand	98.41	1.59		1.59	62		1	0.39877	0.22598	well
50A	2.12872	2.09511	fine sand	98.86	1.14		1.14	86.49		1	0.3863	0.23644	well
51A	2.03452	1.97105	fine sand	97.87	2.13		2.13	45.89		1	0.549	0.34088	moderate
52A	2.11617	2.0967	fine sand	99.07	0.93		0.93	106.65		1	0.38547	0.28383	well
53A	2.12678	2.09862	fine sand	98.71	1.29		1.29	76.31		1	0.42253	0.28767	well
54A	1.64487	1.62085	medium sand	99.44	0.56		0.56	178.51		1	0.45899	0.33055	well
55A	1.73357	1.72195	medium sand	100			0	0			0.30909	0.29712	very well
56A	2.1215	2.09097	fine sand	98.93	1.07		1.07	92.71		1	0.41248	0.28427	well
57A	1.75728	1.73051	medium sand	99.21	0.79		0.79	125.91		1	0.45265	0.33738	well
S1	6.18689	6.19805	fine silt	10.94	73.95	15.11	89.06	0.12	0.2043	0.8303	1.95905	1.89591	poor
S2	7.00761	6.95904	fine silt	3.86	70.06	26.08	96.14	0.04	0.3723	0.7287	2.11517	2.08645	very poor
S3	5.83718	5.78823	medium silt	37.84	38.04	24.12	62.16	0.61	0.6341	0.612	2.76605	2.7215	very poor
S4	2.80507	2.60165	fine sand	94.11	3.68	2.21	5.89	15.97	0.6005	0.6248	1.28874	0.74639	poor
S5	1.76047	1.71232	medium sand	98.01	1.99		1.99	49.37		1	0.65205	0.47274	moderate
S6	1.55771	1.53103	medium sand	99.1	0.9		0.9	110.14		1	0.44547	0.27638	well
S11	2.33224	2.30804	fine sand	98.75	1.25		1.25	79		1	0.44261	0.32752	well
S12	2.33846	2.18385	fine sand	95.92	3.32	0.76	4.08	23.52	0.2289	0.8137	0.97888	0.47505	moderate
S13	6.3928	6.24386	fine silt	22.31	51.87	25.82	77.69	0.29	0.4978	0.6677	2.58217	2.66127	very poor
S14	6.26535	6.0253	fine silt	19.67	60.31	20.02	80.33	0.24	0.332	0.7508	2.34422	2.44399	very poor

Appendix VII: SEDIMENT GEOCHEMISTRY - ANALYTICAL DESCRIPTION

VII-1. MAJOR ELEMENT ANALYSIS (Al, Si, Ti, K, Na, Ca, Fe, Mg, P)

Major element compositions were determined on fused glass discs using X-ray fluorescence following Norrish and Hutton (1969). Ground sediment weighing 0.400 g was added to a preweighed Pt-Au crucible. Added to the crucible was 3.600 g of Spectroflux 105® (47.03% $Li_2B_4O_7$ (lithium tetraborate); 36.63% $LiCO_3$ (lithium carbonate); 16.34% La_2O_3 (lanthanum oxide)) and the mixture was heated in an electric muffle furnace at 1100°C for 30 minutes. Lithium tetraborate and lithium carbonate reduce the melting temperature of the flux to 700°C while lanthanum oxide acts as a heavy absorber increasing the mass absorption of the samples which decreases the matrix absorption contrasts between samples. The crucibles were cooled to room temperature in an aluminum cooling block and then reweighed.

The sample:lanthanum ratio must be kept constant in order to maintain consistent analyses. The weight of the Spectroflux 105® is included in the sample weight and therefore the weight lost when the sample and crucible are heated must be made up to maintain a constant sample:lanthanum ratio. Spectroflux 100® was added to make up the weight lost on fusion due to the oxidation of organic matter and the volatization of H_2O, $CaCO_3$ and other components. Spectroflux 100® only contains $Li_2B_4O_7$ which, upon addition, maintains the sample:La ratio. The sample was reheated over a Meeker burner in a fume hood until melted and then poured into an aluminum mold on a hot plate maintained at 400°C. A brass plunger lowered onto molten sample flattened it into a disc. The disc was allowed to cool slowly, trimmed and stored in a clean plastic bag until further analysis. Results of major element analyses on sediments from Sturgeon Bank are given in VII-6.

VII-2. MINOR ELEMENT ANALYSIS (Rb, Ba, Sr, Co, Cr, Ni, V, Y, Mn, Cu, Zn, Pb, Zr)

Minor element compositions were determined on pressed powder pellets using X-ray fluorescence. Four grams of ground sediment were mixed with one drop of PVA (polyvinyl alcohol $-CH_2CH(OH)-$) binder solution and the sample placed in a stainless steel die and formed into a rigid, borate-backed pellet in a hydraulic press at 10 tons of pressure for one minute. The pellets were labelled and stored face-down in a tissue-lined box until further analysis. Results of minor element analyses on sediments from Sturgeon Bank are given in VII-7.

VII-3. X-RAY FLUORESCENCE SPECTROMETRY

Major and minor element compositions were determined on the fused glass discs and pressed powder pellets using an automated Philips PW 1400 X-ray fluorescence spectrometer. A Rh-target X-ray tube was used for excitation and the spectrometer was controlled by a DEC PDT®-11 microcomputer which calculated the elemental concentrations from the X-ray counts. The instrument settings are listed in VII-8. International geochemical rock standards were placed within the XRF sample runs and were used to monitor the accuracy of results. VII-9 lists the standards used and compares the measured values to those referenced in Abbey (1980).

Analytical precision is represented by the standard deviation (2σ; 95% confidence interval) of a set of replicate samples and the results of standard deviation measurements for all elements are shown in VII-10. Analytical precision was determined by dividing two unique sediment samples into six replicate sub-samples, analyzing them for major and minor element composition, averaging the standard deviations measured for both sets of replicate samples and then displaying them in terms of relative standard deviation (i.e. as a percentage of the mean).

VII-4. TOTAL CARBON AND NITROGEN ANALYSIS

Total carbon and nitrogen were determined by gas chromatography/thermal conductivity on a Carlo-Erba CNS analyzer (model NA-1500). Twenty five to thirty five mg of ground sediment were weighed into tin cups using a Mettler precision balance. The sample was introduced into a combustion column reactor by means of an autosampler and flash combusted at 1050°C in an enriched atmosphere of ultra-pure quality oxygen and helium. The sample and tin container melted at this temperature and the combustion products (CO_2, NO_x and H_2O) were oxidized by passing through a column of Cr_2O_3. The products were then swept through the combustion reactor into a reduction reactor where nitrogen oxides were reduced to N_2 and excess oxygen was removed as the gases passed over copper heated to 650°C. CO_2, N_2 and H_2O were separated on a chromatographic column and then measured by a thermal conductivity detector. The integration of the gas peaks was through the Carlo-Erba "Eager" program that recorded the results on a digital printout Technical specifications of the CNS analyzer give detection limits of 10 ppm with better than 0.1% absolute value reproducibility.

Five acetanilide ($CH_3CONHC_6H_5$; 71.09% C and 10.36% N by weight) samples were placed within the sample run and used to monitor the accuracy of results. Three other standards, PACS-1, MESS-1 and BCSS-1 and a blank cup were analyzed twice each during a sample run of 38 samples. The mean of the two blanks was subtracted from the total counts for each analysis and the constants, K_{carbon} and $K_{nitrogen}$ were calculated using the following formulae:

$$K_{carbon} = \frac{\text{\% C in standard}}{\text{Area}_C \text{ of standard (counts)}}$$

$$= \frac{71.09}{\text{Total counts (C) - blank}}$$

The mean of the constants for the five standards was taken to be K_{carbon} for the run, and the total carbon of the sample was then calculated by

$$\%\,C = \frac{K_C}{\text{Area of sample (counts)/wt. of sample}}$$

Total nitrogen was calculated using 10.36% N in the standard. From the equations $K_{carbon} = 1.813 + 0.0010302x$ ($r = 0.99855$) and $K_{nitrogen} = 2.2118 + 0.0029021x$ ($r = 0.99974$).

Analytical precision was determined by dividing two unique samples into six replicate sub-samples and analyzing them for total carbon and nitrogen content. The precision was measured as the average of twice the standard deviation (2σ) for these analyses, reported as a percentage of the mean and was determined to be $\pm$ 4.84% for carbon and $\pm$ 9.06% for nitrogen (VII-11).

VII-5. INORGANIC CARBON ANALYSIS

Carbonate carbon (inorganic carbon) was determined by coulometry. Approximately 50 to 100 mg of ground sediment were placed in a glass test tube and then connected to a Coulometrics Inc. CO_2 coulometer and carbonate carbon apparatus. Two coulometers, models 5010 and 5011 (coulometers 1 (blue) and 2 (grey), respectively), and two carbonate carbon apparatus, models 5030 and 5130 (coulometers 1 (blue) and 2 (grey), respectively), were used in the analyses. The tube was flushed with CO_2-free air for two minutes to ensure no CO_2 contamination from the atmosphere. After two minutes, while the air continued to flush, 2 ml of 10% HCl were added to the test tube containing the sample and the CO_2 gas evolved was carried to a titration cell. The cell was filled with a solution of ethanolamine and a colorimetric indicator which quantitatively absorbed the CO_2.

The CO_2 reaction with the ethanolamine forms a strong titratable acid, i.e.

$$\underset{\text{(ethanolamine + colorometric indicator)}}{CO_2 + HO\text{-}CH_2\text{-}CH_2\text{-}NH_2} \quad \text{- - ->} \quad \underset{\text{(titratable acid)}}{HO\text{-}CH_2\text{-}CH_2\text{-}NH\text{-}COOH}$$

This reaction causes the blue indicator color to fade, which then causes the transmittance of a light beam through the solution to increase. As the percent transmission increases, a titration current switches on automatically and OH^- ions are generated by reducing H_2O at a silver electrode, i.e.

$$Ag^0 \quad \text{- - ->} \quad Ag^+ + e^-$$
$$H_2O + e^- \quad \text{- - ->} \quad \tfrac{1}{2}H_2 + OH^-$$

The OH^- neutralizes the acid, causing the solution to return to its original color, at which point the current is automatically switched off, i.e.

$$HO\text{-}CH_2\text{-}CH_2\text{-}NH\text{-}COOH + OH^- \text{ - - -> } HO\text{-}CH_2\text{-}CH_2\text{-}NOO^- + H_2O$$

The total amount of current used for the titration is integrated and the result is displayed as μg C. This figure is then converted to % carbonate carbon using the formula:

$$\%\ C_{carb} = \frac{\mu g\ C_{CO2} - \mu g\ C_{blank}\ X\ 100}{\text{sample weight}}$$

Blank samples were run at the beginning of each sample run and ranged in value from 5.0 to 11.03 μg C. Detection limits for both coulometers are 0.01 μg C.

Calcium carbonate (12% C) samples were run at the beginning of each sample run to monitor the accuracy of the results. Measured standard values gave mean values of 11.29, 11.69, and 10.94% carbonate carbon for coulometer (1) on the three days of analyses, respectively and 11.89 and 11.99% carbonate carbon for coulometer (2) on the two days of analyses, respectively which

corresponds to an accuracy of 6%, 2.6%, and 8.8% for coulometer (1) on the three days of analyses, respectively and 0.9% and 0.08% for coulometer (2) on the two days of analyses, respectively.

The precision is measured as the average of twice the standard deviation (2σ) for these analyses and reported as a percentage of the mean. The precision measurements for inorganic carbon was ± 28.63% on coulometer (1) and ± 13.10% on coulometer (2) (VII-12). Random samples were also selected and run on both coulometers for comparison. Upon determination of both % total carbon and % total inorganic carbon, % organic carbon was calculated by difference. Results of carbon and nitrogen analyses are shown in VII-13.

VII-6: MAJOR ELEMENT RESULTS

Sample #	Al (wt. %)	Si (wt. %)	Ti (wt. %)	K (wt. %)	Na (wt. %)	Ca (wt. %)	Fe (wt. %)	Mg (wt. %)	P (wt. %)
1B	5.74494	36.8463	0.258	0.76041	1.13526	1.66595	2.681	0.92259	0.05232
2B	5.49102	36.72488	0.258	0.79236	1.01654	1.52295	2.625	0.89847	0.05232
3B	5.90893	34.24511	0.426	0.92016	1.04622	2.002	3.297	1.39293	0.07412
4B	5.48044	37.08447	0.264	0.77958	0.96089	1.5301	2.31	0.98892	0.04796
5B	6.62837	31.62057	0.51	1.0224	1.09445	2.33805	3.619	1.64619	0.0872
6B	5.61798	36.82295	0.264	0.76041	1.30963	1.6016	2.772	1.07334	0.05232
7B	5.60211	34.82886	0.3	0.74124	1.22059	1.98055	2.933	1.12158	0.05668
8B	5.58095	36.06641	0.258	0.73485	1.08332	1.6159	2.611	0.9648	0.05668
9B	5.49631	35.97768	0.39	0.77958	1.08703	1.83755	3.073	1.10349	0.05232
10B	5.49102	36.32793	0.294	0.79236	0.95718	1.59445	2.73	1.12158	0.05232
11B	5.43812	34.92226	0.45	0.83709	0.95347	1.859	3.276	1.22409	0.06976
12B	5.48044	35.28185	0.348	0.8307	1.00541	1.76605	3.01	1.09143	0.0654
13B	5.6603	34.41323	0.426	0.87543	1.01654	1.8876	3.248	1.24821	0.06104
14B	5.40109	34.62338	0.576	0.78597	0.94234	2.10925	3.829	1.27836	0.06104
15B	5.38522	36.36529	0.264	0.75402	1.02025	1.63735	2.674	1.06128	0.05232
16B	5.17891	36.07108	0.3	0.86265	1.01654	1.4729	2.716	0.95274	0.05232
17B	6.4009	31.89143	0.516	1.03518	0.94976	2.06635	3.857	1.55574	0.0872
18B	6.30568	32.31173	0.45	1.00962	1.05735	1.9162	3.64	1.50147	0.08284
19A	6.1893	31.32169	0.438	1.04796	1.04251	1.82325	3.675	1.39293	0.08284
19B	6.63366	32.83477	0.45	1.06713	1.03138	1.80895	3.689	1.52559	0.0872
19C	6.5067	32.60594	0.438	1.02879	0.99799	1.8447	3.738	1.49544	0.09156
19D	6.38503	32.92817	0.438	1.03518	0.92379	1.80895	3.675	1.5075	0.0872
19E	5.7661	32.42381	0.414	0.97767	0.90524	1.78035	3.388	1.29042	0.06976
20B	5.42225	32.61528	0.384	0.92655	0.92379	1.75175	2.856	1.1457	0.0654
21B	7.22085	29.70587	0.492	1.2141	0.99428	1.85185	4.256	1.68237	0.10028
22B	5.85603	31.59722	0.462	0.93933	0.90153	1.9162	3.612	1.36881	0.07848
23B	6.00944	33.6707	0.51	0.92016	1.0388	2.00915	3.738	1.47132	0.06976
24B	5.29	35.35657	0.36	0.79875	1.10558	1.716	2.975	0.97083	0.05232
25B	5.42225	35.77687	0.33	0.77958	1.00541	1.7589	2.828	1.04922	0.05232
26B	6.22633	31.48047	0.486	1.03518	0.86814	2.002	3.745	1.48338	0.07848
27B	6.37445	31.97082	0.54	0.9585	0.94234	2.18075	3.962	1.56177	0.07848
28B	5.3958	34.56734	0.594	0.74124	1.02767	2.03775	4.123	1.31454	0.06104
29B	5.30587	34.90825	0.42	0.75402	1.06477	1.86615	3.248	1.16379	0.05668
30B	5.34819	33.84349	0.558	0.77958	0.99428	2.13785	3.696	1.3266	0.06976
31B	6.02531	33.23172	0.552	0.87543	1.02396	2.2308	3.815	1.47735	0.0872
32B	5.68675	35.73951	0.54	0.79236	1.04622	2.12355	3.717	1.41705	0.0654
33B	5.07311	34.57201	0.36	0.77958	1.0388	1.9162	2.975	1.12158	0.06104
34B	5.24239	34.76348	0.366	0.75402	1.0017	1.85185	3.094	1.06731	0.05668
35B	5.54392	35.68347	0.36	0.79236	0.96831	1.7732	3.017	1.16982	0.05668
36B	5.40109	33.68471	0.648	0.76041	1.02025	2.2165	4.158	1.31454	0.06976
38B	5.96712	32.69	0.576	0.90099	1.10558	2.13785	4.039	1.56177	0.08284
39B	5.29529	35.3052	0.378	0.77319	1.07961	1.80895	3.227	1.09746	0.05668
40B	6.90874	30.1682	0.51	1.13103	1.09074	2.0449	4.221	1.70649	0.09156
41B	5.21065	36.31392	0.27	0.79875	1.04251	1.4872	2.639	0.85626	0.05232
42B	5.43283	35.31921	0.456	0.77319	0.94605	1.93765	3.458	1.21806	0.06104
43B	5.44341	35.91697	0.3	0.7668	1.03138	1.6731	3.01	1.11555	0.0654
44B	5.24768	35.26317	0.384	0.81153	1.09074	1.8018	3.045	1.12761	0.05232
45B	5.31116	34.40389	0.408	0.73485	1.05364	1.93765	3.255	1.18188	0.04796
46B	5.39051	34.98297	0.39	0.79875	0.99428	1.79465	3.024	1.15173	0.04796
47B	5.64443	33.96491	0.378	0.91377	0.96089	1.69455	3.08	1.05525	0.05668
48B	5.27942	36.55676	0.294	0.79875	1.09074	1.5587	2.485	1.03716	0.04796
49B	4.98847	35.58073	0.288	0.85626	1.16494	1.63735	2.422	1.06731	0.0436
50B	5.25297	36.15047	0.318	0.7668	1.05364	1.79465	2.723	1.13364	0.0436
51B	5.35348	36.1925	0.27	0.77319	1.20204	1.5444	2.499	0.95877	0.0436
52B	5.24768	36.01971	0.282	0.79236	1.03509	1.5587	2.604	1.00098	0.05232
53B	5.60211	35.01566	0.288	0.70929	1.16494	1.89475	2.688	1.07334	0.04796
54B	5.39051	36.893	0.228	0.74124	1.11671	1.4872	2.422	0.77184	0.05232
55B	5.43812	36.51473	0.252	0.7668	1.16865	1.56585	2.492	0.97686	0.0436
56B	5.28471	36.24854	0.294	0.79875	1.06477	1.6302	2.632	1.07937	0.05232
57B	5.51747	35.27251	0.282	0.74763	1.09074	1.86615	2.73	1.09143	0.05232

VII-7: MINOR ELEMENT RESULTS

Sample #	Rb (ppm)	Ba (ppm)	Sr (ppm)	Co (ppm)	Cr (ppm)	Ni (ppm)	V (ppm)	Y (ppm)	Mn (ppm)	Cu (ppm)	Zn (ppm)	Pb (ppm)	Zr (ppm)
1B	31.2	469	265.3	50.6	61.9	28.4	88.9	12.3	975.3	11.1	55	20.8	79.8
2B	28	508.4	252.9	49.3	62.7	30.1	92.4	16	754.9	13	52.7	19.1	87.1
3B	39.8	510.5	267.4	45.1	123.7	35.1	111.9	20.1	535.2	16.6	70.1	19.1	168
4B	33	516.4	251.7	131.8	67.7	26.2	82.7	10.2	471.9	7.2	46.7	12.7	86.2
5B	46.7	537.5	277.1	103.8	124.9	44.2	127.1	22.8	541.2	21	78.8	23.2	194.1
6B	30.2	497.6	255.4	45.9	71.3	30.1	92.3	16.7	640.7	13.5	55.9	11.7	84.7
7B	30.4	468.8	266.5	54.7	97.7	40.4	104.9	13.5	845.2	12.8	55.7	17.8	79.9
8B	28.9	505.3	258.9	39.9	76.8	34.2	94.2	12.7	768.4	13.4	50	7.7	84.3
9B	32.2	512.3	258.3	89.7	132	33.6	111.2	18.4	647.9	9.8	56.4	10.6	139
10B	32.7	513.2	250.7	68.2	88.3	29.7	92.4	15.5	475.4	9.2	55.8	10.1	109.4
11B	40.7	513.2	262.4	49.6	139.1	36.1	116.2	20.5	594.3	11.6	64.9	17.8	182.6
12B	38.2	509.1	255.8	84.6	100.4	33.1	96.4	14.8	536.8	13	60.2	17.1	140.2
13B	39	524	259.7	50.7	126.2	37.7	110.8	17.5	602.2	11.2	64.4	17.1	173.1
14B	33.7	484.5	262.4	69.2	196.8	43.7	132.6	21.2	779.9	9.9	64.3	18.7	247.1
15B	32.6	496.5	248.1	59.4	75.5	28.7	92.7	13.5	560.8	5.6	50	7.5	77.8
16B	35.6	535.4	247.4	54.5	92.1	32.4	91.9	15.2	600.2	9.9	61.9	20.9	121.4
17B	45	547.9	267.2	64.3	140.7	47.7	132.8	26.2	606.7	24.7	82.3	20.8	215.6
18B	46.4	541.2	261	120.9	130.6	47.2	125.6	20.9	585.5	26.9	79.1	15.8	169.3
19A	49.7	552.2	260.9	52.2	129.1	45.8	125.6	23.5	598.5	33.8	88	26.1	153.3
19B	55.3	535	259.7	78.5	129.2	43.6	128.1	19.7	585.1	28.9	89.6	18.2	162
19C	46.4	544.9	259.2	50.6	126.3	42.1	123.5	21.9	611.1	28.4	86.1	21	150.7
19D	52.1	540.5	256.9	31.7	122.2	40.9	117.2	19.4	557.6	29	85.9	23.1	149.4
19E	46.7	528.6	253.6	82	125.6	35	119.8	21.3	587.6	30.1	79.8	18.4	162.2
20B	47.7	541.5	259.1	83.2	123.2	30.6	104.8	19.5	482.8	21.4	74.3	19.4	146.5
21B	59.7	593.1	258.2	47.3	138.1	47.7	142.6	23.7	602.9	49	109.1	26.2	167.6
22B	44.5	518.3	267.4	138.1	131.3	39	123.6	23.1	667.5	18	76.8	15.9	195
23B	43.8	535.7	262.5	50.6	156.9	46.6	131.5	20.7	631.6	20.8	75.6	19.8	205.8
24B	31.8	507	260.4	56.6	121.2	36.5	108	16.7	606.6	10.8	56.2	11	134.8
25B	32.9	502.3	260.6	84.9	99.4	34	100.3	17.1	762.6	10.1	58.8	11.4	100.8
26B	49.6	575.8	265	37.3	134.7	46.3	133.6	19.6	636.8	23.1	81.5	11.5	207.7
27B	47.9	558.2	273.4	53.2	151.9	47.8	139.5	24.3	673.7	20.7	80.9	18.1	244.2

VII-7 cont'd: MINOR ELEMENT RESULTS

Sample #	Rb (ppm)	Ba (ppm)	Sr (ppm)	Co (ppm)	Cr (ppm)	Ni (ppm)	V (ppm)	Y (ppm)	Mn (ppm)	Cu (ppm)	Zn (ppm)	Pb (ppm)	Zr (ppm)
28B	34.5	489.8	263.6	60.2	216.1	42.8	143.7	22.9	769.7	8.6	68.2	17.6	288
29B	34.5	499	262.4	84.1	133.7	35.9	113	17.4	684.6	9.2	60.1	11	181.9
30B	30.8	486.3	264.4	90.6	194.9	43.2	136.7	25	739.8	10.2	66.1	14.5	285.3
31B	40.9	525.4	276.6	60	153.7	43.7	133.8	24.9	626.2	15.8	72.6	18.3	267.7
32B	35.2	500.7	267.4	67.9	164	40.9	128.4	21.7	708.9	9.3	65.5	14	235.5
33B	33.3	516.8	261.3	67.3	126.9	35.4	111.7	13.7	658.7	5.8	58.3	15.7	115.8
34B	27.5	506.1	260.8	54.1	137.4	35.2	116.5	16	633.5	10.9	56.4	13.8	118.9
35B	32.4	489.2	254.5	63.5	104.9	34.2	105.4	17.8	564.7	10.3	57.5	12.7	122
36B	39.4	502.8	265.3	56.5	202.2	43.2	147.5	26.3	792.1	12.1	71.1	14.1	339.6
38B	44.5	508	267.8	67.3	176.3	46.2	141.4	23.5	637.2	15.7	78.1	27.8	301.4
39B	28.3	509.1	252.7	73.9	125.8	37	112.2	16.8	834	9.8	63.2	17.8	135.1
40B	53.7	574.2	264.1	31	130.8	50.9	137.1	25.1	658.9	24.1	90.4	14.4	183.4
41B	36.3	540.6	247.9	58.7	75.5	32.3	87.2	11.4	568.6	7.4	57.8	12.2	85.9
42B	28	530.5	254.5	68.6	159	38.1	128.6	16.3	683.5	9.1	58.6	8.2	157.6
43B	29.3	495.3	245.8	66.9	85.1	37.6	101	13.6	812.3	9.4	61.1	16.2	86.4
44B	31.5	513.9	252.3	42.2	125.7	37.8	115.5	19.3	612.2	8	56	14.4	131.6
45B	29.5	508.8	265.3	43.5	160.2	36.8	122	16.3	699	10.4	55	9.9	142.8
46B	32.9	514.7	251.7	57.6	130.7	38	108.8	18.2	591	9.5	57.3	13	144.2
47B	34.3	524.9	251.5	58.3	130.3	33.8	102.7	18.3	555.7	11.8	56.3	4.4	136.9
48B	34.9	525.9	250.1	102.2	84.4	29.5	91.5	16.8	530.7	8.3	49.8	4.3	101.9
49B	40.1	505.9	252.1	55	83.9	28.8	89.2	15.4	519.5	9.5	47.2	17.8	91.2
50B	33.8	473.9	252.7	67.4	110.1	34.7	99.5	15.7	646.8	9	52.8	13.1	91.5
51B	30.8	521.1	255.1	40.1	77.4	34.5	90.4	11.2	700.4	11.7	50.5	10.8	87.3
52B	34.9	514.2	257.1	83.8	92.6	34	93.3	13.6	655.9	11.8	55.7	10.3	94.7
53B	35.4	490.9	277.6	57.1	91.8	29.8	100.2	15.1	691.4	8	52.6	7.4	87.6
54B	35.5	511.9	253.4	51	54.4	30.7	86.1	12.3	725.8	12.5	50.2	15.9	78.4
55B	34.3	540	260.8	47	68.5	33	89.2	12.5	698	12.1	49.3	7.2	79.9
56B	31.8	542.4	255.2	48.1	99.5	34.2	99.9	14.8	702.3	9	54.5	13.6	93.9
57B	30.2	478.7	264.6	57.2	84.5	31.1	101.2	13.4	683.4	13.1	53.1	6.1	80.7

VII-8: XRF INSTRUMENT SETTINGS

a: MAJOR ELEMENTS

Element *	Tube kv	Tube ma	Crystal ◊	Counter ♡	Peak 2θ (°)	Bkgrd 2θ (°)	Collimator ♧
Si	60	40	T	F	32.23	+2.3/-1.2	C
Al	60	40	T	F	37.88	+1.00	C
Fe	60	40	L	F	63.14	-1.6	C
Ti	60	40	L	F	86.35	+3.0/-1.0	C
Ca	50	10	L	F	113.34	+1.40	C
K	60	40	L	F	136.76	+2.00	F
Mn	50	20	L	F	63.14	-0.86	C
Mg	30	60	T	F	45.21	-1.2	C
P	30	60	G	F	141.12	-1.5	C

b: MINOR ELEMENTS

Element *	Tube kv	Tube ma	Crystal ◊	Counter ♡	Peak 2θ (°)	Bkgrd 2θ (°)	Collimator ♧
Ba	60	40	L	F	87.19	+1.20	F
Co	60	40	L	F	77.9	+0.54/-0.54	F
Cr	60	40	L	F	69.52	+1.00	C
Cu	60	40	L	F/S	45	-0.62	F
Ni	60	40	L	F/S	48.66	+1.2/-0.6	F
Pb	60	40	L	F/S	28.29	+0.5/-0.5	F
Rb	60	40	L	S	26.66	+0.4/-0.9	F
Sr	60	40	L	S	25.2	+0.6/-0.6	F
V	60	40	L	F	77.14	+4.0/-2.6	C
Y	60	40	L	S	23.83	+0.6/-0.6	F
Zn	60	40	L	F/S	41.78	+0.72	F
Zr	60	40	L	S	22.56	+0.74/-0.74	F
Na	30	60	T	F	55.25	+3.4/-1.7	C

* All elements measured on the Kα line, except Ba and Pb (Lβ)
◊ Crystals: L =lithium fluoride (200); T = thallium acid phthalate; G = germanium
♡ Counters: F = flow using 90% Ar & 10% CH4; S = scintillation
♧ Collimators: C = coarse (480 µm); fine (160 µm)

VII-9: ACCURACY OF XRF RESULTS

a: MAJOR ELEMENTS

Element		Al	Fe	Ti	Ca	K	Si	Mg	P	Na
JA2	m	15.37	6.32	0.66	6.35	1.69	56.58	7.52	0.18	3.12
	m	15.16	6.2	0.66	6.24	1.74	56.27	7.98	0.13	3.99
	r	15.32	6.14	0.67	6.48	1.8	56.18	7.68	0.15	3.08
	DFR	-0.02	0.12	-0.01	-0.185	-0.085	0.27	0.07	0.005	0.475
	RA	0.10%	2%	-1.50%	-2.90%	-4.70%	0.50%	0.90%	3.30%	15.40%
JB3	m	17.29	11.74	1.4	9.72	0.73	51.11	5.32	0.3	2.68
	r	16.89	11.88	1.45	9.86	0.78	51.04	5.2	0.29	2.82
	DFR	0.41	-0.18	-0.05	-0.14	-0.05	0.06	0.12	0.01	-0.14
	RA	2.00%	-1.50%	-1.40%	-1.40%	-6.40%	0.10%	2.30%	3.40%	-5%
JG3	m	15.86	3.73	0.46	3.66	2.45	69.39	1.86	0.15	4.21
	r	15.52	3.73	0.48	3.76	2.63	67.1	1.79	0.12	4.03
	DFR	0.38	0	-0.02	-0.1	-0.18	2.3	0.07	0.03	0.18
	RA	2.00%	0	-4.20%	-2.70%	-6.80%	3.40%	3.90%	25.00%	4.50%
JA3	m	15.69	6.58	0.66	6.25	1.3	63.25	3.73	0.14	3.39
	r	15.57	6.59	0.68	6.28	1.41	62.26	3.65	0.11	3.17
	DFR	0.13	-0.01	-0.02	-0.03	-0.09	1.04	0.080.03	0.22	
	RA	0.80%	-0.20%	-2.90%	-0.50%	-6.40%	1.70%	2.20%	27.30%	6.90%
JG2	m	12.87	1.03	0.02	0.71	4.45	80.75	-0.12	0.05	3.78
	r	12.41	0.92	0.04	0.8	4.72	76.95	0.04	0	3.55
	DFR	0.49	0.11	-0.02	-0.09	-0.27	3.85		0.05	0.23
	RA	3.90%	12%	-50%	-11.30%	-5.70%	5%		0	6.50%
G2	m	15.05	2.7	0.47	1.94	4.2	69.27	0.56	0.12	4.37
	r	15.38	2.66	0.48	1.96	4.48	69.08	0.75	0.14	4.08
	DFR	-0.28	0.04	-0.01	-0.02	-0.28	0.22	-0.19	-0.02	0.29
	RA	-1.80%	1.50%	-2%	-1%	-6.30%	0.30%	-25.30%	-14.30%	7.10%

All element concentrations expressed as wt.% oxides

m = measured values

r = recommended values

DFR = difference from reccommended value

RA = relative accuracy

VII-9 cont'd: ACCURACY OF XRF RESULTS

b: MINOR ELEMENTS

Element		Zr	Y	Sr	Rb	Pb	Zn	Cu	Ni	Co	Mn	V	Cr	Ba
JA2	m	112.6	18.1	229.5	69.6	24	64.4	22.7	129.9	28.8	879.7	117.6	445.3	270.8
	m	113.5	21.1	229.3	65	23.3	67.7	24.7	132.5	28.3	904.4	120.6	455.7	273.4
	r	123	18	252	68	19.3	62.7	28.6	142	30		130	465	317
	DFR	-9.95	1.6	-22.6	-0.7	4.35	3.35	-4.9	-10.8	-1.45		-10.9	-14.5	-44.9
	RA	-8.1	8.9	9	-1	22.5	5.3	-17.1	-7.6	-4.8		-8.4	-3.1	-14.2
JB3	m	103.8	20.8	392.2	18.5	20.2	101.1	189.3	36.2	32.4	1274.6	352.4	58.6	226.9
	r	99.4	28	395	13	5.5	106	198	38.8	36.3		383	60.4	251
	DFR	4.4	-7.2	-2.8	5.5	14.7	-4.9	-8.7	-2.6	-3.9		-30.6	-1.8	-24.1
	RA	4.4	-25.7	-0.7	42.3	267.3	-4.6	-4.4	-6.7	-10.7		-8	-3	-9.6
JG3	m	140.2	17.6	352.4	66.6	13.4	46.8	1.3	13.3	11.3	574.7	61.4	22.1	388.2
	r	137	19	372	66	12.3	44.8	6	13	11.4		73	23.6	453
	DFR	3.2	-1.4	-19.6	0.6	1.1	2	-4.7	0.3	-0.1		-11.6	-1.5	-64.8
	RA	2.3	-7.4	-5.3	0.9	8.9	4.5	-78	2.3	-0.9		-15.9	-6.4	-14.3
GSP1	m	490.1	35.7	234.2	239.3	60	107.3	28.6	14.2	6.6	229.7	55.2	9.3	1155.1
	r	530	26	234	254	55	104	33	9	7	326	53	13	1310
	DFR	-39.9	9.7	0.2	-14.7	5	3.3	-4.4	5.2	-0.4	-96.3	2.2	-3.7	-154.9
	RA	-7.5	37.3	0.1	-5.8	9.1	3.2	-13.3	57.8	-5.7	-29.5	4.2	-28.5	-11.8
JG2	m	83.1	87.6	16.9	270.7	36.4	15	-4.4	22.2	4.2	119.5	-23.3	-2.4	-19.4
	r	97	89	16	297	32.8	12.7	0.4	2.1	4.3		3	7.6	67
	DFR	-13.9	-0.98	0.9	-26.3	3.6	2.3			-0.1				
	RA	-14.3	-1.1	5.6	-8.9	11	18			-2.3				
G2	m	312.9	17.9	457.6	160.1	26.2	85.3	9.9	2.3	6.4	208.5	46.7	2.7	1806.8
	r	309	11	478	170	30	86	11	3	5	265	36	9	1882
	DFR	3.9	6.9	-20.4	-9.9	-3.8	-0.7	-1.1	-0.7	1.4	-56.5	10.7	-6.3	-75.2
	RA	12.3	62.7	-4.3	-5.8	-12.7	-0.8	-10	-23.3	28	-21.3	29.7	-70	-4

All element concentrations expressed as ppm (ug/g)

m = measured values

r = recommended values

DFR = difference from reccommended value

RA = relative accuracy

VII-10: ANALYTICAL PRECISION FOR XRF ANALYSES

a: MAJOR ELEMENTS

Sample #	Fe2O3 (wt. %)	TiO2 (wt. %)	CaO (wt. %)	K2O (wt. %)	SiO2 (wt. %)	Al2O3 (wt. %)	MgO (wt. %)	P2O5 (wt. %)	Na2O (wt. %)
5B-A	5.12	0.89	3.32	1.63	68.84	13.14	2.83	0.22	3.09
5B-B	5.4	0.89	3.32	1.6	68.69	13.32	2.78	0.21	2.65
5B-C	5.38	0.89	3.32	1.59	68.89	13.32	2.79	0.21	2.71
5B-D	5.36	0.89	3.32	1.63	68.84	13.25	2.83	0.21	2.87
5B-E	5.3	0.9	3.32	1.61	69.08	13.2	2.79	0.21	2.91
5B-F	5.22	0.89	3.32	1.57	68.07	13.1	2.75	0.2	2.82
SUM	31.78	5.35	19.92	9.63	412.41	79.33	16.77	1.26	17.05
MEAN	5.297	0.892	3.320	1.605	68.735	13.222	2.795	0.210	2.842
STD. DEV.	0.099	0.004	0.000	0.021	0.319	0.084	0.028	0.006	0.142
RSD (%)	3.736	0.836	0.000	2.668	0.927	1.267	2.013	5.499	10.023
21B-A	6	0.85	2.66	1.96	63.79	14.15	2.96	0.24	2.61
21B-B	6.14	0.86	2.63	1.95	64.08	14.3	2.92	0.25	2.61
21B-C	6.27	0.86	2.64	1.93	64.25	14.29	2.88	0.23	2.97
21B-D	6.23	0.86	2.65	1.93	64.53	14.31	2.87	0.25	3.02
21B-E	6.14	0.86	2.65	1.91	64.28	14.25	2.9	0.25	2.88
21B-F	6.28	0.86	2.65	1.92	64.47	14.19	2.86	0.25	2.79
SUM	37.06	5.15	15.88	11.6	385.4	85.49	17.39	1.47	16.88
MEAN	6.177	0.858	2.647	1.933	64.233	14.248	2.898	0.245	2.813
STD. DEV.	0.097	0.004	0.009	0.017	0.247	0.060	0.034	0.008	0.161
RSD (%)	3.132	0.868	0.712	1.758	0.770	0.836	2.337	6.235	11.424

RSD = Relative standard deviation (2 X Std. Dev./Mean) X 100

VII-10: ANALYTICAL PRECISION FOR XRF ANALYSES

b: MINOR ELEMENTS

Sample #	Zr (ppm)	Y (ppm)	Sr (ppm)	Rb (ppm)	Pb (ppm)	Zn (ppm)	Cu (ppm)	Ni (ppm)	Co (ppm)	Mn (ppm)	V (ppm)	Cr (ppm)	Ba (ppm)
5B-A	179.1	21.6	262.1	43	15.7	75.1	20.7	42.9	92.8	600.1	152	145.9	619.8
5B-B	175.2	19.1	258.5	46.2	14.1	76	20.2	37.3	98.9	609.1	155.2	147.6	609.4
5B-C	180.1	21.6	260.5	41.9	6.6	74.9	17.3	41.2	79.4	585.5	151.4	144.7	593.4
5B-D	177.6	19.7	266.1	46.3	11.7	73.1	22.9	42.4	72.5	575	147.2	147.1	587.7
5B-E	177.2	22.6	262.9	40.1	16.3	74	18.2	40.8	68	606.1	150.5	149.5	609.8
5B-F	177.4	22.2	264.3	42.8	7.1	73	21.6	39.2	72.3	602.3	154.3	153.1	621.9
SUM	1066.6	126.8	1574.4	260.3	71.5	446.1	120.9	243.8	483.9	3578.1	910.6	887.9	3642
MEAN	177.767	21.133	262.400	43.383	11.917	74.350	20.150	40.633	80.650	596.350	151.767	147.983	607.000
STD. DEV.	1.543	1.285	2.465	2.233	3.869	1.087	1.910	1.905	11.390	12.115	2.609	2.724	12.629
RSD (%)	1.736	12.165	1.879	10.293	64.932	2.925	18.961	9.376	28.246	4.063	3.439	3.682	4.161
19A-A	148.1	18.1	246.3	43.2	11.7	82.1	32.4	40.6	48.8	613.1	138	138.5	587.2
19A-B	144	19	242.4	43.7	11.6	84.2	32.5	40.9	50	637.4	148.3	140.4	635.3
19A-C	144	20.7	238.9	49.3	14.7	82.2	31.6	42	49	639.3	148	147.8	618.9
19A-D	143.4	18.4	235.1	46.7	13.4	83	32.2	40.9	41.6	608.3	145.9	137.8	601
19A-E	147	21.8	240.5	42.5	15.9	84.2	32.1	43.6	41.1	614.1	146.5	135.1	602.2
19D	149.4	19.4	256.9	52.1	23.1	85.9	29	40.9	31.7	557.6	117.2	122.2	540.5
SUM	875.9	117.4	1460.1	277.5	90.4	501.6	189.8	248.9	262.2	3669.8	843.9	821.8	3585.1
MEAN	145.983	19.567	243.350	46.250	15.067	83.600	31.633	41.483	43.700	611.633	140.650	136.967	597.517
STD.DEV.	2.300	1.300	6.943	3.502	3.905	1.328	1.212	1.045	6.442	26.982	11.040	7.678	29.654
RSD (%)	3.150	13.284	5.706	15.145	51.836	3.177	7.663	5.037	29.481	8.823	15.698	11.212	9.926

RSD = Relative standard deviation (2 X Std. Dev./Mean) X 100

VII-11: ANALYTICAL PRECISION FOR GAS CHROMATOGRAPHY/THERMAL CONDUCTIVITY ANALYSES

Sample #	Total %N	Total %C
5B-A	0.059	1.013
5B-B	0.061	1.025
5B-C	0.055	0.996
5B-D	0.059	0.979
5B-E	0.065	0.984
5B-F	0.054	0.935
5B-G	0.058	0.944
5B-H	0.056	0.965
SUM	0.467	7.839
MEAN	0.058	0.980
STD. DEV.	0.003	0.030
RSD (%)	11.623	6.021
21B-A	0.132	1.238
21B-B	0.144	1.254
21B-C	0.135	1.224
21B-D	0.133	1.231
21B-E	0.138	1.234
21B-F	0.133	1.212
21B-G	0.128	1.184
21B-H	0.136	1.191
SUM	1.080	9.768
MEAN	0.135	1.221
STD. DEV.	0.004	0.022
RSD (%)	6.500	3.658

RSD = Relative standard deviation (2 X Std. Dev./Mean) X 100

VII-12: ANALYTICAL PRECISION FOR COULOMETRY

Instrument : Blue

Test tube #	Sample #	Wt. sample (ug)	ug Carbon	% carb C
14	21Bb	84310	42	0.039
8	21Bc	82720	37	0.034
67	21Bd	98790	40.7	0.032
10	21Be	89840	39.4	0.034
21	21Bf	90710	44.8	0.039
2	21Bg	88670	49.6	0.046
	SUM			0.224
	MEAN			0.037
	STD. DEV.			0.005
	RSD (%)			25.028
3	19Da	97320	33.4	0.025
23	19Db	98760	33.9	0.026
45	19Dd	99020	29.1	0.020
16	19De	87530	27.7	0.021
54	19Df	87910	28.8	0.023
27	19Dg	88170	34.1	0.032
	SUM			0.148
	MEAN			0.025
	STD. DEV.			0.004
	RSD (%)			32.227

Instrument : Grey

Test tube #	Sample #	Wt. sample (ug)	ug Carbon	% carb C
1	21Ba	99150	88.25	0.079
26	21Bb	84410	78.33	0.081
18	21Bc	89040	83.2	0.083
16	21Bd	92190	95.06	0.093
26	21Be	97410	101.14	0.094
9	21Bf	84380	92.23	0.098
	SUM			0.527
	MEAN			0.088
	STD. DEV.			0.007
	RSD (%)			16.177
6	19Da	94380	70.41	0.064
27	19Db	93550	69.5	0.064
2	19Dc	91270	69.69	0.066
24	19Dd	96780	73.84	0.066
46	19De	85700	70.89	0.071
55	19Df	85750	71.92	0.073
	SUM			0.404
	MEAN			0.067
	STD. DEV.			0.003
	RSD (%)			10.015

RSD = Relative standard deviation (2 X Std. Dev./Mean) X 100

VII-13: CARBON AND NITROGEN RESULTS

Sample	Total %N	Total %C	% carbonate C	Instrument	% organic C	C/N ratio
1B	0.021	0.147	0.005	Blue	0.142	6.684
2B	0.022	0.151	0.006	Blue	0.145	6.650
3B	0.036	0.388	0.072	Blue	0.316	8.803
4B	0.021	0.141	0.002	Blue	0.139	6.730
5B	0.055	0.886	0.130	Blue	0.756	13.634
6B	0.021	0.156	0.005	Blue	0.151	7.156
7B	0.022	0.139	0.003	Blue	0.136	6.154
8B	0.023	0.140	0.005	Blue	0.136	5.795
9B	0.022	0.151	0.007	Blue	0.144	6.501
10B	0.019	0.154	0.004	Blue	0.150	7.734
11B	0.025	0.208	0.016	Blue	0.193	7.555
12B	0.029	0.262	0.046	Blue	0.216	7.420
13B	0.029	0.295	0.036	Blue	0.260	9.058
14B	0.023	0.150	0.011	Blue	0.139	6.044
15B	0.022	0.150	0.003	Blue	0.147	6.752
16B	0.038	0.228	0.004	Blue	0.224	5.937
17B	0.052	0.668	0.060	Blue	0.608	11.693
18B	0.051	0.594	0.049	Blue	0.546	10.674
19A	0.083	0.731	0.040	Blue	0.691	8.286
19B	0.073	0.674	0.036	Blue	0.639	8.712
19C	0.079	0.696	0.047	Blue	0.649	8.194
19D	0.076	0.645	0.032	Blue	0.613	8.059
19E	0.062	0.517	0.022	Blue	0.495	7.951
20B	0.054	0.420	0.010	Blue	0.410	7.645
21B	0.128	1.154	0.043	Blue	1.111	8.713
22B	0.049	0.484	0.034	Blue	0.450	9.115
23B	0.047	0.389	0.046	Grey	0.343	7.350
24B	0.022	0.166	0.015	Grey	0.151	6.736
25B	0.028	0.151	0.006	Grey	0.145	5.131
26B	0.042	0.546	0.088	Grey	0.458	11.027

Sample	Total %N	Total %C	% carbonate C	Instrument	% organic C	C/N ratio
27B	0.043	0.518	0.088	Grey	0.430	10.024
28B	0.029	0.168	0.011	Blue	0.157	5.444
29B	0.021	0.158	0.009	Blue	0.150	7.046
30B	0.024	0.212	0.022	Blue	0.190	7.810
31B	0.042	0.397	0.064	Blue	0.333	7.847
32B	0.027	0.181	0.017	Blue	0.164	5.989
33B	0.020	0.134	0.013	Grey	0.121	6.044
34B	0.016	0.122	0.013	Grey	0.109	6.864
35B	0.022	0.175	0.021	Grey	0.154	7.184
36B	0.030	0.199	0.030	Grey	0.168	5.674
38B	0.042	0.426	0.068	Grey	0.358	8.514
39B	0.028	0.185	0.006	Blue	0.179	6.314
40B	0.063	0.775	0.069	Blue	0.706	11.215
41B	0.022	0.161	0.001	Blue	0.160	7.164
42B	0.022	0.167	0.009	Blue	0.158	7.327
43B	0.028	0.204	0.018	Grey	0.186	6.609
44B	0.028	0.156	0.016	Grey	0.141	4.940
45B	0.018	0.130	0.018	Grey	0.112	6.081
46B	0.024	0.177	0.024	Grey	0.154	6.498
47B	0.026	0.165	0.012	Blue	0.154	5.802
48B	0.021	0.153	0.009	Blue	0.144	6.763
49B	0.020	0.140	0.008	Blue	0.132	6.513
50B	0.018	0.125	0.004	Blue	0.122	6.659
51B	0.015	0.147	0.010	Grey	0.137	8.902
52B	0.024	0.148	0.011	Grey	0.137	5.765
53B	0.019	0.140	0.010	Grey	0.129	6.751
54B	0.018	0.139	0.008	Grey	0.131	7.242
55B	0.025	0.144	0.008	Grey	0.136	5.437
56B	0.016	0.129	0.005	Blue	0.124	7.614
57B	0.022	0.145	0.005	Blue	0.140	6.413